



Biochemistry PhD Programme
Cycle XXXIII (2017-2020)

**Anti-trypanosomatidal drug discovery:
a challenge for structural biology**

Supervisor

Dr. Gianni Colotti

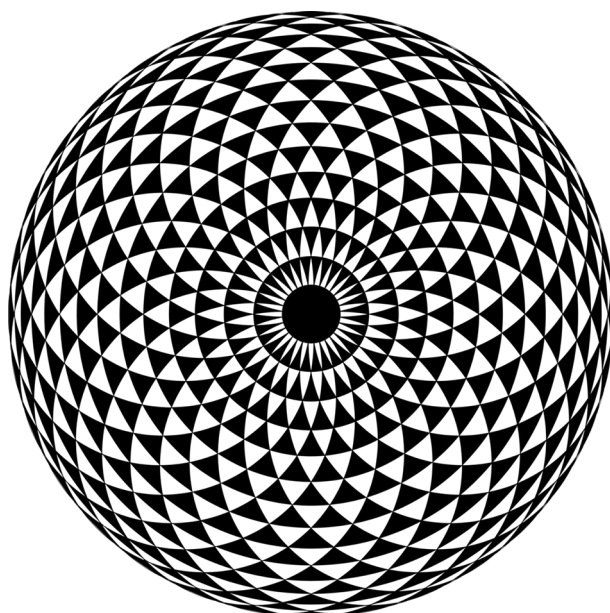
Coordinator

Prof. Stefano Gianni

Prof. Francesco Malatesta

PhD Candidate

Theo Battista





Biochemistry PhD Programme

Cycle XXXIII (2017-2020)

**Anti-trypanosomatidal drug discovery:
a challenge for structural biology**

Supervisor

Dr. Gianni Colotti

Coordinator

Prof. Stefano Gianni

Prof. Francesco Malatesta

PhD Candidate

Theo Battista

INDEX

1. INTRODUCTION	- 1 -
1.1. Drug Discovery	- 1 -
1.1.1. The drug discovery process.....	- 2 -
1.1.2. Drug target identification and validation	- 4 -
1.1.3. Approaches in drug discovery: from hit identification to lead optimization.....	- 6 -
1.1.4. High-throughput screening	- 9 -
1.1.5. Fragment-based screening.....	- 14 -
1.1.6. A rational approach: structure-based drug design.....	- 15 -
1.2. The biological problem: neglected tropical diseases	- 17 -
1.2.1. Trypanosomatid neglected diseases: an overview	- 18 -
1.2.2. Redox homeostasis in Trypanosomatids: the trypanothione metabolism	- 33 -
1.3. The drug target: trypanothione reductase.....	- 41 -
1.3.1. Trypanothione reductase, from structure to function.....	- 41 -
1.3.2. Trypanothione reductase inhibitors.....	- 44 -
2. AIM OF THE STUDY	- 53 -
3. RESULTS AND DISCUSSION	- 55 -
3.1. HTS approach: identification of spiro-containing derivatives.....	- 55 -

3.1.1. HTS assay optimization	- 55 -
3.1.2. Hit identification and confirmation.....	- 56 -
3.1.3. Hit compound binding to TbTR.....	- 63 -
3.1.4. Compound 1 activity in Trypanosoma brucei <i>in vitro</i> culture	- 65 -
3.1.5. X-ray crystal structure of TR in complex with Compound 1	- 67 -
3.1.6. Discussion	- 74 -
3.2. From LeishBox toward a drug against all Kinetoplastids.....	- 76 -
3.2.1. Determination of inhibiting capacity of LeishBox compounds against LiTR.....	- 76 -
3.2.2. Selected inhibitors interact directly with LiTR.....	- 81 -
3.2.3. Structural analysis of the most selective inhibiting compounds	- 82 -
3.2.4. SPR competitive binding experiments.....	- 83 -
3.2.5. Docking of LiTR and hGR with compounds A1/7, C5/7, C10/7 and F1/7 and molecular basis of inhibition specificity	- 84 -
3.2.6. X-ray crystal structure of TR in complex with compound A1/7 ...	- 88 -
3.2.7. Preliminary studies on A1/7 derivatives	- 89 -
3.2.8. Discussion	- 95 -
3.3. Preliminary crystallographic studies for Fragment based screening	- 97 -
4. MATERIALS AND METHODS	- 99 -
4.1. High-throughput screening	- 99 -
4.1.1. Compound collection and similarity search.....	- 99 -

4.1.2. Expression and purification of trypanothione reductase from <i>T. brucei</i> .	- 100 -
4.1.3. Enzymatic assays	- 100 -
4.1.4. Competition assay	- 101 -
4.1.5. Surface plasmon resonance experiments	- 101 -
4.1.6. <i>T. brucei</i> growth inhibition assay	- 102 -
4.1.7. <i>T. brucei</i> lysate thiol formation assay	- 103 -
4.1.8. X-ray structure determination of TbTR-Compound 1 complex ..	- 103 -
4.2. LeishBox compounds identification	- 104 -
4.2.1. Expression and purification of trypanothione reductase from <i>L. infantum</i>	- 104 -
4.2.2. Enzymatic assays	- 105 -
4.2.3. Surface plasmon resonance experiments	- 106 -
4.2.4. Docking of compounds in the active site of TR	- 107 -
4.2.5. X-ray structure determination of TbTR-compound A1/7 complex	- 107 -
4.3. Preliminary crystallographic studies for Fragment based screening	- 108 -
5. CONCLUSIONS AND FUTURE PERSPECTIVES	- 110 -
6. REFERENCES	- 113 -
7. ACKNOWLEDGEMENTS	- 132 -
8. LIST OF PUBLISHED PAPERS	- 133 -
9. ATTACHMENTS	- 135 -

1. INTRODUCTION

1.1. Drug Discovery

Drug discovery and development is a lifelong challenge; disease has been recognized as an enemy of humankind since civilization began, and plagues of infectious diseases appeared as soon as humans began to congregate in settlements about 5000 years ago ¹. This ancient struggle against the diseased condition has pushed humanity toward the conceptualization of “health state” and the implementation of drugs as “weapons” to tackle adverse, unhealthy states. Therapeutics evolved simultaneously with society; despite the emphasis on herbal remedies in early medical concepts, and growing scientific interest in their use as medicines from the 18th century onwards, it was only in the mid-19th century that chemistry and biology advanced sufficiently to give a scientific basis to drug therapy, and it was not until the beginning of the 20th century that this knowledge actually began to be applied to the discovery of new drugs ¹. It is assessed that the foundation of modern, target-directed drug discovery relies on Ehrlich’s (1854 – 1915) catchphrase *Corpora non agunt nisi fixata*, whose belief paved the way for a series of striking improvements and achievements in the field of chemotherapy and, more in general, drug based-therapy.

Grounding on Ehrlich’s statement, research approaches progressed and developed thus far, focusing on specific, “druggable” molecular targets, generally proteins, rather than pathophysiological and/or biochemical mechanisms, like inflammation, blood pressure regulation etc. (the so-called “pre-molecular era”); in the last quarter of the 20th century technologic boost broke out, outlining trends like genomics as an approach to identifying new

drug targets, informatics to store and interpret data, high-throughput screening (HTS) of large compound libraries, based on target-specific assays, as a source of chemical leads and computational/automatic chemistry as a means of systematically synthesizing collections of compounds with drug-like properties in a rational manner ¹.

1.1.1. The drug discovery process

As partially anticipated, drug discovery is nowadays focused on the identification of compounds active against a defined molecular target, moving away from the “pre-molecular”, multivariable approach. It is feasible thanks to the development of molecular technologies and target-directed tools, which define each step of the drug discovery process.

The creation of a new drug goes through different phases, which can be didactically divided in:

- ❖ Drug discovery – from a therapeutic concept applied to a biological problem to the identification of a molecule or a subset of molecules;
- ❖ Drug development – from the molecule to registered product;
- ❖ Commercialization – from the product to therapeutic application and sales ².

It is fundamental to keep in mind that these stages are not independent and/or strictly subsequent the one to the other, but must be considered as a *research continuum*, in which every step can affect and mold, both positively and/or negatively, the previous or the following one. This is the reason why the research teams involved in the project must convey and coordinate, in order to puzzle out all the data and information to gain a successful candidate drug.

Figure 1 exemplifies the workflow that leads from the identification of a drug target to sorting out a valuable candidate drug.

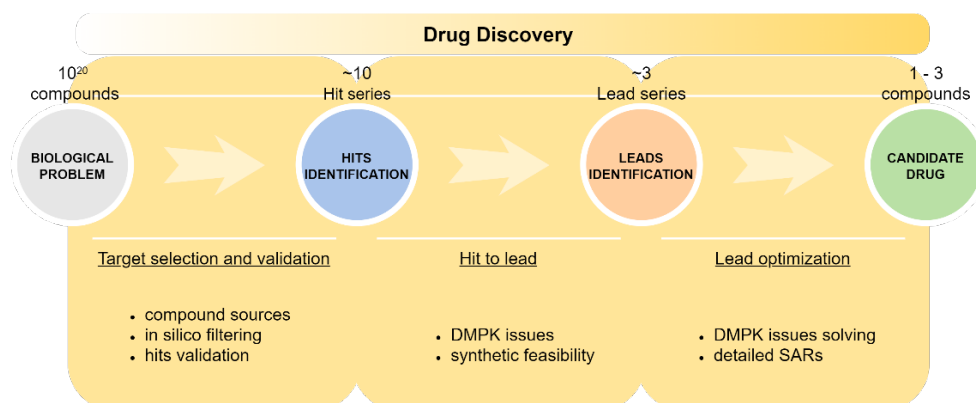


Figure 1. The drug discovery process.

The very first step is, as already mentioned, the identification and validation of a molecular target, responsible for pathophysiological mechanisms (this topic will be broadly discussed in the next section); generally, *in silico* screening aids in filtering a huge number of compounds (from a theoretical number of 10^{20} up to $>10^7$ molecules, available from online data bank like ZINC, ChEMBL, PubChem databases), constituting a starting screening library, to a workable number of compounds (combinatorial libraries are constituted). Readily available “in-house” or “focused” libraries are also employed as a starting point.

HTS is then used to identify “hits”, namely compounds which show a promising activity in the chosen screen ². Here resides one of the numerous bottlenecks of the entire process: the nature and reliability of the HTS assay and the size/quality of the library are crucial as the result is the rejection of up to hundreds or thousands of compounds.

Validation of hits is necessary to eliminate fictitious outcomes, and this may comprise repeating the screening of the hits by exploiting an alternative assay for proving, as well as resynthesis and retesting of the hit compounds ². Simultaneously, structure-activity relationships (SAR) within the library are addressed in order to identify a “hit series” – a family of structurally related compounds – which represents a reasonable starting point for further chemistry ².

In the lead identification stage, the validated hits are subjected to additional investigation, particularly in respect of their pharmacokinetic profile (DMPK issues) and toxicity as well as their feasibility for a synthetic chemistry programme. The “hit series” is consequently reduced to one or a few “lead series”.

Synthetic chemistry then begins; “lead optimization” usually involves parallel synthesis to generate derivatives of the lead series, which are consequently screened and profiled with respect to pharmacology, pharmacokinetics and toxicology, in order to obtain a small number of “drug candidates” (often a single compound), suitable for further development, at which point they are taken into preclinical development ².

1.1.2. Drug target identification and validation

It is extensively proven that the feasibility and likelihood of success of a drug discovery project depends on the selection of an appropriate drug target; commonly drug candidates fail in development and clinical trials mainly because of low potency/specificity and/or unexpected toxicity ^{3,4}.

The broad term “target” includes a range of biological entities such as proteins, genes and RNA, which, to be efficacious, require specific properties, i.e.

clinical relevance and “druggability”. A “druggable” target is accessible to the putative drug molecule, be that a small molecule or larger biologicals, and upon binding, elicit a biological response which may be measured both *in vitro* and *in vivo* ⁵.

Strictly dependent is target’s “assayability”, a fundamental characteristic in target-based drug discovery; the likelihood of discovering a novel modulating molecule depends on the reliability of the screening assay used for investigation. Target characteristics are summarized in Table 1.

<u>WHAT MAKES A GOOD DRUG TARGET?</u>	
Clinical relevance	Disease-modifying and/or proven function in the pathophysiology of a disease
Druggability	Susceptible to binding and modulation in terms of activity
Assayability	Favorable HTS configuration
3D structure	Structure based druggability assessment
Phenotype data	Prediction of potential side effects
Specific expression	Target is unequally expressed throughout districts and/or organisms
Biomarker	Target/disease-specific biomarkers exist to monitor therapeutic efficacy

Table 1. Drug target properties.

The idea for a target can come from a variety of sources including academic, clinical research and the commercial sector. Overall, identifying novel drug targets, mainly proteins that are critically involved in the development and/or progression of a disease, is a multistep endeavor involving various disciplines, including large-scale expression profiling and bioinformatics, structural biology, traditional cell biology, and ultimately functional *in vivo* studies. It may take many years to build up a body of supporting evidence before selecting a target for a costly drug discovery programme ^{5,6}.

Good target identification and validation enables increased confidence in the relationship between target and disease and allows to explore whether target modulation will lead to mechanism-based side effects ⁵.

1.1.3. Approaches in drug discovery: from hit identification to lead optimization

Over the last 25 years remarkable technological progress has been achieved in bioinformatics, high-throughput medicinal chemistry and screening techniques, leading to new approaches in hit identification. Hit identification stage aims at discover molecules able to interact with the validated molecular target in an initial screen, generally performed at a high concentration of compounds, to produce a quantifiable response in a robust, reproducible assay ⁷. Counterscreens have also been developed to eliminate false positives caused by assay interference or aggregation: compounds active in the primary identification assay are retested against another member of the target family under identical assay conditions. In case of observed activity, the hit is likely to be either promiscuous or false positive ⁸.

Several strategies have been adopted so far, in order to identify early hits, including existing drugs, natural ligands and products chemical evaluation, rational structure-based design, fragment-based screening, virtual screening and high-throughput screening (their application will be further discussed). These techniques can be subdivided considering the nature of the compounds used to interrogate the target: drug-like compounds in compliance with Lipinski's Rule of Five⁹ (RO5), or fragment-like molecules for which the Rule of Three¹⁰ (RO3) has been put in forth⁸. 'Drug-likeness' is intended as the overall profile of biophysicochemical properties, determining molecules effective interaction with the target, in a biologically relevant and safe concentration for sufficient duration to produce a therapeutic effect⁷. In the hit compounds chemical space, the drug-likeness concept may be reduced, according to RO3, to a "lead-likeness" definition, being hits the basis for medicinal chemistry and required to display improvable features with the aim to sprout in lead series. Thus, one could infer that an apparent disappointing success rate of compounds screening can be related to the lack of 'drug-likeness' in the collections; in order to avoid this condition, virtual or knowledge-based filtering of screening collections can exclude compounds which do not provide the desired drug-like physicochemical attributes (Ghose filter¹¹). Overall, these drug-/lead-like properties, together with hit clustering over singletons (hit series construction), play a pivotal role in the "hit to lead" (H2L) stage, as prioritization of the confirmed compounds is carried out accounting for selectivity, chemical tractability, binding mechanism, pharmacokinetic properties and patentability rather than potency *per se*⁸.

Properties	Rule of Five	Rule of Three
Molecular weight (daltons)	< 500	< 300
H bond donors	≤ 5	≤ 3
H bond acceptors	≤ 10	≤ 3
Calculated octanol-water partition coefficient (ClogP)	≤ 5	≤ 3
Number of rotatable bonds (NROT)	≤ 10	≤ 3
Polar surface area (PSA) (Å²)	≤ 140	≤ 60

Table 2. RO5 and RO3; Lipinski's RO5 were implemented with NROT and PSA parameters by Veber¹².

The H2L process might involve techniques such as hit evolution, (bio)isosteric replacement and hit fragmentation, or any combination of these⁸. Hit evolution provides analogues of the original hits, synthesized with different substitution patterns. Initial SAR data drive exploratory medicinal chemistry efforts, in order to achieve compounds with an improved lead-like profile. (Bio)isosteric replacements, if applicable, are useful for improving the hit profile while maintaining potency; hit fragmentation, relevant when the scaffold hits are large molecules, basically consists of structural decomposition producing promising fragments (which can be used in turn for a fragment-based screening) or minimalistic pharmacophores. Additionally, minimal core fragments represent a new starting point for fragment expansion; fragmentation can be followed by the combination of moieties coming from different hits (fragment linking or merging).

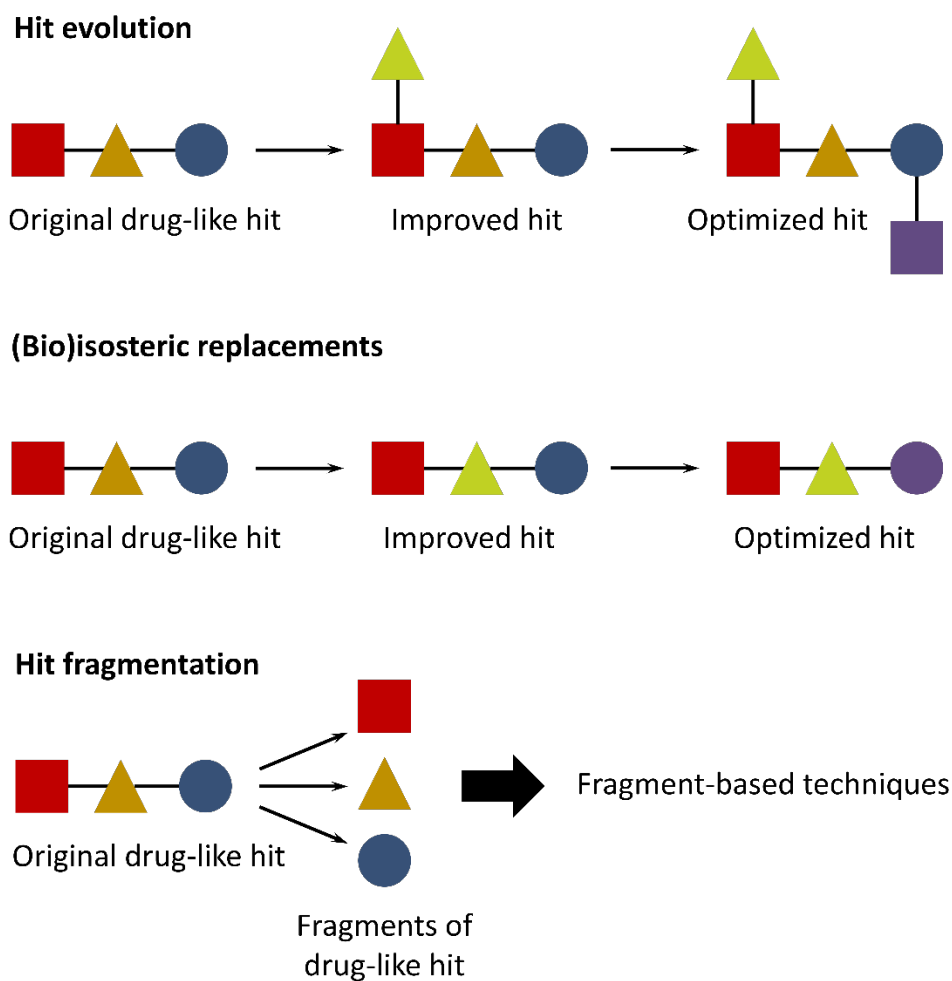


Figure 2. Hit to lead process: major techniques employed for hit optimization.

1.1.4. High-throughput screening

HTS was firstly introduced in the early 1990s and is now routinely employed in the hit identification step; disease-relevant validated targets are incorporated in massive parallel biochemical or cell-based assays and exposed to large numbers of compounds ⁷.

Typically, in HTS, a “primary” screen is performed resulting in the identification of numerous bioactive compounds (“primary hits” or “positives”, usually multiple members of a similar chemical core or chemical series). These undergo through successive rounds of screening (“secondary” screens) to confirm their activity, potency and, if possible, gain an early measure of specificity. Consequently, these hits enter the H2L process, during which specific hit-related compounds are synthesized for testing, in order to develop a rational understanding of SAR of the underlying chemical series ⁷.

Major concepts regarding HTS setup deal with quality criteria of the library to be tested (drug-/lead-likeness, chemical clustering), assay robustness and reproducibility together with parallelization, miniaturization and automation. The principal goal in HTS assay development is ensuring a fast and reliable identification of positives, thus implying the choice of measurable output (e.g. inhibition, stimulation or binding), handling and cost-effectiveness.

In order to identify hits with confidence, only small variations in signal measurements can be tolerated; statistical parameters generally adopted to determine the applicability of an assay for HTS are the calculation of standard deviations (SD), the coefficient of variation (CV), signal-to-noise (S/N) ratio or signal-to-background (S/B) ratio. Inner drawbacks of S/N and S/B criteria is that neither consider the dynamic range of the output signal (expressed as difference between the background, or low control, and the maximum signal, high control) nor the unevenness of the sample and reference control measurements ⁷. Assay quality is generally rated with the Z'-factor equation, instead ^{7,13}:

$$Z' = 1 - \frac{(3(\text{SD of High Control}) + 3(\text{SD of Low Control}))}{|\text{Mean of High Control} - \text{Mean of Low Control}|}$$

Equation 1. Z'-factor equation.

SD are the standard deviations, while low and high controls represent the minimum and the maximum signal to be measured in the assay, respectively. Alternatively to other statistical parameters, the Z'-factor includes, in assay quality assessment, the variability of high and low controls and the separation band between them, which represent the signal window in which the assay must be reliable, sensible and specific to produce an accurate outcome (Figure 3).

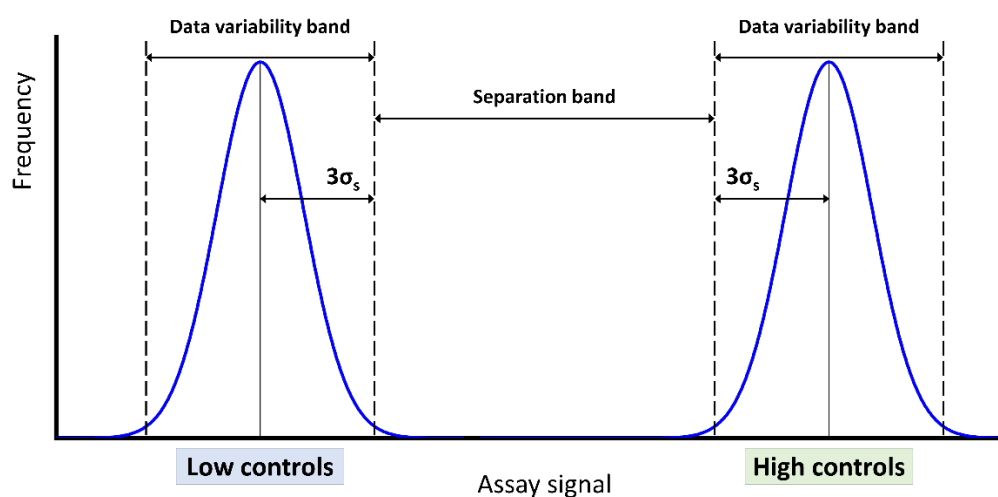


Figure 3. Data variability of high and low controls are taken into account in the Z'-factor, differently from other statistical parameters; separation between them must be high in order to obtain the largest signal window possible and minimize false positive/negative.

Z'-factor fluctuates between 0 and 1, according to the sharpness of controls peaks; a value greater than 0.5 is generally accepted for HTS biochemical

assays, while is decreased to 0.4 in cell-based screenings. From the Z'-factor, a Z-value can be derived, whereby average signal and SD of test set are compared to reference controls ⁷:

$$Z = 1 - \frac{(3(SD \text{ of Test Set}) + 3(SD \text{ of Reference Control}))}{|Mean \text{ of Test Set} - Mean \text{ of Reference Control}|}$$

Equation 2. Z-value equation.

Due to the intrinsic variability of test set compounds, the Z-value is generally lower than Z' score; overall, the simplicity of the equations describing these parameters make them the primary assessment for HTS.

A broad assortment of assays configurations can be outlined in the HTS scenario, even though all fall in two main categories namely biochemical and cell-based assays. Biochemical assays are cell-free *in vitro* systems imitating the biochemistry of cellular processes. These systems provide information on the nature of the molecular interaction (e.g. kinetic data), ranging from simple enzyme/substrate reactions or protein-protein interactions, to more complex systems like *in vitro* transcription systems. Additionally, with respect to cell-based assays, are endowed with a higher solvent tolerance thereby allowing the use of higher compound screening concentration when required. The main limitation is innate in the assay itself, as lack of the cellular context leads to assay being insensitive towards properties like membrane permeability, which governs the effect of compounds on cells ⁷.

Cell-based assays represent a simplified *in vivo* system and are elective for unraveling effects towards those targets unsuitable for screening in simple

systems, such as those involving signal transduction pathways, membrane transport, cell division, cytotoxicity or antibacterial actions ⁷. Through cell-based assays multiple parameters can be inspected: growth, transcriptional activity, changes in cellular metabolism or intracellular levels of messengers like cAMP or calcium, variations in membrane potential. Major issues involving these assays are the complexity of HTS protocols set up (cell cultivation and dedicated automated systems to maintain physiological conditions during screening are required) and frequent off-target effects of test compounds affecting the readout ⁷. Major techniques employed for screening are reported in Figure 4.

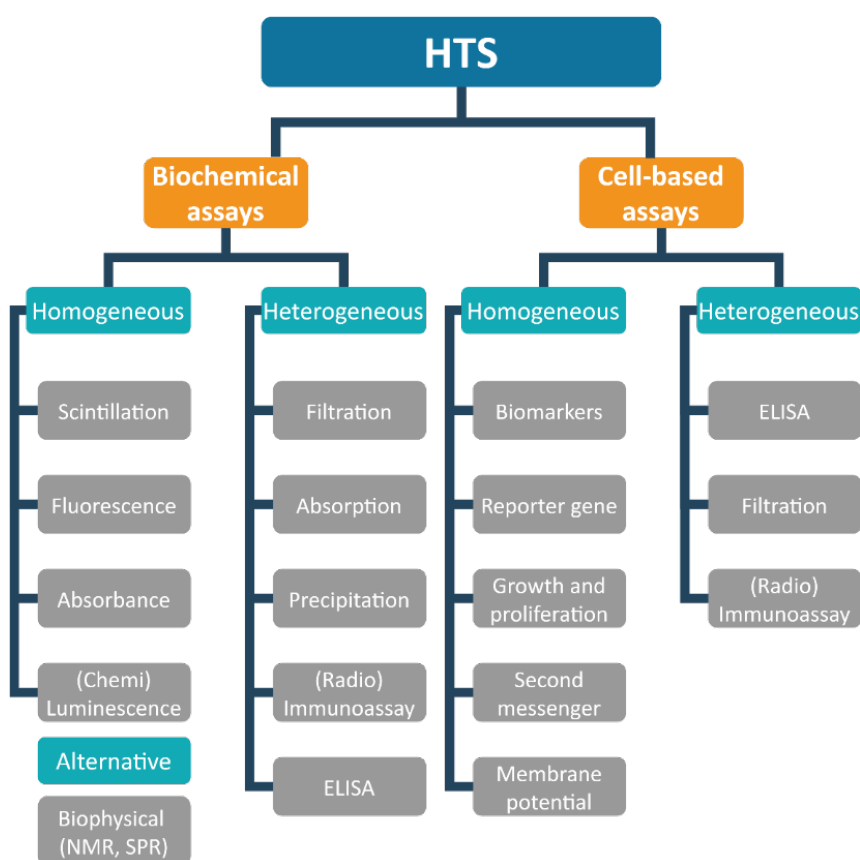


Figure 4. Types of assays generally applied for HTS.

1.1.5. Fragment-based screening

Fragment-based screening (FBS) has simultaneously grown with the other screening technologies, becoming a concrete alternative to more traditional hit identification methods. FBS approach relies on two central guidelines, which set it apart from HTS: (1) the concept that chemical space can be more efficiently probed by handling small fragments (molecules satisfying RO3) instead of large molecules (according to RO5) and (2) the principle that, being these fragments small in size (MW < 300 Da), they should bind with lower affinity to targets with respect to larger molecules but displaying a binding efficiency at least as high as for drug-like compounds ¹⁴.

In Fragment-based drug discover (FBDD), screening methods must be much more sensitive than HTS bioassays (biochemical, biophysical, cell-based assays). The elective strategies are structural biology techniques like NMR or X-ray crystallography, able to detect low affinity binding and to be informative on the fragment-protein interaction. Recent advances in cryo-electron microscopy made it a valuable alternative for FBDD ¹⁵; in any case X-ray crystallography still remains the primary method for FBDD, mainly thanks to dramatic improvements in automatization and therefore time-reduction in obtaining co-crystals structures ¹⁴. Also X-ray data analysis and model building have been improved, with the implementation of automated structure solving pipelines.

Efficient fragment screening requires the soaking of cocktails of fragments into preformed crystals of the target protein; fragment-hits are then subjected to intense SAR studies and undergo chemical optimization through the use of hit optimization techniques discussed in section 1.1.3.

A reliable concept widely used for comparing hits across different series and the effectiveness of compound optimization is “ligand efficiency” (LE). The term LE is defined as the free energy of binding (ΔG) of a ligand for a specific protein averaged for each “heavy atom” (or nonhydrogen atom). The number of heavy atoms is named “heavy atom count” (HAC),

$$LE = -\frac{\Delta G}{HAC} \approx -\frac{RT\ln(IC50)}{HAC}$$

LE is expressed as (kcal/mol)·heavy atom⁻¹ and has been extrapolated that a minimum LE of 0.3 is required in a hit or lead for it to be useful¹⁴. A recent advance of LE is “group efficiency” (GE) which allows the estimation of an individual chemical group’s contribution toward the overall free energy of binding. This analysis requires the comparison of matched pairs of compounds with the result of an additional, fast and informative insight that can direct hit chemistry and SAR studies. ΔG values can be converted into GE similarly to LE:

$$GE = -\frac{\Delta G}{HAC}$$

where HAC is the number of non-hydrogen atoms in a specific group. $GE \geq 0.3$ suggest that the substituent produces an acceptable contribution to the compound’s potency overall, ensuring maintenance of good drug-like properties¹⁴.

1.1.6. A rational approach: structure-based drug design

Structure-based drug design (SBDD) represents a comprehensive, multidisciplinary approach, aiming at overtaking the experimental and economic bottlenecks of other hit/lead identification processes. Actually, the

most recent advances in computer-aided structure predictions and interaction simulations are combined with experimental data, in a knowledge-based fashion, in order to increase the rate of success of focused compound series. In other words, availability of 3D-structures (obtained commonly by X-ray crystallography, NMR but also through homology modeling) helps in the identification of binding sites and interaction determinants which, in turn, guide the selection of possible active molecules and their efficacy improvement.

Once the target is structurally assessed, identification of active compounds can be carried out through three main virtual approaches: ligand-based drug design (LBDD), virtual screening and *de novo* generation¹⁶. LBDD relies on known target's interactors, like substrates or cofactors, which can be further modified in order to increase affinity; in virtual screening, instead, databases of available small molecules are interrogated and tested against the target while in *de novo* generation small fragments are positioned in the characterized binding site. These two last approaches are based on docking techniques, which assess a score and a ranking to each compound, predicting the binding affinity for the target. In LBDD, instead, computational tools like quantitative structure-activity relationship (QSAR) or 3D-QSAR are used to investigate the chemical features that determine binding and to be improved. Descriptors generally taken into account when characterizing active compounds are: binding scores (affinity/specificity), balance between hydrophilicity/lipophilicity, ADMET profile, biodegradation, metabolites. On the basis of these data, compounds improvement and evolution design is generally carried out *in silico* and designed derivatives are again computationally evaluated before being experimentally confirmed *via* biophysical assays or structural characterization; SBDD is, therefore, an iterative process, starting from the identification of

scaffolds and culminating in a rational design, synthesis and testing of derivatives.

1.2. The biological problem: neglected tropical diseases

Various criteria could be applicable when a new drug discovery project begins, regarding scientific and technical issues, strategic and operational concerns (summarized in Figure 5) ¹⁷.

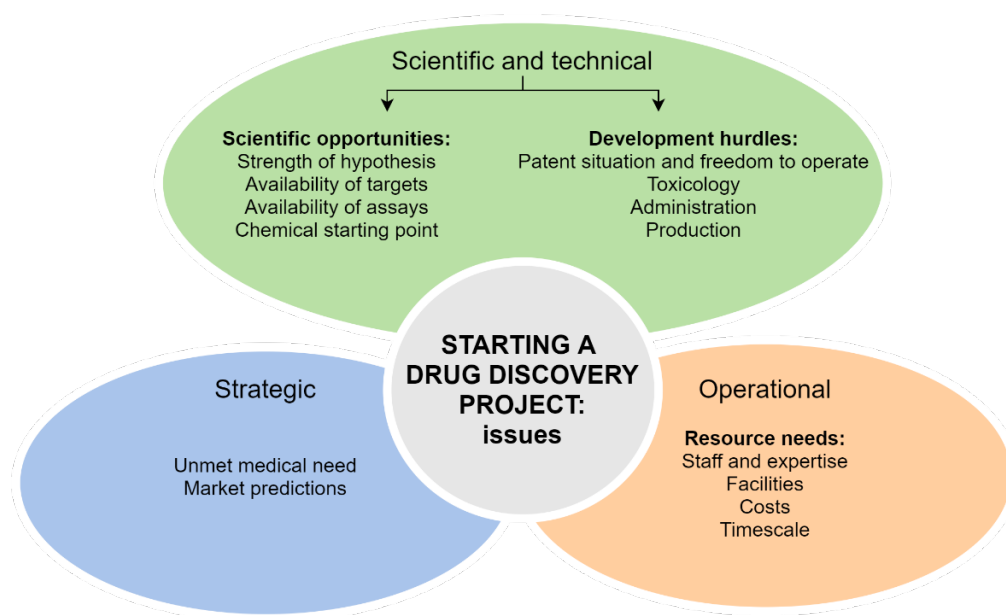


Figure 5. Issues to be taken into account when planning a drug discovery project.

Balance between these features raises possibilities of successfully creating and managing a drug discovery project and must be considered in the initial project assessment. A perfect balance is obviously unlikely, and some issues can be more significant than other; in this perspective most projects are oriented toward well-known and high morbidity diseases, with a conceivable potential

impact on the market while other campaigns are focused on neglected diseases, where the medical need and the freedom to operate represent the driving force of the plan.

The latter is the case of tropical diseases (globally named as “neglected tropical diseases”, NTDs) representing a social plague in the poorest countries worldwide. Research interest is not sufficiently involved because of costs and unfavorable profits, as these diseases generally sweep along with poverty and critical socio-economic conditions. Particularly, parasitic diseases induced by Trypanosomatids represent a large portion of this group and will be discussed in the following sections.

1.2.1. Trypanosomatidal neglected diseases: an overview

Trypanosomatidae represent the broadest family of protozoa belonging to the class of Kinetoplastids¹⁸; all members are exclusively parasitic, found primarily in insects while a few genera have life-cycles involving a secondary host, which may be a vertebrate, invertebrate or plant¹⁸.

The three major human diseases induced by Trypanosomatids are caused by two *genera* of dioxenous parasites, namely *Leishmania* and *Trypanosoma*.

Leishmania spp.

At least 20 species – of which the main are reported in Table 2 – of *Leishmania* (*L.*) are responsible for inducing vector-borne parasitic diseases in humans, transmitted between mammalian hosts by female sandflies¹⁹ (parasite life cycle is outlined in Figure 6). Distinct species of *Leishmania* cause different clinical manifestations, ranging in severity from self-curing cutaneous lesions to life-threatening visceral disease. The outcome is determined by the interplay

of the following: parasite characteristics, vector biology, and host factors, with immune responses taking central stage among the host factors ¹⁹.

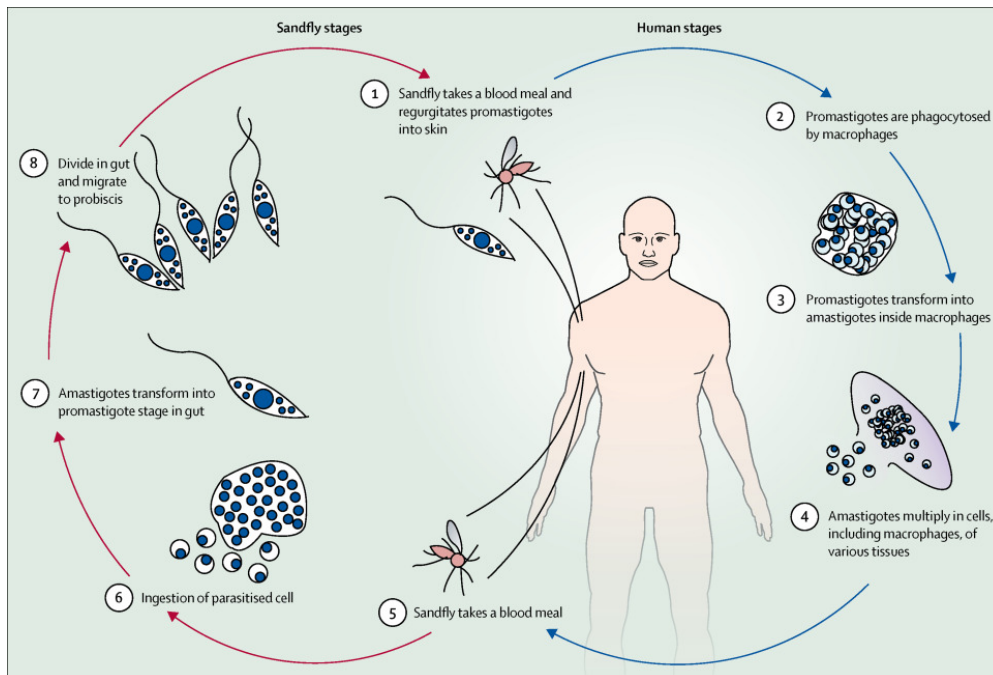


Figure 6. *Leishmania* spp. life cycle ¹⁹.

Visceral Leishmaniasis (VL) – caused by *L. donovani* in Asia and Africa and *L. infantum* in the Mediterranean Basin, the Middle East, central Asia, South America, and Central America – is the most severe, systemic form that is usually fatal unless treated. Post-kala-azar dermal leishmaniasis (PKDL) is a skin manifestation that occurs in otherwise healthy people after treatment of visceral leishmaniasis.

Species	Clinical disease forms	Natural progression	Main reservoirs	High-burden countries or regions	Estimated annual worldwide incidence
<i>L. donovani</i>	VL and PKDL	VL is fatal within 2 years; PKDL lesions self-heal in up to 85% of cases in Africa	Humans	India, Bangladesh, Ethiopia, Sudan and South Sudan	50 000 – 90 000 VL cases
<i>L. tropica</i>	CL, LR and rarely VL	CL lesions often self-heal within 1 year	Humans but zoonotic foci exist	Eastern Mediterranean, Middle East, and northeastern and southern Africa	200 000 – 400 000 CL
<i>L. aethiopica</i>	CL, DCL, DsCL, and oronasal CL	Self-healing, except for DCL, within 2–5 years	Hyraxes	Ethiopia and Kenya	20 000 – 40 000 CL
<i>L. major</i>	CL	Self-healing in >50% of cases within 2–8 months; multiple lesions slow to heal, and severe scarring	Rodents	Iran, Saudi Arabia, north Africa, Middle East, central Asia, and west Africa	230 000 – 430 000 CL
<i>L. infantum</i>	VL and CL	VL is fatal within 2 years; CL lesions self-heal within 1 year; confers individual immunity	Dogs, hares, and humans	China, southern Europe, Brazil, and South America for VL and CL; Central America for CL	6200 – 12 000 cases of OW VL and 4500 – 6800 cases of NW VL
<i>L. mexicana</i>	CL, DCL, DsCL	Often self-healing within 3 – 4 months	Rodents and marsupials	South America	Cases included in 187 200 – 300 000 cases of NW CL
<i>L. amazonensis</i>	CL, DCL, and DsCL	Not well described	Possoms and rodents	South America	Cases included in 187 200 – 300 000 cases of NW CL
<i>L. braziliensis</i>	CL, MCL, DCL, and LR	Might self-heal within 6 months; 2 – 5% of cases progress to MCL	Dogs, humans, rodents, and horses	South America	Majority of 187 200 – 300 000 cases of NW CL
<i>L. guyanensis</i>	CL, DsCL, and MCL	Might self-heal within 6 months	Possoms, sloths, and anteaters	South America	Cases included in 187 200 – 300 000 cases of NW CL

Table 3. Clinical and epidemiological characteristics of the main *Leishmania* species¹⁹. VL = visceral leishmaniasis, PKDL = post-kala-azar dermal leishmaniasis, CL = cutaneous leishmaniasis, LR = leishmaniasis recidivans, DCL = diffuse cutaneous leishmaniasis, DsCL = disseminated cutaneous leishmaniasis, MCL = mucocutaneous leishmaniasis, OW = Old World leishmaniasis, NW = New World leishmaniasis.

Cutaneous leishmaniasis (CL) is usually limited to an ulcer that self-heals over 3-18 months, but can also lead to scarring, disfigurement, and stigmatization as disability outcomes. Depending on parasite species, up to 10% of cutaneous leishmaniasis cases progress to more severe manifestations. These are known as mucocutaneous leishmaniasis (MCL), diffuse cutaneous leishmaniasis (DCL), disseminated cutaneous leishmaniasis (DsCL), and leishmaniasis recidivans (LR) ¹⁹.

For decades, VL was treated by pentavalent antimonial monotherapy, available in two formulations: sodium stibogluconate and meglumine antimoniate. Increasing non-response in India led to increased dosage recommendations, currently up to 20 mg/kg per day either by intramuscular injection or intravenous infusion over the course of 28-30 days.

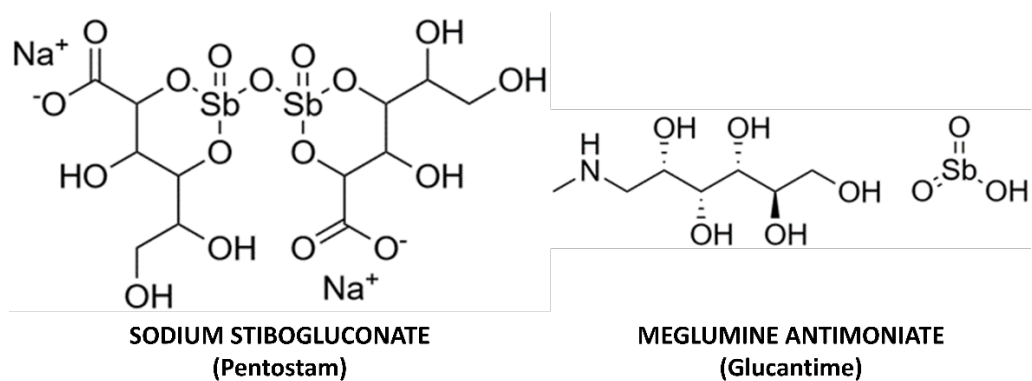


Figure 7. Chemical structure of pentavalent antimonials.

Aside from being painful if administered intramuscularly, antimonials have proven to be cardiotoxic and to induce arrhythmias ^{19,20}, particularly evident in HIV-VL co-infection ^{19,21}. In the Indian subcontinent, sodium stibogluconate

is no longer recommended because of drug resistance^{19,22,23}. Clinical research has then focused on shorter regimens and avoiding resistance^{23,24}. The first breakthrough was oral miltefosine (MF), registered in India in 2002, followed by the injectable paromomycin (PM) in 2006, administered in several short combination regimens, and single-dose liposomal amphotericin B (LAMB).

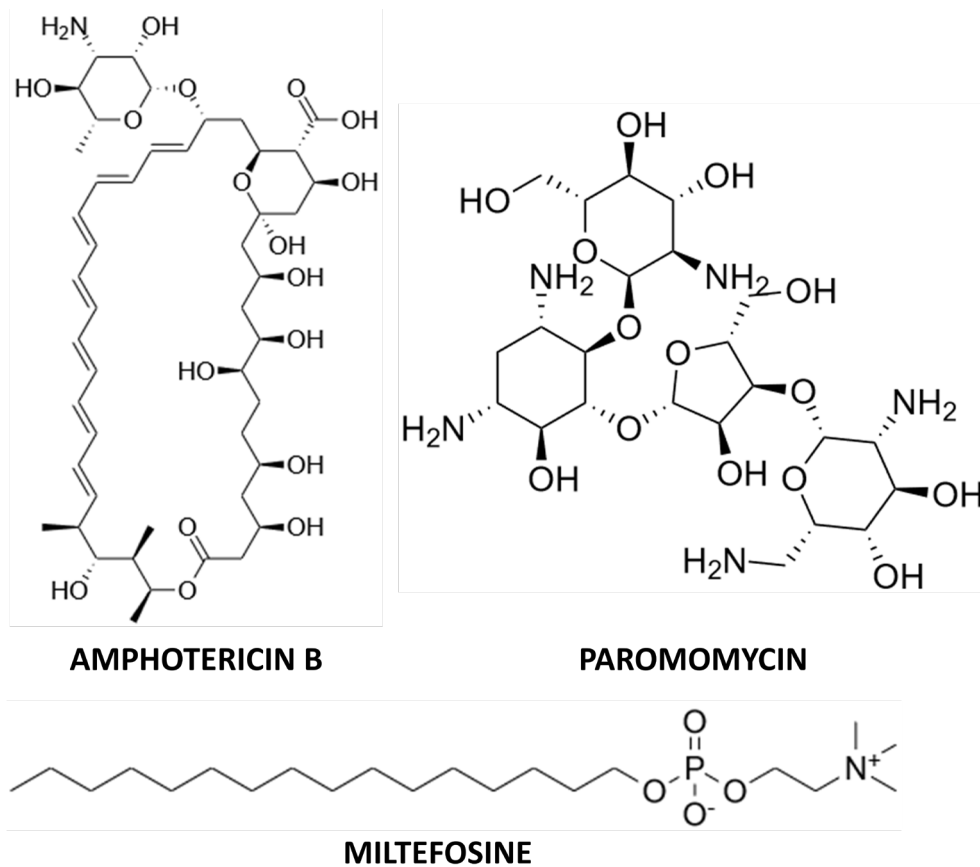


Figure 8. Alternatives to pentavalent antimonials: chemical structures of amphotericin B, PM and MF.

MF was adopted in 2005, as the first-line regimen by the Asian elimination initiative. However, after more than a decade of use there is evidence of reduced effectiveness in both VL and PKDL, while the existing linear dosing recommendations in children are likely to result in under-dosing and treatment failure²⁵. In east Africa, 20 mg/kg per day of sodium stibogluconate, in combination with intramuscular PM (15 mg/kg) over 17 days is the treatment of choice^{23,26}. In general, evidence in this region is limited to end-of-treatment outcomes (rather than the standard 6 months) because of high follow-up loss from migration. In east African patients with complicated VL, or those who are elderly or pregnant, treatment with LAMB is recommended because of its better safety profile¹⁹. However, routine use of LAMB monotherapy in non-severe patients has not proven to be as effective as in Asia and is not recommended. For all VL caused by *L. infantum* and for VL caused by *L. donovani* in Asia, sodium stibogluconate has been superseded by LAMB as first-line treatment. To date, the only LAMB formulation approved by the US Food and Drug Administration (FDA) and WHO for the treatment of VL is AmBisome (Gilead Sciences, Dimas, CA, USA)^{19,27}. Since 2010, for VL caused by *L. donovani* in the Indian subcontinent during the attack phase of elimination, WHO recommends 10 mg/kg of LAMB as a single dose by infusion or 3-5 mg/kg per daily dose infusion over 3-5 days up to a total dose of 15 mg^{19,28}.

An alternative to the LAMB regimen is one of several combination regimens (LAMB + PM, LAMB + MF, LAMB + antimonials), whose use is planned to be adopted once elimination targets have been reached to mitigate the risk of resistance developing to LAMB¹⁹.

Trypanosoma spp.

The genus *Trypanosoma* (*T.*) includes up to 30 relevant species of unicellular parasitic flagellate protozoa. Human-specific pathogens are: *T. brucei*, including *T. brucei gambiense* and *T. brucei rhodesiense* subspecies, and *T. cruzi*, causative agents of Human African trypanosomiasis (HAT, or sleeping sickness) and Chagas disease (or American trypanosomiasis), respectively.

Trypanosoma brucei – Human African trypanosomiasis

HAT occurs in sub-Saharan Africa, within the distributional limits of the vector, the tsetse fly (Diptera, genus *Glossina*). Two forms of the disease exist: the slow-progressing form, caused by *T. brucei gambiense*, which is endemic in western and central Africa; and, the fast-progressing form, caused by *T. brucei rhodesiense*, found in eastern and southern Africa^{29,30}.

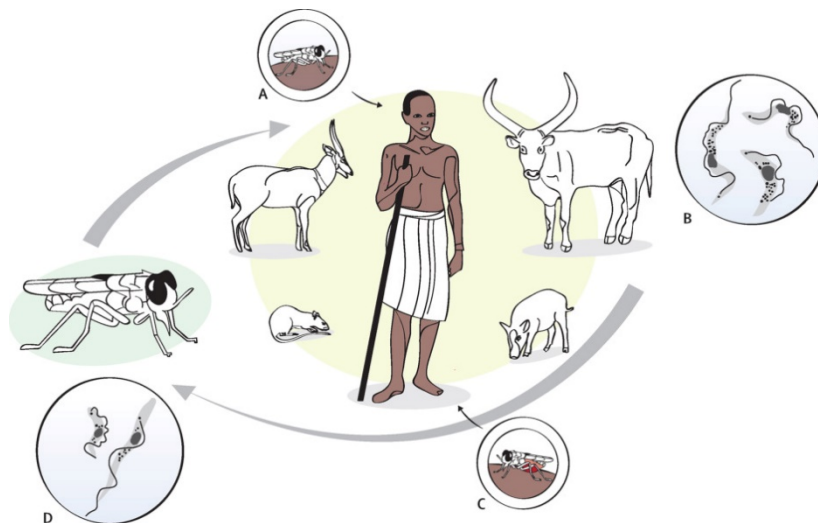
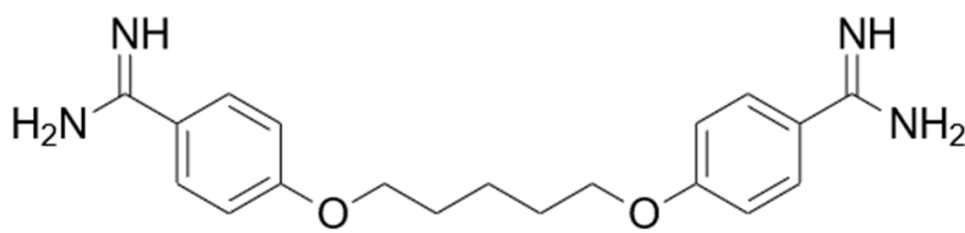


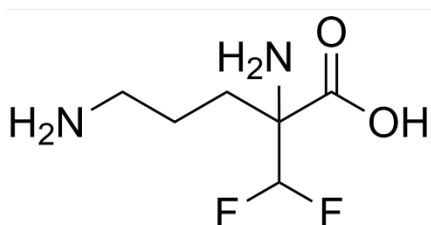
Figure 9. *T. brucei* life cycle: A) Metacyclic trypanosomes are injected into the skin of a mammalian host, during a blood meal. B) In the mammalian host, trypanosomes transform into dividing long slender forms that, via lymph and blood, infiltrate tissues and organs. C) A tsetse fly is infected by taking blood from a human being or other mammal that contains stumpy trypanosomes. D) After about 2 weeks, trypanosomes might have colonized the salivary glands, and can then be transmitted to the next mammalian host²⁹.

Commonly, both forms of the disease are lethal if untreated; even if, for *T. brucei gambiense* disease, healthy carriers and self-cure have been reported in literature ^{29,31}. The disease goes through two stages: a haemolymphatic stage followed by a meningoencephalitic stage in which trypanosomes cross the blood-brain barrier (BBB) and invade the central nervous system (CNS). *T. brucei rhodesiense* disease is generally acute, progressing to second stage within a few weeks, and death in less than 6 months ^{29,32,33}. *T. brucei gambiense* disease follows a chronic progressive course, with a mean duration estimated at 3 years ^{29,33}. Neurological disturbances, including sleep disorder, are typical of second-stage disease while the majority of signs and symptoms (fever, lymphadenopathy, hepatosplenomegaly, endocrine dysfunction) are common to both stages ²⁹.

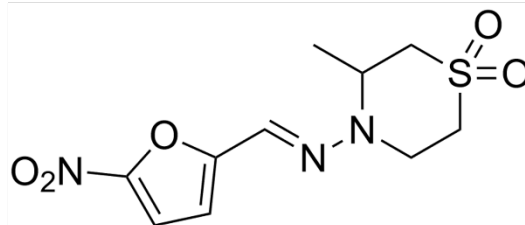
To date, five drugs are available (as monotherapies or in combination regimens) for the treatment of HAT: pentamidine and suramin for the first-stage disease treatment, and melarsoprol, eflornithine (or DFMO), and nifurtimox for second-stage disease ²⁹. A successful recovery rate from HAT strictly depends on promptness of intervention (the earlier, the better in terms of tolerability and cure) while the choice of treatment relies on the causative agent and disease stage. As a general, and proper, rule, drugs for the treatment of first-stage disease are not recommended for the second-stage disease (and *viceversa*), as the latter compels drugs able to cross the BBB, which tend to be more toxic and complex to administer than first-stage drugs ²⁹.



PENTAMIDINE



DFMO



NIFURTIMOX

Figure 10. *T. brucei gambiense* treatment: chemical structures of pentamidine, eflornithine and nifurtimox.

Pentamidine's efficacy against *T. brucei gambiense* disease (95-98%) has been stable for decades; in endemic areas, the most common route of administration is a daily intramuscular injection, for 7 days, but can also be delivered as an intravenous infusion in saline over 2 h. Pentamidine administration should follow the ingestion of sugar (10-20 g) to prevent hypoglycaemia, and has to be succeeded by rest in the supine position for 1-2 h to prevent hypotension. The intramuscular injection causes pain and transient swelling, while additional adverse effects are abdominal pain and gastrointestinal problems^{29,34}. Suramin is used only in the treatment of *T. brucei rhodesiense* disease, in complex treatment schedules lasting up to 1 month. A test dose is generally administered before treatment because of the risk of acute hypersensitivity reactions. Adverse effects are frequent, even if mostly mild and reversible, and

include pyrexia, nephrotoxicity, peripheral neuropathy, agranulocytosis and thrombocytopenia ²⁹.

The first-line treatment for second-stage *T. brucei gambiense* disease is nifurtimox-eflornithine combination therapy (NECT). In 2009, NECT was included in the WHO Essential Medicines List; has higher cure rates (95-98%), lower fatality rates (<1%), less severe adverse events, simpler administration, and is believed to avoid causing drug resistance of the parasite, in comparison to melarsoprol and eflornithine monotherapy. As nifurtimox is not licensed for African trypanosomiasis (but only for Chagas disease) it can only be used to treat patients with African trypanosomiasis off label, subject to express authorization and acceptance of responsibility by national authorities. NECT consists of oral administration of nifurtimox together with intravenous eflornithine. With 14 infusions, instead of the 56 used in eflornithine monotherapy, NECT is easier to administer, demanding fewer hospital resources and reducing costs. Even though eflornithine requires at least four daily infusions for a constant trypanostatic effect, infusions every 12 hours result to be highly effective in combination with oral nifurtimox. The most common adverse events reported for NECT are abdominal pain, vomiting and headache ^{29,35-38}. The toxicity profile replicates that of nifurtimox and eflornithine monotherapies, but with lower frequency and severity, mostly because of the shorter drug exposure. Eflornithine (α -difluoromethylornithine or DFMO) as a monotherapy is an option for *T. brucei gambiense* disease treatment only when nifurtimox is unavailable or contraindicated and is delivered as intravenous infusion for 14 days (generally 56 infusions in total) ²⁹. Frequent adverse effects are fever, pruritus, hypertension, nausea, vomiting, diarrhoea, abdominal pain and myelosuppression but eflornithine is, with a

fatality rate below 2%, safer than melarsoprol, whose use is restricted to the treatment of second-stage *T. brucei rhodesiense* disease^{29,39}.

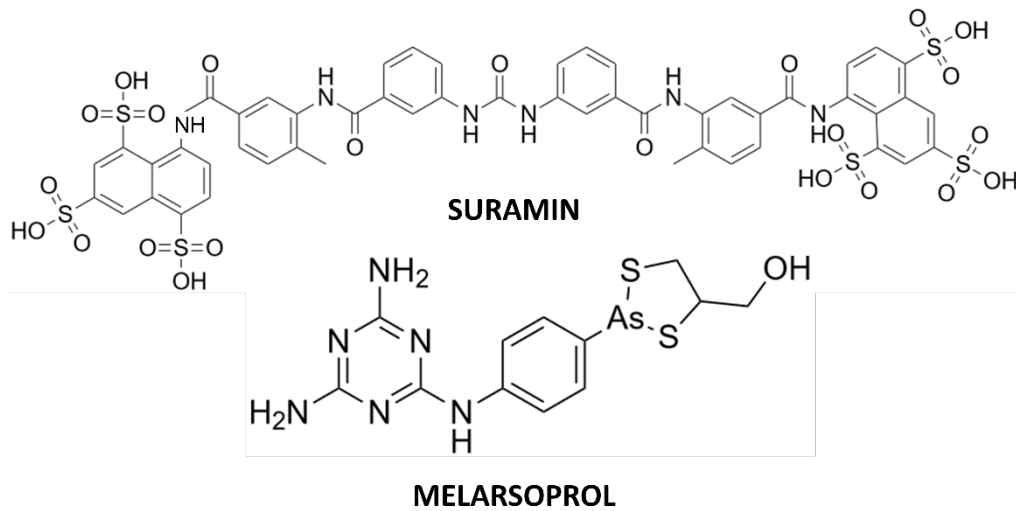


Figure 11. *T. brucei rhodesiense* treatment: chemical structures of suramin and melarsoprol.

Trypanosoma cruzi – Chagas disease

According to WHO, and in common with other neglected tropical diseases, “Chagas disease is a proxy for poverty and disadvantage: it affects populations with low visibility and little political voice, causes stigma and discrimination, is relatively neglected by researchers, and has a considerable impact on morbidity and mortality”^{40,41}; it is an anthroponozoonosis caused by *T. cruzi* (whose life cycle is reported in Figure 12), which is mainly transmitted by various species of three genera of blood-sucking triatomine insects (*Triatoma*, *Panstrongylus* and *Rhodnius*, also known as “kissing bugs”)⁴⁰. Additional routes of transmission are described, which have a major role in non-endemic countries. Mother-to-child transmission rate is estimated about 4-7% while

transmission via blood products settles around 10-25% per infected blood unit. Solid organ transplantation has a role in transmission, particular rates of infection are: 0-19% for kidney recipients, 0-29% for liver recipients and 75-100% for heart recipients⁴²⁻⁴⁶.

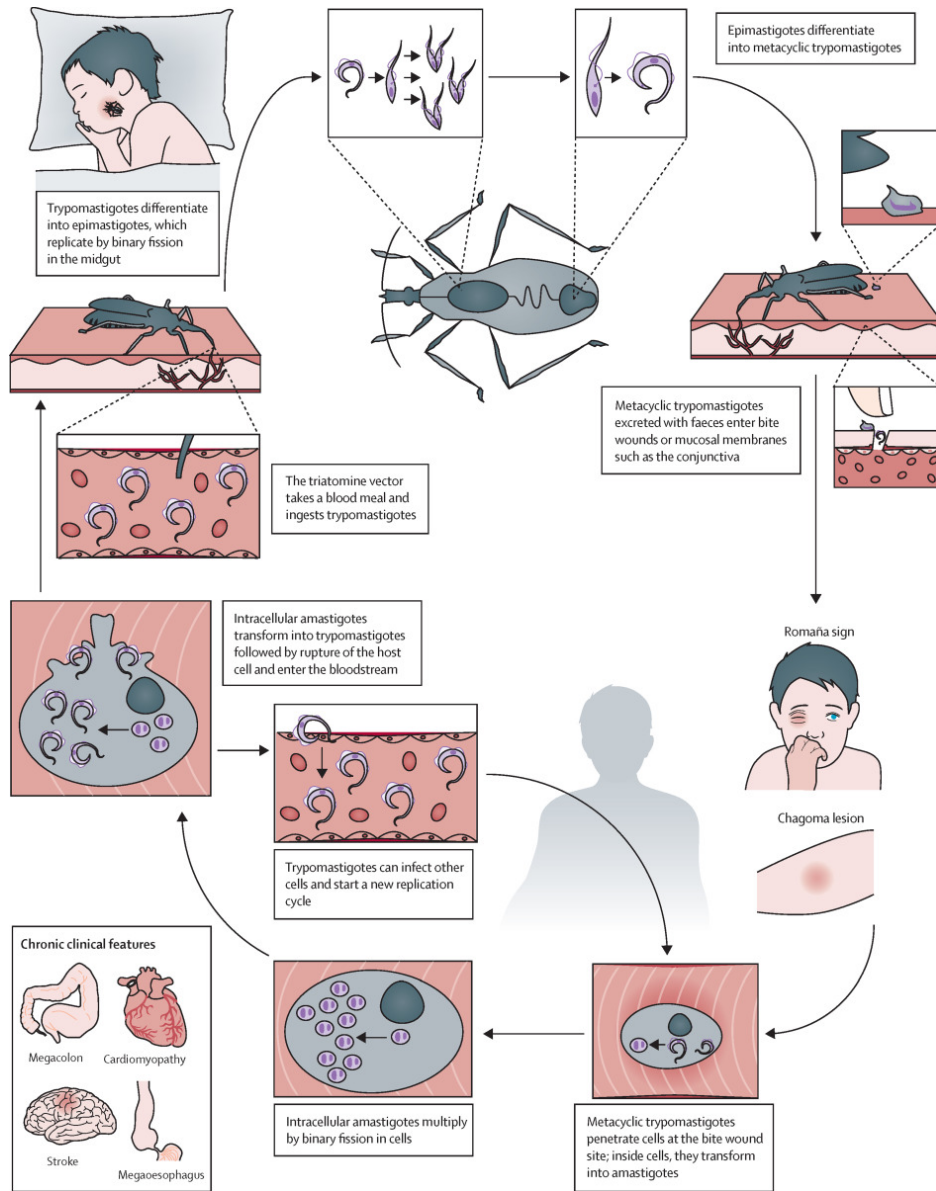


Figure 12. *T. cruzi* life cycle⁴⁰.

Chagas disease is endemic in 21 continental Latin American countries, from southern USA to the north of Argentina and Chile, generally confined to poor, rural areas of Central and South America, where vectorial transmission is the main route of contagion ⁴⁰.

The clinical course of American trypanosomiasis generally begins with an acute phase which can chronicize if untreated, in the second phase. Acute infection occurs at any age and is asymptomatic in most cases. When present, symptoms include fever, local inflammation at the inoculation site (inoculation sore), unilateral palpebral oedema (the so-called Romana sign, in those cases when the conjunctiva is the inoculation site), lymphadenopathy, and hepatosplenomegaly ⁴⁰. The acute phase generally lasts up to 8 weeks, with parasitaemia levels considerably decreasing from 90 days onwards. Severe acute disease occurs in less than 1-5% of patients and including manifestations as acute myocarditis, pericardial effusion and meningoencephalitis ^{40,47-49}. The acute phase generally heals spontaneously but patients commonly evolve to a chronic infection, if untreated; the largest part of patient affected never develop symptoms or visceral involvement, undergoing to an indeterminate form of Chagas disease characterized by seropositivity for *T. cruzi*, absence of clinical signs and symptoms of cardiac and digestive involvement, and normal chest radiography and electrocardiography ^{40,50}. It is estimated that around 30-40% of chronically infected patients can develop organ involvement, mostly cardiomyopathy and megaesophagus and/or megacolon, in 10-30 years after the acute phase. Cardiac implication, primarily affecting myocardium and conduction system, is the most frequent and severe type of organ involvement, occurring in 14-45% of chronically infected patients. Recent studies have demonstrated that progression to cardiac involvement is around 1.4-5% per

year^{40,50-57}. Sudden death is the main cause of death in patients with Chagas heart disease, followed by refractory heart failure and thromboembolism^{40,58}.

Only benznidazole and nifurtimox are licensed for the treatment of Chagas disease to date. Both have been the pillars of parasitocidal treatment for almost 50 years, even though their safety and efficacy profile are far from ideal, with their effectiveness seeming to decrease with time from the primary infection⁴⁰. In this perspective, early detection and intervention are essential requirements for a successful therapy.



Figure 13. American trypanosomiasis treatment: chemical structure of benznidazole.

Nifurtimox is administered orally, in three to four doses for 60-90 days, with recovery rates in the chronic indeterminate phase ranging from 86% in children younger than 14 years to 7-8% in adults^{51,59-62}. The frequency of adverse effects with nifurtimox is quite high (43-97.5%); the most common are anorexia, weight loss and neurological disorders as insomnia, disorientation, paresthesias, and peripheral neuropathy, nausea, vomiting, and, occasionally, fever and rash^{40,61-63}. Benznidazole shows, instead, a better tolerability profile and, possibly, efficacy. It is administered orally in two or three doses usually

for 60 days. Higher doses of up to 15 mg/kg are recommended in cases of meningoencephalitis ^{40,53}. Additionally, 30 days of treatment seems to be useful for chronically infected adults ^{40,53}. Luckily, benznidazole has a noticeable activity in the acute and early phases of *T. cruzi* infection: serological cure is achieved in up to 100% of patients with congenital disease treated during the first year of life and in 76% of patients with acute disease ^{40,64-66}. In the chronic phase, conversely, success rates are much lower: 60-93% in children aged up to 13 years and 2-40% in adults with late chronic disease ^{40,53,66-70}. The most common adverse effects involve hypersensitivity, mainly in the form of skin rash, digestive intolerance, and general symptoms such as anorexia, asthenia, headache and sleeping disorders.

The intent of this limited overview on trypanosomatid induced diseases is to shed light on the social and clinical relevance of these conditions, and how pharmacological therapy is still at its early days, features common to all NTDs. Epidemic loci are spread all around the world, and the burden of these plagues weighs enormously on some of the poorest societies worldwide, leading more than 100 000 people to death every year, comprehensively ⁷¹. It is clear how urgent is the need of new drugs to contrast these diseases; vaccines are unavailable while therapeutic agents used so far are old, endowed with a low tolerability profile and insufficient efficacy. As already discussed in the first part of the introduction, the modern approach in drug discovery is a target-based process, focused on the identification of compounds, active against a specific biomolecule, whose function and essentiality in the development of the disease is generally known; the uniqueness (in the sense of its natural absence in physiological conditions in the patient) of the target plays a critical

role in drug specificity and in avoiding toxic side effects. Trypanosomatidal biology includes feasible targets with these characteristics within a trypanosomatids-specific, unique cellular pathway, i.e. the trypanothione metabolism, whose function is the production and recycling of the spermidine-based dithiol trypanothione (T(SH)₂), a glutathione analogue, necessary, among multiple functions, for redox equilibrium and host immune system resistance. Next sections will deepen the rationale behind choosing this pathway as elective mechanism for antitrypanosomatidal therapy and will focus on one of the enzymes involved in it, the trypanothione reductase (TR), whose ideality as a molecular target, critical activity and structural features will be discussed.

1.2.2. Redox homeostasis in Trypanosomatids: the trypanothione metabolism

Historically, the enigmatic thiol-dependent redox system of trypanosomatids has been puzzled out by the pioneering work of Fairlamb and Cerami ⁷², in 1985. Ten years after the discovery and characterization of an unusual thiol-polyamine conjugate, namely mono(glutathionyl)-spermidine (Gsp) in *E. coli* ⁷³, they firstly identified and put at the crossroads of a novel, trypanosomatids-specific thiol-based redox system, the trypanothione molecule (T(SH)₂); Figure 14), a bis(glutathionyl)-spermidine, almost exclusively found in the order of *Kinetoplastida* and there representing the principal low molecular mass thiol ⁷⁴⁻⁷⁶.

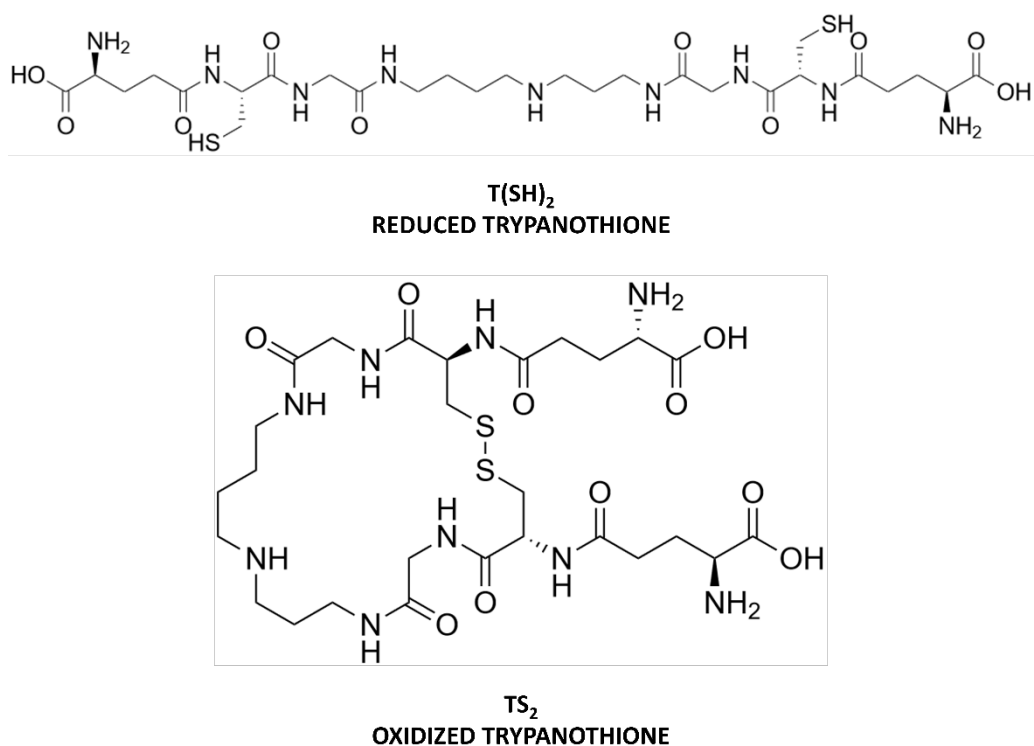


Figure 14. Chemical structures of trypanothione in both the reduced and the oxidized state.

T(SH)₂ utilization required the evolutionary specialization of key redox enzymes, leading to a progressive suppression of NADPH-reductases glutathione reductase (GR) and thioredoxin reductase (TrxR) genes, whose products represent the backbone for redox systems among *Eukaryota* but are absent in all known trypanosomatid genomes⁷⁷⁻⁷⁹. The reconfiguration of a new redox system appears to have gradually occurred in the biological evolution of Trypanosomatids, as TrxR and GR genes are still present in the oldest kinetoplastid ancestor *Euglena gracilis*^{77,80,81}.

Overall, in most living organisms, cellular reducing power and oxidative stress control is mainly governed by GR and TrxR in the glutathione/glutaredoxin

(GSH/Grx) and the thioredoxin (Trx) pathways respectively. Both pathways include the activity of peroxiredoxins for oxidant species neutralization namely glutaredoxin peroxidase (GPx), in the GSH/Grx system, and peroxiredoxin (Prx), in the Trx pathway ^{74,82} (Figure 15).

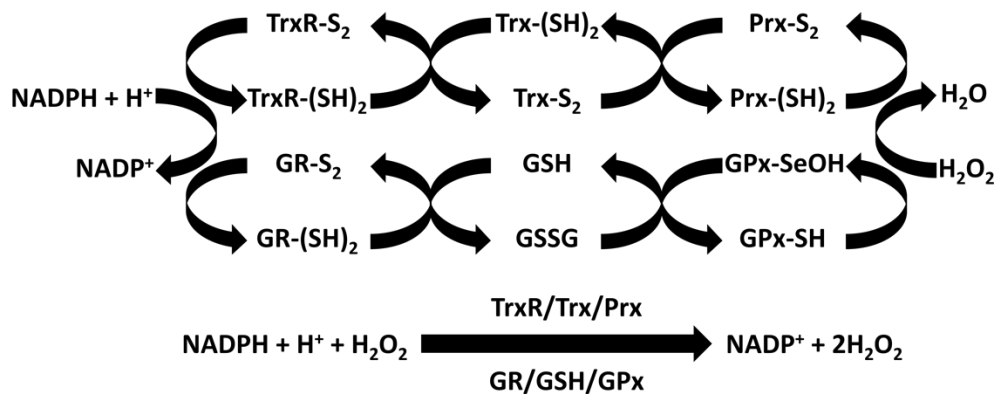


Figure 15. The Trx and the GSH/Grx pathways represent the most common antioxidant systems.

Conversely, Trypanosomatids rely on a minimalistic system composed of trypanothione reductase (TR), T(SH)₂ and the kinetoplastid-specific thioredoxin-like tryparedoxin (TXN), coupled to the tryparedoxin peroxidase (TXNPx) ⁷⁷.

Being trypanothione a spermidine-based dithiol, its synthesis is closely bound to the polyamine (PAs) metabolism (Figure 16). In brief, L-Arginine (L-Arg), the precursor of PAs, is converted in ornithine by the arginase (ARG) enzyme within the very first reaction of the PAs biosynthetic pathway. Ornithine is then converted by the ornithine decarboxylase (ODC) in putrescine. Spermidine (Spd) is synthesized by the enzyme spermidine synthase (SpdS) by addition of

the aminopropyl group of the decarboxylated S-adenosylmethionine (dAdoMet) to putrescine⁸³.

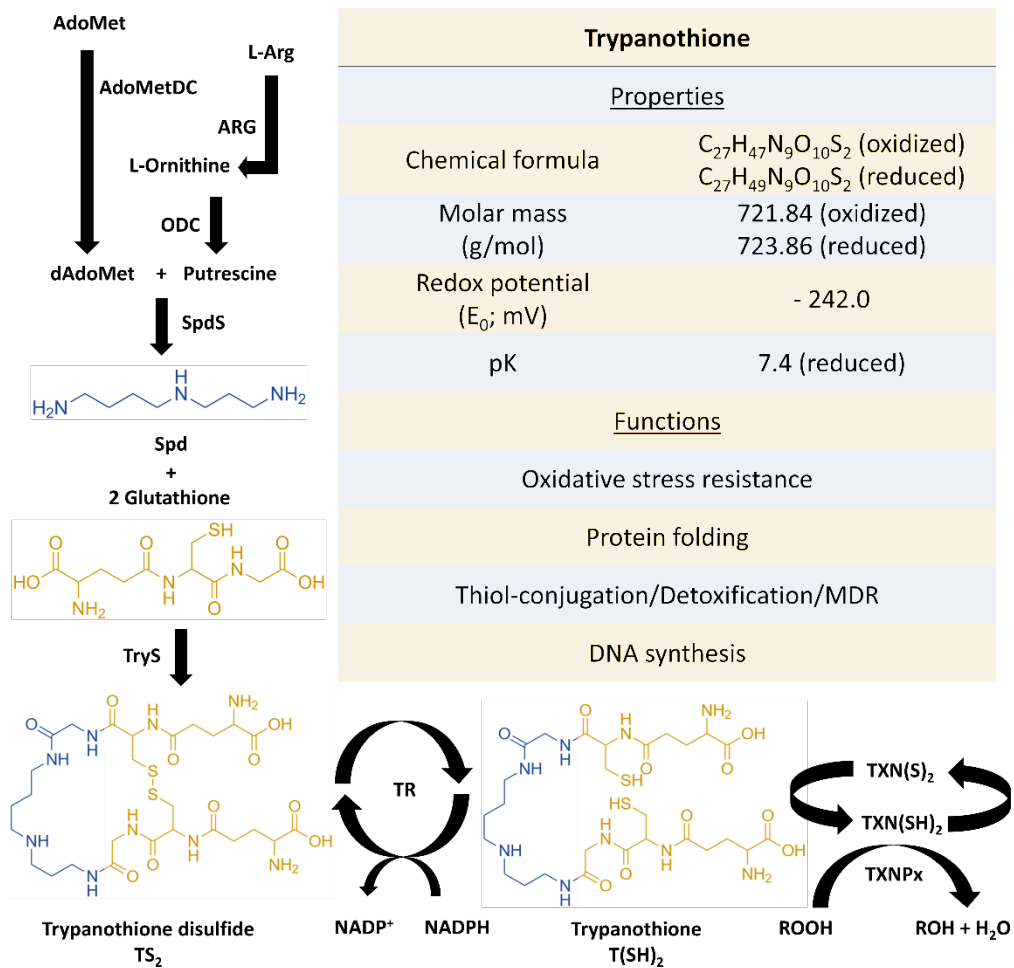


Figure 16. The PAs metabolism represent the very first step of trypanothione synthesis; two molecules of glutathione (in ochre) are condensed to one molecule of spermidine (in blue), to synthesize trypanothione whose chemical-physical properties and functions are summarized in the upper-right table.

Trypanothione is synthesized in a double step reaction by the bifunctional ATP dependent-enzyme trypanothione synthetase-amidase (TryS). The X-ray

crystal structure of TryS from *L. major* was solved by Fyfe and collaborators in 2008 (PDB code: 2VOB, 2VPM, 2VPM) and set the basis for the understanding of the synthetase activity. TryS is a 75 KDa monomeric enzyme presenting a N-terminal amidase domain (residues 1-215, 634-652), by which it is believed to maintain balanced the level of intracellular T(SH)₂, and a C-terminal synthetase domain (216-233), containing a roughly triangle shaped active site⁸⁴. Here, the three vertices represent three binding subpockets S1, S2, S3, able to bind ATP, GSH and Spd, respectively. The current accepted mechanism for the synthetase activity is the following: in the first step of the condensation reaction, the GSH carboxyl group is activated by ATP-dependent phosphorylation, generating an acylphosphate intermediate, stabilized by contributions from Arg328 and two Mg²⁺ ions. The Spd amine carries out nucleophilic attack on the anionic intermediate, which collapses to produce an amide linkage, resulting in the formation of Gsp, with release of ADP and phosphate. The Gsp remains located at S3, with the terminal amine directed toward the active site; S1 and S2 are occupied again by ATP and GSH. The second step takes place in the same manner as the first, with T(SH)₂ released from S3 as final product^{84,85}.

In order to pursue its antioxidant role, T(SH)₂ must be maintained in the reduced state. TR is the designate enzyme for this purpose; *via* NADPH acting as electron donor, a cycle of reduction and charge transfer between FAD, two catalytic cysteines and oxidized trypanothione (TS₂) starts at the active site of the oxidoreductase, from where trypanothione is released in the reduced state⁸⁶. The molecular events that characterize TR's mechanism will be further discussed in the following dedicated sections.

The enzymatic system linking T(SH)₂ to the oxidant species reduction step consists of two protein partners, namely TXN, a thiol disulfide oxidoreductase, and TXNPx, a 2-cysteines (2-cys) peroxiredoxin, which are analogues of thioredoxin and thioredoxin peroxidase, respectively ⁸⁵. In trypanosomatids two isoforms of TXN exist, namely TXN-1 and TXN-2, sharing the same genetic *locus* but endowed with different biochemical and biological properties, and cellular localization (TXN-1 is cytosolic while TXN-2 is mitochondrial) ^{85,87}; tryparedoxins show a WCPPC motif at their catalytic center replacing the WCG/APG motifs found in thioredoxins ⁸⁷ and their role is to provide reducing power to TXNPx, as a consequence of T(SH)₂ reduction. TXNPx is a typical 2-cys peroxiredoxin and forms an obligate homodimer, whose active sites are constituted by the N-proximal peroxidatic cysteine (C_p) from one subunit and a C-proximal resolving cysteine from the other (C_r) ^{87,88}. TXN and TXNPx partake in two distinct reactions. The first takes place upon the formation of a disulfide bridge between the N-terminal Cys40 of TXN and C_r of TXNPx, following the resolution of the intersubunit disulfide bridge (C_p-C_r) ^{87,89}. This inter-protein disulfide bond subsequently undergoes nucleophilic attack by the second cysteine of TXN, in order to leave TXNPx C_r as a thiol or thiolate. TXN returns to the oxidized state to be recharged by T(SH)₂. In the second reaction, the C_p thiolate is oxidized by a peroxide to sulfenic acid that can react with the C_r, reforming the TXNPx intermolecular disulfide bridge; the cycle can then restart.

In addition to oxidative stress defense, fundamental for parasites survival, T(SH)₂ exerts other cellular functions. T(SH)₂ has a role in protein folding because of its reactivity towards disulfide bonds, with effects on protein signaling and transport/secretion; can also act as a scavenger for metals and drugs, tagging molecules (thiol-conjugates) to be exported or sequestered, in

detoxification pathways related to multi-drug resistance (MDR)⁹⁰. The couple T(SH)₂/TXN delivers reducing equivalents also for the parasite synthesis of deoxyribonucleotides; *T. brucei* possesses a typical eukaryotic class I ribonucleotide reductase whose K_m for TXN is 3.7 μM^{90,91}. At high T(SH)₂ levels, the parasite ribonucleotide reductase is directly reduced by the dithiol, with a K_m of 2.1 mM. The TXN-mediated ribonucleotide reductase activity is lowered by more than 60% when 0.1 mM TS₂ is added to an assay containing 1 mM T(SH)₂^{90,91}. The regulation of TXN by the thiol/disulfide ratio of trypanothione represents a control mechanism that links DNA synthesis with the redox state of the cell. The effect is comparable with that observed for the GSH/glutaredoxin system in *E. coli*⁹⁰. Moreover, T(SH)₂ is able to reduce dehydroascorbate ensuring an additional mechanism of defense against hydrogen peroxide⁹⁰. T(SH)₂ ability of undergoing spontaneous reactions (as in the case of ribonucleotide reductase and dehydroascorbate reductions), is notably higher than GSH but does not reside in the difference in redox potentials ($E_{0\ T(SH)_2} = -242\text{ mV}$; $E_{0\ GSH} = -230/250\text{ mV}$), which are rather similar instead. Being T(SH)₂ a dithiol, it is kinetically favoured as disulfide reductant⁹²; moreover, its pK value coincides with the intracellular pH of the parasites (pK_{T(SH)₂} = 7.4), as a consequence of the positively charged nitrogen atom in the Spd moiety, contrarily to GSH pK, ranging from 8.7 to 9.2, with an impact on its reactivity.

In conclusion, it appears clear how the trypanothione metabolism represents a crucial survival pathway in Trypanosomatids. Several cellular events are governed by T(SH)₂; among them, oxidative stress resistance is a first-line defense for parasites against host immune system, which intensely relies on oxidative-species-induced immune protection. Being essential and unique, trypanothione metabolism represents, simultaneously, also a weakness for

Trypanosomatids, as all related enzymes are considered valid candidates for drug development ⁸⁶. Trypanothione reductase (TR), the enzyme directly responsible for keeping trypanothione in the reduced state, has been extensively studied since it fulfills most of the requirements for a good drug target. TR has been validated as a target in both *Leishmania* and *Trypanosoma* species as it is not possible to obtain TR-knockout mutants while expression downregulation causes strong impairment in infectivity ^{86,93,94}. It has also been demonstrated that antimonials interfere with the trypanothione metabolism by inhibiting TR ^{86,95,96}, supporting the idea that targeting this protein is a concrete option for the treatment of trypanosomatidal diseases. Moreover, the high sequence homology of TRs from different species (80-100%) makes it a valuable target for developing a single, broad spectrum drug active against all Trypanosomatids ^{71,86}. The main limitation of TR as a drug target lies in its high efficiency/turnover rate: it is demonstrated that, in order to reach a significant effect over parasite redox state and viability, TR activity must be reduced by at least 90%; consequently only potent inhibitors, with submicromolar affinity, can be considered promising compounds ^{86,93,94}. Many efforts have been made so far to discover new effective hits through *in vitro* and *in silico* screening, in addition to the development of known scaffolds via SAR or structure-based design approaches ⁸⁶, so that several classes of active compounds have been proposed to date. Next sections will discuss TR relevance in the trypanothione metabolism, focusing on its structural insights and the inhibitors so far characterized, in order to offer a comprehensive understanding of its role.

1.3. The drug target: trypanothione reductase

1.3.1. Trypanothione reductase, from structure to function

TR is a NADPH-dependent homodimeric flavo-oxidoreductase (EC 1.8.1.12), enclosing a 2cys-based active site: a “catalytic” cysteine, responsible for the nucleophilic attack on the oxidized substrate, and a “resolving” cysteine, able to attack mixed disulfide intermediates, formed during the oxidoreduction reaction. TR’s structure is thoroughly characterized since the X-ray crystal structure has been solved for several trypanosomatid species (*Crithidia* (*C. fasciculata*, *L. infantum*, *T. brucei* and *T. cruzi*) also in complex with natural substrates and inhibitors⁸⁶. Being TR a homodimer, each of the two subunits, related by a two-fold symmetry, comprises a FAD-binding domain (residues 1-160 and 289-360, *T. brucei* numbering), a NADPH-binding domain (residues 161-288), and an interface domain (residues 361-488; Figure 17A/B). The structure is almost identical for all the characterized species, in accordance with the high degree of sequence similarity (Figure 18). Indeed, TRs from all *Trypanosomatidae* share at least 67% of primary sequence, with >82% identity among *Leishmania spp.* and >80% among *Trypanosoma spp.* Similarity reaches 100% for residues shaping both substrates’ binding sites, proving that the binding mode for ligands is the same in all TRs characterized to date⁸⁶. NADPH and TS₂ bind different cavities facing opposite sides of the isoalloxazine ring of FAD; the TS₂ site, located at the interface between the two subunits, is shaped by residues belonging to both subunits (differentiated with ’ in the enumeration).

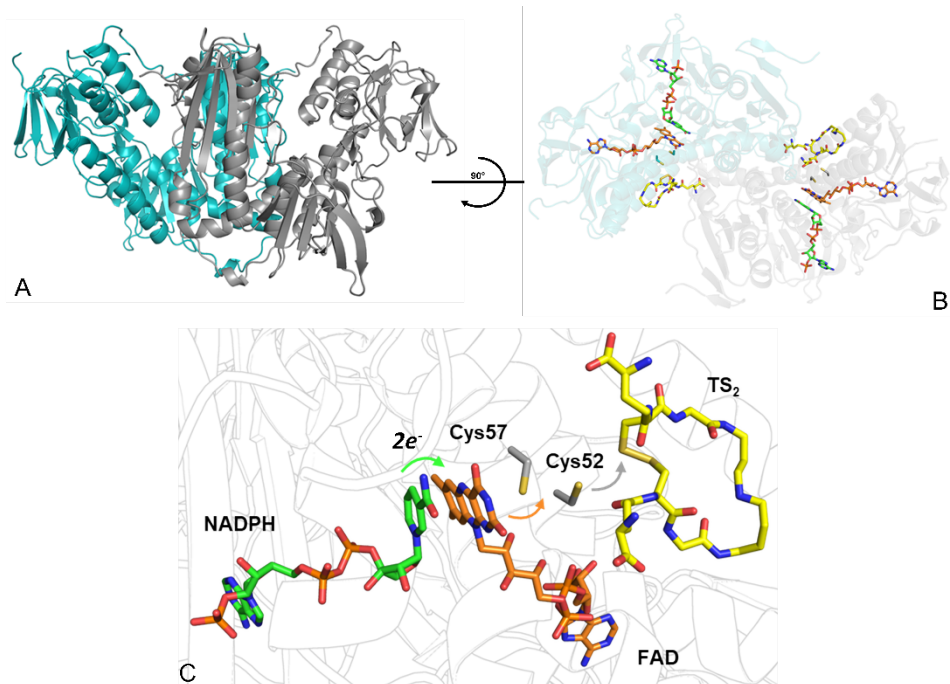


Figure 17. Trypanothione reductase: A) Overall structure; B) 90° projection, substrates are represented as sticks; C) Blow-up of the active site: the electron transfer is directed from NADPH (in green) to the oxidized trypanothione (in yellow), via FAD (in orange) and the couple Cys52/Cys57 (gray).

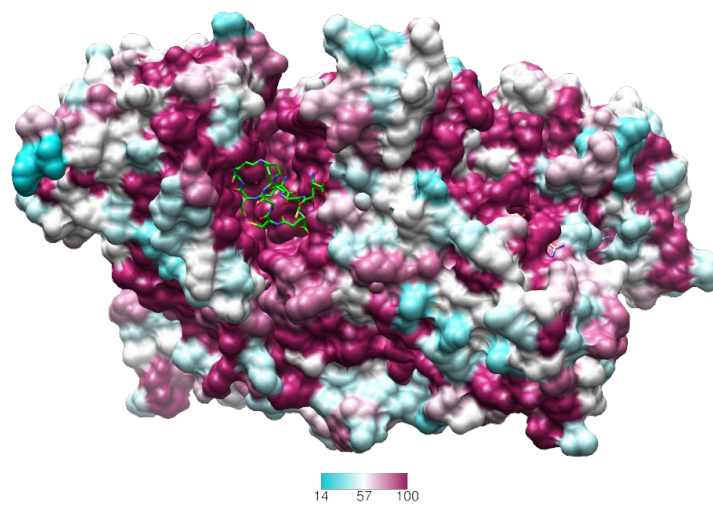


Figure 18. TR from *T. brucei* is colored according to the aminoacids similarity percentage with TRs from other sources: *C. fasciculata*, *T. cruzi*, *T. congolense*, *T. brucei*, *L. braziliensis*, *congolense*, *T. brucei*, *L. braziliensis*, *L. major*, *L. infantum*.

The cyclic mechanism relies on the initial transfer of two electrons from NADPH to the FAD cofactor, which reduces the disulfide bridge between the active site cysteines, Cys52 and Cys57. The oxidized TS₂ binds to the protein, and the catalytic Cys52, deprotonated by the couple His461'-Glu466', attacks the disulfide bridge of the substrate, resulting in the formation of a mixed disulfide. Finally, Cys57 resolves the Cys52-TS₂ bond and reduced T(SH)₂ is released from the active site, while the cysteines come back to the oxidized state, ready for a new cycle. During catalysis, no major structural changes occur, apart from those strictly necessary side chains displacements in the involved residues ⁸⁶.

T(SH)₂ assumes variable conformations in the cavity, as an effect of the “dynamics” of its binding. Accordingly, T(SH)₂ enters as a disulfide but, upon reduction, it is released in an extended conformation. Despite this variability, some interactions emerge to be particularly relevant and specific for binding: Glu18, together with other acidic residues, accounts for the positive charge of the substrate, while the almost hydrophobic patch including Trp21, Tyr110, and Met113 mediates the interaction with the polyamine moiety contained in trypanothione ⁸⁶.

Selectivity over off-targets is a fundamental issue to be taken into account, in order to increase specificity and avoid side effects. GR is the closest human homolog of TR, sharing the same overall fold, with 38% sequence identity, and catalyzing the same reaction on very similar substrates. Both GR and TR reduce a disulfide bridge that is intermolecular for GR (GSSG → 2GSH) and intramolecular for TR (TS₂ → T(SH)₂). The most significant differences between the two enzymes reflect the differences between their cognate substrates: TS₂ is bulkier than GSSG, positively charged due to the spermidine

moiety, which confers at the same time a distinctive hydrophobic character, while GSH bears an exact negative charge, at physiological pH. Therefore, the TS₂ binding site in TR is wider and negatively charged with respect to the GSSG binding site in GR. Precisely, selective interactions take place between the spermidine moiety and residues Glu18, Trp21, Ser109, Tyr110 and Met114 which are not conserved in GR and/or are partially replaced by arginine residues (Arg37, Arg38, and Arg347).

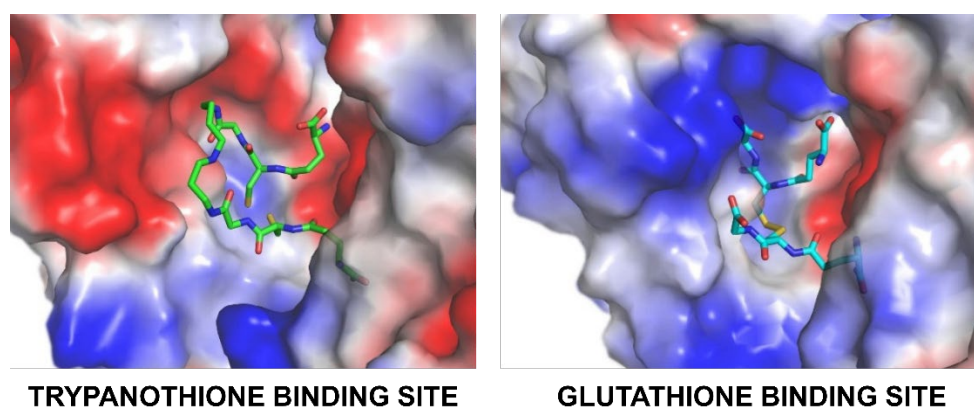


Figure 19. Steric and electrostatic differences between T(SH)₂ binding site and the GSSG binding site.

These steric and electrostatic features (Figure 19) account for the selectivity for substrates and emphasize the potential to generate parasite-specific compounds.

1.3.2. Trypanothione reductase inhibitors

Over the past two decades, structural studies on TR deeply improved the understanding in the molecular recognition of ligands, allowing to identify hot spots for interaction with substrates and inhibitors. This knowledge has been exploited through structure-based design approaches which, in some cases,

have led to a significant improvement in the performances of lead molecules^{86,97-99}. To date, the crystallographic structure of TR in complex with 20 different inhibitors has been solved, revealing 3 major inhibition strategies:

- (i) competition with trypanothione, due to displacement of the substrate at from its binding site, comprising most of the characterized inhibitors;
- (ii) competition with NADPH, similarly to the previous case;
- (iii) redox cysteines inactivation, exerted by molecules able to establish a metal bond with Cys52 and Cys57 in the catalytic site⁸⁶.

A fourth has been recently proposed¹⁰⁰, based on the disassembly of the TR dimer induced by small molecules specifically designed to interfere with protein–protein interaction; however, poor structural information are available so far.

Inhibitors targeting the TS₂ binding cavity

As previously highlighted, TR presents a broad active site, suited to accommodate the voluminous TS₂ substrate. The largest part of the characterized inhibitors bind there, mainly in the so-called “mepacrine binding site” (MBS), a hydrophobic patch located at the entrance of the cavity. Fewer penetrate deeper, closer to the real catalytic site, where the redox cysteines reside and TS₂ reduction takes place.

Mepacrine binding site (MBS)

Mepacrine (or quinacrine) is a notorious antiprotozoal compound, extensively used as antimalarial agent during World War II¹⁰¹. In 1996, Jacoby and coworkers described the crystal structure of *T. cruzi* TR (TcTR) in complex with mepacrine (coordinates not available in the PDB) showing the ligand,

known to be a competitive inhibitor of TS₂, bound at the entrance of the active site^{86,102}. About 20 years later, a detailed description has been provided by Saravanamuthu and collaborators, by solving the crystal structure of TcTR in presence of an alkylating mepacrine derivative (PDB code: 1GXF)¹⁰³. The interaction is governed by 4 key residues, namely Trp21, Met113, Tyr110, and Glu18. Two inhibitor molecules bind in a synergistic fashion as stacking of the planar acridine rings increase the number of binding interactions. Particularly, the aromatic acridine ring of the first mepacrine molecule stacks over Trp21 and is lined by Met113, with the alkylamino chain, kept in position by Glu18, pointing towards the active site, and covalently binding to Cys52 (*T. brucei* numbering); the second acridine is lined by Tyr110 instead. The residues that shape the MBS are involved for TS₂ binding and are not conserved in GR; additionally, mepacrine does not affect human GR.

3,4-dihydroquinazoline derivatives also proved to be able to bind to the MBS⁹⁸, surprisingly inducing the formation of a new subpocket, as a consequence of the displacement of Met113 side chain (PDB code: 2WP5, 2WP6, 2WPC, 2WPE, 2WPF). Herein, the C4-phenyl substituent of the scaffold accommodates. Structural information was subsequently used to design additional inhibitors, including analogues that challenged the induced subpocket leading to the identification of inhibitors with improved potency, among which the best performing showed a 30-fold lower IC₅₀ for *T. brucei* TR (TbTR) with respect to the starting compound, although selectivity remained an issue^{86,98}.

Similarly to mepacrine derivatives, also diarylpyrroles are able to inhibit TR, as displayed in the structure of *L. infantum* TR cocrystallized with a diarylpyrrole derivative (LiTR, PDB code: 4APN)¹⁰⁴. The structure shows that

two molecules of the inhibitor are present at the MBS, without inducing any structural variation (differently from 3,4-dihydroquinazoline derivatives); the compound assumes multiple conformations, due to its intrinsic flexibility and to the absence of stabilizing stacking interactions. Overall, it is a remarkable feature for MBS to be prone to be engaged by diverse unrelated scaffolds.

To date, the most studied class of compounds for structure-based development is 1-(1-(benzo[b]thiophen-2-yl)cyclohexyl)piperidine (BTCP) derivatives. The lead BTCP was initially identified by HTS, together with other tricycles¹⁰⁵; it acts as a competitive inhibitor of TbTR, and is endowed with a considerable activity on *T. brucei* cultures. It was considered to be a promising screening hit for development of new lead compounds because of several drug-like properties such as low molecular weight, lack of activity on GR and capability of crossing the BBB (a crucial requirement for second stage HAT treatment) even though a poor selectivity against mammalian cells was demonstrated¹⁰⁶. Eberle and collaborators proposed the Z-site, a poorly characterized hydrophobic cleft positioned in front of the MBS, as binding site for BTCP¹⁰⁷. Despite that, the co-crystal structure of both TbTR and TcTR with compound 10a, a BTCP analogue in which a thiazole is inserted between the indole and cyclohexyl rings, definitely circumscribed the MBS as the binding site (PDB code: 4NEV, 4NEW). Two key interactions represent the driving force of the interaction namely the protonated tertiary amine of the ligand, which establish a coulombic interaction with Glu18, and the indole moiety, which binds to the hydrophobic wall of MBS (Trp21, Tyr110, Met113), even if the orientation differs between the two structures⁹⁹.

In order to improve properties, particularly water solubility, and potency new BTCP series were synthesized and explored^{97,108}. At first, even though results

in terms of efficacy were not satisfactory, useful structural information emerged ¹⁰⁸. In fact, co-crystal structures of 2 new ligands (18 and 19) confirmed the previously observed binding mode, with the indolylthiazole core adopting identical orientation, and the newly introduced water-solubility-providing substituents oriented toward the periphery of the active site (PDB code: 6BTL, 6BU7) ^{86,108}.

A significant enhancement of potency and selectivity is obtained with compound (+)-2, able to inhibit TbTR with a K_i of 73 nM and fully ineffective against human GR thus claimed to be the most effective non-covalent inhibitor of TR ever reported (although endowed with a relatively high toxicity against mammalian cells) ⁹⁷. Two major chemical modifications led to this result: the addition of the 2-ethylpyrrolidinic substituent on the indole moiety, combined with the introduction onto position 4 of the central thiazole moiety of a propargylic substituent, designed to target a hydrophobic sub-pocket near the catalytic cysteines in the TR active site ⁹⁷. The X-ray crystal structure of (+)-2-TR complex (PDB code: 6OEZ) shows that the indole protonated substituent adds an electrostatic interaction in MBS involving Asp116, while the propargylic moiety, although mobile, locates deeper into the cavity.

Catalytic site

Other compounds have shown affinity towards the innermost portion of the active site. Recently, screening of an in-house collection detected a novel class of diarylsulfides active on *Leishmania* cultures and TR ¹⁰⁹; among them, compound RDS777 (6-(sec-butoxy)-2-((3-chlorophenyl)thio)pyrimidin-4-amine) was found to inhibit TR with high efficiency ($K_i = 0.25 \mu\text{M}$) by competing with TS₂, and to affect parasite growth in the micromolar range ($\text{IC}_{50} = 29 \mu\text{M}$) ^{86,109}. The X-ray crystal structure of RDS777-LiTR complex

(PDB code: 5EBK) revealed the presence of 4 inhibitor molecules, one of which lays at the bottom of TS₂ cavity, engaging hydrogen bonds with catalytic residues, namely Glu466', Cys57 and Cys52. A second molecule is placed closer to the entrance, involved in a stacking interaction with the previous one. The additional two molecules interact with the NADPH-binding site and are discussed later. Based on the structural information, a new series of derivatives have been synthesized, one of which has a higher activity on parasitic cultures (IC₅₀ = 11 μM), is able to decrease the reduced T(SH)₂ concentration in cell but is less effective on TR (K_i = 12 μM). Docking studies suggest that it prefers the second outermost binding site, indicating that it likely has other intracellular targets besides TR. Other diarylsulfides have been previously proposed and predicted to bind at the MBP and Z-site, differently from RDS777¹¹⁰; in conclusion, it must be considered that bonding is plausibly influenced more by the nature of the aryl substituents than by the thioether itself.

Metal inhibitors

As previously described, metal-based drugs, such as antimonials, are currently used in trypanosomatid infections treatment, despite severe side effects and resistance phenomena. It is known that these drugs, at least in part, act on TR by seizing catalytic cysteines. Baiocco et al. demonstrated that Sb(III) efficiently inhibits reduced TR (K_i = 1.5 μM) by forming a stable complex with the catalytic residues, namely Cys52, Cys57, His461' and Thr335 (PDB code: 2W0H)¹¹¹. Together with antimony, silver and gold were proven to be even more efficient with K_i down to 20 nM¹¹²⁻¹¹⁴. Particularly interesting is the case of auranofin, a gold-containing drug used to treat rheumatoid arthritis, 10-fold more potent than Sb on TR (K_i = 0.15 μM) and active *via* a double mechanism

of action. In addition to the expected gold complexation, the thiosugar moiety of auranofin contributes to inhibition by binding the inner region of TS₂ site (PDB code: 2YAU). Comprehensively, this finding embodies the opportunity to combine metal-free scaffolds capable of binding the outer TS₂ cavity with metal-coordinating moieties to exploit a double inhibition mechanism, promoting a selective targeting of otherwise poorly specific metal inhibitors.

Inhibitors targeting NADPH binding site

NADPH-binding cavity is reasonably considered less appealing for specific TR inhibitors development, due to the ubiquitous role of this cofactor actually involved in a number of pathways in all organisms. Nevertheless, a couple of TR inhibitors have been found to bind to this site. As anticipated, diarylsulfide RDS777 binds the NADPH-binding site, in addition to the catalytic one, at the entrance where the adenosine moiety of NADPH usually settles¹⁰⁹. In contrast to the structural data, kinetic characterization denied competition for the cofactor, so it can be hypothesized that binding is weak or due to crystallographic artifact⁸⁶.

Interestingly a new hit compound (“compound 3”) targeting the NADPH-binding site was identified by HTS on LiTR, in 2018¹¹⁵. The inhibitor is not particularly potent (IC₅₀ = 7.5 μM) but shows attractive characteristics. Indeed, it competes for NADPH but is inactive on both human GR and TrxR and is endowed with dose-dependent anti-proliferative activity *L. infantum* promastigotes at micromolar concentration (IC₅₀ = 12.4 μM). Crystallographic analysis of the complex (PDB code: 6ER5) revealed that the compound binds at the entrance of NADPH site, similarly to RDS777, but in a cleft not conserved in human GR. Even if cytotoxicity data are not available and the compound could be active on other NADPH-dependent human enzymes, it

represents the first proof of the existence of a druggable site in NADPH cavity

86.

Site	Scaffold	PDB code	Source	Potency (μM)	Ref
MBS	Acridine	N.A.	Tc	K _i : 25	92
		1GXF	Tb	Irreversible	93
	3,4-dihydroquinazoline	2WP5	Tb	IC ₅₀ : 6.8	88
		2WP6	Tb	IC ₅₀ : 0.93	
		2WPC	Tb	IC ₅₀ : 0.42	
		2WPE	Tb	IC ₅₀ : 0.86	
		2WPF	Tb	IC ₅₀ : 0.23	
		4NEV	Tb	K _i : 12	
	4NEW	Tc	K _i : 4	89	
	BTCP	6BTL	Tb	K _i : 3.8	98
		6BU7	Tb	K _i : 6.4	
		6OEZ	Tb	K _i : 0.73	
	Diarylpyrrole	4APN	Li	K _i : 4.6	94
	Pyrrolopyrimidine	6I7N	Li	IC ₅₀ : 52.2	90
	Catalytic site	Diarylsulfide	5EBK	Li	K _i : 0.25
Catalytic site/ Cysteines	Metal/Thiosugar	2YAU	Li	K _i : 0.15	103
Cysteines	Metal	2W0H	Li	K _i (SbIII): 1.5	85
		2X50	Li	K _i (AgI): 0.5 K _i (Ag0): 0.05	102
NADPH cavity	3-amino-1-arylpropan-1-one	6ER5	Li	IC ₅₀ : 12.4	105

Table 4. Crystallized TR-inhibitor complexes, available in the PDB so far.

The pivotal role of TR distinctly emerges on two different but related levels. TR plays a crucial part for parasite survival, being the pillar of the trypanothione metabolism and actively involved in host immune response resistance. On the other hand, its uniqueness, specificity and conservation among species set the basis for antitrypanosomatidal drug discovery, as supported by the efforts made so far in the identification of new active scaffolds and their structural characterization.

2. AIM OF THE STUDY

The line of research of this work is to pursue the identification of novel compounds endowed with inhibitory activity towards the trypanosomatidal NADPH-dependent flavoenzyme trypanothione reductase, whose role is to maintain the redox metabolism of Trypanosomatids balanced.

Trypanosomatids are causative agents of a series of vector-borne neglected diseases as leishmaniasis, Chagas disease and human African trypanosomiases, affecting millions of people worldwide and leading to death more than 100'000 humans per year, comprehensively. TR is an ideal drug target, being a unique and essential enzyme, exclusively present in the parasitic family of *Trypanosomatidae* and absent in mammals. TR is highly conserved in all the trypanosomatidal species (66-100% sequence identity; 80-100% sequence homology), and selectivity over the human homologous glutathione reductase (34-37% sequence identity; 51-54% sequence homology) can be achieved on the basis of the sequence diversity and the different dimension and charge of the active site.

Thus far, vaccines are unavailable while a limited number of drugs are accessible for the treatment of these life-threatening conditions; all of these display an insufficient efficacy, poor safety and inadequate pharmacokinetic profiles ⁷¹. In this framework our research drops in, aiming at discovering family-specific, rather than species-specific, novel compounds, by targeting TR. *Via* both a high-throughput and a rational design approach, together with the use of biophysical assays and especially of X-ray crystallography, new active molecules are identified, paving the way for the design and synthesis of new potent broad spectrum inhibitors, effective over the different parasitic trypanosomatidal species.

In collaboration with the pharmaceutical company IRBM (Pomezia, Rome) an HTS assay has been set up: 3097 compounds were assayed against TbTR and a novel hit series of spiro-containing derivatives has been identified. Among these, Compound 1 activity has been validated through SPR and demonstrated activity against LiTR also, while the solution of the crystal structure in complex with TbTR revealed the structural basis of inhibition. Additionally, antiparasitic power of Compound 1 was evaluated against *T. brucei* *in vitro* culture.

Contemporarily, starting from LeishBox, a 192-molecule set of best antileishmanial compounds identified by GlaxoSmithKline (GSK) HTS (based on 1.8 million compounds, which were used to build up also a HATBox and a ChagasBox)¹¹⁶, specific competitive inhibitors of LiTR have been identified through SPR and kinetic experiments. Structural information was obtained *via* docking predictions; only recently we could build a preliminary model of the crystal structure of compound A1/7 in complex with TbTR thus obtaining additional structural details, which confirmed the mechanism of inhibition. Interestingly, compound A1/7 is contained in all GSK boxes, so it has been used, in collaboration with the medicinal chemistry group of Prof. Giuseppe Campiani (University of Siena, Italy), to rationally generate derivatives, which are being tested, in order to yield a single inhibitor for TR from all sources.

Additionally, preliminary crystallographic studies have been conducted on TbTR, as an FBS is programmed in the near future at the XCHEM-Fragment Screening platform, at Diamond Light Source (Didcot, UK): specific growth conditions for reproducible, DMSO-resistant, high resolution-diffracting crystals have been settled.

3. RESULTS AND DISCUSSION

3.1. HTS approach: identification of spiro-containing derivatives

3.1.1. HTS assay optimization

The TbTR enzyme, expressed in *E. coli*, was purified as described in Materials and Methods (Figure 20A) and used to develop an *in vitro* enzyme assay. In order to measure TbTR activity, a luminescent assay was optimized starting from a design previously described¹¹⁵. At first, the linearity range of NADPH detection signal via NADPH-Glo kit was determined, resulting to be 50 μM (Figure 20B). The apparent K_m value for TS₂ was calculated using 1 nM TbTR in presence of serial dilutions of TS₂ and a fixed concentration of 40 μM NADPH. The luminescence signal was detected in the first 10 min of reaction. NADPH depletion, calculated using the NADPH standard curve, allowed the determination of the apparent K_m values by the Michaelis-Menten kinetic (Figure 20C). The K_m for TS₂ was calculated to be $4.0 \pm 0.7 \mu\text{M}$. To further optimize the assay, a time course experiment was carried out. Different concentrations of the TbTR enzyme, ranging from 0.025 to 0.2 nM, were used, while the TS₂ concentration was fixed near the K_m value (5 μM) and the NADPH concentration was 20 μM , falling within the linearity range observed for the NADPH standard curve. 0.1 nM TbTR and 60 min of incubation were judged to be an optimal compromise for preserving the reaction linearity along with a good S/B ratio (Fig 20D), allowing a suitable time for the screening operations. The final conditions used for the screening were: 0.1 nM TbTR, 5 μM TS₂, 20 μM NADPH with an incubation time of reaction of 60 minutes.

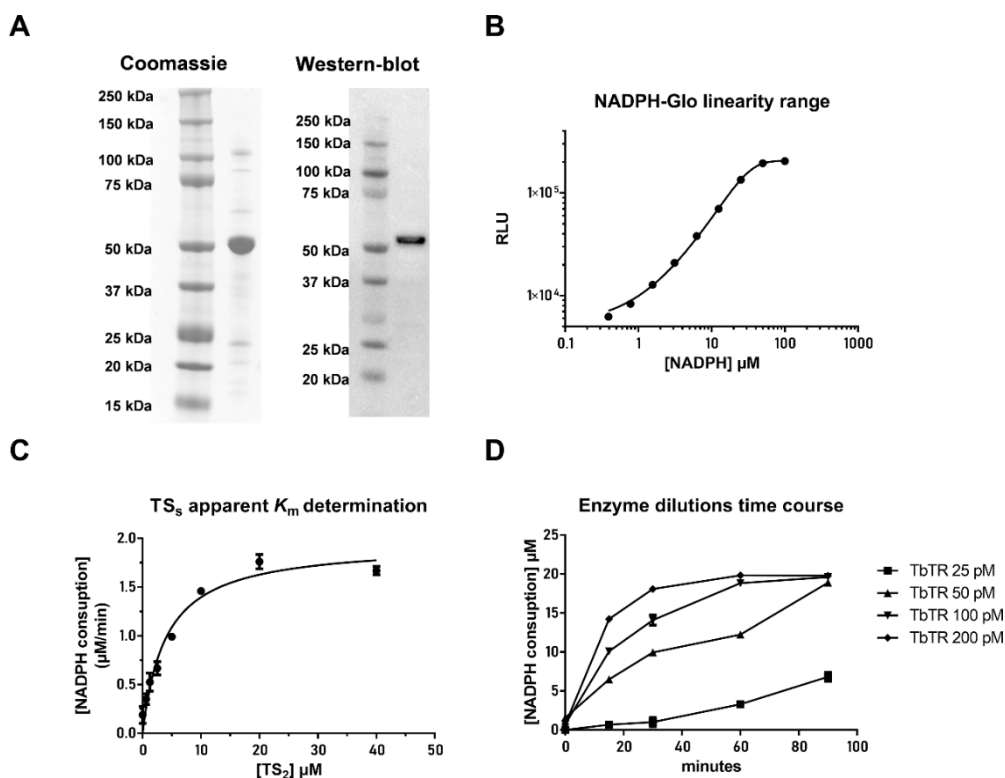


Figure 20. A) Purification of recombinant TbTR (MW= 54 KDa). A western blot analysis with an anti-His tag antibody has been performed to confirm protein identity; B) Sensitivity and linearity of NADPH detection using the NADPH-Glo detection kit; (C) Determination of the TS₂ apparent K_m at 1 nM TbTR and 40 μM NADPH; (D) Time course and TbTR titration using TS₂ and NADPH at fixed concentrations of 10 μM and 20 μM , respectively. For all graphs, the plotted points are the average of three independent replicates.

3.1.2. Hit identification and confirmation

A collection of 3097 compounds present in our library and previously reported to be active in PubChem Trypanosomatid proliferation assays was screened at 10 μM using the protocol previously described. The Z' values were found to be greater than 0.5 for all screening plates indicating that the assay was sufficiently robust to be used to test the compounds (Figure 21). The distribution of the compound activities converges to normal distribution (or

Gaussian distribution) (Figure 21); therefore, compounds with an activity equal to or greater than the average activity plus three standard deviations were considered hit compounds. Eight compounds, namely 0.26% of the total, were identified as active in the primary screening and subjected to the confirmation assays. The design of the primary assay which produces a positive luciferase signal in the presence of an inhibitor meant that no luciferase inhibition counterscreen was necessary.

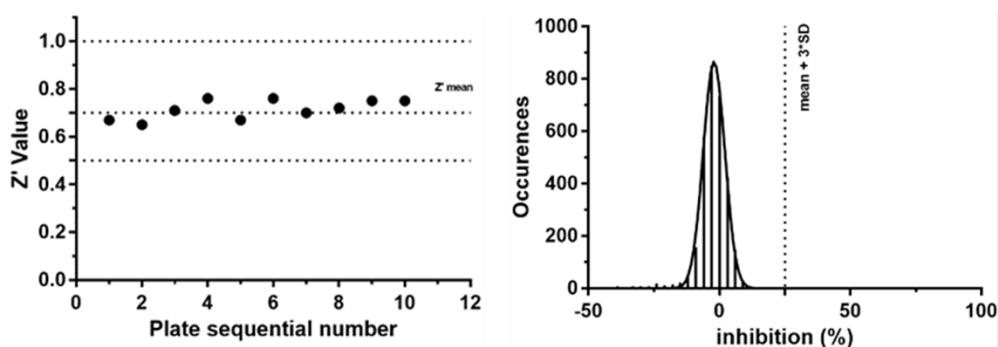


Figure 21. Screening result; Left panel) The Z' factors of all the 384-well plates are represented by solid dots. The dashed line indicates the Z' mean of 0.71; Right panel) Occurrence distribution of compound activity is plotted as Z-factor with respect to the whole sample average and standard deviation.

In order to confirm hit compounds, they were tested in a dose-response fashion starting from 85 μM in the TbTR luminescence assay. Four of eight compounds were confirmed to be TbTR inhibitors, with IC_{50} values ranging from 3 μM to 34 μM . Structural analysis of active compounds (reported in Table 5, at the end of this section) revealed the presence of a 1-phenyl-1,3,8-triazaspiro[4.5]decan-4-one moiety (Figure 22A) as a recurrent central core, in which the simultaneous substitution of central core by R and R' seems to be required for activity (Figure 22).

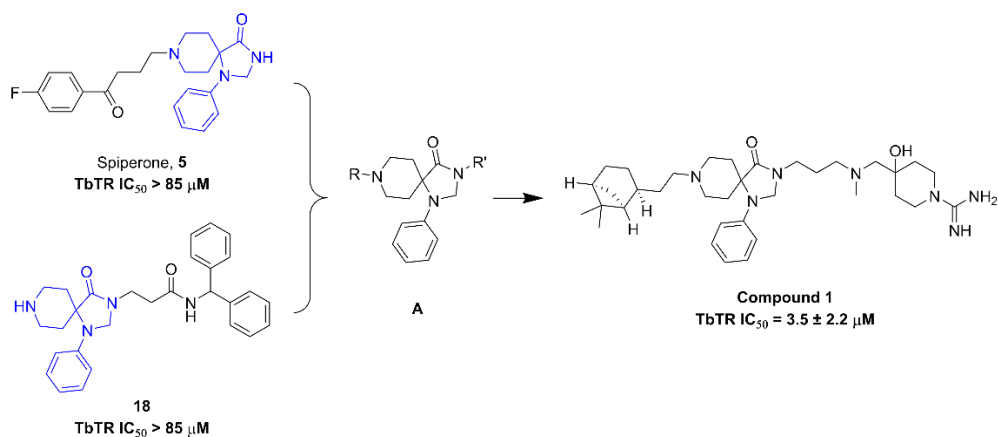
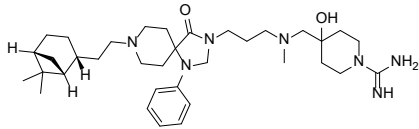
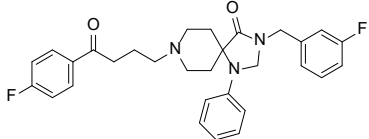
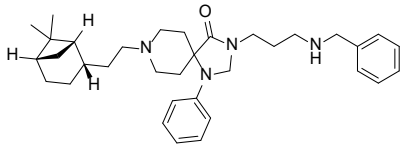
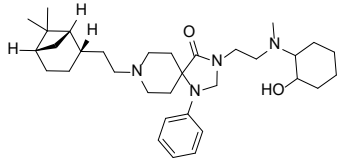
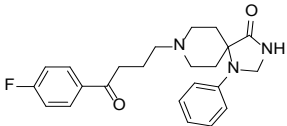
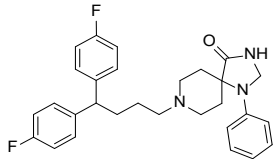
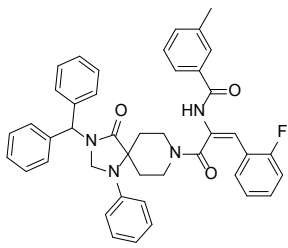
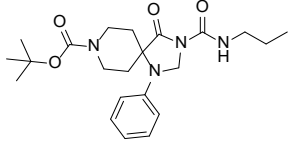
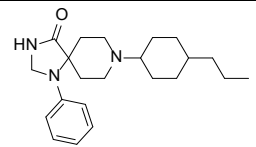
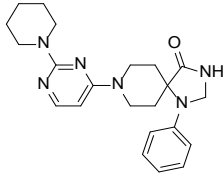
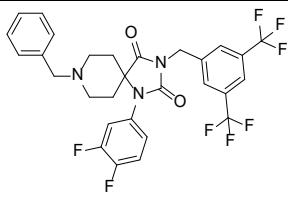
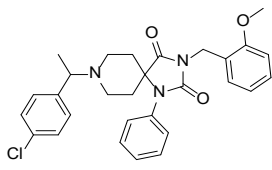
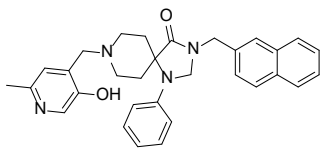


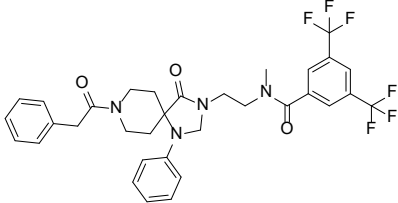
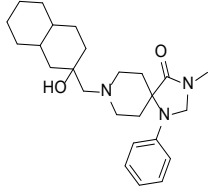
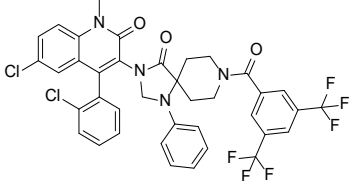
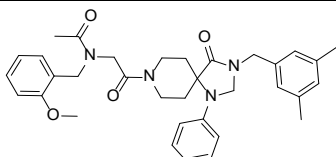
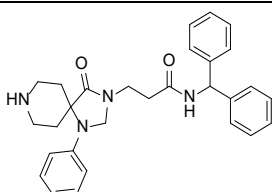
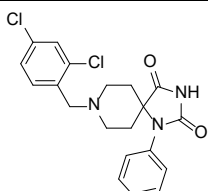
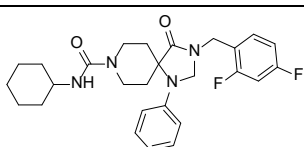
Figure 22. General structures of hit series and representative molecule with TR inhibition potency.

To further expand structure activity relationships (SAR) around the 4 hits, 22 structurally similar analogues from either the original screening set (potential false negatives) or CNCCS entire chemical collection were selected. The selection was performed based on structural similarity to the central core or closed analogues (visual inspection). Active hit compounds were also tested for confirmation in the standard DTNB absorbance assay as previously reported¹¹⁷. Further, to evaluate their specificity they were tested against the hGR as reported by Turcano and collaborators¹¹⁵, using glutathione as substrate. Results from this follow up are summarized in Table 5. Although this follow up did not lead improved activity, the confirmation of the hit compounds as micromolar inhibitors of TbTR in enzymatic assays, with high selectivity for the parasite (IC₅₀ values on hGR were uniformly above 50 μM) provided a level of comfort that the new compound series represents a *bona fide* class of TbTR inhibitors. Compound 1 (IUPAC nomenclature: 4-(((3-(8-(2-((1*S*,2*S*,5*S*)-6,6-dimethylbicyclo[3.1.1]heptan-2-yl)ethyl)-4-oxo-1-phenyl-1,3,8-triazaspiro[4.5]decan-3-yl)propyl)(methyl)amino)methyl)-4-

hydroxypiperidine-1-carboximidamide), was selected for further profiling studies based on its acceptable *in vitro* potency ($3.5 \pm 2.2 \mu\text{M}$) and on its high solubility ($185.1 \mu\text{M}$ in PBS buffer pH 7.4).

ID	Structure	TbTR	DTNB	hGR	MS [M+H] ⁺ Found
		assay IC ₅₀ (nM) n=4	assay IC ₅₀ (nM) n=4	assay IC ₅₀ (nM) n=2	
1		3501 ± 2187	966 ± 68	> 50000	608
2		20351 ± 4888	20364 ± 3098	> 50000	504
3		23270 ± 4884	16644 ± 3219	> 50000	529
4		34098 ± 4850	27337 ± 7866	> 50000	537
5		> 85000	--	--	395
6		> 85000	--	--	476

7		> 85000	--		679
8		>85000	--	--	417
9		> 85000	--	--	356
10		> 85000	--	--	393
11		> 85000	--	--	598
12		> 85000	--	--	505
13		> 85000	--	--	493

14		> 85000	--	--	647
15		> 85000	--	--	412
16		> 85000	--	--	774
17		> 85000	--	--	569
18		> 85000	--	--	469
19		> 85000	--	--	405
20		> 85000	--	--	483

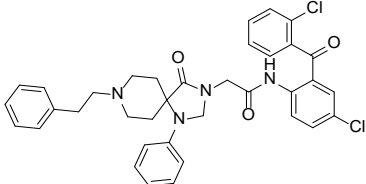
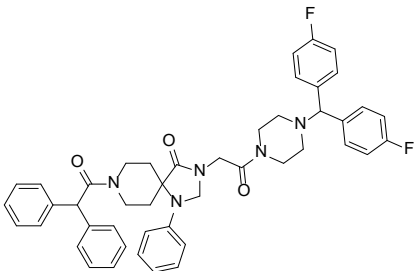
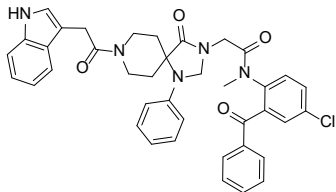
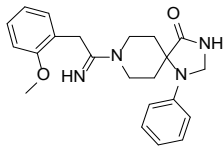
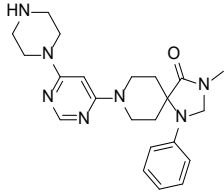
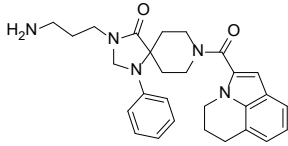
21		> 85000	--	--	642
22		> 85000	--	--	754
23		> 85000	--	--	675
24		> 85000	--	--	379
25		> 85000	--	--	407
26		> 85000	--	--	472

Table 5. Biological data for hits resulted from HTS and selected follow-up compounds.

3.1.3. Hit compound binding to TbTR

The binding between TbTR and Compound 1 was evaluated by SPR. To this purpose, TbTR was covalently immobilized at high density (c. 9,000 Δ RU) to a CM4 sensor chip, then the compound was injected over the surface at different concentrations ranging from 0.3125 to 20 μ M (Figure 23). The hit showed a reversible binding to the enzyme, but it was not possible to calculate the kinetic parameters (k_{on} and k_{off}) using a simple 1:1 Langmuir binding model. Thus, the kinetic parameters were calculated from the sensorgrams applying an heterogeneous ligand model¹¹⁸. The analysis suggested the presence of two binding sites with different affinities. For the higher affinity site, the apparent K_d resulted to be in the high micromolar range ($K_d = 10.3 \pm 2.9$ μ M, $k_{on} = 3.3 \pm 0.5$ 1/Ms, $k_{off} = 0.035 \pm 0.014$ 1/Ms). It was not possible to calculate reliable constants for the lower affinity site. Subsequently, the ability of hit Compound 1 to compete with the TS₂ substrate for TbTR was investigated. To this aim a serial dilution of TS₂ starting from 100 μ M, plus 20 μ M NADPH, was assayed in the TbTR enzyme in the presence of vehicle, 5 or 25 μ M Compound 1.

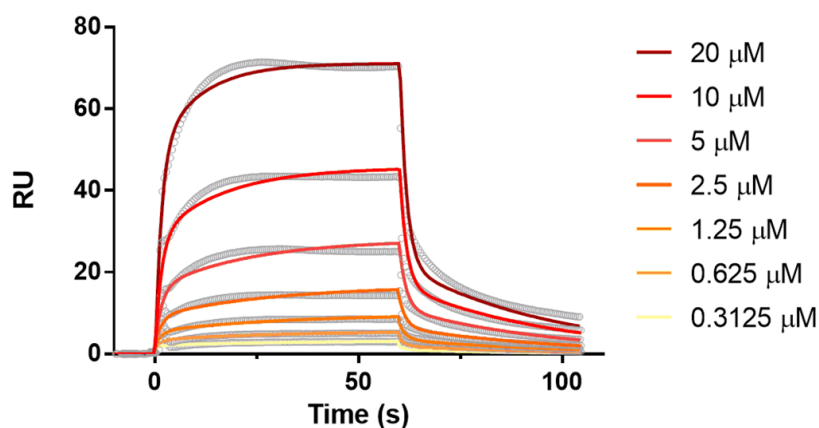


Figure 23. Compound 1 binding sensorgrams.

Compound 1 was found to be competitive with TS₂ (Figure 24) for TbTR with the apparent K_m of TS₂ shifting to the right with the increase of the inhibitor concentration. No changes in calculated V_{max} were observed.

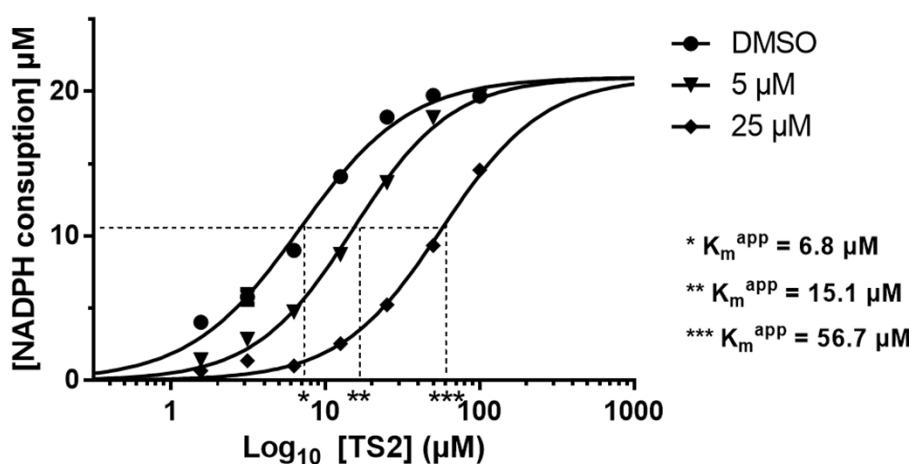


Figure 24. Competition assay of Compound 1 against TS₂. TS₂ was titrated against 1 nM TbTR in presence of vehicle (dots) or against two concentrations of Compound 1: 5 μM (triangles) and 25 μM (diamonds). The assay run for 10 minutes using 20 μM NADPH. Each experimental point is the average of three replicates.

In order to investigate the inhibitory power towards TR of other parasites, Compound 1 was tested against LiTR, in a kinetic assay previously published¹¹⁵. The IC₅₀ of Compound 1 resulted to be $3.8 \pm 0.6 \mu\text{M}$ (Figure 25), in line with the one on TbTR.

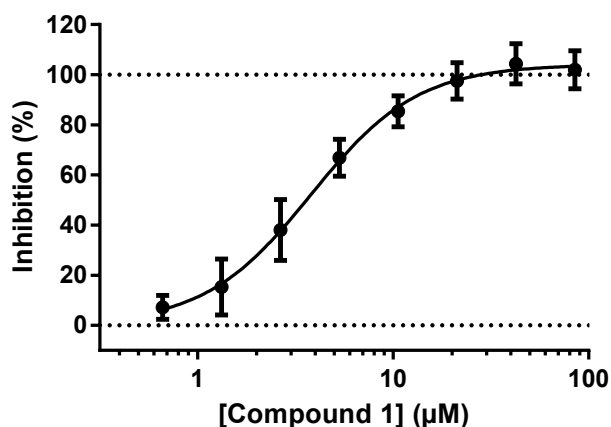


Figure 25. Inhibition of LiTR by Compound 1. Each experimental point is the average of three replicates.

3.1.4. Compound 1 activity in *Trypanosoma brucei* *in vitro* culture

To evaluate the ability of Compound 1 to inhibit endogenous TbTR activity, a titration experiment was performed. Different concentrations of Compound 1 were incubated with a lysate of *T. brucei*, supplemented with 50 μM of TS₂, 200 μM NADPH and 100 μM DTNB. The increased absorbance signal at 412 nm can be attributed to the increase in reduced thiols, a reasonable surrogate of the TbTR activity. Figure 26 shows that Compound 1 is active in a dose-response fashion, with an IC₅₀ value of $5.7 \pm 0.6 \mu\text{M}$.

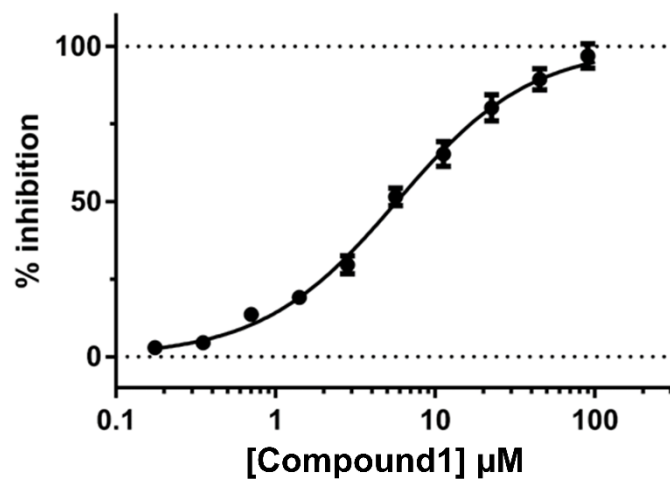


Figure 26. Inhibition of endogenous TbTR activity.

Additionally, the anti-proliferative activity of serial dilution of Compound 1 on a *T. brucei* culture, treated for 24 hours, resulted in an IC_{50} of $2.2 \pm 2.4 \mu\text{M}$ (Figure 27).

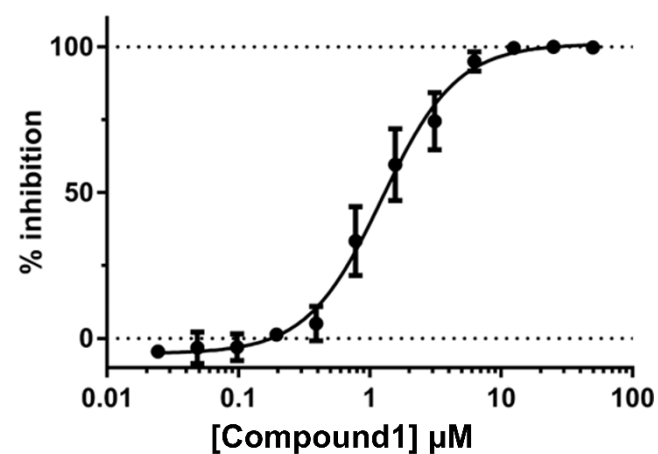


Figure 27. Effect of the hit inhibitory Compound 1 on *T. brucei* growth.

3.1.5. X-ray crystal structure of TR in complex with Compound 1

The structure of the complex between TbTR and Compound 1 (TR-1) was determined by X-ray crystallography at 1.98 Å resolution, allowing the identification of the binding sites and a detailed description of the interaction. Crystal parameters, data collection and refinement statistics are reported in Table 6.

Crystal parameters	
PDB code	6RB5
Space group	P2 ₁ 2 ₁ 2 ₁
Unit cell dimension (a,b,c) (Å)	63.1, 132.6, 161.0
Asymmetric unit composition (molecule, amount, modelled residue range)	TbTR, dimer (A:1-489, B:1-488) FAD, 2 Compound 1, 4 Sulfate ions, 9 Glycerol, 6 H ₂ O, 486
Wilson B-factor (Å ²)	31.5
Data analysis statistics	
Resolution range (highest resolution shell) (Å)	102.39-1.98 (2.01-1.98)
Unique reflections	94907 (4693)
Completeness (%)	99.7 (99.9)
Redundancy	5.5 (5.4)
Rmerge (%)	7.1 (78.6)
CC(1/2) (%)	99.9 (78.8)
$\langle I/\sigma(I) \rangle$	13.3 (1.1)
Model Refinement statistics	
Resolution range (highest resolution bin)	102.39-1.98 (2.03-1.98)

R_{crys} (%)	18.3 (28.1)
R_{free} (%)	20.6 (28.7)
rms (angles) ($^{\circ}$)	1.533
rms (bonds) (\AA)	0.009
Mean B value (\AA^2)	37.55
Residues in allowed region of Ramachandran plot / generously allowed (%)	100/2

Table 6 Crystal parameters, data analysis and refinement statistics for TR-1 complex.

TR-1 structure is similar to TbTR both in the apo and in the substrate-bound form (PDB CODE: 2WOI, 2WOW), thus indicating that Compound 1 binding does not induce global or local conformational variations. Inspection of electron density revealed two binding sites on each TbTR monomer, unequivocally attributed to Compound 1 (Figure 28).

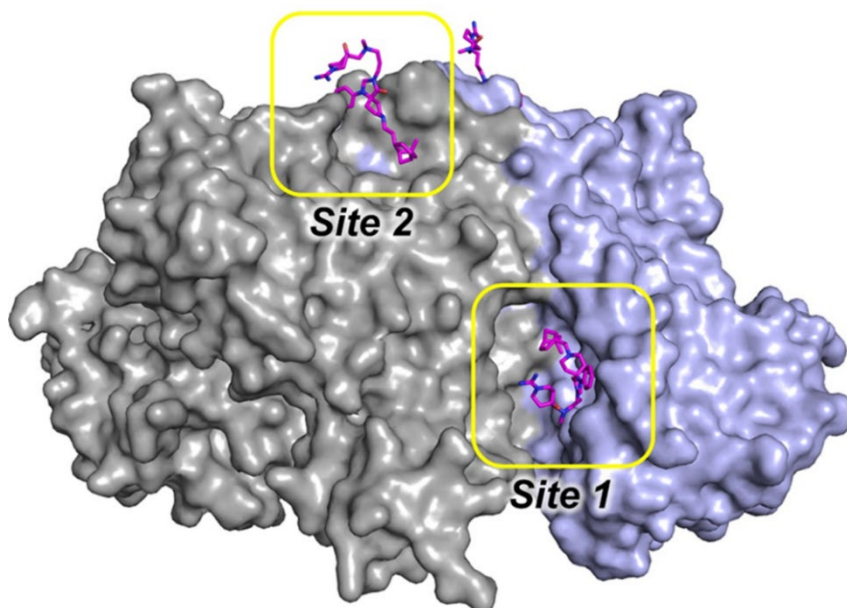


Figure 28. Overall fold of TR in complex with Compound 1. The accessible solvent areas of the two-fold symmetry related monomers are indicated in grey and blue respectively; the sites 1 and 2 are indicated by yellow boxes and Compound 1 is represented as magenta sticks.

Indeed, the peculiar shape of the spiro moiety, with two rings sharing a sp^3 carbon and therefore forced to lie on perpendicular planes, can be identified and modeled with high confidence in the electron density map (Figure 29).

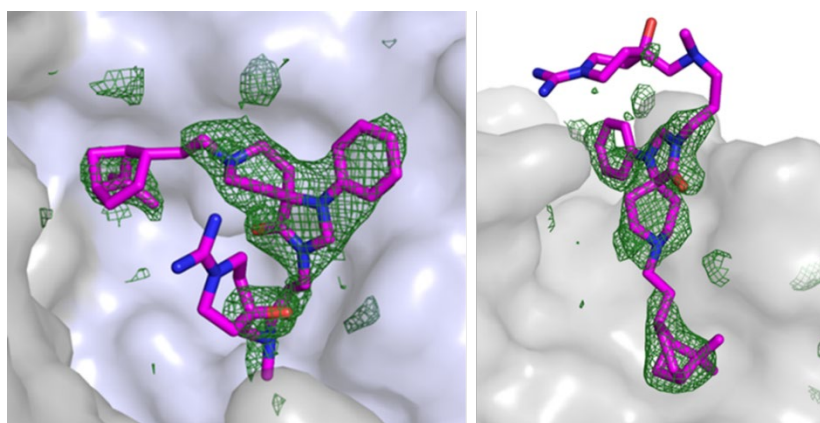


Figure 29. Electron density map of Compound 1 bound to site 1 (left) and site 2 (right).

The most significant of the two binding sites, indicated as site 1, is located inside the wide trypanothione binding cavity, where it partially overlaps with MBS. Binding is dominated by the hydrophobic interactions established by the central core of Compound 1 while the flexible arms of the molecule point towards the inside and outside of the cavity. The phenyl-triazaspiro scaffold of compound 1 fits well the hydrophobic/aromatic patch composed by Trp21, Met113 and Tyr110.

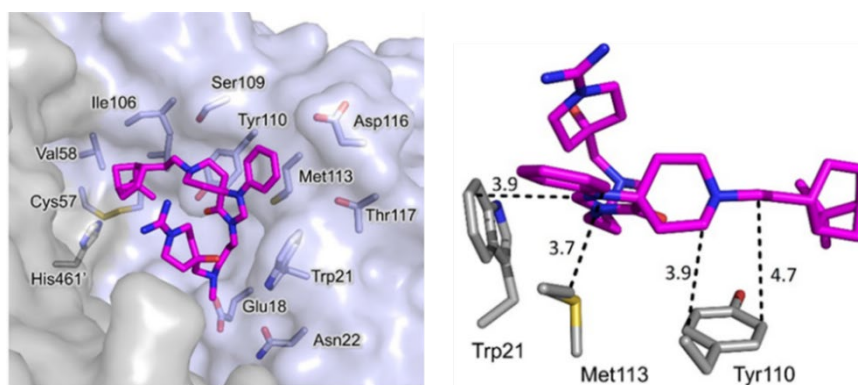


Figure 30. Left) Binding site 1: the residues lining the binding site and the catalytic residues are represented as sticks. Compound 1 carbon atoms are colored in magenta and the protein residues carbon atoms in grey. The accessible solvent area of the cavity is colored grey; Right) Detail of the Compound 1-TR interaction. Compound 1, Trp21, Met113 and Tyr110 are represented as sticks.

In particular, i) the phenyl and the diazole rings, almost coplanar, lay along the side chain of Met113, ii) the indole ring of Trp21 establishes a π -CH interaction with the perpendicular diazole ring, iii) the cyclohexyl moiety interacts with the aromatic ring of Tyr110 (all described interactions are within 4 Å) (Figure 30). The arms of Compound 1 establish weaker interactions with the protein, consistent with what indicated by the electron density map that is poorly defined for these portions of the molecule (Figure 29). The bicycle-heptane moiety extends deeper in the cavity, into the hydrophobic subpocket

lined by Val53, Val58, Ile106 and Leu399, and is just 6-7 Å away from the catalytic Cys52 and Cys57 residues. The hydrophilic carboximidamide moiety fluctuates inside the cavity, towards the entrance, and only a weak electrostatic interaction (4.4 Å) takes place between the tertiary amino group of the arm and Glu18. However, the positive charge dispersed on the arm, due to the presence of amino groups, contributes to the binding by interacting with the overall negative charge of the cavity, suited to accommodate the positive TS₂ substrate. The comparison of TR-1 with the TbTR structure in complex with TS₂ (PDB CODE: 2WOW) clearly shows that compound 1 occupies the site allocated to spermidine and glutathionyl moieties of TS₂ during catalysis (Figure 31).

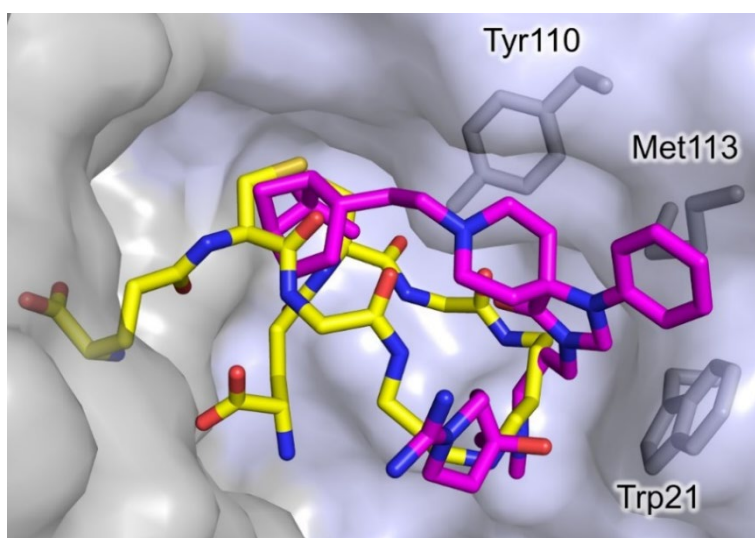


Figure 31. Superposition of TR-1 and TbTR in complex with TS₂ (PDB CODE: 2WOW). Carbon atoms of Compound 1 are colored in magenta whereas the carbon atoms of TS₂ are colored in yellow. Trp21, Met113 and Tyr110 are indicated. The solvent accessible area is represented and colored in grey.

Accordingly, binding of Compound 1 in the cavity is incompatible with the simultaneous binding of TS₂, consistent with the competitive inhibition

observed by kinetic characterization. The second molecule of Compound 1 binds an almost hydrophobic cleft, indicated as site 2, close to the dimerization interface of TR. The phenyl moiety inserts between Pro213 and Lys89, guided by π -CH interactions, the spiro moiety interacts with the backbone of Gly85 and Ser86, while the bicycle-heptane arm points toward a hydrophobic pocket lined by Met70, Leu73, Arg74 and Phe83 (Figure 32). The hydrophilic arm does not contribute to binding, as a consequence of its flexibility; it protrudes out of the cleft and is completely exposed to the solvent. This binding site is far away from both the NADPH and the TS₂ binding cavities and, up to now, no specific function has been attributed to this region. Therefore, it is reasonable to assume that the binding of Compound 1 in site 2 has no effect on the catalytic activity of TbTR and that the observed inhibition is due exclusively to the binding at site 1.

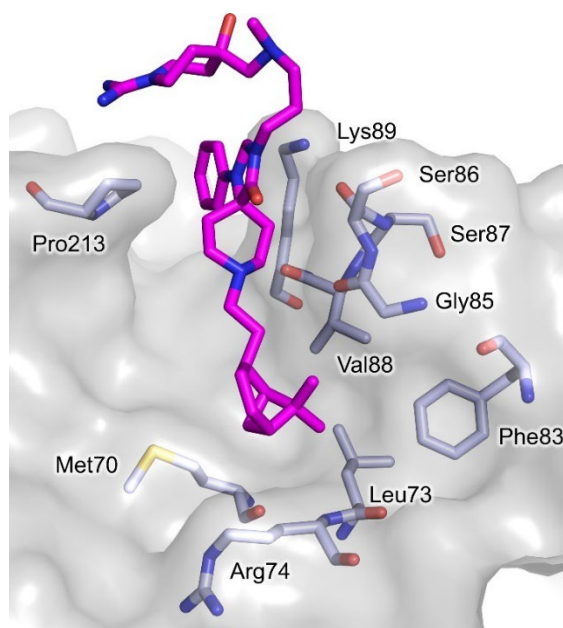


Figure 32. Binding site 2: the residues lining the binding site and the catalytic residues are represented as sticks. Compound 1 carbon atoms are colored in magenta and the protein residues carbon atoms in grey. The accessible solvent area of the cavity is represented and colored grey.

On the contrary, binding to site 2 might explain the SPR results. The binding mode proposed for Compound 1 in TR-1 justifies the selectivity shown against hGR. Indeed, residues composition of site 1 discloses important differences in hGR able to prevent inhibitor binding, while site 2 cleft is completely absent in hGR. Specifically, residues Trp21 and Met113, critical for Compound 1 binding in site 1, are replaced by Arg37 and Asn117 in hGR. Moreover, while the explicit positive electrostatic potential of the hGR substrate binding cavity is unsuitable for accommodating Compound 1, consequently to the presence of positively charged carboximidamide arm and tertiary amino group (Figure 33),

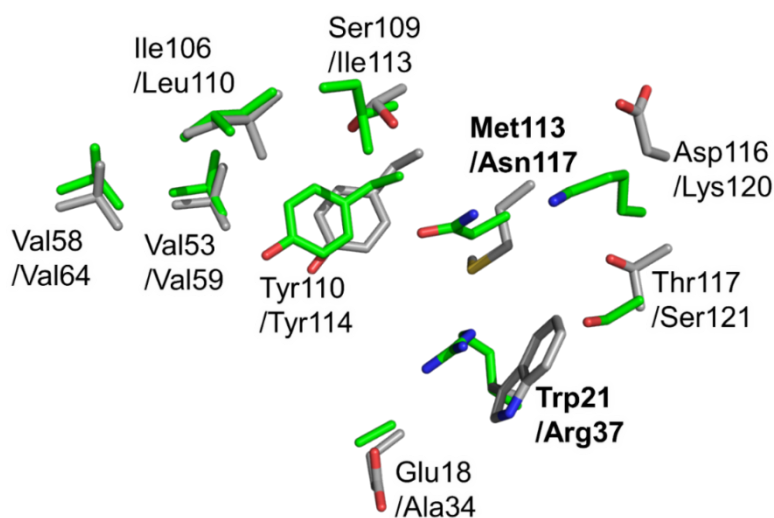


Figure 33. The positive electrostatic potential of the hGR substrate binding cavity is unsuitable for accommodating Compound 1 due to the presence of positively charged carboximidamide arm and tertiary amino group (green lateral chains) whereas the TbTR cavity surface electrostatic potential (grey lateral chains) appears to be compatible with the Compound 1 binding.

the hydrophobic and positively charged moieties of Compound 1 appear to be complementary to the TbTR cavity surface (Figure 34).

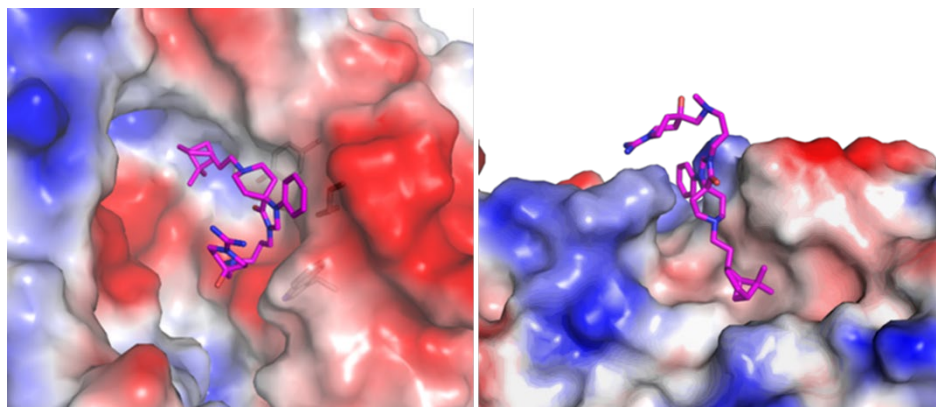


Figure 34. The hydrophobic and positively charged moieties of Compound 1 appear to be complementary to the TbTR cavity surface: site 1 (left) and site 2 (right).

3.1.6. Discussion

By screening 3097 compounds previously reported in PubChem to be inhibitors of Trypanosomatid growth, a new series based on a 1-phenyl-1,3,8-triazaspiro[4.5]decan-4-one scaffold has been identified to be able to inhibit TbTR in the micromolar range. Among these, Compound 1 has been characterized as a reversible TS_2 competitive inhibitor, able to inhibit endogenous reductase activity and parasite growth. The X-ray crystal structure of the complex TR-1 has been solved at 1.98 Å of resolution, providing essential insights on the mechanism of inhibition. Two binding sites are present, as also demonstrated by SPR, none of these inducing global or local conformational variations. Site 2 is located close to the dimeric interface of TR, while site 1 is located in the trypanothione binding cavity and partially overlaps with the mepacrine binding site: the phenyl-triazaspiro core anchors Compound 1 to the cleft *via* a conserved hydrophobic patch (formed by the Trp21, Met113 and Tyr110 residues), while the flexible arms of the inhibitor cause steric hindrance both at the bottom (close to the catalytic cysteines) and at the entrance of the cavity, thus preventing the entry of the substrate into the

catalytic site. The binding mode proposed in TR-1 justifies the selectivity shown against human GR since the residues Trp21 and Met113, critical for Compound 1 binding to site 1, are replaced by Arg37 and Asn117 in hGR and the distinctly positive electrostatic potential of the hGR substrate binding cavity is unsuitable for accommodating the inhibitor, which in turn is positively charged due to the presence of carboximidamide arm. Unexpectedly, the bicycle-heptane moiety of Compound 1 extends deeper in the cavity, into a new hydrophobic sub-pocket lined by Val53, Val58, Ile106 and Leu399 residues. For these reasons, Compound 1 represents a new lead compound suitable to develop new drugs against HAT. Additionally, Compound 1 displays a comparable activity on LiTR, reasonably due to the conserved structural features present in the targets which stabilize the interaction. Further, the spiro central core of the hit series was previously reported in PubChem to be active against *T. brucei* and *T. cruzi* proliferation. Compound 1 potency resulted to be similar (between ≈ 2 and $5 \mu\text{M}$) in all the assays namely TbTR *in vitro* activity, TbTR activity in *T. brucei* lysate and the *T. brucei* proliferation assay, thus suggesting the ability of this compound to reach the target in the parasite with no significant potency shift. The Compound 1 chemotype, being the central spiro core the key for the interaction with TR, is a relevant starting point from a drug development perspective as molecules containing a central spiro core, like spiperone¹¹⁹ and fluspirilene¹²⁰, were proven to be brain penetrant in humans. Even if several rounds of optimization together with improvement of drug-like properties are needed, this chemotype represents an intriguing new avenue for the future treatment of the CNS phase of *T. brucei* infections.

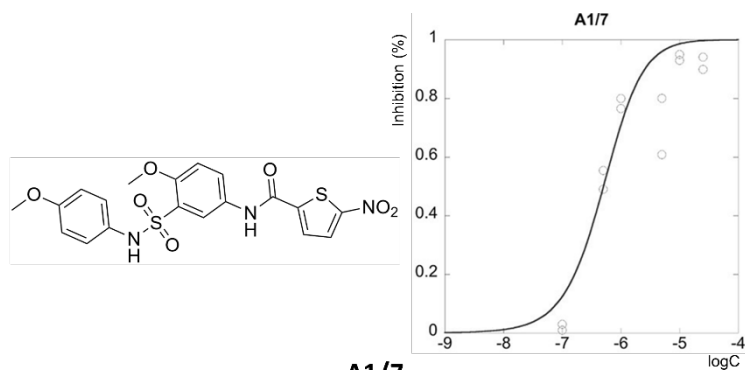
3.2. From LeishBox toward a drug against all Kinetoplastids

3.2.1. Determination of inhibiting capacity of LeishBox compounds against LiTR

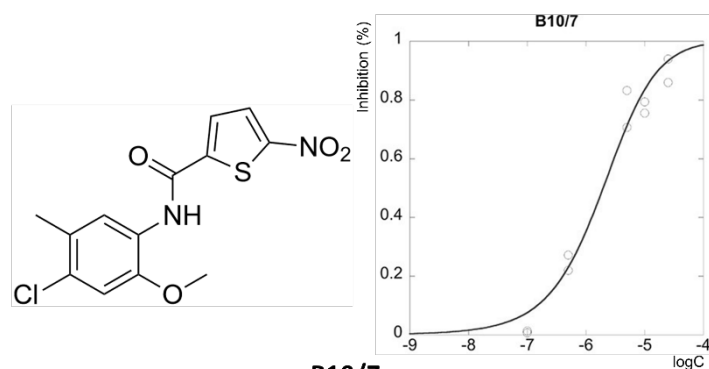
All 192 compounds of the LeishBox, identified by GlaxoSmithKline in HTS from 1.8 million compounds against *L. donovani*¹¹⁶, were first tested for their ability to inhibit LiTR enzymatic activity. A first screen was carried out at a concentration of 25 μM to measure their efficacy in inhibiting LiTR. Sixteen out of 192 compounds (8.3% of the whole set) are able to decrease the velocity of TS₂ reduction by at least 50%, while 7 compounds (3.6% of tested compounds) inhibit TR by at least 80%. These 7 compounds, i.e., compounds A1/7, B10/7, C5/7, C10/7, F1/7, G1/9, and G2/9 (Figure 35), were then tested at lower concentrations (between 10 and 0.02 μM) to determine their IC₅₀.

	pIC ₅₀									
	MW	Aring	ClogP	Hba	Hbd	Heavy	Tpsa	L.d.	T. c.	T. b.
A1/7	463.84	3	2.713	4	1	31	139.55	6.1-6.3	7.2	6.8
B10/7	326.76	2	3.213	2	1	25	84.15	5.3-5.3	6.2	6.3
C5/7	381.43	2	2.541	4	1	25	112.3	5.8-6.0	6.7	6.8
C10/7	341.18	2	3.985	2	1	19	74.92	5.5-5.8	6.6	6.5
F1/7	442.55	3	3.782	5	1	30	92.26	5.8-6.8	6.4	6.7
G1/9	427.48	3	3.551	3	0	29	78.97	6.0-6.4	5.6	5
G2/9	297.38	3	4.188	2	1	21	46.92	5.2-5.3	5.5	5.5

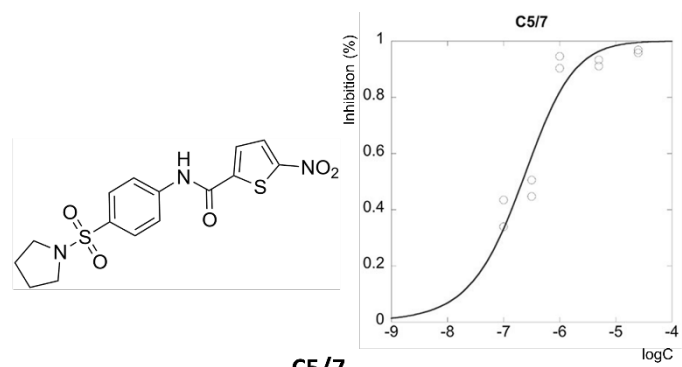
Table 7. Chemicophysical properties of the best selective TR inhibitors¹¹⁶. MW = Molecular weight; Aring = number of aromatic rings; Clogp = calculated partition-coefficient between n-octanol and water; Hba = hydrogen-bond acceptor; Hbd = hydrogen-bond donor; Heavy = number of heavy atoms (no hydrogen atoms); Tpsa = total polar surface area; pIC₅₀: $-\log(\text{IC}_{50})$.



A1/7
 N-{4-methoxy-3-[(4-methoxyphenyl)sulfonyl]phenyl}-5-nitrothiophene-2-carboxamide

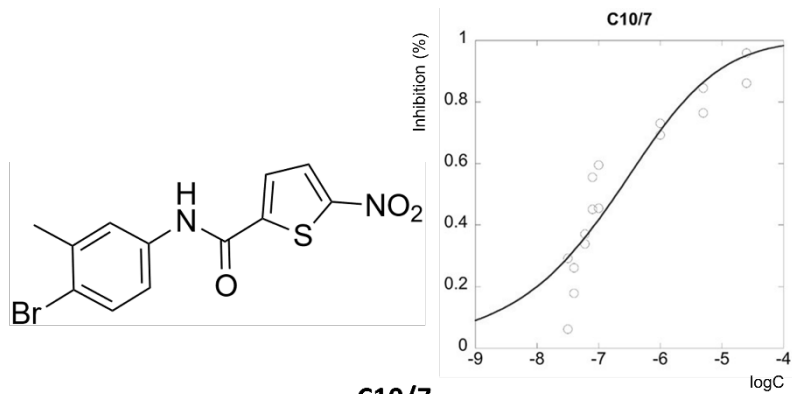


B10/7
 N-(4-chloro-2-methoxy-5-methylphenyl)-5-nitrothiophene-2-carboxamide



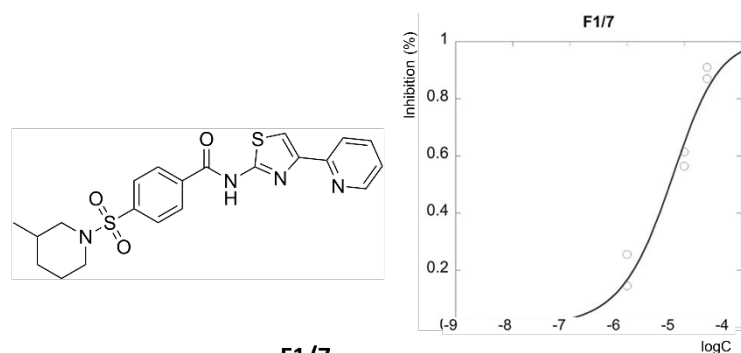
C5/7
 5-nitro-N-[4-(1-pyrrolidinylsulfonyl)phenyl]-2-thiophenecarboxamide

Figure 35. Chemical structure and inhibition experiments of active compounds against LiTR.



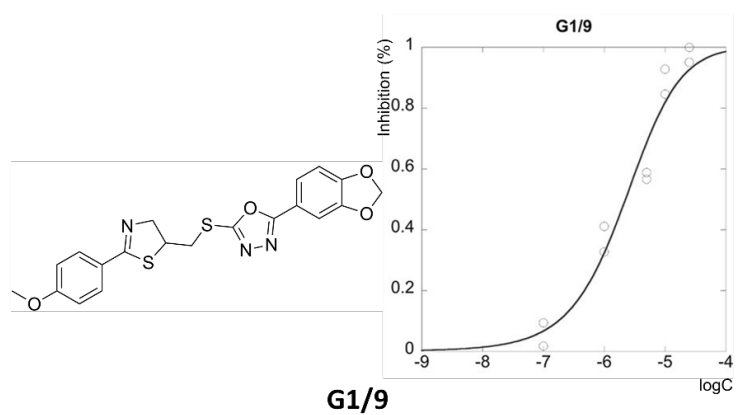
C10/7

N-(4-bromo-3-methylphenyl)-5-nitrothiophene-2-carboxamide



F1/7

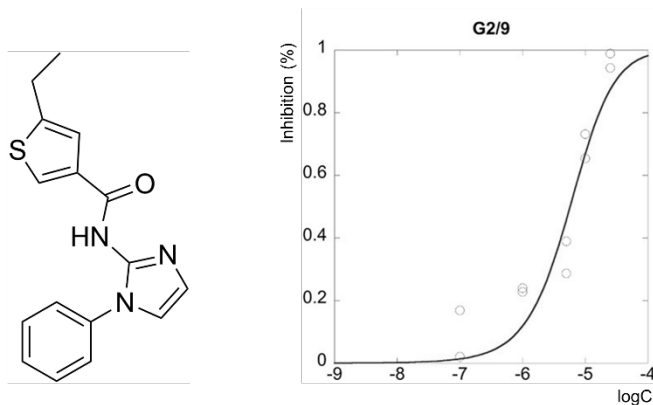
4-[(3-methylpiperidin-1-yl)sulfonyl]-N-[4-(pyridin-2-yl)-1,3-thiazol-2-yl]-benzamide



G1/9

2-(2H-1,3-benzodioxol-5-yl)-5-({[2-(4-methoxyphenyl)-4,5-dihydro-1,3-thiazol-5-yl]methyl}sulfanyl)-1,3,4-oxadiazole

Figure 35. (following) Chemical structure and inhibition experiments of active compounds against LiTR



G2/9

5-ethyl-N-(1-phenyl-1H-imidazol-2-yl)-3-thiophenecarboxamide

Figure 35. (following) Chemical structure and inhibition experiments of active compounds against LiTR

	LiTR inhibition IC ₅₀ (μM)	hGR inhibition IC ₅₀ (μM)	Selectivity index (IC ₅₀ hGR/ IC ₅₀ LiTR)
A1/7	0.52 ± 0.14	no inhibition at 25	≫50
B10/7	1.96 ± 0.30	3.7	1.9
C5/7	0.22 ± 0.05	3.2	15
C10/7	0.19 ± 0.08	no inhibition at 25	≫100
F1/7	5.58 ± 0.86	no inhibition at 25	≫5
G1/9	2.24 ± 0.52	>25	>11
G2/9	5.96 ± 0.84	>25	>4

Table 8. LiTR vs hGR inhibition. IC₅₀ for each inhibitor has been calculated by fitting the experiments in Figure 35.

All of these compounds display an IC₅₀ value below 6 μM (Table 8); three of them (compounds C10/7, C5/7 and compound A1/7) have the highest potency,

with IC_{50} values in the nanomolar range. To rule out whether these compounds containing a nitro group were able to be reduced by NADPH or could serve as pseudosubstrates of TR, control kinetics experiments using 25 μ M compound C10/7 in the absence of TS_2 and LiTR were carried out.

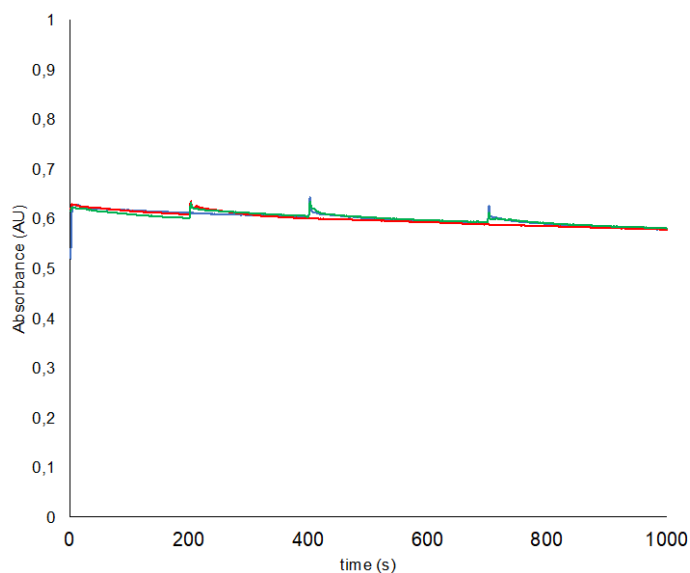


Figure 36. Control experiments with and without compound C10/7 (25 μ M concentration). (A, red): the assay was initiated by addition of NADPH 100 μ M to a solution containing buffer; TR 5 nM was added after 200 s; (B, blue): the assay was initiated by addition of NADPH 100 μ M to a solution containing buffer and inhibitor C10/7 at 25 μ M; TR 5 nM was added after 400 s; a new addition of TR 5 nM was performed after 700 s. (C, green): the assay was initiated by addition of NADPH 100 μ M to a solution containing buffer; inhibitor C10/7 at 25 μ M was added after 200 s; TR 5 nM was added after 400 s; a new addition of TR 5 nM was performed after 700 s.

A very slow absorbance decrease occurs at 340 nm in all conditions, indicating a slow oxygen-dependent NADPH oxidation. No C10/7-dependent oxidation of NADPH takes place; C10/7 is not a pseudo-substrate of LiTR.

3.2.2. Selected inhibitors interact directly with LiTR

The ability of inhibiting compounds to interact with LiTR was evaluated by SPR experiments. These were carried out by immobilizing LiTR onto COOH5 sensorchips and adding compounds as analytes. Figure 37 shows the sensorgrams of eight evaluated interactions, namely compounds A1/7, B10/7, C5/7, C10/7, F1/7, G1/9, and two control noninhibiting compounds (B1/7 and B2/7); the experiment indicates that binding of the inhibitor compounds to LiTR occurs, while the two control compounds do not appear to bind to the target enzyme.

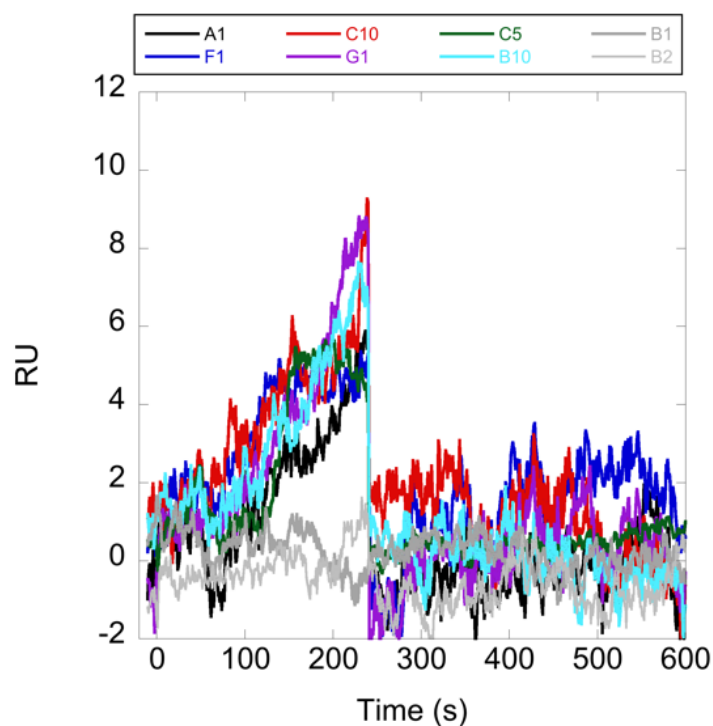


Figure 37. SPR experiment. Sensorgrams of the interaction between LiTR immobilized on a COOH5 sensorchip and compounds of the LeishBox at a concentration of 20 μ M.

3.2.3. Structural analysis of the most selective inhibiting compounds

The most selective inhibitors identified have quite similar structures, as shown by Figure 35. The phenyl-5-nitrothiophene-2-carboxamide moiety (Figure 38) of N-(4-bromo-3-methylphenyl)-5-nitrothiophene-2-carboxamide (compound C10/7) is the core of the A1/7 and C5/7 compounds, i.e., the compounds that show the highest potency against TR.

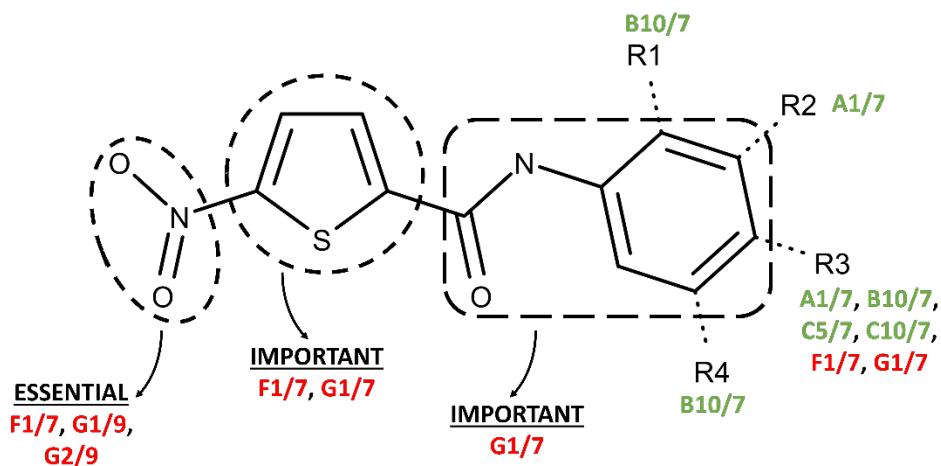


Figure 38. The phenyl-5-nitrothiophene-2-carboxamide moiety; in green are reported those compounds in which modifications of the core induce a positive effect on potency over TR, on the contrary, in red, are indicated those compounds in which potency is impaired.

From Figure 38 it is possible to infer that potency is particularly relevant only when the nitrothiophene portion is conserved; in G2/7, even the substitution of only the nitro group with an aliphatic chain induces an impairment in activity, while the thiophene ring is maintained untouched. The phenylcarboxamide moiety is replaced only in G1/7, and seems to be associated to a general potency impairment; in any case, it is not possible to state whether it strictly depends from this modification or from the nitrothiophene absence.

Interestingly, those modifications associated to the phenyl ring induce a general potency improvement; this is particularly true for those compounds presenting a sulfonyl group (A1/7, C5/7), in addition to the phenyl-5-nitrothiophene-2-carboxamide moiety, contrarily to F1/7, in which substitution on R3 position of the phenyl ring does not induce the same effect. Interestingly compound B10/7 is the unique presenting three substituents on the phenyl ring, which apparently enhance this compounds inhibition against TR but probably play a role in the aspecific activity against hGR as is endowed with the lowest specificity index in the series ($IC_{50} \text{ hGR} / IC_{50} \text{ LiTR} = 1.9$).

3.2.4. SPR competitive binding experiments

TS₂ and compounds A1/7 and C10/7, were singularly injected in 20 mM Hepes pH 7.4, 150 mM NaCl + 0.005% surfactant P20 + 2% DMSO at a concentration of 20 μM on the sensor chip at a constant flow (30 μL/min); in addition, mixtures of compound A1/7 + TS₂ or of compound C10/7 + TS₂, each at a concentration of 20 μM, were injected in the same conditions to test whether the compounds compete with TS₂ (Figure 39). The increase in RU relative to the baseline (0-120 s) indicates complex formation, whereas the decrease in RU after 120 s represents the dissociation of the compounds and/or TS₂ from the immobilized ligand after injection of the buffer.

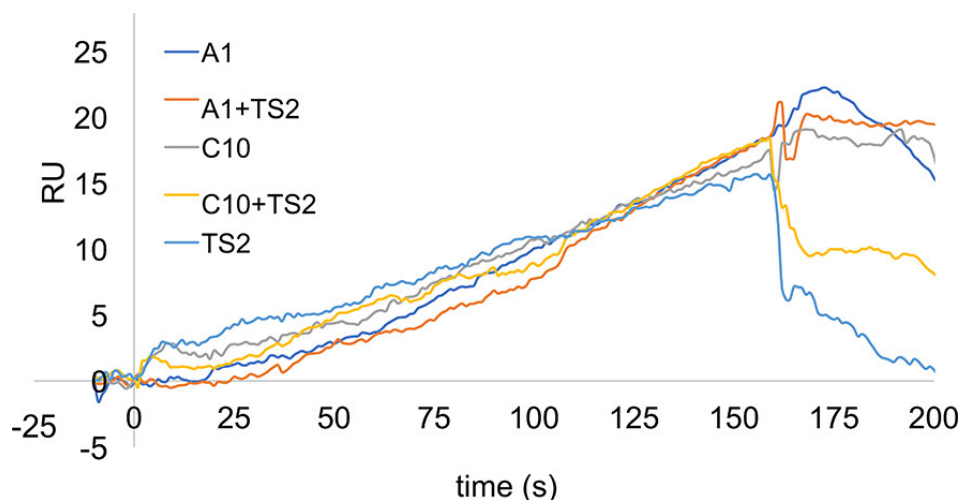


Figure 39. SPR competition experiment between oxidized trypanothione (TS₂) and compounds C10/7 and A1/7.

The experiments on one side show that TS₂ and compounds A1/7 and C10/7 appear to bind with similar curves to TR; even more importantly, sensorgrams carried out by injecting mixtures of compound A1/7 + TS₂ or of compound C10/7 + TS₂ do not show increased (additive) binding with respect to injection of TS₂ or of inhibitors alone. The experiments clearly show that competition occurs between trypanothione and inhibitors, and the inhibitors act by binding to the trypanothione binding site.

3.2.5. Docking of LiTR and hGR with compounds A1/7, C5/7, C10/7 and F1/7 and molecular basis of inhibition specificity

Docking experiments were performed with compounds A1/7, C5/7, C10/7, and F1/7 using AutoDock4 and selecting the positions of binding to LiTR on the basis of the lowest estimated free energy of binding, as calculated by the suite (= van der Waals energy + H bond energy + desolvation energy + electrostatic energy + final total internal energy + torsional free energy – unbound system's energy). Compounds result to bind to the same region of LiTR active site,

comprising catalytic C52, C57, H461', and E466', with similar orientations and very favorable calculated affinities. Figure 40 reports the best docked poses for A1/7 in the trypanothione pocket: two different models, where the inhibitor is bound with different torsions between residues C57, K61, H461', and E466' on one side, and to P336 and the loop, including F396, P398, L399, and M400, on the other side.

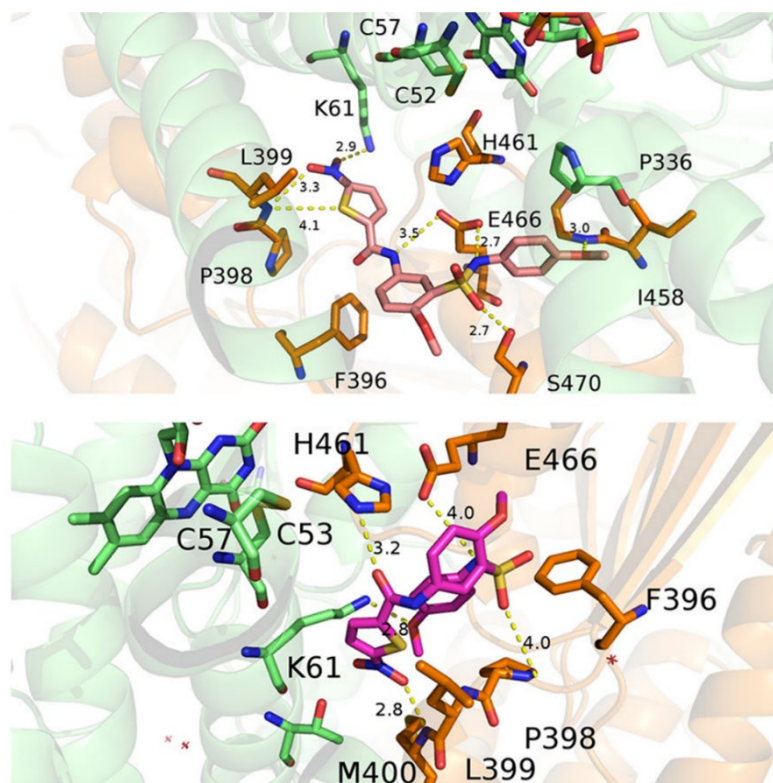


Figure 40. Best docked poses for A1/7.

The two models were predicted to bind with an estimated free energy of binding of -7.88 kcal/mol (Figure 40, upper panel; estimated inhibition constant, $K_i = 1.69 \mu\text{M}$ at 298.15 K) and -7.55 kcal/mol (Figure 40, lower panel; estimated inhibition constant, $K_i = 2.90 \mu\text{M}$ at 298.15 K), respectively,

values of the same order of magnitude of measured IC_{50} . Figure 41 shows the docking of compound C5/7 with TR, identifying the very same region of interaction with respect to compound A1/7. The docking yielded a model where C5/7 binds to TR with an estimated free energy of binding of -7.75 kcal/mol (Figure 41, upper panel; estimated inhibition constant, $K_i = 2.10 \mu\text{M}$ at 298.15 K). Compound F1/7 binds to TR with an estimated free energy of binding of -9.58 kcal/mol (Figure 42; estimated inhibition constant, $K_i = 94.68 \text{ nM}$ at 298.15 K). Compound C10/7 binds to TR with an estimated free energy of binding of -6.68 kcal/mol (Figure 41, lower panel; estimated inhibition constant, $K_i = 12.61 \mu\text{M}$ at 298.15 K).

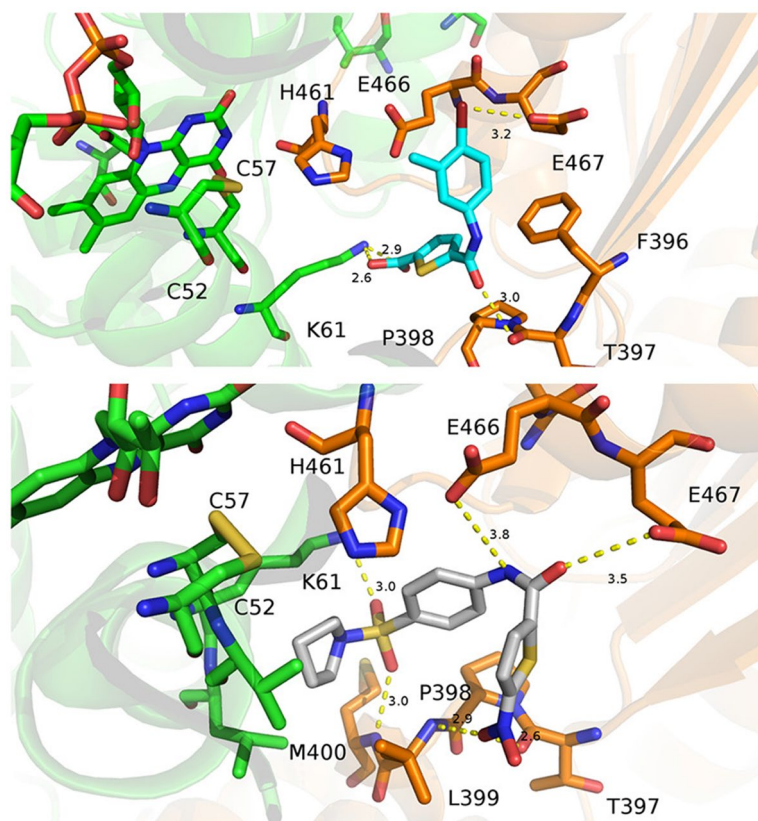


Figure 41. Best docked poses for C5/7 and C10/7 (upper and lower panel respectively).

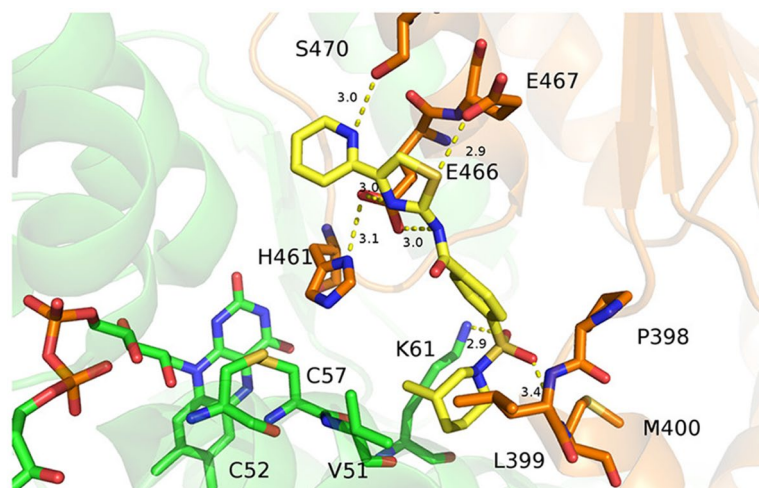


Figure 42. Best docked pose for F1/7.

In particular, all of these compounds appear to bind with the nitro group establishing bonds (with the possible exception of compound C10/7) with the nitrogen atoms of the peptide bonds P398-L399 and L399-M400.

Additionally, superposition of the inhibitors A1/7, C5/7, C10/7, and F1/7 modeled by docking to the TR active site by the glutathione binding site of hGR was calculated (Figure 43). In particular, in the position where the compounds are bound to hGR in the modeled structures, three residues (L399, M400, and N402) are replaced by M450, Y451, and A452, respectively, and the loop 396-402 (447-453 in hGR) is bulkier and negatively charged.

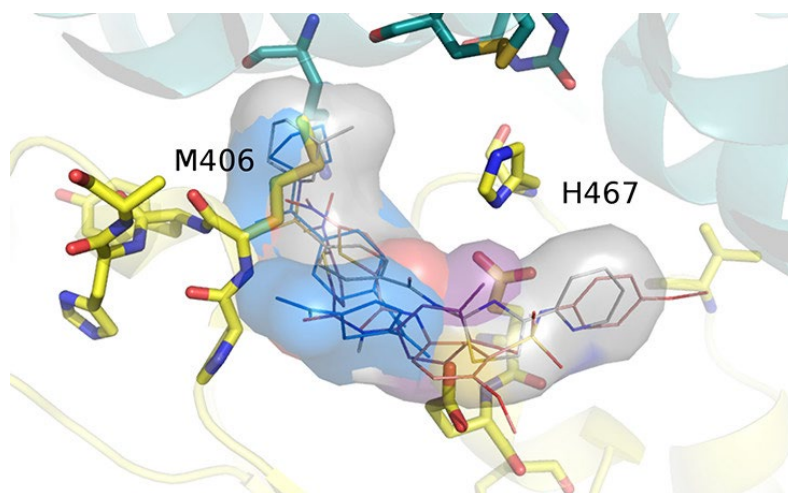


Figure 43. Superposition of A1/7, F1/7, C5/1, and C10/7 (gray) modeled by docking to the TR active site and to the glutathione binding site of human GR (yellow).

A clash between the compound and the loop 447-453 of hGR (396-402, LiTR numeration) impairs inhibitor binding to hGR, and it is possibly responsible for the molecular basis of the specificity of action of these compounds toward LiTR.

3.2.6. X-ray crystal structure of TR in complex with compound A1/7

A preliminary model for the complex TR-A1/7 has been built, starting from a dataset collected at 2.1 Å. A wide tubular shaped electron density was found at the entrance of both the TS₂ binding site and modelled as a molecule of compound A1/7. The inhibitor seems to settle at about 10 Å far from the catalytic cysteines, thus preventing substrate binding, in a similar fashion to docking prediction and confirming the competitive behavior determined by SPR. Accordingly, the nitrothiophene moiety seems to be the driving force of the interaction; particularly the nitro group seizes K61 while the thiophene ring

is sandwiched by the sidechains of two proline residues, namely P398 and P462 (Figure 44).

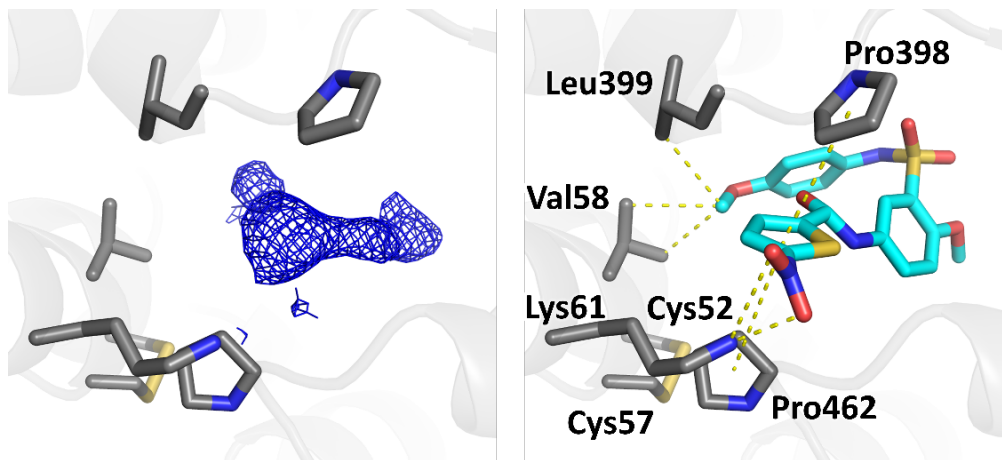


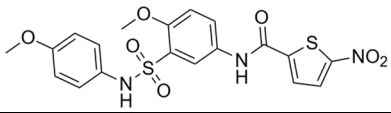
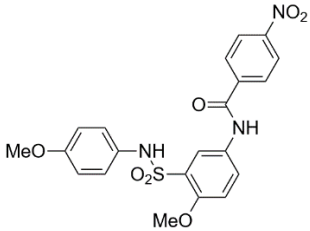
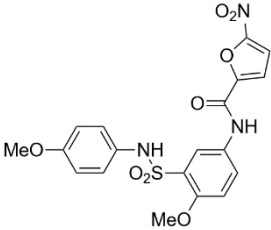
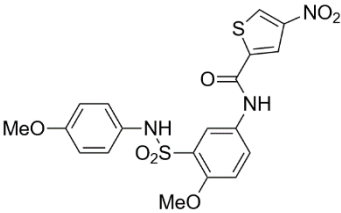
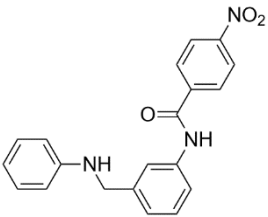
Figure 44. Left) 2Fo-Fc map, contoured at 1σ , of compound A1/7 at the entrance of the trypanothione binding site; Right) A1/7 modeled in the cleft.

The remaining part of the compound is much less informative because of lack of electron density: rotability of the S-N bond and absence of a stabilizing surrounding probably induce this portion of the inhibitor to flap inside the cleft; it is possible hypothesize a bonding interplay between the methoxy group and the L399 and V58 residues, known to stabilize TS₂.

3.2.7. Preliminary studies on A1/7 derivatives

One of the most intriguing features of compound A1/7, besides being one of the most potent against LiTR, is certainly its presence in all the three GSK boxes, which provides the basis for a broad spectrum drug development. In this perspective a series of 12 derivatives has been synthesized, in collaboration with the medicinal chemistry group of Prof Giuseppe Campiani (University of

Siena, Italy). At this time, kinetic screening of derivatives is ongoing; derivatives structures together with IC₅₀ values are reported in Table 9.

Compound	Structure	MW (g/mol)	pIC ₅₀
A1/7 (scaffold)		463.48	6.28
NF2856		457.46	4.30
NF2857		447.42	5.27
NF2858		463.48	4.00
NF2859		347.37	5.21

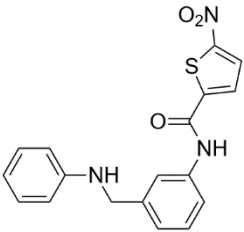
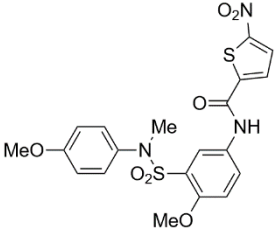
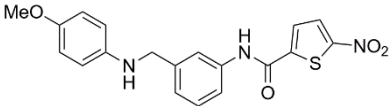
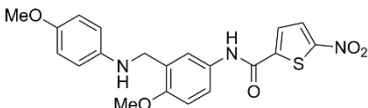
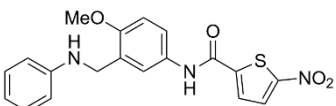
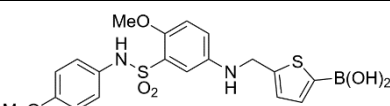
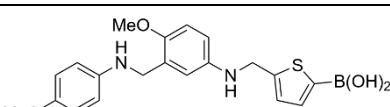
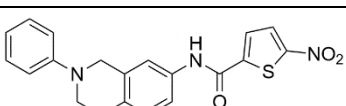
NF2860		353.39	7.2
NF2862		477.51	5.72
NF2890		383.42	6.14
NF2891		413.45	5.71
NF2894		383.42	5.62
NF2895		448.32	4.67
NF2896		398.28	4.95
NF2897		381.41	6.81

Table 9. Series of twelve A1/7 analogues.

Compounds NF2860, NF2890, NF2897 are the most active ones among the set, as are endowed with a potency in the same order of magnitude of the

scaffold. Even if structural insights would be extremely helpful in identifying positive and negative effects originating from A1/7 modification, some considerations can be addressed (summarized in Figure 46); the most noticeable is that the modification of the nitrothiophene moiety causes a clear drop in terms of potency, particularly evident in compounds NF2856, NF2858, NF2895, NF2896 ($pIC_{50} < 5$). Actually, in compound NF2856, the thiophene core is replaced by a phenyl ring; even if a nitro group is present in position *para*, potency results impaired. In compound NF2858, the effect is even more remarkable when the nitro group is shifted from position 5 to position 4 of the thiophene ring. In compounds NF2895 and NF2896, a boronic substituent is present in position 5, being a class generally prone to establish reversible covalent bonds; unfortunately, an adequate effect is not achieved in this case. Comprehensively these observations suggest that the nitrothiophene plays an important part in the inhibition mechanism, and even small alterations, as in NF2858, induce a loss of potency.

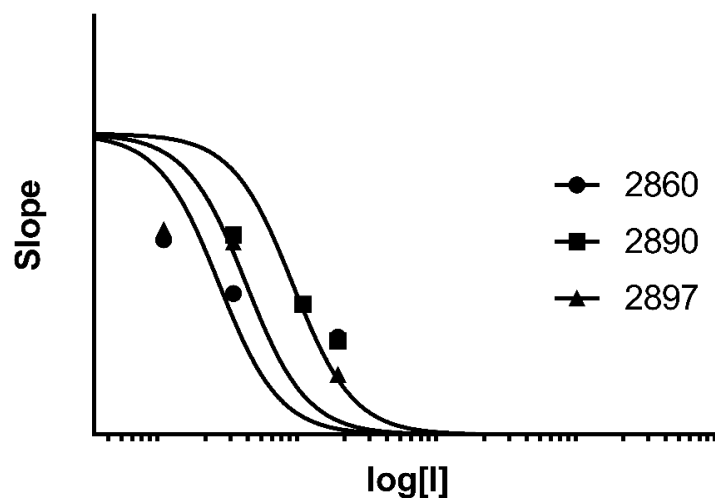


Figure 45. Kinetic experiment of compounds NF2860, NF2890, NF2897 carried out against LiTR.

Conversely, in compounds NF2860 and NF2897 a gain of potency is clear, while NF2890 shows an IC₅₀ comparable to the scaffold (inhibition kinetic against LiTR is depicted in Figure 45); the molecular weight is lower than A1/7 and the 5-nitrothiophene-2-carboxamide moiety is conserved.

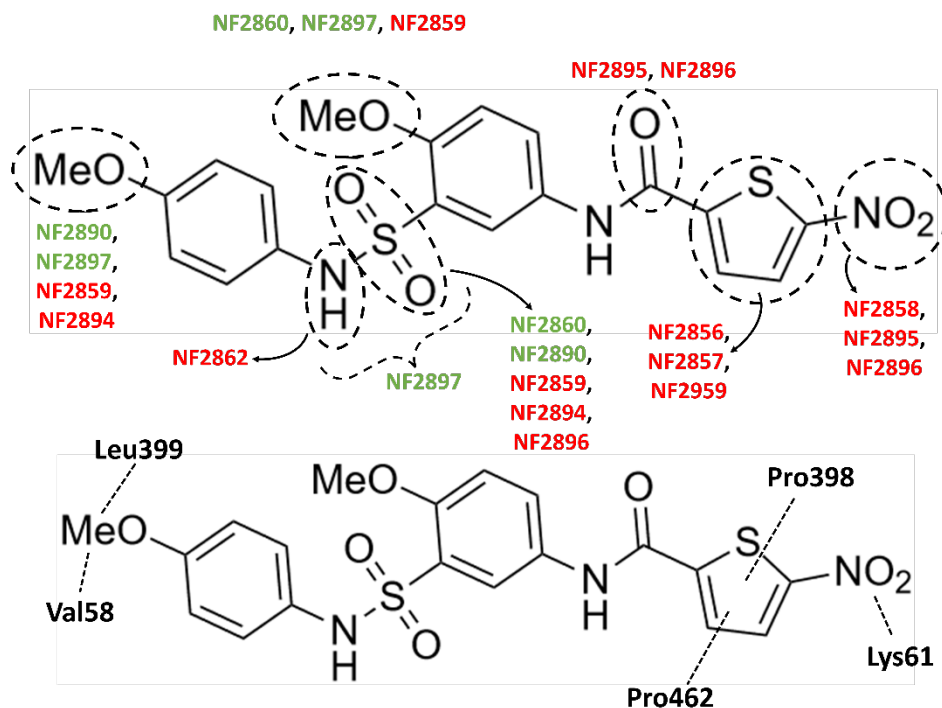


Figure 46. Upper panel) 2D representation of chemical modifications performed on A1/7; in green are reported those compounds in which modifications of the scaffold induce a positive effect on potency over TR, on the contrary, in red, are indicated those compounds in which potency is impaired; Lower panel) 2D plot of the interactions occurring between TbTR and A1/7 (based on the preliminary crystallographic model).

NF2860 is a “simplified” version of the scaffold as it is deprived of the sulfonyl group and two methoxy group, suggesting that these groups may not be strictly necessary for the interaction. NF2890 seems to confirm, in part, this hypothesis

as the presence of only one methoxy group, placed in position 4 of the terminal phenyl ring, preserve a considerable potency, which is, however, decreased with respect to NF2860. NF2897 represents a *sui generis* derivative as a heterocyclic group is introduced; the secondary amine function converges with the methoxy group in order to form a 1,3-oxazinane, conferring a higher overall planarity to the molecule. From Figure 46 it is also possible to appreciate how those modifications associated to an impairment in terms of potency fall into the determinants of interaction identified by the X-ray crystal structure of TR-A1/7 complex; as already mentioned, the nitrothiophene moiety is definitely the most important fragment, and all the worst compounds of the series contain alterations of this group. In general, this variation not only specifically alters K61 seizing, but probably has an effect on the steric hindrance of the compound, which, when lowered, permits a more efficient exposure of residues Pro398, Pro462 and the nearby His461 (involved in the catalytic cycle) towards TS₂ substrate. Moreover, absence of the phenylic methoxy group in compounds NF2859 and NF2894 probably determines potency decreasing, even if the nitro group is conserved. Differently, NF2897 displays interesting features as the phenylic methoxy group is absent, and so, probably, binding to Val58 and Leu399 but still shows a high potency against TR. This is probably due to the simultaneous modification of the sulfamoyl group, which is converted in a rigid 2-rings system; the final effect is likely to be the avoidance of the flapping of the remaining part of the compound hypothesized on the basis of the X-ray structure (electron density is actually absent in that region, due to the inner flexibility of the compound), with a consequent enhanced stability of the compound in the binding cleft.

3.2.8. Discussion

Starting from LeishBox, a set of 192 best antileishmanial compounds identified by GlaxoSmithKline in an HTS from 1.8 million compounds against *L. donovani*, 7 compounds resulted being highly potent TR inhibitors (3.6% of tested compounds). Among these, 3 (1.6% of tested compounds) are also selective, as do not show activity against hGR. Selectivity relies on the structural differences among TR and hGR; in TR compounds seem to bind at the trypanothione binding site and the interaction is driven by two key residues, namely L399 and M400, which are replaced by a methionine and a tyrosine, respectively, in the human homologue thus preventing compounds from entering. In hGR, these residues form a bulky loop that impairs inhibitor binding: this may provide an explanation for the ability of these compounds to efficiently kill *Leishmania* parasites in both axenic promastigote and microphage-infecting amastigote forms, while having little effect with respect to human cells¹¹⁶. In addition, the same pocket is conserved in TRs from all major Trypanosomatids, namely *L. donovani*, *L. infantum*, *T. cruzi* and *T. brucei*, setting the basis for a potential broad spectrum antikinoplastid therapy. Structural analysis of four best compounds (A1/7, C5/7, C10/7, F1/7) shows that the phenyl-5-nitrothiophene-2-carboxamide moiety of N-(4-bromo-3-methylphenyl)-5-nitrothiophene-2-carboxamide (compound C10/7) is the core of the A1/7 compound and of the C5/7 compound, which may bind in the same position at the trypanothione binding site. Similarly, F1/7 encloses a core with a phenyl group, a carboxamide (reversed with respect to C10/7), and a thiazol group instead of a thiophene, and is able to bind the same site of C10/7, A1/7, and C5/7 compounds. Docking studies of A1/7, C5/7, F1/7, and C10/7 demonstrate that they all locate at the same site and suppress TR activity with the same competitive mechanism. SPR competitive binding experiments show

that competition occurs between trypanothione and inhibitors and confirm that the inhibitors act by binding to the trypanothione binding site. The experiment was carried out using TR in the oxidized state to avoid further complication of the analysis, since a nucleophilic attack by the NADPH-reduced cysteines of the active site to the nitrothiophene moiety of some inhibitors is, in principle, possible ¹²¹. This is not irrelevant as a nitrothiophene is present in the most effective inhibitors: docking shows that the nitro group can interact with the nitrogen of the peptide bond at L399 and/or with the amino group of the side chain of K61. This behavior is also confirmed in a preliminary model of the crystal structure of TR-A1/7 complex; the inhibitor seems to approximately bind the same region, in which the nitro group interacts with the K61 side chain. It is worth noting that the most selective inhibitors identified in this study were already demonstrated to be effective by whole-cell phenotypic assays against *L. donovani*, *T. cruzi*, and *T. brucei* ¹¹⁶, and that one of these compounds (compound A1/7) is the only present in all three LeishBox, ChagasBox, and HATBox. For this reason, A1/7 has been used as scaffold for the synthesis of a set of 12 derivatives, produced in collaboration with the medicinal chemistry group of Prof. Giuseppe Campiani (University of Siena, Italy). Three out of twelve compounds (NF2860, NF2890, NF2897) display a higher and/or comparable pIC₅₀ with respect to the scaffold, in a kinetic screening assay against LiTR; further intense SAR studies will broaden the knowledge regarding the determinants of inhibition in order to synthesize more potent derivatives.

3.3. Preliminary crystallographic studies for Fragment based screening

Recently a proposal for FBS to be carried out on TbTR has been accepted by the XCHEM-Fragment screening platform at Diamond Light Source (Didcot, UK). In order to meet XCHEM-Fragment screening platform pre-requirements (reported in Materials and Methods section), preliminary crystallographic studies on TbTR have been carried out. An automatic protocol for TbTR crystallization was successfully set up, resulting in achieving 30-55 μm cryoprotected crystals. Data collection statistics for “native” (non-soaked crystals), DMSO-soaked and Compound 1-soaked crystals are reported in Table 10.

	Native	10% DMSO	Compound 1
Crystal parameters			
Space group	P2 ₁ 2 ₁ 2 ₁	P2 ₁ 2 ₁ 2 ₁	P2 ₁ 2 ₁ 2 ₁
Unit cell dimension (a,b,c) (Å)	80.45 109.99 113.38	80.24 109.97 113.69	80.94 109.55 113.36
Asymmetric unit composition (molecule, amount)	TbTR, dimer FAD, 2	TbTR, dimer FAD, 2	TbTR, dimer FAD, 2 Compound 1, 4
Data analysis statistics			
Resolution range (highest resolution shell) (Å)	55.00-2.06 (2.09-2.06)	56-85-2.12 (2.15-2.12)	78.78-1.78 (1.81-1.78)
Unique reflections	63128 (3106)	57981 (2830)	97064 (4838)
Completeness (%)	99.9 (100)	99.9 (100)	99.9 (99.9)
Redundancy	8.8 (8.9)	8.8 (8.6)	8.8 (8.6)
R _{meas} (%)	6.9 (115.8)	9.2 (107.1)	5.3 (111.7)
CC(1/2) (%)	100 (70)	100 (80)	100 (70)
$\langle I/\sigma(I) \rangle$	19.1 (2.1)	14.8 (2.3)	24.1 (2.2)

Table 10. Crystal parameters and data collection statistics for native, DMSO-soaked and Compound 1-soaked crystals.

Diffraction data confirm the suitability of these crystallization conditions for FBS, as crystals are resistant to DMSO, which is the solvent for fragments stock solutions; DMSO soaking does not affect diffraction quality, which is preserved with respect to “native” crystals. Additionally, soaking with Compound 1 demonstrates how the new crystal packing does not affect ligand binding, as the binding sites still remain accessible to the candidate ligand. Moreover, the possibility of flash-freezing crystals overtaking the cryoprotection step represents an important feature in avoiding a technical bottleneck when working on a very large scale of crystal samples.

4. MATERIALS AND METHODS

Being two approaches adopted for active compounds identification, the experimental section will be subdivided in two main portions in order to facilitate the understanding of each strategy's workflow.

4.1. High-throughput screening

4.1.1. Compound collection and similarity search

The compounds that are made available through the CNCCS collection (c. 150'000 compounds - www.cnccs.it) were crossed with the PubChem database to select those that were reported to be active in confirmatory Trypanosomatid survival assays. 3'097 compounds were identified that were cherry-picked from 10 mM DMSO solutions and arrayed for testing.

After hit confirmation, compound similarity searches were performed by generation of circular Morgan fingerprints (radius 2, 2018 bits) for the test compounds using open source RDKit software (<http://www.rdkit.org/>). The molecular representations generated were used to perform ligand based virtual screening against the target database that is described above or a subset of the public ZINC database (<https://zinc.docking.org>). Similarity was assessed by the Tanimoto index between the reference and target structures using a cut-off (or threshold) of 0.6. Similar compounds were clustered using Taylor-Butina clustering, a non-hierarchical clustering method that ensures that each cluster contains molecules with a set cut-off distance from the central compound. Compounds selected for purchase or screening follow up were chosen from the most populated clusters, with either the central compound or closed analogues

(based on visual inspection) being used to represent the compound cluster. All selected compounds were quality controlled by UPLC-MS prior to testing.

4.1.2. Expression and purification of trypanothione reductase from *T. brucei*

The gene coding for the enzyme (aa 1-492) was codon optimized for the expression in *E. coli* and obtained from GenScript. The coding sequence was cloned in the pET15b vector in order to express an N-terminal fused 6xHisTag for affinity chromatography. *E. coli* BL21(DE3) transfected cells were induced with 0.5 mM IPTG for 18 h at 37°C. Cells were then pelleted at 4000 rpm, for 30 min at 4°C, and then resuspended in lysis buffer (25 mM Tris pH 7.4, 0.5 M NaCl, 10% glycerol, protease inhibitor cocktail), incubated on ice for 30 min and lysed by high pressure homogenization (PANDA PLUS instrument, 900 bar). The soluble fraction was clarified by centrifugation (16000 RPM, 30 min at 4°C) and incubated with NiNTA resin (Qiagen) for 1 h at 25°C on a rotating wheel. After removing the unbound fraction, the resin was washed with 20 mM imidazole and the recombinant protein subsequently eluted by a single step elution with 500 mM imidazole. Finally, the buffer was exchanged with 25 mM Tris pH 7.4, 150 mM NaCl, 50% glycerol by dialysis and the purified enzyme flash frozen in liquid nitrogen.

4.1.3. Enzymatic assays

Compounds from 10 mM stock solutions were transferred to assay plates by acoustic transfer (EDC Biosystems, Milmont, CA). The TbTR luminescent assay was performed in 384-well white plate (Greiner Bio One, Frickenhausen, Germany). The following components were added to the plates to a final volume of 30 µl: 0.1 nM TR, 20 µM NADPH, 10 µM TS₂ in 50 mM HEPES

pH 7.4, 40 mM NaCl, 0.01% BSA. After 60 min of incubation at room temperature the residual amount of NADPH was measured by addition of an equal volume of NADPH-Glo as per the manufacturer's protocol and the luminescent signal was acquired by an EnVision plate reader (PerkinElmer, Waltham, MA). The DTNB assay was performed in a final volume of 50 μ l by addition of 2 nM TR, 100 μ M NADPH, 4 μ M TS₂ and 200 μ M DTNB in 40 mM HEPES pH 7.4, 1 mM EDTA, 0.01% BSA and 0.05% Tween-20. After 10 minutes of incubation at room temperature the absorbance signal was detected at 412 nm using the Safire2 plate reader (Tecan, Switzerland). The human glutathione reductase (hGR) activity assay was carried out as described by Turcano and coworkers¹¹⁵. Results were analyzed using Prism software (GraphPad, San Diego, CA) and Vortex (Dotmatics, Bioshops Stortford, UK). Dose-response curves were fitted by four-parameter logistic regression.

4.1.4. Competition assay

Competition experiments were performed at two different compound concentrations (5 μ M and 25 μ M) by TbTR luminescent assay. The apparent K_m values for TS₂ in presence of 20 μ M NADPH were calculated using 1 nM TR after 10 min incubation. The signal was revealed by the addition of an equal volume of NADPH-Glo. The luminescent signal was measured using the EnVision plate reader (PerkinElmer, USA). IC₅₀, V_{max}, and K_m values were calculated using Prism software (GraphPad, San Diego, CA).

4.1.5. Surface plasmon resonance experiments

Surface plasmon resonance (SPR) interaction analysis was performed using a Biacore T200 (GE Healthcare, Uppsala, Sweden). TbTR was immobilized on a CM4 chip by amine coupling according to manufacturer's instructions

(Amine Coupling Kit, GE Healthcare, Uppsala, Sweden). Briefly, the surface of the sensor chip was activated for 7 minutes using a mixture of 0.1 M N-hydroxy succinimide (NHS) and 0.4 M N-ethyl-N'-[3-dimethylaminopropyl]carbodiimide (EDC) then 30 µg/ml of Tx3 in 10 mM sodium acetate pH 4.5 was injected for 360 s at 10 µl/min. Finally, residual activated groups on the surface were blocked by a 7 min injection of 1 M ethanolamine pH 8.5. A reference channel for background subtraction was prepared by activation with EDC/NHS mixture (0.1 M/0.4 M as per ligand immobilization), followed by blocking with 1 M ethanolamine. The binding of the selected hit to the immobilized ligand was evaluated by a multi-cycle kinetic procedure in PBS-P (GE Healthcare Lifescience) supplemented with 2% DMSO (Sigma Aldrich). The analyte was injected for 60 s at 50 µl/min until equilibrium and dissociation monitored for 600 s. A standard curve of DMSO was included for solvent correction. Biomolecular binding events were reported as changes of resonance units (RUs) over time. The data were analyzed by the Biacore T200 evaluation software. The sensorgrams were obtained by subtracting the signals of the reference channel to those of the TbTR-immobilized one and corrected for DMSO interference using the DMSO standard curve. The binding affinity was evaluated from kinetic parameters (k_{off}/k_{on}) calculated according to a heterogeneous ligand binding model¹¹⁸.

4.1.6. *T. brucei* growth inhibition assay

The anti-proliferative effect of testing compounds on *T. brucei* in vitro cultures was carried out by incubating compounds with 1.5×10^3 parasites per well followed by a 24 h incubation at 37°C and in presence of 5% CO₂. The parasite viability was measured by CellTiter-Glo according to the manufacturer's instructions.

4.1.7. *T. brucei* lysate thiol formation assay

T. brucei parasites were grown on IMDM medium (Iscove's Modified Dulbecco's Medium) supplied with 3 g/L sodium bicarbonate, 136 mg/L hypoxanthine, 39 mg/L thymidine, 28.2 mg/L bathocuproine sulfonic acid, 0.5 mM cysteine, 0.001% β -mercaptoethanol and 10% heat-inactivated Calf serum. 1.5×10^6 compound treated parasite per well were lysed using 1 mM EDTA, 40 mM HEPES pH 7.5, 50 mM Tris-HCl pH 7.5, 2% Triton-X100 and protease inhibitors cocktail (Sigma). 200 μ M NADPH, 50 μ M TS₂, 100 μ M DTNB were added in each well to trigger the TbTR activity. After 30 min incubation the absorbance signal was detected at 412 nm using the Safire2 plate reader (Tecan, Switzerland).

4.1.8. X-ray structure determination of TbTR-Compound 1 complex

The TbTR-compound 1 complex was crystallized at 294 K by hanging drop vapor diffusion method, using 12 mg/ml TbTR to prepare symmetrical drops (1+1 μ l) equilibrated over a reservoir solution of 500 μ l. Streak seeding and soaking techniques were used. First, TbTR was crystallized according to published conditions¹²² consisting of ammonium sulfate 2.0-2.2 M, HEPES 0.1 M pH 7-8, polyethylene glycol 400 (PEG400) 5% v/v. This condition was used for soaking and co-crystallization but diffraction data did not show compound 1 binding. A tubular density peak, instead, was found in TS₂ binding site and was modeled as PEG400. Streak seeding was then performed in absence of PEG400 aiming at obtaining PEG400-free crystals. Crystals were soaked with a solution containing 10 mM compound 1 and 10% DMSO. After 1 h of soaking, crystals were cryo-protected in 20% glycerol and frozen in liquid N₂. Single wavelength dataset ($\lambda = 0.976254$ Å) was collected at ID23 beamline, at Synchrotron Radiation Source ESRF, Grenoble (France) using a

Dectris Pilatus 6M detector at a temperature of 100 K. The datasets were processed and scaled with XDS ¹²³. The structure was solved by molecular replacement with the program Molrep ¹²⁴ using native TbTR (PDB code: 2WBA) as search model. Refinement was performed using the program REFMAC5 ¹²⁵ and model building was carried out with COOT ¹²⁶.

4.2. LeishBox compounds identification

4.2.1. Expression and purification of trypanothione reductase from *L. infantum*

Coding sequence for LiTR was cloned into a pET28b(+) vector (Novagen, Madison, WI, USA) to obtain LiTR in frame with a hexa-histidine tag at its N-terminus, with a thrombin cleavage site between the histidine tag and the protein sequence and kanamycin as resistance marker. BL21(DE3) strain *E. coli* cells were transformed via heat-shock and grown in LB broth supplied with 30 mg/L kanamycin, at 37 °C for 4 h. Protein expression was induced with 1 mM IPTG, when growth reached an OD₆₀₀ = 0.6, yielding up to 20 mg protein/L of culture. Cells were subsequently harvested and centrifuged; the cellular pellet was resuspended in lysis buffer (20 mM Tris-HCl buffer, pH 7.4, 500 mM NaCl, 5 mM imidazole, 1 mM phenylmethylsulphonyl fluoride (PMSF), 5 U DNase, and 1 tablet of Protease Inhibitor Cocktail (Roche)) and lysed by sonication. LiTR was purified by affinity chromatography on HiTrap-Ni (GE Healthcare, Italy), previously equilibrated with buffer A (20 mM Tris-HCl buffer, pH 7.4, 500 mM NaCl, 5 mM imidazole) before protein loading; elution was carried out with a linear gradient of 5-500 mM imidazole. Purified LiTR was finally dialysed against 20 mM Hepes, pH 7.4 and protein aliquots flash frozen in liquid N₂.

4.2.2. Enzymatic assays

Enzymatic inhibition assays were performed at 20 °C using a diode-array HP8453 spectrophotometer. In order to optimize the assay, different buffers together with different enzyme and substrate concentrations were tried out. The chosen experimental conditions allowed for the determination of specific activity and K_m values for NADPH and TS₂ (K_m , NADPH = 12 μ M; K_m , TS₂ = 72 μ M; k_{cat} , TS₂ = 4800 min^{-1}). LeishBox compounds were firstly tested at a final concentration of 25 μ M. The solution containing buffer 50 mM HEPES pH 7.4, 40 mM NaCl, 5 nM LiTR, 150 μ M TS₂, and 25 μ M inhibitor were allowed to equilibrate for 2 min in a quartz Hellma 104-QS cuvette (final reaction volume = 800 μ L). Assays were initiated by adding 100 μ M NADPH, and its oxidation was followed at 340 nm. Inhibition was calculated for each experiment by measuring the velocity of oxidation of NADPH with respect to the experiments carried out in the absence of the inhibitor. The active compounds (inhibition >80%) were tested at lower concentrations (between 10 and 0.02 μ M) using the same assay, in duplicate, in order to determine compound potency (IC_{50}). To verify selectivity, these inhibitors were also tested on hGR; the experiment was performed, similarly to TR inhibition assay, in the following conditions: 5 nM hGR, 150 μ M GSSG, 25 μ M inhibitor, and the final addition of 100 μ M NADPH, in buffer 50 mM HEPES pH 7.4, 40 mM NaCl. NADPH concentration was calculated using the molar extinction coefficient $\epsilon_{340\text{ nm}} = 6222\text{ M}^{-1}\cdot\text{cm}^{-1}$. TS₂ (Bachem), NADPH (Sigma-Aldrich), hGR (Sigma-Aldrich), and GSSG (Sigma-Aldrich) were used for the experiments.

4.2.3. Surface plasmon resonance experiments

SPR experiments were carried out using a SensiQ Pioneer system. The sensor chip (COOH5) was activated chemically by a 35 μL injection of a 1:1 mixture of EDC (200 mM) and NHS (50 mM) at a flow rate of 5 $\mu\text{L}/\text{min}$. LiTR (at a concentration of 100 nM) was immobilized on activated sensor chips via amine coupling. Immobilizations were carried out in 20 mM sodium acetate at pH 4.5; the remaining groups were blocked by injecting 1 M ethanolamine hydrochloride (35 μL). A total of 800 resonance units (RU) of TR was immobilized onto the chip for the NADPH-dependent oxidation experiment; a total of 3000 RU of TR was immobilized onto the chip for the competitive binding experiment. Compounds interacting with the ligand (in 20 mM Hepes pH 7.4, 150 mM NaCl + 0.005% surfactant P20 + 2% DMSO) were injected at a concentration of 25 μM on the sensor chip at a constant flow (30 $\mu\text{L}/\text{min}$). As a negative control, sensor chips were treated as described above in the absence of immobilized TR. Regeneration procedures are based on two long (2000 and 500 s) injections of buffer, separated by a brief (5 s) injection of 10 mM NaOH. For the competitive binding experiment, TS₂, compounds A1/7 and C10/7 were injected in 20 mM Hepes pH 7.4, 150 mM NaCl + 0.005% surfactant P20 + 2% DMSO, at a concentration of 20 μM on the sensor chip at a constant flow (30 $\mu\text{L}/\text{min}$); in addition, mixtures of compound A1/7 + TS₂ or of compound C10/7 + TS₂, each at a concentration of 20 μM , were injected in the same conditions to test whether the compounds compete with TS₂. The increase in RU relative to the baseline (0-160 s) indicates complex formation, whereas the decrease in RU after 160 s represents the dissociation of compounds and/or TS₂ from the immobilized ligand after injection of the buffer. As a negative control, sensor chips were treated as described above in the absence of immobilized TR. Regeneration procedures were based on two

long (2000 and 500 s) injections of buffer, separated by a brief (5 s) injection of 10 mM NaOH. The sensorgrams were analyzed using the SensiQ Qdat program.

4.2.4. Docking of compounds in the active site of TR

The AutoDock4 docking package was used for ligand flexible docking simulations. The structure of LiTR in oxidized form, downloaded from the protein data bank (PDB code: 2JK6), was set up as the receptor for docking protocol. The .pdb coordinates of compounds A1/7, C5/7, F1/7, and C10/7 were generated using the PRODRG2 server¹²⁷. The LiTR structure was edited using the software from the ADT package to remove all water molecules and add hydrogen atoms. Nonpolar hydrogens and lone pairs were then merged into each atom within the macromolecule, and the ligands were assigned with a Gasteiger partial charge. The .pdbqt files for protein and ligands were generated with ADT. A grid box of $72 \times 42 \times 50$ points, with a spacing of 0.436 Å, was positioned at the active-site gorge. The Lamarckian genetic algorithm (LGA) was employed to run the docking job for each ligand with the maximum number of generations and energy evaluations of 27'000 and 2'500'000, respectively.

4.2.5. X-ray structure determination of TbTR-compound A1/7 complex

The TbTR-A1/7 complex was cocrystallized at 294 K by hanging drop vapor diffusion method, using a solution containing 12 mg/ml TbTR and 2 mM A1/7 to prepare symmetrical drops (1+1 µl) equilibrated over a reservoir solution of 500 µl; additionally, streak seeding was used. Reservoir solutions were prepared using ammonium sulfate 2.0-2.2 M and HEPES 0.1 M pH 7-8. Crystals were cryo-protected in 20% glycerol and frozen in liquid N₂. Single

wavelength dataset ($\lambda = 0.99999 \text{ \AA}$) was collected at XRD2 beamline, at Elettra Sincrotrone Trieste, using a Dectris Pilatus 6M detector at a temperature of 100 K. The datasets were processed and scaled with XDS¹²³. The structure was solved by molecular replacement with the program Molrep¹²⁴ using native TbTR (PDB code: 2WBA) as search model. Refinement was performed using the program REFMAC5¹²⁵ and model building was carried out with COOT¹²⁶.

4.3. Preliminary crystallographic studies for Fragment based screening

Before proceeding with FBS specific requirements must be met:

- robust crystallization condition that yields reproducible high quality crystals (reservoir volume of 30 μL and drop size of 200-600 nL);
- more than 50% of the drops in the plate will have crystals of reasonable diffraction quality (2.6 \AA) and at least 35 μm size;
- consistent diffraction quality of crystals (ideally all crystals tested diffract to 2.6 \AA or better);
- structural accessibility of the site of interest, i.e. the site of interest is not involved in the crystal packing or blocked (source: <https://www.diamond.ac.uk/Instruments/Mx/Fragment-Screening>).

In order to fulfil these conditions, preliminary crystallographic studies have been performed. In sequence, reproducible crystal growth conditions, already reported in literature by Patterson and collaborators⁹⁸, on 96-wells crystallization plates were settled, using as reservoir 20-30% v/v MPD, 10-20% v/v PEG3350 and 40 mM imidazole pH 8. TbTR was concentrated to a

final concentration of 12 mg/mL, in 20 mM Hepes pH 7.5, 50 mM NaBr buffer. 0.3 nL + 0.3 nL sitting drops were prepared by using a Crystal Phoenix robot (ArtRobbins) and let equilibrate against 30 μ L of reservoir; 30-55 μ m crystals grew up in 3-7 days. In order to test diffraction quality, crystals from different drops were sampled (“native” crystals); a number of these were exposed to soaking with various concentrations of DMSO (maximum 10% v/v in reservoir solution) to test crystal resistance. Additionally, the same soaking performed to obtain TR-1 complex structure, reported in section 4.1.8, was conducted, to check if the new crystal packing was consistent with ligand binding. Finally crystals were fished and cryo-cooled in liquid nitrogen; no cryoprotectant was needed as 20-30% MPD already conferred cryoprotection⁹⁸. Single wavelength datasets ($\lambda = 0,99990$ Å) were collected at XRD2 beamline, at Elettra Sincrotrone Trieste, using a Dectris Pilatus 6M detector.

5. CONCLUSIONS AND FUTURE PERSPECTIVES

The modern approach in drug discovery relies on the identification, validation and targeting of specific, unique and druggable molecular target. So far, huge efforts have been made in order to maximize the number of active compounds identified in the lowest time possible, as in the case of large scale HTS or FBS; at the same time computational tools together with biophysical methods, as X-ray crystallography, evolved so fast to make structure-based drug design a primary approach for drug development. These colossal knowledge and technology are now fundamental for the advancement in medicinal chemistry. The line of research on which this work is focused, regards some of the most life-threatening and neglected diseases, globally named Neglected tropical diseases, namely Leishmaniasis, Human Africa trypanosomiasis and American trypanosomiasis. The causative agents are all belonging to the parasitic family of Trypanosomatids and even if phenotypical characteristics are different from species to species, they all share unique and specific molecular features which can be targeted for the identification and development of new broad-spectrum compounds, in order to supersede current therapies, endowed with high toxicity and inefficacy profiles.

With this aim, the trypanothione reductase (TR), a NADPH-dependent flavoenzyme, has been targeted as it fulfills all the requirements to be considered a good drug target: it is unique, as is present only in trypanosomatidal species and absent in the host, essential, playing a central role in the redox equilibrium of parasites and it is druggable, as can be efficiently addressed, and thus inhibited, by specific compounds.

Employing different approaches new active hit compounds against TR have been identified; through an HTS a spiro-containing derivative, Compound 1,

has been fully characterized. Its competitive mechanism of inhibition has been assessed and confirmed by SPR and X-ray crystallography and demonstrated to be able to inhibit the same enzyme from different sources, with selectivity over the human homologue glutathione reductase. The most intriguing feature is represented by its chemotype, which is known to be able to cross the brain-blood barrier, particular important in the treatment of the central nervous system phase of HAT. Simultaneously, screening of the 192 compounds contained in the LeishBox led to a list of seven compounds active against TR from *L. infantum*; SPR experiments and docking predictions, together with a preliminary model of the crystal structure of TR in complex with compound A1/7, assessed the competitive fashion of the inhibition. A1/7 is among the most potent inhibitors identified in the series and is contained also in the HATBox and ChagasBox, setting the basis for a broad-spectrum drug development. For this reason, it has been used as a scaffold for the synthesis of twelve derivatives, which are being tested at this time; three out of twelve display a better and/or comparable affinity with respect to A1/7, providing important information regarding the chemical modifications to be applied to boost affinity. Finally, preliminary crystallographic studies have been performed, in order to fulfil pre-requirements needed for an FBS, to be performed at the Xchem-Screening platform, at Diamond Light Source. Reproducible high-diffracting, DMSO-resistant and ligand accessible crystals have been obtained by setting up an automated protocol.

Future steps are those typical of the hit optimization round; the information so far collected will be used for intense SAR studies in order to obtain more potent and specific inhibitors. Efforts will be carried out in order to acquire structural information *via* X-ray crystallography, to proceed with a structure-based campaign. FBS results will help in designing new scaffolds and

pharmacophores, facilitating the discovery of a single inhibitor for this conserved target.

6. REFERENCES

1. Rang HP. *The Development of the Pharmaceutical Industry*. Second Edi. Elsevier Ltd; 2013. doi:10.1016/B978-0-7020-4299-7.00001-9
2. Rang HP, Hill RG. *The Drug Discovery Process: General Principles and Some Case Histories*. Second Edi. Elsevier Ltd; 2012. doi:10.1016/B978-0-7020-4299-7.00004-4
3. Gashaw I, Ellinghaus P, Sommer A, Asadullah K. What makes a good drug target? *Drug Discov Today*. 2011;16(23-24):1037-1043. doi:10.1016/j.drudis.2011.09.007
4. Arrowsmith J. Trial watch: Phase II failures: 2008-2010. *Nat Rev Drug Discov*. 2011;10(5):328-329. doi:10.1038/nrd3439
5. Hughes JP, Rees SS, Kalindjian SB, Philpott KL. Principles of early drug discovery. *Br J Pharmacol*. 2011;162(6):1239-1249. doi:10.1111/j.1476-5381.2010.01127.x
6. Egner U, Krätzschar J, Kreft B, Pohlenz HD, Schneider M. The target discovery process. *ChemBioChem*. 2005;6(3):468-479. doi:10.1002/cbic.200400158
7. Cronk D. *High-Throughput Screening*. Second Edi. Elsevier Ltd; 2013. doi:10.1016/B978-0-7020-4299-7.00008-1
8. Keseru GM, Makara GM. Hit discovery and hit-to-lead approaches. *Drug Discov Today*. 2006;11(15-16):741-748. doi:10.1016/j.drudis.2006.06.016
9. Lipinski CA, Lombardo F, Dominy BW, Feeney PJ. Experimental and computational approaches to estimate solubility and permeability in

- drug discovery and development settings. *Adv Drug Deliv Rev.* 1997;23(1-3):3-25. doi:10.1016/S0169-409X(96)00423-1
10. Congreve M, Carr R, Murray C, Jhoti H. A 'Rule of Three' for fragment-based lead discovery? *Drug Discov Today.* 2003;8(19):876-877. doi:10.1016/S1359-6446(03)02831-9
 11. Ghose AK, Viswanadhan VN, Wendoloski JJ. A knowledge-based approach in designing combinatorial or medicinal chemistry libraries for drug discovery. 1. A qualitative and quantitative characterization of known drug databases. *J Comb Chem.* 1999;1(1):55-68. doi:10.1021/cc9800071
 12. Veber DF, Johnson SR, Cheng H-Y, Smith BR, Ward KW, Kopple KD. Molecular properties that influence the oral bioavailability of drug candidates. *J Med Chem.* 2002;45(12):2615-2623. doi:10.1021/jm020017n
 13. Zhang J-H, Chung TDY, Oldenburg KR. A Simple Statistical Parameter for Use in Evaluation and Validation of High Throughput Screening Assays. *J Biomol Screen.* 1999;4(2):67-73. doi:10.1177/108705719900400206
 14. Congreve M, Chessari G, Tisi D, Woodhead AJ. Recent developments in fragment-based drug discovery. *J Med Chem.* 2008;51(13):3661-3680. doi:10.1021/jm8000373
 15. Saur M, Hartshorn MJ, Dong J, et al. Fragment-based drug discovery using cryo-EM. *Drug Discov Today.* 2020;25(3):485-490. doi:10.1016/j.drudis.2019.12.006

16. Anderson AC. The Process of Structure-Based Drug Design. *Chem Biol.* 2003;10(9):787-797. doi:10.1016/j.chembiol.2003.09.002
17. Rang HP, Hill RG. *Choosing the Project*. Second Edi. Elsevier Ltd; 2013. doi:10.1016/B978-0-7020-4299-7.00005-6
18. Simpson AGB, Stevens JR, Lukeš J. The evolution and diversity of kinetoplastid flagellates. *Trends Parasitol.* 2006;22(4):168-174. doi:10.1016/j.pt.2006.02.006
19. Burza S, Croft SL, Boelaert M. Leishmaniasis. *Lancet.* 2018;392(10151):951-970. doi:10.1016/S0140-6736(18)31204-2
20. Sundar S, Chakravarty J. Antimony toxicity. *Int J Environ Res Public Health.* 2010;7(12):4267-4277. doi:10.3390/ijerph7124267
21. Ritmeijer K, Veeken H, Melaku Y, et al. Ethiopian visceral leishmaniasis: Generic and proprietary sodium stibogluconate are equivalent; HIV co-infected patients have a poor outcome. *Trans R Soc Trop Med Hyg.* 2001;95(6):668-672. doi:10.1016/S0035-9203(01)90110-5
22. Sundar S, More DK, Singh MK, et al. Failure of pentavalent antimony in visceral leishmaniasis in India: Report from the center of the Indian epidemic. *Clin Infect Dis.* 2000;31(4):1104-1107. doi:10.1086/318121
23. World Health Organization. Control of the leishmaniases. *World Health Organ Tech Rep Ser.* 2010;(949):22-26.
24. van Griensven J, Balasegaram M, Meheus F, Alvar J, Lynen L, Boelaert M. Combination therapy for visceral leishmaniasis. *Lancet Infect Dis.* 2010;10(3):184-194. doi:10.1016/S1473-3099(10)70011-6

25. Dorlo TPC, Huitema ADR, Beijnen JH, De Vries PJ. Optimal dosing of miltefosine in children and adults with visceral leishmaniasis. *Antimicrob Agents Chemother.* 2012;56(7):3864-3872. doi:10.1128/AAC.00292-12
26. Kimutai R, Musa AM, Njoroge S, et al. Safety and Effectiveness of Sodium Stibogluconate and Paromomycin Combination for the Treatment of Visceral Leishmaniasis in Eastern Africa: Results from a Pharmacovigilance Programme. *Clin Drug Investig.* 2017;37(3):259-272. doi:10.1007/s40261-016-0481-0
27. Balasegaram M, Ritmeijer K, Lima MA, Burza S. Liposomal amphotericin B as a treatment for human leishmaniasis. *Expert Opin Emerg Drugs.* Published online 2012:493-510.
28. Sundar S, Chakravarty J, Agarwal D, Rai M, Murray HW. Single-Dose Liposomal Amphotericin B for Visceral Leishmaniasis in India. *N Engl J Med.* 2010;362(6):504-512. doi:10.1056/NEJMoa0903627
29. Büscher P, Cecchi G, Jamonneau V, Priotto G. Human African trypanosomiasis. *Lancet.* 2017;390(10110):2397-2409. doi:10.1016/S0140-6736(17)31510-6
30. Simarro PP, Cecchi G, Paone M, et al. The Atlas of human African trypanosomiasis: A contribution to global mapping of neglected tropical diseases. *Int J Health Geogr.* 2010;9(1):57. doi:10.1186/1476-072X-9-57
31. Jamonneau V, Ilboudo H, Kaboré J, et al. Untreated human infections by trypanosoma brucei gambiense are not 100% fatal. *PLoS Negl Trop Dis.* 2012;6(6). doi:10.1371/journal.pntd.0001691

32. Odiit M, Kansiime F, Enyary JC. Duration of symptoms and case fatality of sleeping sickness caused by *Trypanosoma brucei rhodesiense* in Tororo, Uganda. *East Afr Med J*. 1997;74:792—795. <http://europepmc.org/abstract/MED/9557424>
33. Checchi F, Filipe JAN, Barrett MP, Chandramohan D. The natural progression of gambiense sleeping sickness: What is the evidence? *PLoS Negl Trop Dis*. 2008;2(12). doi:10.1371/journal.pntd.0000303
34. Pohlig G, Bernhard SC, Blum J, et al. Efficacy and Safety of Pafuramidine versus Pentamidine Maleate for Treatment of First Stage Sleeping Sickness in a Randomized, Comparator-Controlled, International Phase 3 Clinical Trial. *PLoS Negl Trop Dis*. 2016;10(2):1-17. doi:10.1371/journal.pntd.0004363
35. Priotto G, Kasparian S, Mutombo W, et al. Nifurtimox-eflornithine combination therapy for second-stage African *Trypanosoma brucei gambiense* trypanosomiasis: a multicentre, randomised, phase III, non-inferiority trial. *Lancet*. 2009;374(9683):56-64. doi:10.1016/S0140-6736(09)61117-X
36. Franco J, Pere S, Diarra, Ruiz-Postigo, Samo, Jannin. Monitoring the use of nifurtimox-eflornithine combination therapy (NECT) in the treatment of second stage gambiense human African trypanosomiasis. *Res Rep Trop Med*. Published online 2012:93. doi:10.2147/rrtm.s34399
37. Lutje V, Seixas J, Kennedy A. Chemotherapy for second-stage Human African trypanosomiasis. *Cochrane Database Syst Rev*. 2013;2013(6). doi:10.1002/14651858.CD006201.pub3

38. Alirol E, Schruppf D, Amici Heradi J, et al. Nifurtimox-eflornithine combination therapy for second-stage gambiense human African trypanosomiasis: Médecins Sans Frontières experience in the Democratic Republic of the Congo. *Clin Infect Dis*. 2013;56(2):195-203. doi:10.1093/cid/cis886
39. Balasegaram M, Harris S, Checchi F, Hamel C, Karunakara U. Treatment outcomes and risk factors for relapse in patients with early-stage human African trypanosomiasis (HAT) in the Republic of the Congo. *Bull World Health Organ*. 2006;84(10):777-782. doi:10.2471/BLT.05.028399
40. Pérez-Molina JA, Molina I. Chagas disease. *Lancet*. 2018;391(10115):82-94. doi:10.1016/S0140-6736(17)31612-4
41. WHO. First WHO report on neglected tropical diseases: working to overcome the global impact of neglected tropical diseases. *World Health Organ*. Published online 2010:1-184. doi:10.1177/1757913912449575
42. Riarte A, Luna C, Sabatiello R, et al. Chagas' disease in patients with kidney transplants: 7 years of experience 1989-1996. *Clin Infect Dis*. 1999;29(3):561-567. doi:10.1086/598634
43. Huprikar S, Bosserman E, Patel G, et al. Donor-derived *Trypanosoma cruzi* infection in solid organ recipients in the United States, 2001-2011. *Am J Transplant*. 2013;13(9):2418-2425. doi:10.1111/ajt.12340
44. Chin-Hong P V., Schwartz BS, Bern C, et al. Screening and treatment of chagas disease in organ transplant recipients in the United States: Recommendations from the chagas in transplant working group. *Am J Transplant*. 2011;11(4):672-680. doi:10.1111/j.1600-

6143.2011.03444.x

45. Kun H, Moore A, Mascola L, et al. Transmission of *Trypanosoma cruzi* by heart transplantation. *Clin Infect Dis*. 2009;48(11):1534-1540. doi:10.1086/598931
46. Chagas' Disease Argentine Collaborative Transplant Consortium, Casadei D. Chagas' disease and solid organ transplantation. *Transplant Proc*. 2010;42(9):3354-3359. doi:10.1016/j.transproceed.2010.09.019
47. Wegner DH, Rohwedder RW. The effect of nifurtimox in acute Chagas' infection. *Arzneimittelforschung*. 1972;22(9):1624-1635. <http://www.ncbi.nlm.nih.gov/pubmed/4630485>
48. DIAS E, LARANJA FS, MIRANDA A, NOBREGA G. Chagas' disease; a clinical, epidemiologic, and pathologic study. *Circulation*. 1956;14(6):1035-1060. doi:10.1161/01.cir.14.6.1035
49. Pinto AY das N, Valente SA, Valente V da C, Ferreira Junior AG, Coura JR. Fase aguda da doença de Chagas na Amazônia brasileira: estudo de 233 casos do Pará, Amapá e Maranhão observados entre 1988 e 2005. *Rev Soc Bras Med Trop*. 2008;41(6):602-614. doi:10.1590/S0037-86822008000600011
50. Dias JCP. The indeterminate form of human chronic Chagas' disease: a clinical epidemiological review. *Rev Soc Bras Med Trop*. 1989;22(3):147-156. doi:10.1590/S0037-86821989000300007
51. Oms. CONTROL OF CHAGAS DISEASE Second report of the WHO Expert Committee World Health Organization. *WHO Technical*

Report Series. 2002;905:1-109.

52. Coura JR, Abreu LL de, Pereira JB, Willcox HP. Morbidade da doença de Chagas: IV. Estudo longitudinal de dez anos em Pains e Iguatama, Minas Gerais, Brasil. *Mem Inst Oswaldo Cruz*. 1985;80(1):73-80. doi:10.1590/S0074-02761985000100011
53. Viotti R, Vigliano C, Lococo B, et al. Long-term cardiac outcomes of treating chronic Chagas disease with benznidazole versus no treatment: a nonrandomized trial. *Ann Intern Med*. 2006;144(10):724-734. doi:10.7326/0003-4819-144-10-200605160-00006
54. Sabino EC, Ribeiro AL, Salemi VMC, et al. Ten-Year Incidence of Chagas Cardiomyopathy Among Asymptomatic *Trypanosoma cruzi* – Seropositive Former Blood Donors. *Circulation*. 2013;127(10):1105-1115. doi:10.1161/CIRCULATIONAHA.112.123612
55. Machado-de-Assis GF, Diniz GA, Montoya RA, et al. A serological, parasitological and clinical evaluation of untreated Chagas disease patients and those treated with benznidazole before and thirteen years after intervention. *Mem Inst Oswaldo Cruz*. 2013;108(7):873-880. doi:10.1590/0074-0276130122
56. Pérez-Ayala A, Pérez-Molina JA, Norman F, et al. Chagas disease in Latin American migrants: A Spanish challenge. *Clin Microbiol Infect*. 2011;17(7):1108-1113. doi:10.1111/j.1469-0691.2010.03423.x
57. Salvador F, Treviño B, Sulleiro E, et al. *Trypanosoma cruzi* infection in a non-endemic country: Epidemiological and clinical profile. *Clin Microbiol Infect*. 2014;20(7):706-712. doi:10.1111/1469-0691.12443

58. Rassi Jr A, Rassi SG, Rassi A. Sudden death in Chagas' disease. *Arq Bras Cardiol.* 2001;76(1). doi:10.1590/S0066-782X2001000100008
59. Bern C, Montgomery SP, Herwaldt BL, et al. Evaluation and treatment of chagas disease in the United States: A systematic review. *J Am Med Assoc.* 2007;298(18):2171-2181. doi:10.1001/jama.298.18.2171
60. Andrade JP de, Marin Neto JA, Paola AAV de, et al. I Diretriz Latino-Americana para o diagnóstico e tratamento da cardiopatia chagásica: resumo executivo. *Arq Bras Cardiol.* 2011;96(6):434-442. doi:10.1590/S0066-782X2011000600002
61. Coura JR, Castro SL de. A Critical Review on Chagas Disease Chemotherapy. *Mem Inst Oswaldo Cruz.* 2002;97(1):3-24. doi:10.1590/S0074-02762002000100001
62. Streiger ML, Barco ML del, Fabbro DL, Arias ED, Amicone NA. Estudo longitudinal e quimioterapia específica em crianças, com doença de Chagas crônica, residentes em área de baixa endemicidade da República Argentina. *Rev Soc Bras Med Trop.* 2004;37(5):365-375. doi:10.1590/S0037-86822004000500001
63. Jackson Y, Alirol E, Getaz L, Wolff H, Combescure C, Chappuis F. Tolerance and safety of nifurtimox in patients with chronic Chagas disease. *Clin Infect Dis.* 2010;51(10):6-12. doi:10.1086/656917
64. Russomando G, De Tomassone MMC, De Guillen I, et al. Treatment of congenital chagas' disease diagnosed and followed up by the polymerase chain reaction. *Am J Trop Med Hyg.* 1998;59(3):487-491. doi:10.4269/ajtmh.1998.59.487

65. Schijman AG, Altcheh J, Burgos JM, et al. Aetiological treatment of congenital Chagas' disease diagnosed and monitored by the polymerase chain reaction. *J Antimicrob Chemother.* 2003;52(3):441-449. doi:10.1093/jac/dkg338
66. Cançado JR. Criteria of Chagas disease cure. *Mem Inst Oswaldo Cruz.* 1999;94(suppl 1):331-335. doi:10.1590/S0074-02761999000700064
67. Estani SS, Segura EL, Ruiz AM, Velazquez E, Porcel BM, Yampotis C. Efficacy of chemotherapy with benznidazole in children in the indeterminate phase of Chagas' disease. *Am J Trop Med Hyg.* 1998;59(4):526-529. doi:10.4269/ajtmh.1998.59.526
68. de Andrade AL, Zicker F, de Oliveira RM, et al. Randomised trial of efficacy of benznidazole in treatment of early *Trypanosoma cruzi* infection. *Lancet (London, England).* 1996;348(9039):1407-1413. doi:10.1016/s0140-6736(96)04128-1
69. Yun O, Lima MA, Ellman T, et al. Feasibility, drug safety, and effectiveness of etiological treatment programs for Chagas disease in Honduras, Guatemala, and Bolivia: 10-Year experience of Médecins Sans Frontières. *PLoS Negl Trop Dis.* 2009;3(7):1-8. doi:10.1371/journal.pntd.0000488
70. Fabbro DL, Streiger ML, Arias ED, Bizai ML, Del Barco M, Amicone NA. Trypanocide treatment among adults with chronic Chagas disease living in Santa Fe City (Argentina), over a mean follow-up of 21 years: Parasitological, serological and clinical evolution. *Rev Soc Bras Med Trop.* 2007;40(1):1-10. doi:10.1590/s0037-86822007000100001
71. Ilari A, Genovese I, Fiorillo F, et al. Toward a Drug Against All

- Kinetoplastids: From LeishBox to Specific and Potent Trypanothione Reductase Inhibitors. *Mol Pharm.* 2018;15(8):3069-3078.
doi:10.1021/acs.molpharmaceut.8b00185
72. Fairlamb A, Blackburn P, Ulrich P, Chait B, Cerami A. Trypanothione: a novel bis(glutathionyl)spermidine cofactor for glutathione reductase in trypanosomatids. *Science (80-)*. 1985;227(4693):1485-1487. doi:10.1126/science.3883489
73. Tabor H, Tabor CW. Glutathionylspermidine in Escherichia coli. *Ital J Biochem.* 1974;25(1):70-76.
<http://www.ncbi.nlm.nih.gov/pubmed/773896>
74. Comini MA, Flohé L. Trypanothione-Based Redox Metabolism of Trypanosomatids. *Trypanos Dis Mol Routes to Drug Discov.* Published online 2013:167-199. doi:10.1002/9783527670383.ch9
75. Krauth-Siegel RL, Comini MA. Redox control in trypanosomatids, parasitic protozoa with trypanothione-based thiol metabolism. *Biochim Biophys Acta - Gen Subj.* 2008;1780(11):1236-1248.
doi:10.1016/j.bbagen.2008.03.006
76. Krauth-Siegel RL, Leroux AE. Low-Molecular-Mass Antioxidants in Parasites. *Antioxid Redox Signal.* 2012;17(4):583-607.
doi:10.1089/ars.2011.4392
77. Manta B, Bonilla M, Fiestas L, et al. Polyamine-Based Thiols in Trypanosomatids: Evolution, Protein Structural Adaptations, and Biological Functions. *Antioxidants Redox Signal.* 2018;28(6):463-486.
doi:10.1089/ars.2017.7133

78. Ivens AC. The Genome of the Kinetoplastid Parasite, *Leishmania major*. *Science* (80-). 2005;309(5733):436-442.
doi:10.1126/science.1112680
79. El-Sayed NM. The Genome Sequence of *Trypanosoma cruzi*, Etiologic Agent of Chagas Disease. *Science* (80-). 2005;309(5733):409-415. doi:10.1126/science.1112631
80. O'Neill EC, Trick M, Hill L, et al. The transcriptome of *Euglena gracilis* reveals unexpected metabolic capabilities for carbohydrate and natural product biochemistry. *Mol Biosyst*. 2015;11(10):2808-2820.
doi:10.1039/C5MB00319A
81. Montrichard F, Le Guen F, Laval-Martin DL, Davioud-Charvet E. Evidence for the co-existence of glutathione reductase and trypanothione reductase in the non-trypanosomatid Euglenozoa: *Euglena gracilis* Z. *FEBS Lett*. 1999;442(1):29-33. doi:10.1016/S0014-5793(98)01606-8
82. Couto N, Wood J, Barber J. The role of glutathione reductase and related enzymes on cellular redox homeostasis network. *Free Radic Biol Med*. 2016;95:27-42. doi:10.1016/j.freeradbiomed.2016.02.028
83. Ilari A, Fiorillo A, Baiocco P, Poser E, Angiulli G, Colotti G. Targeting Polyamine Metabolism for Finding New Drugs Against Leishmaniasis: A Review. *Mini-Reviews Med Chem*. 2015;15(3):243-252. doi:10.2174/138955751503150312141044
84. Fyfe PK, Oza SL, Fairlamb AH, Hunter WN. *Leishmania* trypanothione synthetase-amidase structure reveals a basis for regulation of conflicting synthetic and hydrolytic activities. *J Biol*

- Chem.* 2008;283(25):17672-17680. doi:10.1074/jbc.M801850200
85. Colotti G, Ilari A. Polyamine metabolism in Leishmania: From arginine to trypanothione. *Amino Acids.* 2011;40(2):269-285. doi:10.1007/s00726-010-0630-3
 86. Battista T, Colotti G, Ilari A, Fiorillo A. Targeting trypanothione reductase, a key enzyme in the redox trypanosomatid metabolism, to develop new drugs against leishmaniasis and trypanosomiasis. *Molecules.* 2020;25(8). doi:10.3390/molecules25081924
 87. Fiorillo A, Colotti G, Boffi A, Baiocco P, Ilari A. The Crystal Structures of the Tryparedoxin-Tryparedoxin Peroxidase Couple Unveil the Structural Determinants of Leishmania Detoxification Pathway. *PLoS Negl Trop Dis.* 2012;6(8). doi:10.1371/journal.pntd.0001781
 88. Wood ZA. Peroxiredoxin Evolution and the Regulation of Hydrogen Peroxide Signaling. *Science (80-).* 2003;300(5619):650-653. doi:10.1126/science.1080405
 89. Alphey MS, Leonard GA, Gourley DG, Tetaud E, Fairlamb AH, Hunter WN. The high resolution crystal structure of recombinant *Crithidia fasciculata* tryparedoxin-I. *J Biol Chem.* 1999;274(36):25613-25622. doi:10.1074/jbc.274.36.25613
 90. Krauth-Siegel RL, Meiering SK, Schmidt H. The parasite-specific trypanothione metabolism of trypanosoma and leishmania. *Biol Chem.* 2003;384(4):539-549. doi:10.1515/BC.2003.062
 91. Dormeyer M, Reckenfelderbäumer N, Lüdemann H, Krauth-Siegel

- RL. Trypanothione-dependent Synthesis of Deoxyribonucleotides by Trypanosoma brucei Ribonucleotide Reductase. *J Biol Chem.* 2001;276(14):10602-10606. doi:10.1074/jbc.M010352200
92. Gilbert HF. Molecular and Cellular Aspects of Thiol-Disulfide Exchange. In: ; 2006:69-172. doi:10.1002/9780470123096.ch2
93. Tovar J, Cunningham ML, Smith AC, Croft SL, Fairlamb AH. Down-regulation of Leishmania donovani trypanothione reductase by heterologous expression of a trans-dominant mutant homologue: Effect on parasite intracellular survival. *Proc Natl Acad Sci U S A.* 1998;95(9):5311-5316. doi:10.1073/pnas.95.9.5311
94. Krieger S, Schwarz W, Arlyanayagam MR, Fairlamb AH, Krauth-Siegel RL, Clayton C. Trypanosomes lacking trypanothione reductase are avirulent and show increased sensitivity to oxidative stress. *Mol Microbiol.* 2000;35(3):542-552. doi:10.1046/j.1365-2958.2000.01721.x
95. Baiocco P, Colotti G, Franceschini S, Ilari A. Molecular basis of antimony treatment in Leishmaniasis. *J Med Chem.* 2009;52(8):2603-2612. doi:10.1021/jm900185q
96. Cunningham ML, Fairlamb AH. Trypanothione Reductase from Leishmania donovani. Purification, Characterisation and Inhibition by Trivalent Antimonials. *Eur J Biochem.* 1995;230(2):460-468. doi:10.1111/j.1432-1033.1995.tb20583.x
97. De Gasparo R, Halgas O, Harangozo D, et al. Targeting a Large Active Site: Structure-Based Design of Nanomolar Inhibitors of Trypanosoma brucei Trypanothione Reductase. *Chem - A Eur J.*

2019;25(49):11416-11421. doi:10.1002/chem.201901664

98. Patterson S, Alphey MS, Jones DC, et al. Dihydroquinazolines as a novel class of Trypanosoma brucei trypanothione reductase inhibitors: Discovery, synthesis, and characterization of their binding mode by protein crystallography. *J Med Chem*. 2011;54(19):6514-6530. doi:10.1021/jm200312v
99. Persch E, Bryson S, Todoroff NK, et al. Binding to large enzyme pockets: Small-molecule inhibitors of trypanothione reductase. *ChemMedChem*. 2014;9(8):1880-1891. doi:10.1002/cmcd.201402032
100. Revuelto A, Ruiz-Santaquiteria M, De Lucio H, et al. Pyrrolopyrimidine vs Imidazole-Phenyl-Thiazole Scaffolds in Nonpeptidic Dimerization Inhibitors of Leishmania infantum Trypanothione Reductase. *ACS Infect Dis*. 2019;5(6):873-891. doi:10.1021/acsinfecdis.8b00355
101. *Mepacrine.*; 2012. <http://www.ncbi.nlm.nih.gov/pubmed/31643202>
102. Jacoby EM, Schlichting I, Lantwin CB, Kabsch W, Krauth-Siegel RL. Crystal structure of the Trypanosoma cruzi trypanothione reductase·mepacrine complex. *Proteins Struct Funct Genet*. 1996;24(1):73-80. doi:10.1002/(SICI)1097-0134(199601)24:1<73::AID-PROT5>3.0.CO;2-P
103. Saravanamuthu A, Vickers TJ, Bond CS, Peterson MR, Hunter WN, Fairlamb AH. Two interacting binding sites for quinacrine derivatives in the active site of trypanothione reductase: A template for drug design. *J Biol Chem*. 2004;279(28):29493-29500. doi:10.1074/jbc.M403187200

104. Baiocco P, Poce G, Alfonso S, et al. Inhibition of *Leishmania infantum* trypanothione reductase by azole-based compounds: A comparative analysis with its physiological substrate by x-ray crystallography. *ChemMedChem*. 2013;8(7):1175-1183. doi:10.1002/cmdc.201300176
105. Richardson JL, Nett IRE, Jones DC, Abdille MH, Gilbert IH, Fairlamb AH. Improved tricyclic inhibitors of trypanothione reductase by screening and chemical synthesis. *ChemMedChem*. 2009;4(8):1333-1340. doi:10.1002/cmdc.200900097
106. Patterson S, Jones DC, Shanks EJ, et al. Synthesis and evaluation of 1-(1-(benzo[b]thiophen-2-yl)cyclohexyl) piperidine (BTCP) analogues as inhibitors of trypanothione reductase. *ChemMedChem*. 2009;4(8):1341-1353. doi:10.1002/cmdc.200900098
107. Eberle C, Lauber BS, Fankhauser D, et al. Improved Inhibitors of Trypanothione Reductase by Combination of Motifs: Synthesis, Inhibitory Potency, Binding Mode, and Antiprotozoal Activities. *ChemMedChem*. 2011;6(2):292-301. doi:10.1002/cmdc.201000420
108. De Gasparo R, Brodbeck-Persch E, Bryson S, et al. Biological Evaluation and X-ray Co-crystal Structures of Cyclohexylpyrrolidine Ligands for Trypanothione Reductase, an Enzyme from the Redox Metabolism of *Trypanosoma*. *ChemMedChem*. 2018;13(9):957-967. doi:10.1002/cmdc.201800067
109. Saccoliti F, Angiulli G, Pupo G, et al. Inhibition of *Leishmania infantum* trypanothione reductase by diaryl sulfide derivatives. *J Enzyme Inhib Med Chem*. 2017;32(1):304-310.

doi:10.1080/14756366.2016.1250755

110. Stump B, Eberle C, Kaiser M, Brun R, Krauth-Siegel RL, Diederich F. Diaryl sulfide-based inhibitors of trypanothione reductase: inhibition potency, revised binding mode and antiprotozoal activities. *Org Biomol Chem*. 2008;6(21):3935. doi:10.1039/b806371k
111. Baiocco P, Colotti G, Franceschini S, Ilari A. Molecular Basis of Antimony Treatment in Leishmaniasis †. *J Med Chem*. 2009;52(8):2603-2612. doi:10.1021/jm900185q
112. Baiocco P, Ilari A, Ceci P, et al. Inhibitory Effect of Silver Nanoparticles on Trypanothione Reductase Activity and Leishmania infantum Proliferation. *ACS Med Chem Lett*. 2011;2(3):230-233. doi:10.1021/ml1002629
113. Ilari A, Baiocco P, Messori L, et al. A gold-containing drug against parasitic polyamine metabolism: the X-ray structure of trypanothione reductase from Leishmania infantum in complex with auranofin reveals a dual mechanism of enzyme inhibition. *Amino Acids*. 2012;42(2-3):803-811. doi:10.1007/s00726-011-0997-9
114. Colotti G, Ilari A, Fiorillo A, et al. Metal-Based Compounds as Prospective Antileishmanial Agents: Inhibition of Trypanothione Reductase by Selected Gold Complexes. *ChemMedChem*. Published online August 23, 2013:n/a-n/a. doi:10.1002/cmdc.201300276
115. Turcano L, Torrente E, Missineo A, et al. Identification and binding mode of a novel Leishmania Trypanothione reductase inhibitor from high throughput screening. Kortagere S, ed. *PLoS Negl Trop Dis*. 2018;12(11):e0006969. doi:10.1371/journal.pntd.0006969

116. Peña I, Pilar Manzano M, Cantizani J, et al. New compound sets identified from high throughput phenotypic screening against three kinetoplastid parasites: An open resource. *Sci Rep.* 2015;5. doi:10.1038/srep08771
117. Hamilton CJ, Saravanamuthu A, Eggleston IM, Fairlamb AH. Ellman's-reagent-mediated regeneration of trypanothione in situ: substrate-economical microplate and time-dependent inhibition assays for trypanothione reductase. *Biochem J.* 2003;369(Pt 3):529-537. doi:10.1042/BJ20021298
118. Edwards PR, Gill A, Pollard-Knight D V, et al. Kinetics of protein-protein interactions at the surface of an optical biosensor. *Anal Biochem.* 1995;231(1):210-217. doi:10.1006/abio.1995.1522
119. Leung K. *3-N-(2-[18F]Fluoroethyl)Spiperone.*; 2004. <http://www.ncbi.nlm.nih.gov/pubmed/20641672>
120. Spanarello S, La Ferla T. The pharmacokinetics of long-acting antipsychotic medications. *Curr Clin Pharmacol.* 2014;9(3):310-317. doi:10.2174/15748847113089990051
121. Morley JO, Matthews TP. Structure-activity relationships in nitrothiophenes. *Bioorg Med Chem.* 2006;14(23):8099-8108. doi:10.1016/j.bmc.2006.07.032
122. Jones DC, Ariza A, Chow W-HA, Oza SL, Fairlamb AH. Comparative structural, kinetic and inhibitor studies of *Trypanosoma brucei* trypanothione reductase with *T. cruzi*. *Mol Biochem Parasitol.* 2010;169(1):12-19. doi:10.1016/j.molbiopara.2009.09.002

123. Kabsch W. XDS. *Acta Crystallogr D Biol Crystallogr*. 2010;66(Pt 2):125-132. doi:10.1107/S0907444909047337
124. Vagin A, Teplyakov A. Molecular replacement with MOLREP. *Acta Crystallogr D Biol Crystallogr*. 2010;66(Pt 1):22-25. doi:10.1107/S0907444909042589
125. Murshudov GN, Vagin AA, Dodson EJ. Refinement of macromolecular structures by the maximum-likelihood method. *Acta Crystallogr D Biol Crystallogr*. 1997;53(Pt 3):240-255. doi:10.1107/S0907444996012255
126. Emsley P, Lohkamp B, Scott WG, Cowtan K. Features and development of Coot. *Acta Crystallogr D Biol Crystallogr*. 2010;66(Pt 4):486-501. doi:10.1107/S0907444910007493
127. Schüttelkopf AW, van Aalten DMF. PRODRG: a tool for high-throughput crystallography of protein-ligand complexes. *Acta Crystallogr D Biol Crystallogr*. 2004;60(Pt 8):1355-1363. doi:10.1107/S0907444904011679

7. ACKNOWLEDGEMENTS

At the end of a journey it is difficult to settle down and recollect; the last three years have been particularly intense. Looking back at the experiences, the persons met, the achievements and failures, everything seems to blend into a melting pot of feelings and considerations, suggesting that at least a minimal portion of life is ruled by our decisions, and I have been extremely lucky to have the chance to take certain.

I am truly grateful to Dr. Gianni Colotti for being my supervisor; his lab has been my shelter for five years.

Everything would not have tasted the same without my mates Ilaria, Valerio and Stefano, as the time, fears and happiness shared together welded our complementarity, the key of our rare, precious and meaningful equilibrium.

My gratitude is for Dr. Annarita Fiorillo, for her unbearable, relentless passion that I always intended as the clue to overstep the shallowness of things.

I owe the most to Dr. Andrea Ilari, for the constant respect he always showed to me, my sacrifices and my growth, for his continuous guidance and trust that always pushed me to improve; ultimately, for being a true, authentic mentor.

8. LIST OF PUBLISHED PAPERS

- ❖ Turcano, L., Battista, T., De Haro, E. T., Missineo, A., Alli, C., Paonessa, G., Colotti, G., Harper, S., Fiorillo, A., Ilari, A., & Bresciani, A. (2020). **Spiro-containing derivatives show antiparasitic activity against trypanosoma brucei through inhibition of the trypanothione reductase enzyme.** *PLoS Neglected Tropical Diseases*, *14*(5), 1–17.
- ❖ Battista, T., Colotti, G., Ilari, A., & Fiorillo, A. (2020). **Targeting Trypanothione Reductase, a Key Enzyme in the Redox Trypanosomatid Metabolism, to Develop New Drugs against Leishmaniasis and Trypanosomiases.** *Molecules*, *25*(8), 1924.
- ❖ Colotti, G., Saccoliti, F., Gramiccia, M., Di Muccio, T., Prakash, J., Yadav, S., Dubey, V. K., Vistoli, G., Battista, T., Mocci, S., Fiorillo, A., Bibi, A., Madia, V. N., Messore, A., Costi, R., Di Santo, R., & Ilari, A. (2020). **Structure-guided approach to identify a novel class of anti-leishmaniasis diaryl sulfide compounds targeting the trypanothione metabolism.** *Amino Acids*, *52*(2), 247–259.
- ❖ Ilari, A., Genovese, I., Fiorillo, F., Battista, T., De Ionna, I., Fiorillo, A., & Colotti, G. (2018). **Toward a Drug Against All Kinetoplastids: From LeishBox to Specific and Potent Trypanothione Reductase Inhibitors.** *Molecular Pharmaceutics*, *15*(8), 3069–3078.

- ❖ Ortalli, M., Ilari, A., Colotti, G., De Ionna, I., Battista, T., Bisi, A., Gobbi, S., Rampa, A., Di Martino, R. M. C., Gentilomi, G. A., Varani, S., & Belluti, F. (2018). **Identification of chalcone-based antileishmanial agents targeting trypanothione reductase.** *European Journal of Medicinal Chemistry*, *152*, 527–541.

Published papers on PhD side projects

- ❖ Genovese, I., Carotti, A., Ilari, A., Fiorillo, A., Battista, T., Colotti, G., & Ivarsson, Y. (2020). **Profiling calcium-dependent interactions between Sorcin and intrinsically disordered regions of human proteome.** *Biochimica et Biophysica Acta (BBA) - General Subjects*, *1864*(8), 129618.
- ❖ Battista, T., Fiorillo, A., Chiarini, V., Genovese, I., Ilari, A., & Colotti, G. (2020). **Roles of Sorcin in Drug Resistance in Cancer: One Protein, Many Mechanisms, for a Novel Potential Anticancer Drug Target.** *Cancers*, *12*(4), 887.
- ❖ Genovese, I., Giamogante, F., Barazzuol, L., Battista, T., Fiorillo, A., Vicario, M., D'Alessandro, G., Cipriani, R., Limatola, C., Rossi, D., Sorrentino, V., Poser, E., Mosca, L., Squitieri, F., Perluigi, M., Arena, A., van Petegem, F., Tito, C., Fazi, F., ... Colotti, G. (2020). **Sorcin is an early marker of neurodegeneration, Ca²⁺ dysregulation and endoplasmic reticulum stress associated to neurodegenerative diseases.** *Cell Death & Disease*, *11*(10), 861.

9. ATTACHMENTS

RESEARCH ARTICLE

Spiro-containing derivatives show antiparasitic activity against *Trypanosoma brucei* through inhibition of the trypanothione reductase enzyme

Lorenzo Turcano¹, Theo Battista², Esther Torrente De Haro³, Antonino Missineo¹, Cristina Alli¹, Giacomo Paonessa¹, Gianni Colotti⁴, Steven Harper^{3†}, Annarita Fiorillo², Andrea Ilari^{4*}, Alberto Bresciani^{1*}

1 Department of Translational and Discovery Research, Pomezia (Roma) Italy, **2** Dipartimento di Scienze Biochimiche, Sapienza Università di Roma, Roma, Italy, **3** Department of Drug Discovery, Pomezia (Roma) Italy, **4** Istituto di Biologia e Patologia Molecolari del CNR c/o Dipartimento di Scienze Biochimiche, Sapienza Università di Roma, Roma, Italy

☞ These authors contributed equally to this work.

† Deceased.

* andrea.ilari@cnr.it (AI); a.bresciani@irbm.com (AB)



OPEN ACCESS

Citation: Turcano L, Battista T, De Haro ET, Missineo A, Alli C, Paonessa G, et al. (2020) Spiro-containing derivatives show antiparasitic activity against *Trypanosoma brucei* through inhibition of the trypanothione reductase enzyme. PLoS Negl Trop Dis 14(5): e0008339. <https://doi.org/10.1371/journal.pntd.0008339>

Editor: Grace Adira Murilla, KARI-Trypanosomiasis Res Centre, KENYA

Received: December 19, 2019

Accepted: April 30, 2020

Published: May 21, 2020

Peer Review History: PLOS recognizes the benefits of transparency in the peer review process; therefore, we enable the publication of all of the content of peer review and author responses alongside final, published articles. The editorial history of this article is available here: <https://doi.org/10.1371/journal.pntd.0008339>

Copyright: © 2020 Turcano et al. This is an open access article distributed under the terms of the [Creative Commons Attribution License](https://creativecommons.org/licenses/by/4.0/), which permits unrestricted use, distribution, and reproduction in any medium, provided the original author and source are credited.

Data Availability Statement: Crystallography data is available from the PDB database (accession number 6RB5).

Abstract

Trypanothione reductase (TR) is a key enzyme that catalyzes the reduction of trypanothione, an antioxidant dithiol that protects Trypanosomatid parasites from oxidative stress induced by mammalian host defense systems. TR is considered an attractive target for the development of novel anti-parasitic agents as it is essential for parasite survival but has no close homologue in humans. We report here the identification of spiro-containing derivatives as inhibitors of TR from *Trypanosoma brucei* (*TbTR*), the parasite responsible for Human African Trypanosomiasis. The hit series, identified by high throughput screening, was shown to bind *TbTR* reversibly and to compete with the trypanothione (TS₂) substrate. The prototype compound **1** from this series was also found to impede the growth of *Trypanosoma brucei* parasites *in vitro*. The X-ray crystal structure of *TbTR* in complex with compound **1** solved at 1.98 Å allowed the identification of the hydrophobic pocket where the inhibitor binds, placed close to the catalytic histidine (His 461') and lined by Trp21, Val53, Ile106, Tyr110 and Met113. This new inhibitor is specific for *TbTR* and no activity was detected against the structurally similar human glutathione reductase (hGR). The central spiro scaffold is known to be suitable for brain active compounds in humans thus representing an attractive starting point for the future treatment of the central nervous system stage of *T. brucei* infections.

Author summary

Trypanosoma brucei is a parasite responsible for neglected pathologies such as human African trypanosomiasis, also known as sleeping sickness. This disease is endemic in sub-

Funding: All authors were funded by CNCCS s.c.a.r.l. (National Collection of Chemical Compounds and Screening Center, www.cnccs.it); TB, GC, AF and AI were also funded by MIUR PRIN 20154JRJPP. The funders had no role in study design, data collection and analysis, decision to publish, or preparation of the manuscript.

Competing interests: The authors have declared that no competing interests exist.

Saharan Africa, with 70 million people at risk of infection. Current treatments for this type of disease are limited by their toxicity, administration in endemic countries and treatment resistance. Therapies against infectious diseases typically rely on targeting one or more components of the parasite that are not present in humans to ensure the best possible therapeutic window. In this case we aimed at targeting the *Trypanosoma brucei* trypanothione reductase (TR), one enzyme that synthesizes the reduced trypanothione a key molecule for preserving the parasite redox balance. This enzyme does not exist in humans that have glutathione instead of trypanothione. Past attempts to identify novel inhibitors of this target has failed to generate drug-like molecules. To overcome this limitation we employed a recent, higher quality, TR activity assay to test a collection of compounds previously reported to be active against these parasites. This approach led to the identification and validation of a new chemotype with a unique mode of inhibition of TR. This chemical series is a drug-like starting point, in fact its core (spiro) is present in drugs approved for human use.

Introduction

Trypanosoma spp. and *Leishmania* spp. are parasites belonging to Trypanosomatidae family that includes important pathogens of both human and animal. It is estimated that about 25 million people worldwide are affected by these two protozoa [1]. In particular *Trypanosoma brucei* is responsible for neglected pathologies such as chronic and acute human African trypanosomiasis (HAT), also known as sleeping sickness [2]. HAT is endemic in sub-Saharan Africa, with 70 million people at risk of infection. Late-stage HAT is always fatal if untreated. The current therapeutic approaches for the treatment of trypanosomiasis such as HAT include the use of organoarsenic compounds (e.g. melarsoprol) or diamidine derivatives (e.g. pentamidine)[3,4]. More recently, oral compounds like fexinidazole or oxaboroles have come to fruition.[5] Fexinidazole, in particular is the first all-oral drug targeting both early and late stages of *T. brucei gambiense* sleeping sickness. [6] However, the inherent toxicity of some of these treatments, together with the dissemination of drug resistance [2,7,8], and the limited central nervous system (CNS) penetration to treat late stage HAT has limited the employment of these molecules, highlighting the need for new therapies to treat *Trypanosoma* parasite infections [2,8]. In recent years, new biochemical pathways essential for parasite survival have emerged as possible therapeutic target for the development of new drugs against trypanosomiasis [9]. Of these, Trypanothione reductase (TR), a flavoenzyme that reduces trypanothione (TS₂) to its T(SH)₂ form [10], is of significant interest. T(SH)₂ and TR represent a major defense system against oxidative stress for *Trypanosoma* parasites, similar to the glutathione (GSH)–glutathione reductase (GR) system found in humans. Despite the three-dimensional similarity between TR and GR, these enzymes recognize specific substrates (trypanothione vs. glutathione), suggesting the possibility to design specific and selective inhibitors of the parasite enzyme without off-target activity on the host[11]. *T. brucei* cells lacking TR show an increased sensitivity to oxidative stress and limited virulent characteristics [12]. Targeting TR thus represents a viable approach to reduce *Trypanosoma* virulence. Several molecules have been characterized as TR inhibitors, such as polyamine, peptide derivative, benzimidazole, nitrobenzene derivative, quinazoline [13–19]. However, despite the large number of TR inhibitors reported in the literature, none of these series has reached drug development stages due to them being not drug-like.[20] These compound potency, toxicity and pharmacokinetics profiles [21] are often suboptimal and the large hydrophobic active site of TR [22] makes its inhibition by small

molecules challenging. As a consequence the discovery and of new scaffolds able to inhibit TR activity is compulsory.

In the present work we identify a new inhibitor of *T. brucei* TR (*TbTR*) by small molecule screening using an optimized luminescence assay able to measure *in vitro* *TbTR* activity [23]. Compound **1**, a hit compound representative of the new class of TR inhibitors is shown to kill the *T. brucei* parasite *in vitro*. The X-ray structure of the *TbTR*/compound **1** complex allowed the identification of a new pocket in the TS₂ binding site where compound **1** binds.

Methods

Compound collection

The compounds that are made available through the CNCCS collection (c. 150000 compounds - www.cnccs.it) were crossed with the PubChem database to select those that were reported to be active in confirmatory Trypanosomatid survival assays. 3097 compounds were identified that were cherry-picked from 10 mM DMSO solutions and arrayed for testing in the present work.

Materials

Bovine serum albumin (BSA), NADPH, human glutathione reductase (hGR), oxidized glutathione (GSSG) and 5,5'-Dithiobis(2-nitrobenzoic acid) (DTNB), IMDM medium (Iscove's Modified Dulbecco's Medium), sodium bicarbonate, hypoxanthine, thymidine, bathocuprione sulfonic acid, cysteine, β-mercaptoethanol, heat-inactivated Calf serum, triton-X 100, anti-His tag antibody and protease inhibitors cocktail were purchased from Sigma-Aldrich (St. Louis, USA); oxidized trypanothione (TS₂) was purchased from Bachem (Bubendorf, Switzerland); NADPH-Glo kit and CellTiter-Glo were purchased from Promega (Madison, WI).

TbTR cloning, expression and purification

The production of the *TbTR* enzyme was performed as previously described[24] with minor modifications. Briefly, the gene coding for the enzyme (aa 1–492) was codon optimized for the expression in *E.coli* and obtained from GenScript. The coding sequence was then cloned in the pET15b vector in order to have an N-terminal fused 6xHisTag for purification purpose. *E. coli* BL21(DE3) transfected cells were treated with 0.5 mM IPTG for 18 h at 37°C. Cells pelleted (4000 RPM, 30 min at 4°C), then re-suspended in lysis buffer (25 mM Tris pH 7.4, 0.5 M NaCl, 10% glycerol, protease inhibitor cocktail SIGMA FAST), incubated on ice for 30 min and lysed by high pressure homogenization (PANDA PLUS instrument, 900 bar). The soluble fraction was clarified by centrifugation (16000 RPM, 30 min at 4°C) and incubated with NiNTA resin (Qiagen) for 1 h at 25°C on a rotating wheel. After removing the unbound fraction the resin was washed with 20 mM imidazole and the recombinant protein subsequently eluted by a single step elution with 500 mM imidazole. Finally, the buffer was exchanged with 25 mM Tris pH 7.4, 150 mM NaCl, 50% glycerol by dialysis and the purified enzyme flash frozen in liquid nitrogen. The purity of recombinant *TbTR* was evaluated by Western blot by an anti-His tag antibody[25]. The signal was revealed by the Pierce Pico-west luminol reagent and detected on a Chemidoc imaging system (Biorad, USA).

TbTR in vitro assays

Compounds from 10 mM stock solutions were transferred to assay plates by acoustic transfer (EDC Biosystems, Milmont, CA). The *TbTR* luminescent assay was performed in 384-well white plate (Greiner Bio One, Frickenhausen, Germany). The following components were

added to the plates to a final volume of 30 μ L: 0.1 nM TR, 20 μ M NADPH, 10 μ M TS₂ in 50 mM HEPES (pH 7.4), 40 mM NaCl, 0.01% BSA. After 60 min of incubation at room temperature the residual amount of NADPH was measured by addition of an equal volume of NADPH-Glo as per the manufacturer's protocol and the luminescent signal was acquired by an EnVision plate reader (PerkinElmer, Waltham, MA). The DTNB assay was performed in a final volume of 50 μ l by addition of 2 nM TR, 100 μ M NADPH, 4 μ M TS₂ and 200 μ M DTNB in 40 mM HEPES (pH 7.4), 1 mM EDTA, 0.01% BSA and 0.05% Tween-20. After 10 minutes of incubation at room temperature the absorbance signal (412 nm) was detected using the Safire2 plate reader (Tecan, Switzerland). The human glutathione reductase (hGR) activity assay was carried out as described by Turcano *et al.*[23]. Results were analyzed using Prism software (GraphPad, San Diego, CA) and Vortex (Dotmatics, Bioshops Stortford, UK). Dose-response curves were fitted by four-parameter logistic regression.

Compound similarity search

After hit confirmation, compound similarity searches were performed by generation of circular Morgan fingerprints (radius 2, 2048 bits) for the test compounds using open source RDKit software (<http://www.rdkit.org/> release 2014_09_2). The molecular representations generated were used to perform ligand based virtual screening against the target database (i.e. our own screening collection) that is described above or a subset of the public ZINC database (<https://zinc.docking.org/>). Similarity was assessed by the Tanimoto index between the reference and target structures using a cut-off (or threshold) of 0.6. Similar compounds were clustered using Taylor-Butina clustering, a non-hierarchical clustering method that ensures that each cluster contains molecules with a set cut-off distance from the central compound. Compounds selected for purchase or screening follow up were chosen from the most populated clusters, with either the central compound or closed analogues (based on visual inspection) being used to represent the compound cluster. All selected compounds were quality controlled by UPLC-MS prior to testing.

Chemistry

Compounds were obtained from commercial suppliers and were tested without further purification. Purity of final compounds were determined using MS and UPLC. UPLC-MS analyses were performed on a Waters Acquity UPLCTM, equipped with a diode array and a ZQ mass spectrometer, using a Waters BEH C₁₈ column (1.7 μ m, 2.1 x 50 mm). The mobile phase comprised a linear gradient of binary mixtures of H₂O containing 0.1% formic acid (A), and MeCN containing 0.1% formic acid (B). The following linear gradient was used (A): 90% (0.1 min), 90%-0% (2.6 min), 0% (0.3 min), 0%-90% (0.1 min). The flow rate was 0.5 mL/min. The purity of final compounds was in all cases \geq 95%. ¹H NMR spectra were recorded on a Bruker AV400 spectrometer operating at 400 MHz. Chemical shifts (δ) are reported in parts per million downfield from TMS and are determined using the residual (undeuterated) NMR solvent peak as an internal standard.

The solubility testing was carried out as previously reported [26,27].

4-(((3-(8-(2-((1S,2S,5S)-6,6-dimethylbicyclo[3.1.1]heptan-2-yl)ethyl)-4-oxo-1-phenyl-1,3,8-triazaspiro[4.5]decan-3-yl)propyl)(methyl)amino)methyl)-4-hydroxypiperidine-1-carboximidamide (**1**). Compound **1** was purchased as a white solid from Prestwick, ¹H NMR (600 MHz, DMSO-d₆) δ 7.36 (s, 3 H), 7.31 (t, *J* = 7.9 Hz, 2 H), 7.03 (d, *J* = 7.33 Hz, 2 H), 6.88 (br t, *J* = 7.33 Hz, 1 H), 6.88 (t, *J* = 7.33 Hz, 1 H), 5.61–5.48 (m, 1 H), 4.76 (s, 2 H), 3.71–3.68 (m, 2 H), 3.60–3.53 (m, 4 H), 3.49–3.40 (m, 4 H), 2.34–3.28 (m, 2 H), 3.14–3.08 (m, 2 H), 2.89 (m, 2 H), 2.38–2.32 (m, 2 H), 2.05–1.84 (m, 14 H), 1.73–1.51 (m, 2 H), 1.21 (s, 3 H), 1.06 (s, 3 H); UPLC RT 0.97 min (peak area 95%); MS (ES⁺) 608 (M+H)⁺.

Competition assay

Competition experiments were performed at two different compound concentrations (5 μM and 25 μM) by *TbTR* luminescent assay. The apparent K_m values for TS_2 in presence of 20 μM NADPH were calculated using 1 nM TR after 10 min incubation. The signal was revealed by the addition of an equal volume of NADPH-Glo. The luminescent signal was measured using the EnVision plate reader (PerkinElmer, USA). IC_{50} , V_{max} and K_m values were calculated using Prism software (GraphPad, San Diego, CA).

Binding assay by SPR

Surface Plasmon resonance (SPR) interaction analysis were performed using a Biacore T200 (GE Healthcare, Uppsala, Sweden). *TbTR* was immobilized on a CM4 chip by amine coupling according to manufacturer's instructions (Amine Coupling Kit, GE Healthcare, Uppsala, Sweden). Briefly, the surface of the sensor chip was activated for 7 minutes using a mixture of 0.1 M N-hydroxy succinimide (NHS) and 0.4 M N-ethyl-N'-[3-dimethyl-aminopropyl] carbodiimide (EDC) then 30 $\mu\text{g}/\text{ml}$ of Tx3 in 10 mM sodium acetate (pH 4.5) was injected for 360 s at 10 $\mu\text{l}/\text{min}$, finally residual activated groups on the surface were blocked by a 7 min injection of 1 M ethanolamine (pH 8.5). A reference channel for background subtraction was prepared by activation with EDC/NHS mixture (0.1 M/0.4 M as per ligand immobilization), followed by blocking with 1 M ethanolamine. The binding of the selected hit to the immobilized ligand was evaluated by a multi-cycle kinetic procedure in PBS-P (GE Healthcare Lifescience) supplemented with 2% DMSO (Sigma Aldrich). The analyte was injected for 60 s at 50 $\mu\text{l}/\text{min}$ until equilibrium and dissociation monitored for 600 s. A standard curve of DMSO was included for solvent correction.

Biomolecular binding events were reported as changes of resonance units (RUs) over time. The data were analyzed by the Biacore T200 evaluation software. The sensorgrams were obtained, by subtracting the signals of the reference channel to those of the *TbTR*-immobilized one, and corrected for DMSO interference using the DMSO standard curve. The binding affinity was evaluated from kinetic parameters ($k_{\text{off}}/k_{\text{on}}$) calculated according to a heterogeneous ligand binding model [28].

X-ray structure determination

The *TbTR*-compound **1** complex was crystallized at 294 K by the hanging drop vapor diffusion method, using 12 mg/ml *TbTR* to prepare symmetrical drops (1+1 μl) equilibrated over a reservoir solution of 500 μl . Streak seeding and soaking techniques were applied. First, we crystallized *TbTR* according to already published condition [29] [30] consisting in ammonium sulfate 2.0–2.2 M, HEPES 0.1M pH 7–8, polyethylene glycol 400 (PEG400) 5% v/v. We used this condition for soaking and co-crystallization but diffraction data did not show compound **1** binding, instead we found a tubular density peak in TS_2 binding site that we modeled as PEG400 likely competing with compound **1** for binding. Then, we performed streak seeding in absence of PEG400 to obtain PEG400-free crystals and avoid competition. We soaked the crystals in a solution containing 10 mM compound **1** and 10% DMSO (stock solution 100 mM compound **1** in DMSO diluted 1:10 with mother liquor). After 1 h of soaking, crystals were cryo-protected with 20% glycerol and frozen in liquid N_2 .

Single wavelength data set ($\lambda = 0.976254 \text{ \AA}$) was collected at the beamline ID23 at the Synchrotron Radiation Source ESRF, Grenoble (France) using a Dectris Pilatus 6M detector at a temperature of 100 K. The data sets were processed and scaled with XDS [31]. The structure was solved by molecular replacement with the program Molrep [32] using native *TbTR* (PDB code: 2WBA) as search model. Refinement was performed using the program REFMAC5 [33]

and model building was carried out using the program COOT [34]. Crystal parameters, data collection statistics and refinement statistics are reported in S2 Table (S2 Table).

***T. brucei* lysate thiol formation assay**

T. brucei parasites were grown on IMDM medium (Iscove's Modified Dulbecco's Medium) supplied with 3 gr/L sodium bicarbonate, 136 mg/L hypoxanthine, 39 mg/L thymidine, 28.2 mg/L bathocuprione sulfonic acid, 0.5 mM cysteine, 0.001% β -mercaptoethanol and 10% heat-inactivated Calf serum. 1.5×10^6 compound treated parasite per well were lysed using 1 mM EDTA, 40 mM Hepes pH 7.5, 50 mM Tris-HCl pH 7.5, 2% Triton-X100 and protease inhibitors cocktail (Sigma). 200 μ M NADPH, 50 μ M TS₂, 100 μ M DTNB were added in each well to trigger the *Tb*TR activity. After 30 min incubation the absorbance signal (412 nm) was detected using the Safire2 plate reader (Tecan, Switzerland).

***T. brucei* growth inhibition assay**

The anti-proliferative effect of testing compounds on *T. brucei* in vitro cultures was carried out by incubating compounds with 1.5×10^3 parasite per well followed by 24 incubation at 37°C and 5% CO₂. The parasite viability was measured by CellTiter-Glo according to the manufacturer's instructions.

Results

TR assay optimization

The *Tb*TR enzyme was produced in bacteria, purified as described in materials and methods and used to develop an in vitro enzyme assay (Fig 1A). To measure *Tb*TR activity, a luminescent assay was optimized starting from a design that we previously described [23]. First we determined the linearity range of the NADPH detection signal via NADPH-Glo kit that was determined to be 50 μ M (Fig 1B). The K_m (apparent) value for TS₂ was calculated using 1 nM TR in the presence of serial dilutions of TS₂ and a fixed concentration of 40 μ M NADPH. The luminescence signal was detected in the first 10 min of reaction. NADPH depletion, calculated using the NADPH standard curve (Fig 1B), allowed the determination of the apparent K_m values by the Michaelis-Menten kinetic (Fig 1C). The K_m for TS₂ was calculated to be 4.0 ± 0.7 μ M. To further optimize the assay, a time course experiment was carried out. Different concentrations of the *Tb*TR enzyme, ranging from 0.025 to 0.2 nM, were used, while the TS₂ concentration was fixed near the K_m value (5 μ M) and the NADPH concentration was 20 μ M that falls within the linearity range observed for the NADPH standard curve. 0.1 nM *Tb*TR at and 60 min of incubation were judged to be an optimal compromise for preserving the reaction linearity along with a good signal to background ratio (Fig 1D) and allowing a suitable time for the screening operations. The final conditions used for the screening were: 0.1 nM *Tb*TR, 5 μ M TS₂, 20 μ M NADPH with the incubation time of the reaction being 60 minutes.

Hit identification

A collection of 3097 compounds present in our library and previously reported to be active in PubChem Trypanosomatid proliferation assays (see materials) was screened at 10 μ M using the protocol described above. The Z' values [35] were found to be greater than 0.5 for all screening plates indicating that the assay was sufficiently robust to be used to test the compounds (Fig 2A). The distribution of the compound activities converges to normal distribution (or Gaussian distribution) (Fig 2B); therefore, compounds with an activity equal to or

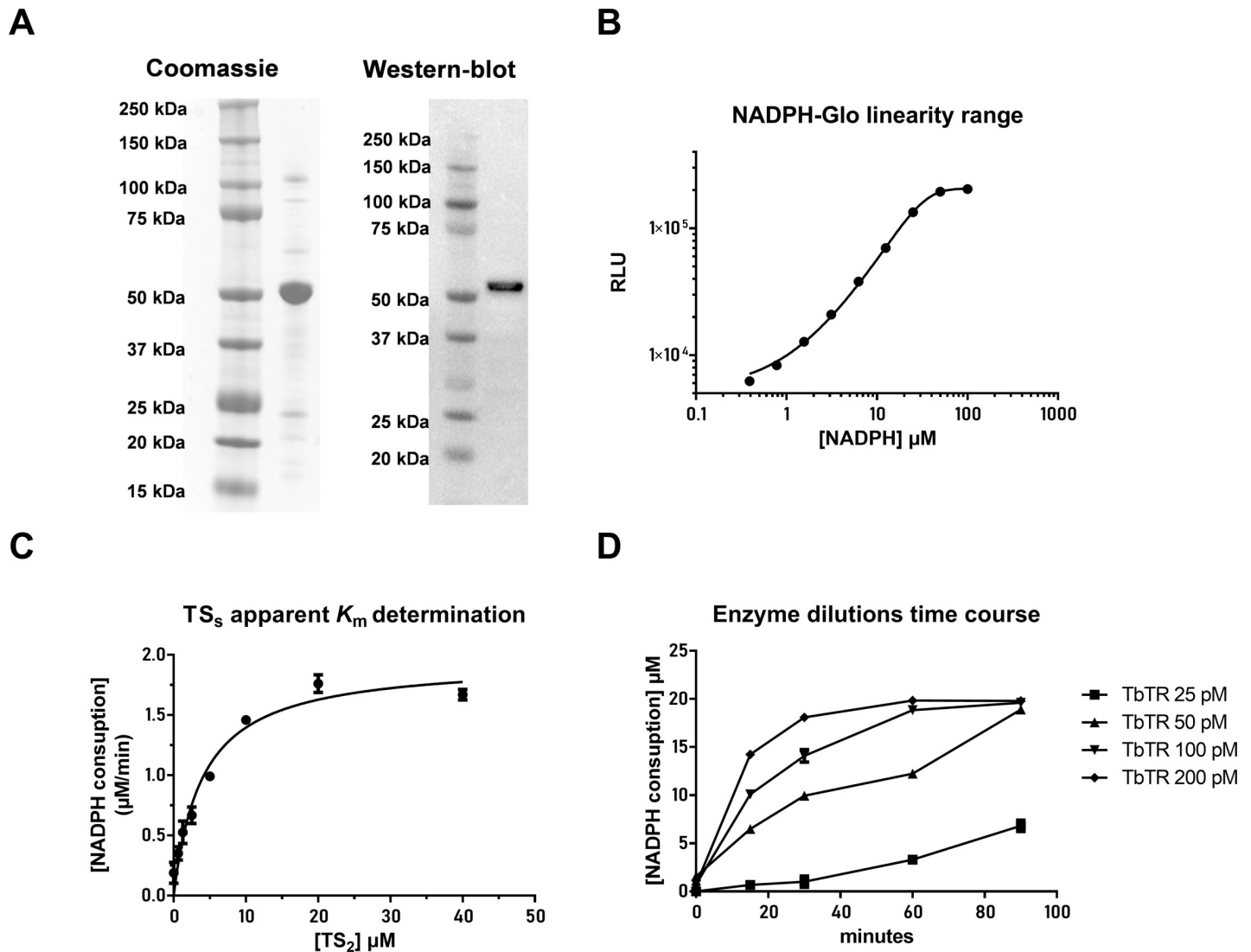


Fig 1. (A) Expression and purification of the recombinant *TbTR* protein. A distinct band around 50 kDa was detected after stimulation of *E. coli* BL21 (DE3) cells with IPTG followed by purification on NiNTA resin. Western blot with anti-His tag antibody to confirm the identity of the recombinant *TbTR*. (B) Sensitivity and linearity of the NADPH detection using the NADPH-Glo detection kit. (C) Determination of the TS_2 apparent K_m at 1 nM *TbTR* and 40 μM NADPH. (D) Time course and *TbTR* titration using TS_2 and NADPH at fixed concentrations of 10 μM and 20 μM respectively. For all graphs, the plotted points are the average of three independent replicates.

<https://doi.org/10.1371/journal.pntd.0008339.g001>

greater than the average activity plus three standard deviations were considered hit compounds. Eight compounds, i.e. 0.26% of the total, were identified as active in the primary screening and subjected to the confirmation assays. The design of the primary assay which produces a positive luciferase signal in the presence of an inhibitor meant that no luciferase inhibition counter-screen was necessary.

Hit confirmation

In order to confirm hit compounds, they were tested in a dose-response fashion starting from 85 μM in the *TbTR* luminescence assay. Four of eight compounds were confirmed to be *TbTR* inhibitors, with IC_{50} values ranging from 3 μM to 34 μM . Structural analysis of active

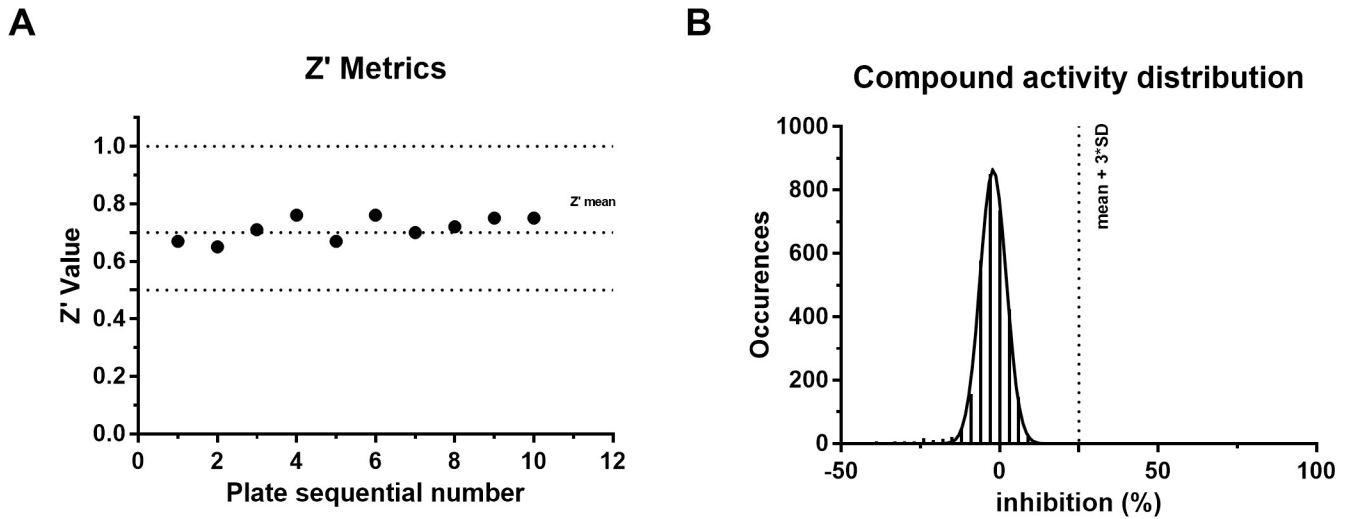


Fig 2. Screening result. (A) The Z' factors of all the 384-well plates are represented by solid dots. The dashed line indicates the Z' mean of 0.71. (B) Occurrence distribution of compound activity is plotted as Z-factor with respect to the whole sample average and standard deviation.

<https://doi.org/10.1371/journal.pntd.0008339.g002>

compounds (S1 Table) revealed the presence of a 1-phenyl-1,3,8-triazaspiro[4.5]decan-4-one moiety (i.e. A, Fig 3) as a recurrent central core, in which the simultaneous substitution of central core by R and R' seems to be required for activity (Fig 3).

To further expand structure activity relationships (SAR) around the 4 hits, 22 structurally similar analogues from either the original screening set (potential false negatives) or our entire chemical collection were selected. The selection was performed based on structural similarity to the central core or closed analogues (visual inspection). Active hit compounds were also tested for confirmation in the standard DTNB absorbance assay as reported by Hamilton *et al.* [36]. Further, to evaluate their specificity they were tested against the homolog human

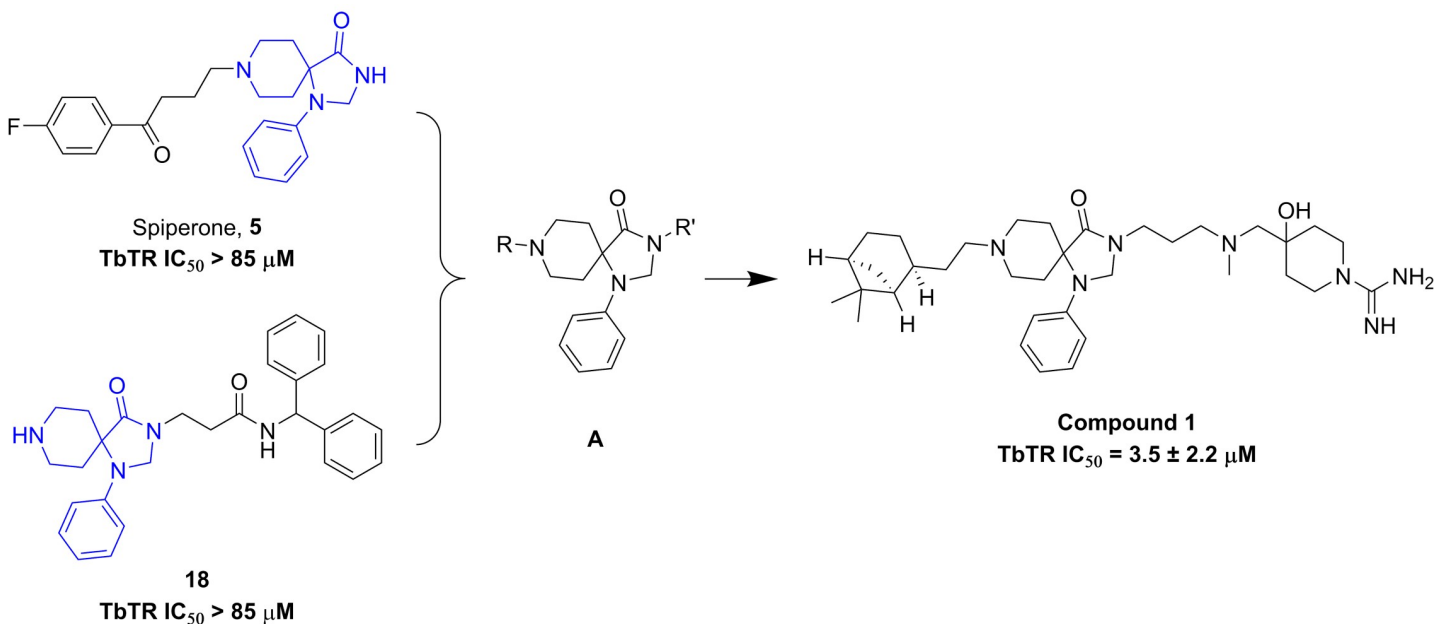


Fig 3. General structures of hit series and representative molecule with TR inhibition potency.

<https://doi.org/10.1371/journal.pntd.0008339.g003>

glutathione reductase enzyme (hGR), as reported by Turcano *et al.* [23], using glutathione as a substrate. Results from this follow up are summarized in **S1 Table**. Although this follow up did not lead improved activity, the confirmation of the hit compounds as micromolar inhibitors of *Tb*TR in enzymatic assays, with strong selectivity for the parasite (IC₅₀ values on hGR were uniformly above 50 μ M) provided a level of comfort that our new compound series represents a *bona fide* class of *Tb*TR inhibitors. Compound **1**, 4-(((3-(8-(2-((1*S*,2*S*,5*S*)-6,6-dimethylbicyclo[3.1.1]heptan-2-yl)ethyl)-4-oxo-1-phenyl-1,3,8-triazaspiro[4.5]decan-3-yl)propyl)(methyl)amino)methyl)-4-hydroxypiperidine-1-carboximidamide (identity by ¹H NMR is provided in **S1 Fig**), was selected for further profiling studies based on its acceptable *in vitro* potency (3.5 ± 2.2 μ M, **Fig 3**) and on its high solubility (185.1 μ M in assay PBS buffer at pH 7.4).

Hit compound binding to TR

The binding between *Tb*TR and compound **1** was evaluated by surface plasmon resonance (SPR). To this purpose, *Tb*TR was covalently immobilized at high density (c. 9,000 Δ RU) to a CM4 sensor chip, then the compound was injected over the surface at different concentrations ranging from 0.3125 to 20 μ M. The hit showed a reversible binding to the enzyme, but it was not possible to calculate the kinetic parameters (k_{on} and k_{off}) using a simple 1:1 Langmuir binding model. Thus, the kinetic parameters (k_{on} and k_{off}) were calculated from the sensorgrams applying an heterogeneous ligand model[28]. The analysis suggested the presence of two binding sites with different affinities. For the higher affinity site, the apparent K_d resulted to be in the high micro molar range ($K_d = 10.3 \pm 2.9$ μ M, $k_{on} = 3.3 \pm 0.5$ 1/Ms, $k_{off} = 0.035 \pm 0.014$). It was not possible to calculate reliable constants for the lower affinity site.

Subsequently, the ability of hit compound **1** to compete with the TS₂ substrate for *Tb*TR was investigated. To this aim a serial dilution of TS₂ starting from 100 μ M, plus 20 μ M NADPH, was assayed in the *Tb*TR enzyme in the presence of vehicle, 5 or 25 μ M Compound **1**. Compound **1** was found to be competitive with TS₂ (**Fig 4B**) for *Tb*TR the apparent K_m (K_m^{app}) of TS₂ shifting to the right with the increase of the inhibitor concentration. No changes in calculated V_{max} were observed.

X-ray crystal structure of TR in complex with Compound 1

The structure of the complex between *Tb*TR and compound **1** (TR-1) was determined by X-ray crystallography at 1.98 \AA resolution, allowing the identification of the binding sites of the

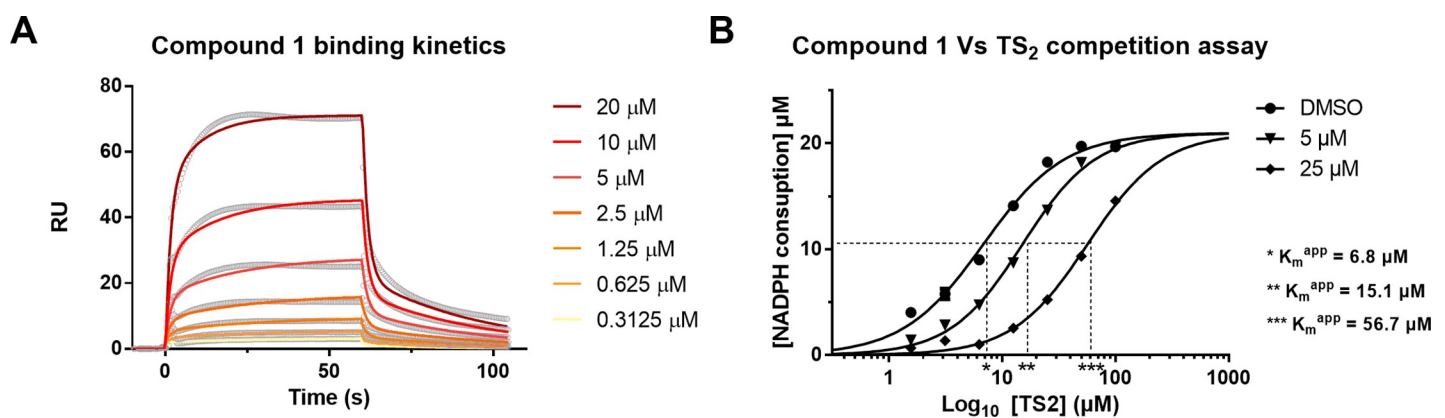


Fig 4. Study of the interaction of compound 1 with *Tb*TR. (A) Binding kinetics of compound 1 to *Tb*TR that was immobilized on a CM5 SPR chip. The image shows a representative experiment of four replicates. (B) Competition assay of compound 1 against TS₂. TS₂ was titrated against 1 nM *Tb*TR in presence of vehicle (dots) or against two concentrations of compound 1: 5 μ M (triangles) and 25 μ M (diamond). The assay run for 10 minutes using 20 μ M NADPH. Each experimental point is the average of three replicates.

<https://doi.org/10.1371/journal.pntd.0008339.g004>

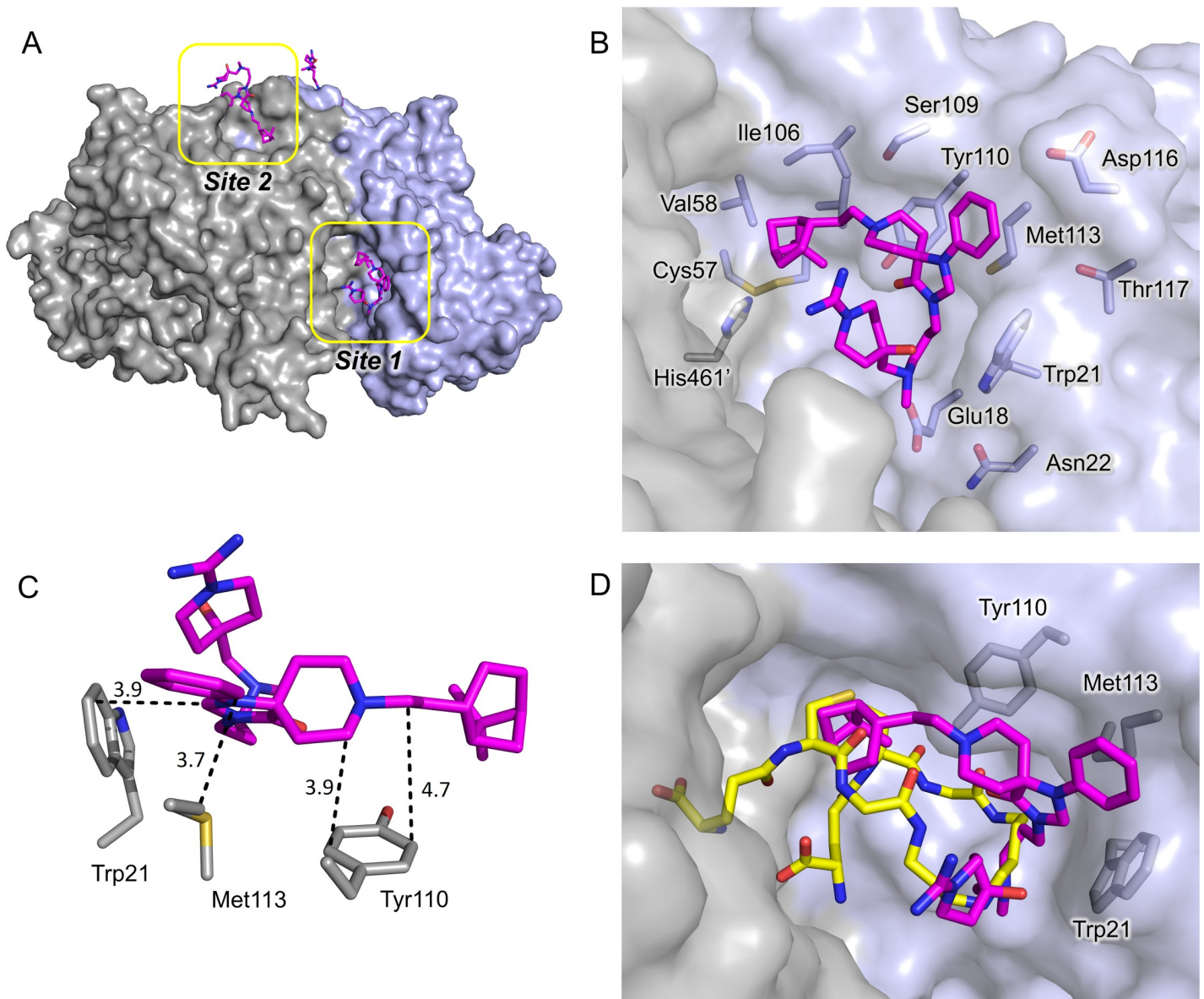


Fig 5. X-ray structure of 1-TR. (A) Overall fold of TR in complex with compound 1. The accessible solvent areas of the two-fold symmetry related monomers are indicated in grey and blue respectively; the sites 1 and 2 are indicated by yellow boxes and compound 1 is represented as magenta sticks. (B) Binding site 1: the residues lining the binding site and the catalytic residues are represented as sticks. Compound 1 carbon atoms are colored in magenta and the protein residues carbon atoms in grey. The accessible solvent area of the cavity is colored grey. (C) Detail of the compound 1-*Tb*TR interaction. Compound 1, Trp21, Met113 and Tyr110 are represented as sticks. (D) Superposition of TR-1 and *Tb*TR in complex with TS₂ (pdb: 2wow). Carbon atoms of compound 1 are colored in magenta whereas the carbon atoms of TS₂ are colored yellow. Trp21, Met113 and Tyr110 are indicated. The solvent accessible area is represented and colored in grey. The pictures were obtained using PyMOL (The PyMOL Molecular Graphics System, Version 2.0 Schrödinger, LLC).

<https://doi.org/10.1371/journal.pntd.0008339.g005>

inhibitor and the definitions of the details of the interaction (see [S2 Table](#) for crystal parameters, data collection and refinement statistics).

TR-1 structure is very similar to *Tb*TR either in the apo form or bound to the substrates (pdb: 2woi, 2wow) indicating that compound 1 binding does not induce global or local conformational variations.

Inspection of electron density revealed two binding sites on each *Tb*TR monomer, unequivocally attributed to compound 1 ([Fig 5A](#)). Indeed, the peculiar shape of the spiro moiety, with

two rings sharing a sp^3 carbon and therefore forced to lie on perpendicular planes, can be identified and modeled with high confidence in the electron density map (S2 Fig, supporting material).

The most significant of the two binding sites, indicated as site 1, is located inside the wide trypanothione binding cavity, where it partially overlaps with the so-called mepacrine binding site [37]. The binding is dominated by the hydrophobic interactions made by the core of compound **1** while the arms of the molecule are more flexible and point respectively towards the inside and the outside of the cavity. The phenyl-triazaspiro scaffold of compound **1** fits well the hydrophobic/aromatic patch composed by Trp21, Met113 and Tyr110. In particular, i) the phenyl and the diazole rings, almost coplanar, lay along the side chain of Met113, ii) the indole ring of Trp21, perpendicular to diazole ring, makes π -CH interaction with it, iii) the cyclohexyl moiety interacts with the aromatic ring of Tyr110 (all described interactions are within 4Å) (Fig 5B and 5C).

The arms of compound **1** establish weaker interactions with the protein, consistent with what indicated by the electron density map that is poorly defined for these portions of the molecule (S2 Fig). The bicycle-heptane moiety extends deeper in the cavity, into the hydrophobic subpocket lined by Val53, Val58, Ile106 and Leu399, and is just 6-7Å away from the catalytic Cys52 and Cys57 residues. The hydrophilic carboximidamide moiety fluctuates in the cavity towards the entrance and only a weak electrostatic interaction (4.4Å) takes place between the tertiary amino group of the arm and Glu18. However, the positive charge of the arm, due to the presence of amino groups, can contribute to the binding by interacting with the overall negative charge of the cavity, suited to accommodate the positive TS_2 substrate.

The comparison of TR-1 with the *Tb*TR structure in complex with TS_2 (pdb: 2wow) clearly shows that compound **1** occupies the site reserved to spermidine and glutathionyl moieties of TS_2 during catalysis (Fig 5D). Thus, the binding of compound **1** in the cavity is incompatible with the binding of TS_2 , consistent with the competitive inhibition observed by kinetic characterization.

The second molecule of compound **1** binds an almost hydrophobic cleft, indicated as site 2, close to the dimeric interface of TR. The phenyl moiety is inserted between Pro213 and Lys89, making π -CH interactions, the spiro moiety interacts with the backbone of residues Gly85 and Ser86, while the bicycle-heptane arm points toward a hydrophobic pocket lined by Met70, Leu73, Arg74, Phe83 (Fig 6). The hydrophilic arm of compound **1** does not contribute to binding but is very mobile. It protrudes out of the cleft and is completely exposed to the solvent. This binding site is far away from both the NADPH and the TS_2 binding cavities and, up to now, no specific function has been attributed to this region. Therefore, it is reasonable to assume that the binding of compound **1** in site 2 has no effect on the catalytic activity of *Tb*TR and that the observed inhibition is due exclusively to the binding at site 1. Moreover, binding to additional sites other than site 1 might explain the SPR results.

The mode of binding proposed for compound **1** in TR-1 justifies the selectivity shown against human GR. Indeed, residues composition of site 1 presents important differences in hGR able to prevent inhibitor binding, while the cleft of site 2 is absent in hGR. In particular, residues Trp21 and Met113, critical for compound **1** binding in site 1, are replaced by Arg37 and Asn117 in hGR. Moreover, while the distinctly positive electrostatic potential of the GR substrate binding cavity is unsuitable for accommodating compound **1**, due to the presence of positively charged carboximidamide arm and tertiary amino group (S3 Fig), the hydrophobic and positively charged moieties of compound **1** appear to be complementary to the *Tb*TR cavity surface (S4 Fig).

Other low molecular weight inhibitors competing with TS_2 have been previously identified for TRs from *Trypanosoma* spp. as well as for *Leishmania* spp. A detailed structural characterization is available for some of them, revealing that most inhibitors bind to the hydrophobic

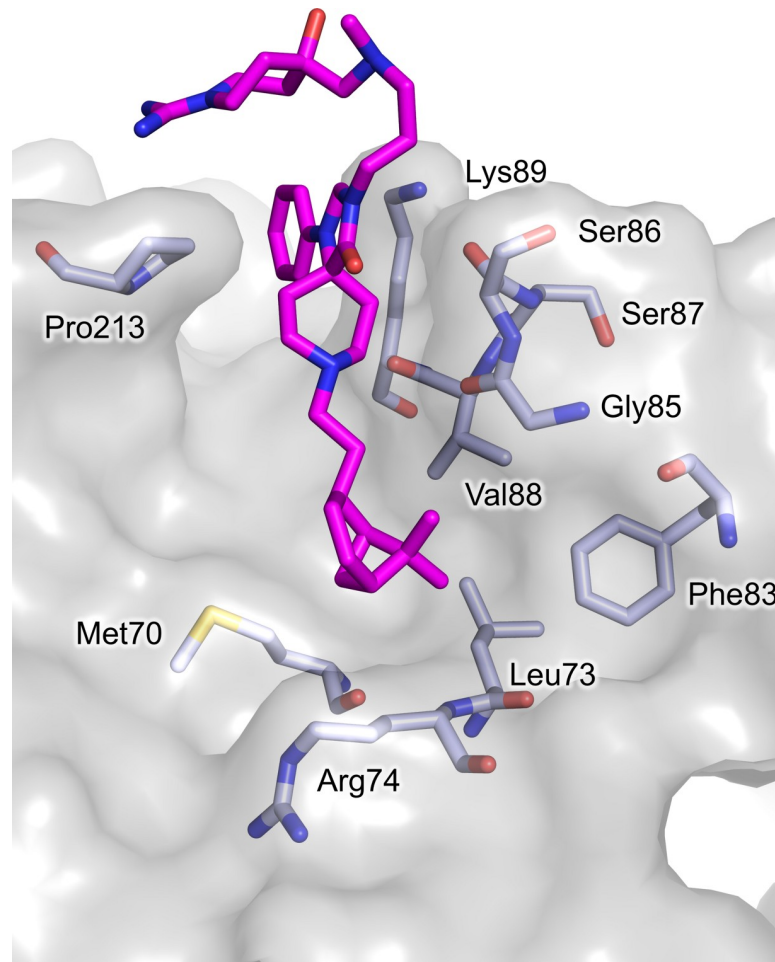


Fig 6. Binding site 2: the residues lining the binding site and the catalytic residues are represented as sticks. Compound 1 carbon atoms are colored in magenta and the protein residues carbon atoms in grey. The accessible solvent area of the cavity is represented and colored grey. The picture was obtained using PyMOL (The PyMOL Molecular Graphics System, Version 2.0 Schrödinger, LLC.).

<https://doi.org/10.1371/journal.pntd.0008339.g006>

patch Trp21-Tyr110-Met113 as compound 1, known as mepacrine binding site. The first crystal structure solved represents *T. cruzi* TR in complex with mepacrine[38] (pdb: 1gxf), from which the site was named. In order to confirm that the binding site is common to TR of other parasites, we tested compound 1 against the *Leishmania infantum* TR according to our previous work.[23] The IC_{50} of compound 1 was found to be $3.8 \pm 0.6 \mu\text{M}$ (S5 Fig) well in line with the one on *Tb*TR confirming the above hypothesis.

Compound 1 activity in *Trypanosoma brucei* in vitro culture

To evaluate the ability of Compound 1 to inhibit endogenous *Tb*TR activity, a titration of it was incubated with a lysate of *T. brucei*, supplemented with $50 \mu\text{M}$ of TS_2 , $200 \mu\text{M}$ NADPH and $100 \mu\text{M}$ DTNB. The increased absorbance signal at 412 nm can be attributed to the increase in reduced thiols, a reasonable surrogate of the *Tb*TR activity. Fig 7A shows that compound 1 is active in a dose-response manner, with an IC_{50} value of $5.7 \pm 0.6 \mu\text{M}$. Finally, the anti-proliferative activity of serial dilution of Compound 1 on a *T. brucei* culture, treated for 24 hours, resulted in an IC_{50} of $2.2 \pm 2.4 \mu\text{M}$ (Fig 7B).

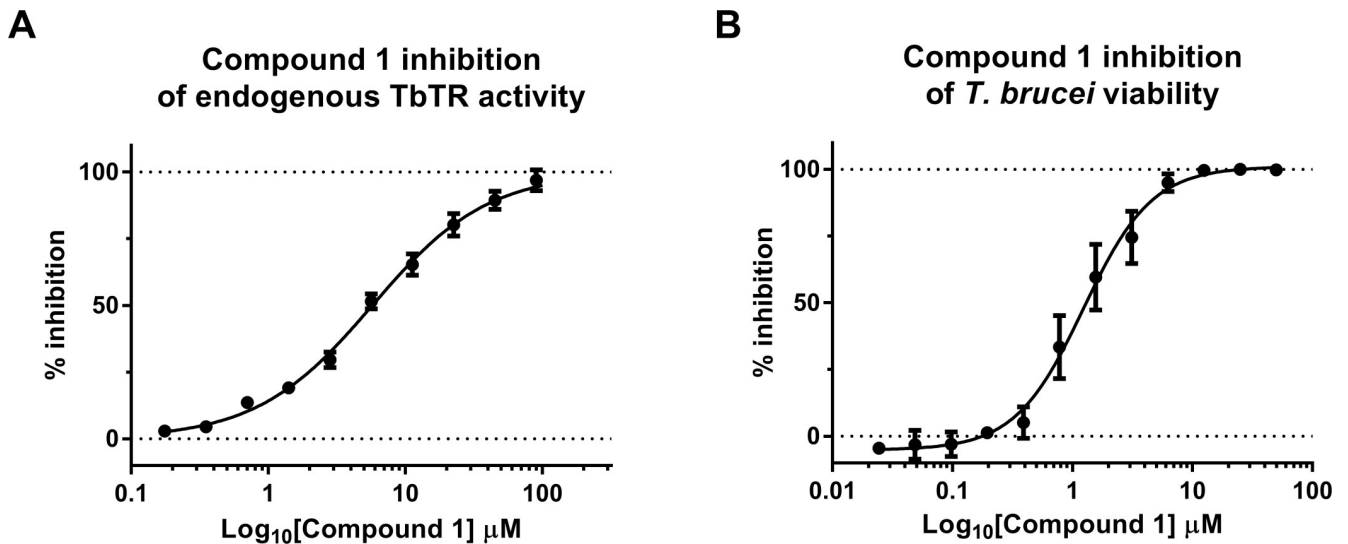


Fig 7. (A) Compound 1 inhibition of endogenous *TbTR* activity. A *T. brucei* lysate was incubated with a compound 1 serial dilution plus 200 μM NADPH, 50 μM TS₂ and 100 μM DTNB. The absorbance signal was measured at 412 nm after 30 min of incubation. IC₅₀ value of $5.7 \pm 0.6 \mu\text{M}$ (B) Effect of the hit inhibitory compound on *T. brucei* growth. Parasites were seeded at 1.5×10^3 per well and incubated with compound 1 for 24 h. Cell viability was measured using the CellTiter-Glo. IC₅₀ of $2.2 \pm 2.4 \mu\text{M}$. All results of the present figure are the average of two independent experiments, each consisting of three technical replicates.

<https://doi.org/10.1371/journal.pntd.0008339.g007>

Discussion

In this work, we presented the identification and validation of a new series of *TbTR* inhibitors by the screening of 3097 compounds previously reported in PubChem to be active in inhibiting Trypanosomatid growth. These compounds, based on a 1-phenyl-1,3,8-triazaspiro[4.5]decan-4-one scaffold, were able to inhibit the *TbTR* enzyme in the low micromolar range. The mode of action of a representative compound **1** was investigated. It was found to be a reversible TS₂ competitive inhibitor. The ability of this compound to inhibit endogenous reductase activity of *TbTR* and *T. brucei* growth was confirmed.

The structure of the complex between *TbTR* and compound **1** (TR-1) determined by X-ray crystallography at 1.98 Å resolution, allowed us to identify two binding sites of the inhibitor and to define the details of the interaction. TR-1 structure is very similar to *TbTR* in the apo form or bound to the substrates indicating that compound **1** binding does not induce global or local conformational variations. According to SPR data, compound **1** was demonstrated to bind to two sites of TR. Site 2 is located close to the dimeric interface of TR, while site 1 is located in the trypanothione binding cavity and partially overlaps with the so-called mepacrine binding site: the phenyl-triazaspiro core anchors the molecule to the trypanothione binding cavity through a conserved hydrophobic patch (formed by the Trp21, Met113 and Tyr110 residues), while the arms cause steric hindrance both at the bottom (close to the catalytic cysteines) and at the entrance of the cavity, thus preventing the entry of the substrate into the catalytic site (Fig 5, Fig 8). The mode of binding proposed for compound **1** in TR-1 justifies the selectivity shown against human GR since the residues Trp21 and Met113, critical for compound **1** binding to site 1, are replaced by Arg37 and Asn117 in GR and the distinctly positive electrostatic potential of the GR substrate binding cavity is unsuitable for accommodating compound **1**, which in turn is positively charged due to the presence of carboximidamide arm.

Other low molecular weight inhibitors of TR competing with TS₂ and binding to mepacrine binding site, have been previously identified for *Trypanosoma* as well as for *Leishmania*. However, the bicycle-heptane moiety of compound **1** extends deeper in the cavity, into a new

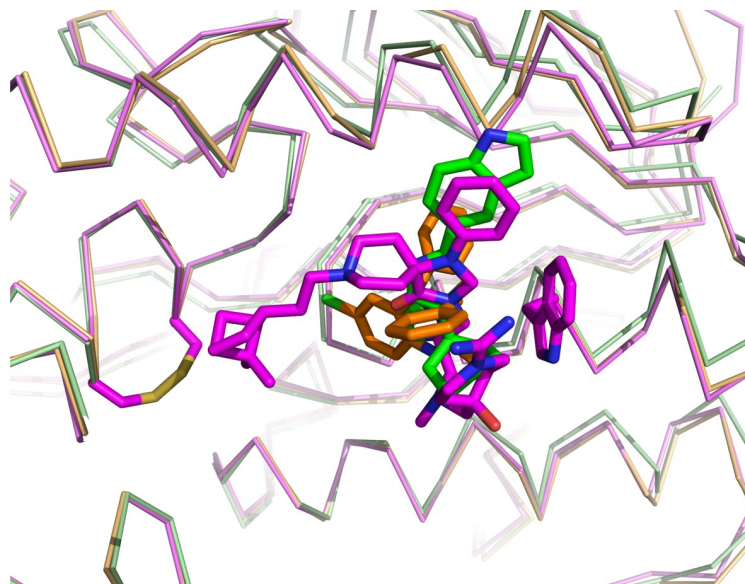


Fig 8. Comparison of TR inhibitors mode of binding to the catalytic cavity. The figure shows the overlay of TR in complex with compound 1 (magenta, pdb code: 6RB5) and other two representative inhibitors: cyclohexylpiperolidine derivative (green, pdb code: 4NEV) [Persch 2014] and dihydroquinazoline (orange, pdb: 2WP6) [22].

<https://doi.org/10.1371/journal.pntd.0008339.g008>

hydrophobic sub-pocket lined by Val53, Val58, Ile106 and Leu399 residues. For these reasons, compound **1** represent a new lead compound suitable to find new drugs against the HAT. Moreover, compound **1** is equally active on *Li*TR given that all the structural features responsible for compound **1** binding to *Tb*TR are present also in the *Leishmania* TR suggesting that TRs can be the target of anti-kinetoplastids drugs.[39] Further, The spiro central core of the present hit compound series was previously reported in pubchem to be active against the growth of *T. brucei* and *T. cruzi*.

The potency of compound **1** was found to be aligned (between c. 2 and 5 μ M) among the *Tb*TR activity, the TR activity in the *T. brucei* lysate and the *T. brucei* proliferation assays suggesting that this molecule is able to reach the target in the parasite with no major potency shift.

The compound **1** chemotype, being the central spiro core that is key for the interaction with *Tb*TR, is an attractive starting point from a drug discovery and development perspective. In fact molecules containing the central spiro core, like the spiperone [40] and the fluspirilene [41], were shown to be brain penetrant in humans. Though several rounds of optimization to increase the potency, install drug-like properties and to sort out possible human off-targets are needed, the present chemotype represents an intriguing new avenue for the future treatment of the central nervous system phase of *T. brucei* infections.

Supporting information

S1 Table. Biological data for hits resulted from HTS and selected follow-up compounds. (PDF)

S2 Table. Crystal parameters, data collection statistics and refinement statistics of 1-TR complex. (PDF)

S1 Fig. ^1H NMR spectrum for compound **1** ^1H NMR spectrum for compound **1**. (PDF)

S2 Fig. Electron density map of compound 1 bound to site 1 (A) or site 2 (B).
(PDF)

S3 Fig. The distinctly positive electrostatic potential of the GR substrate binding cavity is unsuitable for accommodating compound 1 due to the presence of positively charged carboximidamide arm and tertiary ammino group (green lateral chains) whereas the *TbTR* cavity surface electrostatic potential (grey lateral chains) appears to be compatible with the binding of compound 1.
(PDF)

S4 Fig. The hydrophobic and positively charged moieties of compound 1 appear to be complementary to the *TbTR* cavity surface. site 1 (A) or site 2 (B).
(PDF)

S5 Fig. Inhibition of *Leishmania infantum* trypanothione reductase (*LiTR*) by Compound 1. Each experimental point is the average of three replicates.
(PDF)

Acknowledgments

This work is dedicated to our beloved college and friend Steven Harper who passed away at the age of 51.

The authors would like to thank Rita Graziani and Nadia Gennari for providing support with the *Trypanosoma brucei* cultures and Letizia Lazzaro for her support with the quality control of the hit molecules.

Author Contributions

Conceptualization: Gianni Colotti, Andrea Ilari, Alberto Bresciani.

Data curation: Lorenzo Turcano, Esther Torrente De Haro, Steven Harper, Annarita Fiorillo, Andrea Ilari, Alberto Bresciani.

Funding acquisition: Alberto Bresciani.

Investigation: Lorenzo Turcano, Theo Battista, Esther Torrente De Haro, Antonino Missineo, Cristina Alli, Annarita Fiorillo.

Supervision: Giacomo Paonessa, Gianni Colotti, Steven Harper, Alberto Bresciani.

Visualization: Lorenzo Turcano, Theo Battista, Antonino Missineo, Cristina Alli, Gianni Colotti, Annarita Fiorillo, Alberto Bresciani.

Writing – original draft: Andrea Ilari, Alberto Bresciani.

Writing – review & editing: Giacomo Paonessa, Gianni Colotti, Steven Harper, Andrea Ilari, Alberto Bresciani.

References

1. de Morais CGV, Castro Lima AK, Terra R, dos Santos RF, Da-Silva SAG, Dutra PML. The Dialogue of the Host-Parasite Relationship: *Leishmania* spp. and *Trypanosoma cruzi* Infection. *Biomed Res Int*. 2015; 2015: 324915. <https://doi.org/10.1155/2015/324915> PMID: 26090399
2. Fairlamb AH, Horn D. Melarsoprol Resistance in African Trypanosomiasis. *Trends Parasitol*. 2018; 34: 481–492. <https://doi.org/10.1016/j.pt.2018.04.002> PMID: 29705579

3. Bernardes LSC, Zani CL, Carvalho I. Trypanosomatidae Diseases: From the Current Therapy to the Efficacious Role of Trypanothione Reductase in Drug Discovery. 2013; 2673–2696.
4. Richardson JL, Nett IRE, Jones DC, Abdille MH, Gilbert IH, Fairlamb AH. Improved Tricyclic Inhibitors of Trypanothione Reductase by Screening and Chemical Synthesis. 2009; 1333–1340. <https://doi.org/10.1002/cmdc.200900097> PMID: 19557801
5. Steinmann P, Stone CM, Sutherland CS, Tanner M, Tediosi F. Contemporary and emerging strategies for eliminating human African trypanosomiasis due to *Trypanosoma brucei gambiense*: review. *Trop Med Int Health*. 2015; 20: 707–18. <https://doi.org/10.1111/tmi.12483> PMID: 25694261
6. Mesu VKBK, Kalonji WM, Bardonneau C, Mordt OV, Blesson S, Simon F, et al. Oral fexinidazole for late-stage African *Trypanosoma brucei gambiense* trypanosomiasis: a pivotal multicentre, randomised, non-inferiority trial. *Lancet (London, England)*. 2018; 391: 144–154. [https://doi.org/10.1016/S0140-6736\(17\)32758-7](https://doi.org/10.1016/S0140-6736(17)32758-7)
7. Hancock REW, Speert DP. Antibiotic resistance in *Pseudomonas aeruginosa*: mechanisms and impact on treatment. *Drug Resist Updat*. 2000; 3: 247–255. <https://doi.org/10.1054/drup.2000.0152> PMID: 11498392
8. Baker N, de Koning HP, Mäser P, Horn D. Drug resistance in African trypanosomiasis: the melarsoprol and pentamidine story. *Trends Parasitol*. 2013; 29: 110–8. <https://doi.org/10.1016/j.pt.2012.12.005> PMID: 23375541
9. Ferrins L, Rahmani R, Baell JB. Drug discovery and human African trypanosomiasis: a disease less neglected? *Future Med Chem*. 2013; 5: 1801–41. <https://doi.org/10.4155/fmc.13.162> PMID: 24144414
10. Angiulli G, Lantella A, Forte E, Angelucci F, Colotti G, Ilari A, et al. Leishmania infantum trypanothione reductase is a promiscuous enzyme carrying an NADPH:O₂ oxidoreductase activity shared by glutathione reductase. *Biochim Biophys Acta*. 2015; 1850: 1891–7. <https://doi.org/10.1016/j.bbagen.2015.05.022> PMID: 26033467
11. Vázquez K, Paulino M, Salas CO, Zarate-Ramos JJ, Vera B, Rivera G. Trypanothione Reductase: A Target for the Development of Anti- *Trypanosoma cruzi* Drugs. *Mini Rev Med Chem*. 2017; 17: 939–946. <https://doi.org/10.2174/1389557517666170315145410> PMID: 28302040
12. Krieger S, Schwarz W, Ariyanayagam MR, Fairlamb AH, Krauth-Siegel RL, Clayton C. Trypanosomes lacking trypanothione reductase are avirulent and show increased sensitivity to oxidative stress. *Mol Microbiol*. 2000; 35: 542–52. <https://doi.org/10.1046/j.1365-2958.2000.01721.x> PMID: 10672177
13. Holloway GA, Charman WN, Fairlamb AH, Brun R, Kaiser M, Kostewicz E, et al. Trypanothione reductase high-throughput screening campaign identifies novel classes of inhibitors with antiparasitic activity. *Antimicrob Agents Chemother*. 2009; 53: 2824–33. <https://doi.org/10.1128/AAC.01568-08> PMID: 19364854
14. Khan MO, Austin SE, Chan C, Yin H, Marks D, Vaghjiani SN, et al. Use of an additional hydrophobic binding site, the Z site, in the rational drug design of a new class of stronger trypanothione reductase inhibitor, quaternary alkylammonium phenothiazines. *J Med Chem*. 2000; 43: 3148–56. <https://doi.org/10.1021/jm000156+> PMID: 10956223
15. Parveen S, Khan MOF, Austin SE, Croft SL, Yardley V, Rock P, et al. Antitrypanosomal, antileishmanial, and antimalarial activities of quaternary arylalkylammonium 2-amino-4-chlorophenyl phenyl sulfides, a new class of trypanothione reductase inhibitor, and of N-acyl derivatives of 2-amino-4-chlorophenyl phenyl sulfide. *J Med Chem*. 2005; 48: 8087–97. <https://doi.org/10.1021/jm050819t> PMID: 16335933
16. Stump B, Eberle C, Schweizer WB, Kaiser M, Brun R, Krauth-Siegel RL, et al. Pentafluorosulfanyl as a novel building block for enzyme inhibitors: trypanothione reductase inhibition and antiprotozoal activities of diarylamines. *Chembiochem*. 2009; 10: 79–83. <https://doi.org/10.1002/cbic.200800565> PMID: 19058274
17. Cavalli A, Lizzi F, Bongarzone S, Brun R, Luise Krauth-Siegel R, Bolognesi ML. Privileged structure-guided synthesis of quinazoline derivatives as inhibitors of trypanothione reductase. *Bioorg Med Chem Lett*. 2009; 19: 3031–5. <https://doi.org/10.1016/j.bmcl.2009.04.060> PMID: 19414258
18. Kumar S, Ali MR, Bawa S. Mini review on tricyclic compounds as an inhibitor of trypanothione reductase. *J Pharm Bioallied Sci*. 2014; 6: 222–8. <https://doi.org/10.4103/0975-7406.142943> PMID: 25400403
19. Maya JD, Salas CO, Aguilera-Venegas B, Diaz M V, López-Muñoz R. Key proteins in the polyamine-trypanothione pathway as drug targets against *Trypanosoma cruzi*. *Curr Med Chem*. 2014; 21: 1757–71. <https://doi.org/10.2174/0929867320666131119122145> PMID: 24251576
20. Leroux AE, Krauth-Siegel RL. Thiol redox biology of trypanosomatids and potential targets for chemotherapy. *Mol Biochem Parasitol*. 2006; 156: 67–74. <https://doi.org/10.1016/j.molbiopara.2015.11.003> PMID: 26592324

21. Field MC, Horn D, Fairlamb AH, Ferguson MAJ, Gray DW, Read KD, et al. Anti-trypanosomatid drug discovery: an ongoing challenge and a continuing need. *Nat Rev Microbiol*. 2017; 15: 217–231. <https://doi.org/10.1038/nrmicro.2016.193> PMID: 28239154
22. Patterson S, Alphey MS, Jones DC, Shanks EJ, Street IP, Frearson JA, et al. Dihydroquinazolines as a novel class of *Trypanosoma brucei* trypanothione reductase inhibitors: discovery, synthesis, and characterization of their binding mode by protein crystallography. *J Med Chem*. 2011; 54: 6514–30. <https://doi.org/10.1021/jm200312v> PMID: 21851087
23. Turcano L, Torrente E, Missineo A, Andreini M, Gramiccia M, Di Muccio T, et al. Identification and binding mode of a novel *Leishmania* Trypanothione reductase inhibitor from high throughput screening. *PLoS Negl Trop Dis*. 2018; 12: e0006969. <https://doi.org/10.1371/journal.pntd.0006969> PMID: 30475811
24. Baiocco P, Franceschini S, Ilari A, Colotti G. Trypanothione reductase from *Leishmania infantum*: cloning, expression, purification, crystallization and preliminary X-ray data analysis. *Protein Pept Lett*. 2009; 16: 196–200. <https://doi.org/10.2174/092986609787316306> PMID: 19200044
25. Mohammadi Tashakkori M, Tabatabaei M, Tebianian M, Mosavari N. Production of MPT-64 recombinant protein from virulent strain of *Mycobacterium bovis*. *Iran J Vet Res*. 2018; 19: 108–112. PMID: 30046321
26. Ahmad NM. Solubility-driven lead optimisation: Recent examples and personal perspectives. *Bioorg Med Chem Lett*. 2016; 26: 2975–2979. <https://doi.org/10.1016/j.bmcl.2016.04.049> PMID: 27161281
27. Saal C, Petereit AC. Optimizing solubility: kinetic versus thermodynamic solubility temptations and risks. *Eur J Pharm Sci*. 2012; 47: 589–95. <https://doi.org/10.1016/j.ejps.2012.07.019> PMID: 22885099
28. Edwards PR, Gill A, Pollard-Knight D V, Hoare M, Buckle PE, Lowe PA, et al. Kinetics of protein-protein interactions at the surface of an optical biosensor. *Anal Biochem*. 1995; 231: 210–7. <https://doi.org/10.1006/abio.1995.1522> PMID: 8678303
29. Jones DC, Ariza A, Chow WA, Oza SL, Fairlamb AH. Molecular & Biochemical Parasitology Comparative structural, kinetic and inhibitor studies of *Trypanosoma brucei* trypanothione reductase with *T. cruzi*. 2010; 169: 12–19. <https://doi.org/10.1016/j.molbiopara.2009.09.002> PMID: 19747949
30. Jones DC, Ariza A, Chow W-HA, Oza SL, Fairlamb AH. Comparative structural, kinetic and inhibitor studies of *Trypanosoma brucei* trypanothione reductase with *T. cruzi*. *Mol Biochem Parasitol*. 2010; 169: 12–9. <https://doi.org/10.1016/j.molbiopara.2009.09.002> PMID: 19747949
31. Kabsch W. XDS. *Acta Crystallogr D Biol Crystallogr*. 2010; 66: 125–32. <https://doi.org/10.1107/S0907444909047337> PMID: 20124692
32. Vagin A, Teplyakov A. Molecular replacement with MOLREP. *Acta Crystallogr D Biol Crystallogr*. 2010; 66: 22–5. <https://doi.org/10.1107/S0907444909042589> PMID: 20057045
33. Murshudov GN, Vagin AA, Dodson EJ. Refinement of macromolecular structures by the maximum-likelihood method. *Acta Crystallogr D Biol Crystallogr*. 1997; 53: 240–55. <https://doi.org/10.1107/S0907444996012255> PMID: 15299926
34. Emsley P, Lohkamp B, Scott WG, Cowtan K. Features and development of Coot. *Acta Crystallogr D Biol Crystallogr*. 2010; 66: 486–501. <https://doi.org/10.1107/S0907444910007493> PMID: 20383002
35. Zhang J-H, Chung TDY, Oldenburg KR. A Simple Statistical Parameter for Use in Evaluation and Validation of High Throughput Screening Assays. *Journal of Biomolecular Screening*. 1999. pp. 67–73. <https://doi.org/10.1177/108705719900400206> PMID: 10838414
36. Hamilton CJ, Saravanamuthu A, Eggleston IM, Fairlamb AH. Ellman's-reagent-mediated regeneration of trypanothione in situ: substrate-economical microplate and time-dependent inhibition assays for trypanothione reductase. *Biochem J*. 2003; 369: 529–37. <https://doi.org/10.1042/BJ20021298> PMID: 12416994
37. Jacoby EM, Schlichting I, Lantwin CB, Kabsch W, Krauth-Siegel RL. Crystal structure of the *Trypanosoma cruzi* trypanothione reductase-mepacrine complex. *Proteins*. 1996; 24: 73–80. [https://doi.org/10.1002/\(SICI\)1097-0134\(199601\)24:1<73::AID-PROT5>3.0.CO;2-P](https://doi.org/10.1002/(SICI)1097-0134(199601)24:1<73::AID-PROT5>3.0.CO;2-P) PMID: 8628734
38. Saravanamuthu A, Vickers TJ, Bond CS, Peterson MR, Hunter WN, Fairlamb AH. Two interacting binding sites for quinacrine derivatives in the active site of trypanothione reductase: a template for drug design. *J Biol Chem*. 2004; 279: 29493–500. <https://doi.org/10.1074/jbc.M403187200> PMID: 15102853
39. Ilari A, Genovese I, Fiorillo F, Battista T, De Ionna I, Fiorillo A, et al. Toward a Drug Against All Kinetoplastids: From LeishBox to Specific and Potent Trypanothione Reductase Inhibitors. *Mol Pharm*. 2018; 15: 3069–3078. <https://doi.org/10.1021/acs.molpharmaceut.8b00185> PMID: 29897765
40. Leung K. 3-N-(2-[18F]Fluoroethyl)spiperone [Internet]. Molecular Imaging and Contrast Agent Database (MICAD). 2004. Available: <http://www.ncbi.nlm.nih.gov/pubmed/20641672>
41. Spanarello S, La Ferla T. The pharmacokinetics of long-acting antipsychotic medications. *Curr Clin Pharmacol*. 2014; 9: 310–7. Available: <http://www.ncbi.nlm.nih.gov/pubmed/23343447> <https://doi.org/10.2174/15748847113089990051> PMID: 23343447

Review

Targeting Trypanothione Reductase, a Key Enzyme in the Redox Trypanosomatid Metabolism, to Develop New Drugs against Leishmaniasis and Trypanosomiases

Theo Battista ¹, Gianni Colotti ², Andrea Ilari ² and Annarita Fiorillo ^{1,*}

¹ Department of Biochemical Sciences, Sapienza University, P.le A.Moro 5, 00185 Rome, Italy; theo.battista@uniroma1.it

² Institute of Molecular Biology and Pathology, Italian National Research Council, IBPM-CNR, c/o Department of Biochemical Sciences, Sapienza University, P.le A.Moro 5, 00185 Rome, Italy; gianni.colotti@cnr.it (G.C.); andrea.ilari@cnr.it (A.I.)

* Correspondence: annarita.fiorillo@uniroma1.it; Tel.: +39-064-991-0910

Academic Editor: Sandra Gemma

Received: 4 April 2020; Accepted: 20 April 2020; Published: 21 April 2020



Abstract: The protozoans *Leishmania* and *Trypanosoma*, belonging to the same Trypanosomatidae family, are the causative agents of Leishmaniasis, Chagas disease, and human African trypanosomiasis. Overall, these infections affect millions of people worldwide, posing a serious health issue as well as socio-economical concern. Current treatments are inadequate, mainly due to poor efficacy, toxicity, and emerging resistance; therefore, there is an urgent need for new drugs. Among several molecular targets proposed, trypanothione reductase (TR) is of particular interest for its critical role in controlling the parasite's redox homeostasis and several classes of active compounds that inhibit TR have been proposed so far. This review provides a comprehensive overview of TR's structural characterization. In particular, we discuss all the structural features of TR relevant for drug discovery, with a focus on the recent advances made in the understanding of inhibitor binding. The reported cases show how, on the basis of the detailed structural information provided by the crystallographic analysis, it is possible to rationally modify molecular scaffolds to improve their properties.

Keywords: trypanosomatid infection; structure-based drug design; trypanothione reductase; rational drug discovery; protein crystallography

1. Introduction

Leishmaniasis, Chagas disease, and human African trypanosomiasis (HAT), also known as sleeping sickness, are vector borne zoonosis that affect millions of people worldwide and lead to the death of about 100,000 humans per year. These diseases are caused by infection with the trypanosomatids *Leishmania* (*L.*), *Trypanosoma* (*T.*) *cruzi*, and *Trypanosoma brucei*, respectively.

Several species of *Leishmania* parasites, transmitted by the bite of infected female phlebotomine sandflies, cause three main forms of leishmaniases: visceral (VL), cutaneous (CL), and mucocutaneous (MCL). There are an estimated 700,000 to 100,000,000 new cases of Leishmaniases annually in the world, widely distributed in tropical and subtropical climate zones, which lead to 26,000 to 65,000 deaths [1].

Chagas disease, also known as American trypanosomiasis, is found mainly in endemic areas of 21 continental Latin American countries, where it affects about 6 to 7 million people. Chagas disease is transmitted to humans by contact with feces or urine of triatomine bugs, known as “kissing bugs”. *Trypanosoma cruzei* infection is curable if treatment is initiated soon after infection; if the disease becomes chronic, the patient may develop cardiac, digestive, and/or neurological alterations [2].

Sleeping sickness is endemic in 36 sub-Saharan African countries, where it is transmitted by tsetse flies. *Trypanosoma brucei gambiense* accounts for more than 98% of reported cases of the disease. Sustained control efforts have reduced the number of new cases so that in 2009 the number of reported cases dropped below 10,000 for the first time, and in 2018 there were only 977 cases recorded [3].

These diseases affect some of the poorest countries in the world and are often associated with malnutrition, population migration, poor housing, weak immune systems, such that they are generally recognized as neglected tropical diseases. However, the Mediterranean Basin is included in the affected areas, and climate change will exacerbate the ecological risk of human exposure in regions out of the current range of the disease; therefore, the issue concerns developed countries as well. Moreover, animal infection represents a further socio-economic problem: both domestic and wild animals are a reservoir for human infection, as in the case of endemic canine leishmaniasis in the Mediterranean area; in addition, livestock infection can cause significant economic losses in rural areas, as in the case of Nagana disease in Africa.

The therapeutic arsenal currently available for these diseases includes suramin, pentamidine, melarsoprol, and eflornithine for HAT; benznidazole and nifurtimox for Chagas disease; miltefosine, amphotericin B in liposomal formulation, pentavalent antimonials, and paromomycin for visceral leishmaniasis. Despite the need, these drugs are unsatisfactory because of a number of reasons: they are poorly effective, manifest severe side effects, episodes of resistance are increasingly frequent, and most treatments require prolonged and parenteral administration not suited for therapy in poor countries. Antimonials, for example, have a low therapeutic index and invoke extreme toxicities; therefore, they are administered only if strictly needed, in case of resistance to other treatments. Many different approaches have been attempted to date to develop new trypanocidal drugs, ranging from target based to phenotypic based and repositioning, and some compounds have been moved to clinical trials, but further efforts will be needed for new drugs to hit the market [4].

Leishmania and *Trypanosoma* parasites share many features, including gene conservation, high amino acid identity among proteins, the presence of subcellular structures such as glycosomes and the kinetoplastid, and genome architecture; such conservations may make drug development family-specific, rather than species-specific, i.e., based on the inhibition of a common, conserved target. Many unique metabolic pathways and cellular functions, divergent from other eukaryotes, are attractive target sources for drug discovery [4].

Oxidative stress plays an essential role in the host immune fight against infection, so that parasite survival mainly depends on the capability to resist this attack [5]. Infective trypanosomatids lack catalase [6] and other conventional redox controlling systems [7,8], and they base their defense on trypanothione, an unusual variant of glutathione, main actor in maintaining thiols' homeostasis. Being essential and peculiar, trypanothione is a weakness for these parasites, and all related enzymes are considered interesting candidates for drug development [9]. Among these, trypanothione reductase (TR), the enzyme directly responsible for keeping trypanothione in the reduced state, has been extensively studied since it fulfills most of the requirements for a good drug target [10]. Indeed, TR is: (i) essential for parasite survival; (ii) absent in the host, in which TR is replaced by glutathione reductase (GR); (iii) druggable, in that it can be efficiently addressed by inhibitors.

TR has been validated as a target in both *Leishmania* and *Trypanosoma* as it is not possible to obtain TR-knockout mutants and its downregulation causes strong impairment of infectivity [11,12]. It has also been proven that antimonials, among the drugs currently in use to treat leishmaniasis, interfere with the trypanothione metabolism and inhibit TR [13,14], reinforcing the idea that targeting this protein is a concrete option for the treatment of these diseases. Moreover, the high sequence homology of TRs from different sources (80–100%) makes it a valuable target for developing a single, broad spectrum drug active against all trypanosomatids [15].

The main limitation of TR as a drug target lies in its high efficiency/turnover: it was shown that, in order to have a significant effect on parasite redox state and viability, TR activity must be reduced by

at least 90%, meaning that only potent inhibitors, with submicromolar IC_{50} , can be considered very promising lead compounds [11,12].

Many efforts have been made in order to find new effective hits through in vitro and in silico screening, in addition to the development of known scaffolds via SAR or structure-based design approaches [15–33], so that several classes of active compounds have been proposed to date.

This article provides an overview of the attempts made so far to rationalize the interaction between TR and known inhibitors through a detailed experimental structural characterization. Based on this information, as shown by some examples reported, it is possible to plan chemical modification of selected molecules in order to improve their potency and selectivity or to alter other characteristics, such as solubility, pharmacokinetics, and dynamics, without affecting affinity.

2. Relevant Structural Features of TR

Before addressing the binding mode of inhibitors, it is appropriate to describe the main structural features of TR, the mechanism of catalysis, and the recognition of substrates.

The structure of TR is thoroughly characterized, since the crystal structure has been solved for several species, namely *Crithidia fasciculata*, *L. infantum*, *T. brucei*, and *T. cruzi*, also in complex with substrates [14,34–37]. TR is an obligate homodimer with each of the two individual subunits, related by two-fold symmetry, comprising an FAD-binding domain (residues 1–160 and 289–360), an NADPH-binding domain (residues 161–288), and an interface domain (residues 361–488, *T. brucei* numbering).

The protein catalyzes the reduction of the dithiol trypanothione (from TS_2 to $T(SH)_2$) at the expense of the co-substrate NADPH. NADPH and TS_2 bind different cavities facing opposite sides of the isoalloxazine ring of FAD. The TS_2 site, located at the interface between the two subunits, is shaped by residues belonging to both subunits. The reaction mechanism relies on the transfer of two electrons from NADPH to two catalytic cysteines (Cys52 and Cys57), via the FAD cofactor. Once the cysteines are reduced, the oxidized TS_2 binds to the protein, and Cys52, deprotonated by the couple His461'-Glu466', attacks the disulfide bridge of the substrate, resulting in the formation of a mixed disulfide. Finally, the attack of Cys57 on Cys52 enables the release of the reduced $T(SH)_2$ (Figure 1). During catalysis, no major structural changes occur, apart from the strictly necessary displacements of the side chains of the residues involved.

The structure is almost identical for all the characterized species, in accordance with the high degree of sequence similarity (Figure 1, panel D). Indeed, TRs from all Trypanosomatidae share at least 67% of primary sequence, with >82% identity among *Leishmania* spp. and >80% among *Trypanosoma* spp. Similarity reaches 100% for residues shaping both substrates' binding sites, with the fact that the mode of binding of ligands is the same for all TRs characterized to date [34–36]. The trypanothione assumes variable conformations in the wide cavity, as an effect of the "dynamics" of its binding. In fact, trypanothione enters as a disulfide but, upon reduction, it is released in an extended conformation. Despite this variability, some interactions emerge to be particularly relevant and specific for binding: Glu18, together with other acidic residues, accounts for the positive charge of the substrate, while the almost hydrophobic patch including Trp21, Tyr110, and Met113 mediates the interaction with the polyamine moiety contained in trypanothione.

This observation suggests that, in the search for new inhibitors, results can be transferred from one TR to the others, and the chance exists to find a common inhibitor active on all TRs that can lead to the development of a broad spectrum trypanocidal drug. This is clearly an ambitious goal because differences in biology and lifestyle of these parasites, although they are closely related genetically, could cause species-specific efficacy, as in the case of eflornithine (DFMO). Indeed, DFMO, a suicide inhibitor of ornithine decarboxylase from any source, is the treatment of choice for advanced stage of the sleeping sickness caused by *T. brucei* but is rather ineffective on other infections [9].

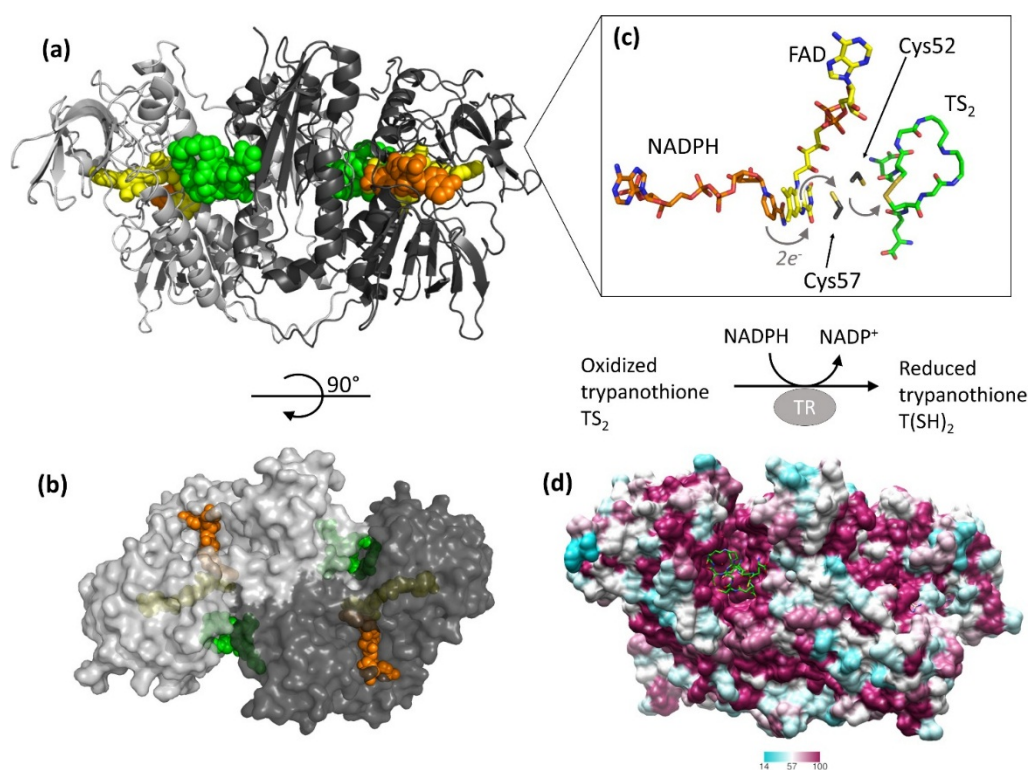


Figure 1. Structure and activity of trypanothione reductase (TR). (a,b) Two views of TR dimer from *T. brucei* (PDB: 2w0w) are shown. NADPH (orange), FAD (yellow), and trypanothione (green) are represented as spheres to highlight the binding sites. (c) The detail shows all entities involved in the electron transfer from NADPH to trypanothione. For clarity, trypanothione is depicted as modeled in TR from *T. cruzi* (PDB: 1bzl), where a single oxidized conformation is observed in the absence of NADPH. (d) Sequence conservation of TR. The dimer of TR from *T. brucei* (PDB: 2w0w) is colored according to the percentage of amino acid identity with respect to other representative TR sequences (*C. fasciculata*, *T. cruzi*, *T. congolense*, *T. brucei*, *L. braziliensis*, *L. infantum*, *L. major*). Trypanothione, represented as green sticks, assumes multiple conformations in the wide and highly conserved binding cavity.

3. Off-Target Evaluation: Comparison with Glutathione Reductase (GR)

Selectivity is a fundamental parameter in the evaluation of a potential pharmacological target. For the development of an antiparasitic drug, it is important to choose a target that has substantial differences compared to the host homolog(s), the so-called off-target(s), in order to promote specific action and minimize side effects.

The trypanothione/TR couple replaces many of the antioxidant and metabolic functions of the glutathione/glutathione reductase (GSH/GR) and thioredoxin/thioredoxin reductase (Trx/TrxT) systems present in the host [38].

GR is the closest human homolog of TR as they have the same overall fold, with 38% sequence identity, and catalyze the same reaction on very similar substrates. Both GR and TR reduce a disulfide bridge that is intermolecular for GR ($GSSG \rightarrow 2 GSH$) and intramolecular for TR ($TS_2 \rightarrow T(SH)_2$). Indeed, trypanothione is an analog of glutathione, comprised of two glutathione molecules linked by amide bonds occurring between the glycyl carboxylate groups of each GSH and the primary amines of the polyamine spermidine.

The most significant differences between the two proteins reflect the differences between their cognate substrates: TS_2 is bulkier than GSSG and positively charged due to the spermidine moiety, while GSH has a net negative charge at physiological pH. As a consequence, the TS_2 binding site in TR is wider and negatively charged with respect to the GSSG binding site in GR (Figure 2). In particular, selective interactions take place between the spermidine moiety and residues Glu18, Trp21, Ser109,

Tyr110, and Met114 that are not conserved in GR and are partially replaced by arginine residues (Arg37, Arg38, and Arg347).

These steric and electrostatic differences account for the selectivity for substrates [39] and emphasize the potential to generate parasite-specific compounds.

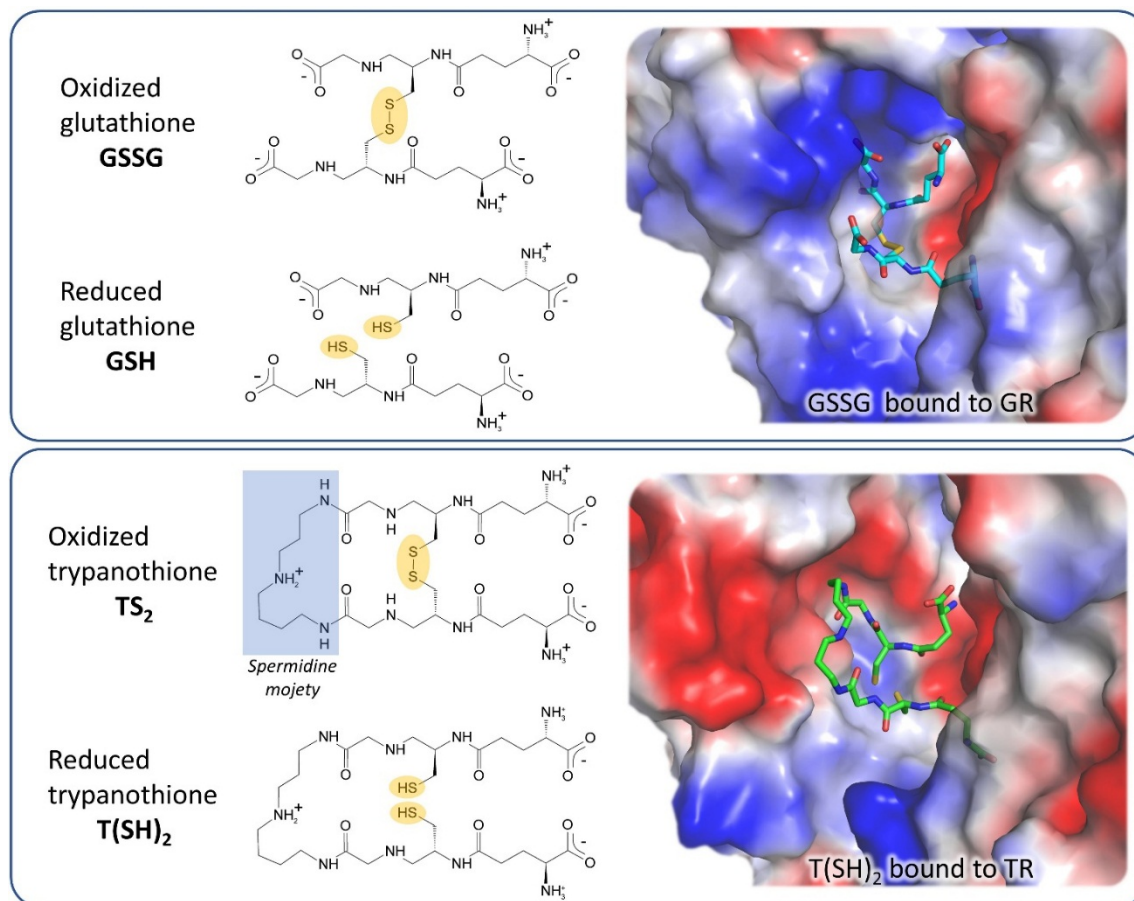


Figure 2. Substrates and active site of glutathione reductase (GR) and TR. The comparison between the electrostatic potential surfaces of GR (upper panel, PDB: 1gra) and TR (lower panel, PDB: 1bzl) highlights the difference in size and charge of substrate binding sites, related to substrates features.

4. Structural Characterization of TR Inhibitors

Structural studies on TR, intensified over the past 10 years, strongly improved the understanding of the molecular basis of ligand binding, allowing to identify hot-spots for interaction with substrates and inhibitors. This knowledge has been exploited in few structure-based design approaches which, in some cases, have led to a significant improvement in the performances of lead molecules [27,37,40].

To date, the crystallographic structure of TR in complex with 21 different inhibitors has been defined (see Table 1 and Table S1 and Figure 3). These can be grouped into 3 main inhibition modes: (i) competition with trypanothione, due to binding to the wide TS₂ cavity, comprising most of the characterized inhibitors; (ii) competition with NADPH, due to the binding to NADPH cavity; (iii) redox cysteines inactivation, due to a metal binding to Cys52 and Cys57 in the catalytic site. A fourth inhibition mode has been recently proposed [41], based on the disassembly of the TR dimer induced by small molecules designed to interfere with protein–protein interaction. However, poor structural information is available for this case.

Below is a description of the various classes of characterized inhibitors, divided according to mode of action and binding site, with attention to how the structural information was used to guide the design of better molecules.

4.1. Inhibitors Targeting the TS₂ Binding Cavity

As mentioned above, TR has a wide active site, suited to accommodate the voluminous trypanothione substrate. Most of the characterized inhibitors bind to this cavity, mainly in the so-called “mepacrine binding site” (MBS), a hydrophobic patch located at the entrance. Fewer ligands bind deeper in the cavity, closer to the real catalytic site, where the redox cysteines are located and TS₂ reduction takes place (Figure 4).

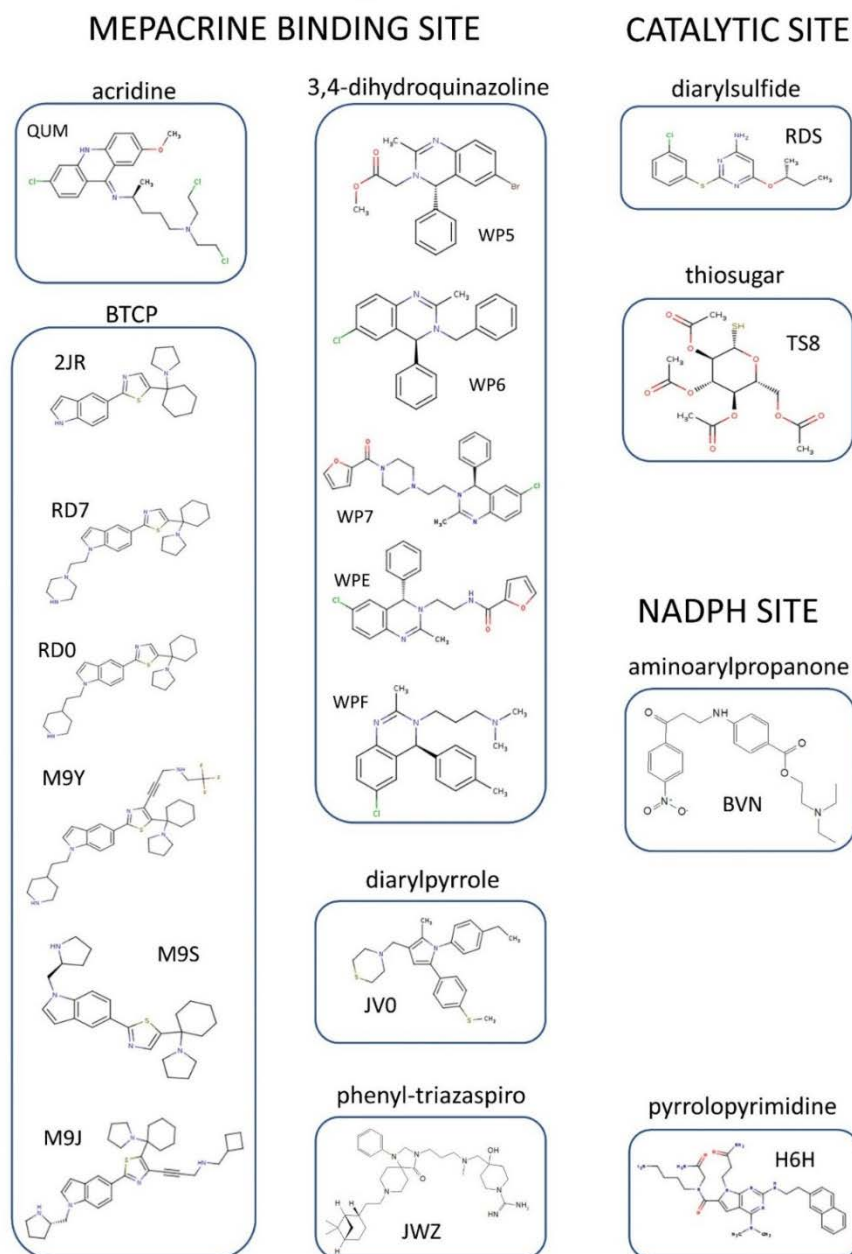
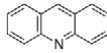
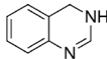
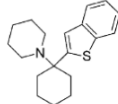


Figure 3. Organic inhibitors co-crystallized with TR, grouped by binding site and molecular scaffold. Molecules are named by PDB 3-digit ID.

Table 1. All inhibitors co-crystallized with TR.

Site	Scaffold	PDB Code	Source	Inhibitor PDB ID (Paper ID ^a)	Potency ^b	Reference	
MBS	Acridine 	<i>Not available</i>	Tc	(Quinacrine or mepacrine)	K _i : 25 μM	Jacoby, 1996	
		1gxf	Tb	QUM (Quin. mustard)	<i>Irreversible inhibition</i>	Saravanamuthu, 2004	
	3,4-dihydroquinazoline 	2wp5	Tb	WP5 (1a)	IC ₅₀ : 6.8 μM	Patterson, 2011	
		2wp6	Tb	WP6 (6a)	IC ₅₀ : 0.93 μM		
		2wpc	Tb	WP7 (13e)	IC ₅₀ : 0.42 μM		
		2wpe	Tb	WPE (11e)	IC ₅₀ : 0.86 μM		
		2wpf	Tb	WPF (29a)	IC ₅₀ : 0.23 μM		
		BTCP 	4nev	Tb	2JR (10a)	K _i : 12 μM Inh. [%] ^b : 43	Persch, 2014
			4new	Tc	2JR (10a)	K _i : 4 μM Inh. [%] ^b : 79	
			6bt1	Tb	RD7 (18)	K _i : 3.8 μM Inh. [%] ^c : 80	De Gasparo, 2018
			6bu7	Tb	RD0 (19)	K _i : 6.4 μM Inh. [%] ^c : 78	
			6oez	Tb	M9J ((+)-2)	K _i : 73 nM	De Gasparo, 2019
			6oey	Tb	M9S ((+)-4)	K _i : 2.1 μM	
			6oex	Tb	M9Y (5)	K _i : 1.5 μM	
		diarylpyrrole	4apn (B)	Li	JV0 (1)	K _i : 4.6 μM IC ₅₀ : 13.8 μM	Baiocco, 2013
		phenyl-triazaspiro	6br5	Tb	JWZ (1)	IC ₅₀ : 5.7 μM	Turcano, 2020
		Pyrrrolopyrimidine	6i7n (B)	Li	H6H (2f)	IC ₅₀ : 52.2 μM	Revuelto, 2019
Catalytic site	diaryl sulfide	5ebk	Li	RDS (RDS 777)	K _i : 0.25 μM	Saccoliti, 2017	
Catalytic site/cysteines	Metal/thiosugar	2yau	Li	AU-TS8 (auranofin)	K _i : 0.15 μM	Ilari, 2012	
Catalytic cysteines	Metal	2w0h	Li	SB	K _i : 1.5 μM	Baiocco, 2009	
		2x50	Li	AG	K _i (Ag1): 500 nM K _i (Ag0): 50 nM	Baiocco, 2010	
NADPH-cavity	3-amino-1-arylpropan-1-one	6er5	Li	BVN (3)	IC ₅₀ : 12.4 μM	Turcano, 2018	

^a identification code of the inhibitor as reported in the original paper. ^b K_i, IC₅₀ and/or percentage of inhibition are reported when available in literature. ^c Percent inhibition by 40 mM inhibitor in the presence of 40 mM dithiol trypanothione (TS₂).

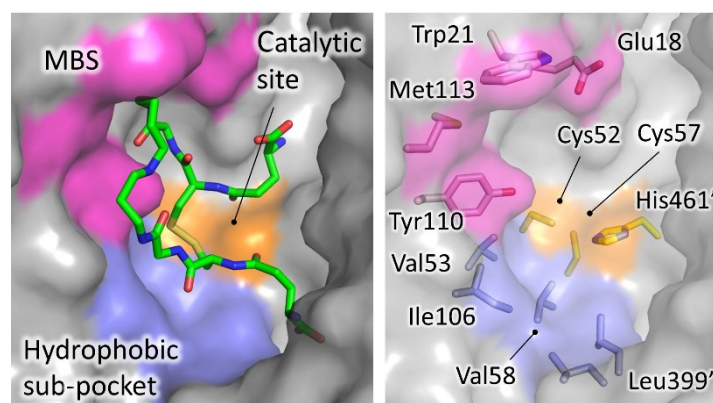


Figure 4. Trypanothione binding cavity. Surface representation of TR from *T. brucei* (pdb: 2wow). The most significant areas for ligand interaction are highlighted with different colors. TS₂, extracted from *T. cruzi* structure (pdb: 1bzl) is shown as sticks.

4.1.1. Mepacraine Binding Site (MBS)

Mepacraine, also named quinacrine, is a well-known antiprotozoal compound, superseded by safer and more effective agents. In 1996, Jacoby and coworkers described the crystal structure of *T. cruzi* TR in complex with mepacraine [42] (coordinates not available in the PDB). The ligand, known to compete with TS₂, was found on the edge of the active site. Later, Saravanamuthu and coworkers [43], added details to this interaction, by solving the structure of TR with an alkylating mepacraine derivative at higher resolution. The interaction is dominated by 4 residues, namely Trp21, Met113, Tyr110, and Glu18. They found that two molecules of the inhibitor bind in a synergistic way by stacking of planar acridine ring, thereby gaining an increased number of binding interactions. In particular, the aromatic acridine ring of the first mepacraine molecule stacks over Trp21 and is lined by Met113, while the alkylamino chain points inside the active site, held in position by Glu18, and covalently binds to Cys52 (*T. brucei* numbering); the second stacked acridine is lined by Tyr110. The site immediately turned out to be interesting since the residues that shape it are important for TS₂ binding and are not conserved in GR. Indeed, mepacraine does not affect human GR.

Since then, other scaffolds besides tricyclic acridine have been found to bind to MBS. In 2011, Patterson et al. [37] developed a new class of TR inhibitors based on a 3,4-dihydroquinazoline scaffold, by an elegant combination of chemical-driven and structure-based approaches. Starting from a high-throughput screen hit [17], indicated as compound 1a, they composed and tested a small commercial collection of molecules. On the basis of the structure–activity relationship (SAR) analysis of these compounds, the authors planned the synthesis of new derivatives. The crystal structure of hit 1a (WP5 in PDB) and another 3 representative inhibitors in complex with TR from *T. brucei* revealed the mode of binding and helped to rationalize SAR analysis. All derivatives bind to the TS₂ cavity at the MBS and surprisingly induce a structural variation of the active site that was revealed to be critical for binding. Indeed, a new subpocket, which accommodates the C4-phenyl substituent of the scaffold, is generated by the displacement of Met113 side chain. Structural information was subsequently used to design other inhibitors, including analogs that challenged the induced subpocket. Overall, this hit-to-lead approach resulted in the development of inhibitors with improved potency, among which the best performing has a 30-fold lower IC₅₀ for *T. brucei* TR with respect to starting compound (1a, WP5 in PDB: 6.8 μM; 29a, WPF in PDB: 0.23 μM), although selectivity remained an issue (Figure 5).

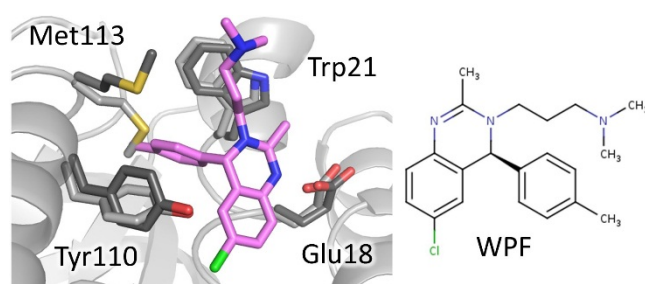


Figure 5. Mode of binding of 3,4-dihydroquinazoline derivatives. Compound WPF, best performing compound of the series, binds to mepacrine binding site (MBS). Critical residues are shown as sticks, light grey for inhibitor-free (PDB: 2wow) and dark grey for inhibitor-bound TR (PDB: 2wpf). Note the displacement of Met113 to accommodate the C4-phenyl substituent.

In 2013, Ilari and collaborators [35] described the binding of a diarylpyrrole to TR from *L. infantum*. The compound was selected from an in-house collection on the base of activity on amastigote form of *L. donovani* and docking studies on TR. The structure shows that, as observed for mepacrine derivative, two molecules bind to MBS without inducing any variation in the cavity, but the mode of binding differs considerably. In this case, the compound assumes multiple conformations, likely due to its intrinsic flexibility, and no stacking to Trp21 takes place, indicating that MBS has the capability to interact in different ways with unrelated scaffolds.

Derivatives of 1-(1-(Benzo[b]thiophen-2-yl)cyclohexyl)piperidine (BTCP), another class of compounds able to bind MBS, are probably, to date, the most explored compounds for structure-based development. Identified by HTS together with many other tricycles [21], the lead BTCP was found to be a competitive inhibitor of TbTR, active on *T. brucei* cultures but endowed with poor selectivity against mammalian cells. However, it was considered to be a promising screening hit for further development due to some drug-like characteristics such as low molecular weight, lack of activity on GR, capability of crossing the blood–brain barrier, and critical property for treating HAT [44]. The first attempt to describe the binding to plan a structure-based improvement of BTCP's properties was carried out by Persch et al. [40]. Previous work suggested that binding of BTCP occurs at the so-called Z-site, a hydrophobic region in front of MBS [45]. However, the conjunction of mutation studies and virtual ligand docking simulations led to the prediction that the binding takes place at MBS. This was confirmed by the co-crystal structure of both *T. brucei* and *T. cruzi* TR with compound 10a (2JR 3-digit code in PDB), a BTCP analog in which a thiazole is inserted between indole and cyclohexyl rings (Figure 6). Two key interactions appear to control binding: the protonated tertiary amine of the ligand makes a Coulombic interaction with Glu18, while the indole moiety binds to the hydrophobic wall of MBS (Trp21, Tyr110, Met113) even if it adopts different orientations in the two structures [40].

Further efforts for improving properties and potency of this class have been recently undertaken by De Gasparo and colleagues [27,46]. They explored the possibility to combine the 2 different binding modes observed for compound 10a by introducing other substituents on the thiazole to be able to increase water solubility and binding affinity. At first, three new series of BTCP derivatives were synthesized and tested for activity on TR and parasites, but the results were not very satisfactory in terms of efficacy, though useful structural information emerged [46]. In fact, co-crystal structures of 2 new ligands (18 and 19) confirmed the mode of binding previously observed, with the indolyl-thiazole core adopting identical orientation, and the newly introduced water-solubility-providing substituents oriented toward the periphery of the active site.

Later, new substitutions resulted in a significant improvement of potency and selectivity. Indeed, compound (+)-2 (M9J in PDB), claimed to be the most effective non-covalent inhibitor of TR ever reported, inhibits *T. brucei* TR with an inhibition constant K_i of 73 nM and is fully ineffective against human GR, even if its toxicity against mammalian cells is relatively high [27]. Two major structural changes led to this result: the modification of the substituent on the indole moiety, combined with

the introduction onto position 4 of the central thiazole moiety of a propargylic substituent, designed to target a hydrophobic sub-pocket near the catalytic cysteines in the TR active site. The structure of inhibitor (+)-2-TR complex confirmed the prediction, showing that the indole protonated substituent expands the interaction in MBS to Asp116, while the propargylic moiety, although mobile, locates deeper into the cavity. Moreover, a HEPES molecule, found in close proximity to propargylic substituent, suggests the opportunity to further modify the lead to reach another anchor point in the wide TS₂ cavity (Figure 6).

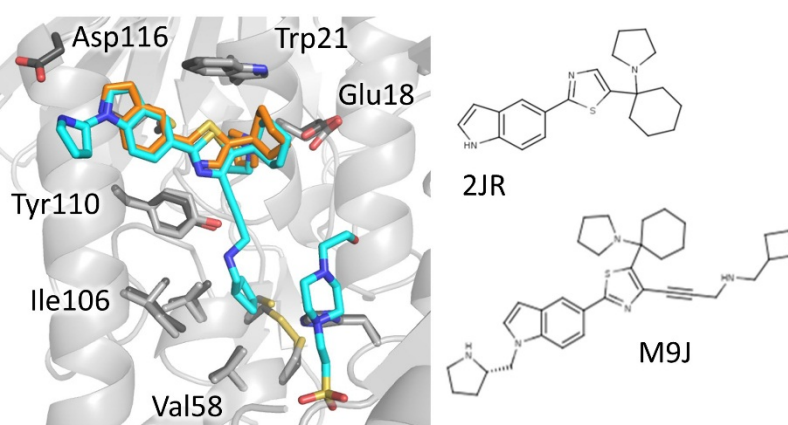


Figure 6. Mode of binding of 1-(1-(benzo[b]thiophen-2-yl)cyclohexyl)piperidine (BTCP)-derivatives. Compound 2JR (orange) binds to MBS while its best performing evolution M9J (cyan) extends to the catalytic site and, in addition, a HEPES molecule binds deeper in the cavity (cyan). Critical residues are shown as sticks, light grey for inhibitor-free (PDB: 2wov) and dark grey inhibitor-bound TR (PDB: 6oez).

Very recently, a new spiro-containing series has been found to bind trypanothione cavity, resembling the mode of binding of compound M9J [47]. The hit, identified by HTS on *T. brucei* TR, was found to inhibit both the recombinant enzyme and the enzyme in cell lysate, as well as parasite proliferation in the low micromolar range (2–5 μ M) while being inactive on human GR. Crystallographic studies confirmed the hot-spots for interaction already found for BTCP-derivatives (Figure 7). Indeed, the phenyl-triazaspiro core anchors the molecule to the MBS (Trp21, Met113, and Tyr110) while the arms cause steric hindrance both at the bottom and at the entrance of the cavity: the tertiary amino group of the hydrophilic carboximidamide arm, fluctuating toward the entrance, engages a weak electrostatic interaction with Glu18 and, in general, with the negative environment; the hydrophobic bicycle-heptane moiety extends deeper in the cavity, pointing to the same hydrophobic sub-pocket targeted by the propargylic substituent of (+)-2 BTCP-derivative (Val53, Val58, Ile106, and Leu399). A second binding site is located at the dimeric interface but seems to be not significant for activity. Though several rounds of optimization are needed, what makes this spiro-core particularly interesting is the fact that, as for BTCP, molecules containing this moiety are known to be able to penetrate the brain, a very appealing characteristic for the treatment of the second stage of sleeping sickness, affecting the central nervous system [48,49].

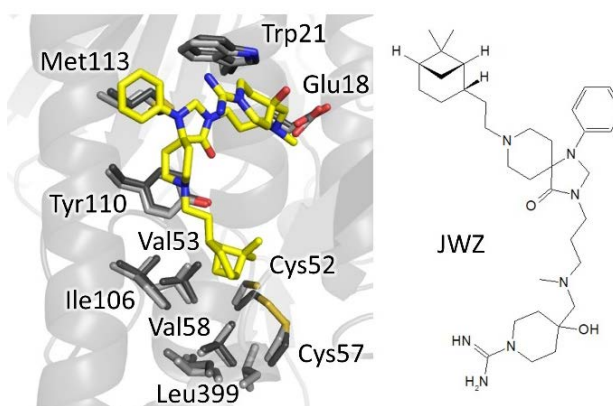


Figure 7. The binding mode of spiro-containing derivative. The phenyl-triazaspiro core seizes the MBS while the bicyclo-heptane moiety accommodates in the hydrophobic sub-pocket. Involved residues are shown as sticks, light grey for inhibitor-free (PDB: 2w0w) and dark grey for inhibitor-bound TR (PDB: 6rb5).

4.1.2. Catalytic Site

Other compounds have shown the capability to bind the inner part of the active site. Recently, screening of an in-house collection detected a novel class of diarylsulfides active on *Leishmania* culture and TR [32]. In particular, the compound RDS777 (6-(sec-butoxy)-2-((3-chlorophenyl)thio)pyrimidin-4-amine) was found to inhibit TR with high efficiency (K_i 0.25 μM) by competing with TS_2 , and to affect parasites in the micromolar range (IC_{50} 29 μM). The crystal structure of RDS777 (RDS in PDB) in complex with *L. infantum* TR revealed the binding of 4 inhibitor molecules, one of which lays at the bottom of TS_2 cavity, in direct contact with catalytic site by establishing hydrogen bonds with the residues involved in catalysis, namely Glu466', Cys57, and Cys52. A second molecule is found in one out of two cavities, placed closer to the entrance, engaged in a stacking interaction with the first one. The other two molecules interact with the NADPH-binding site and are discussed later. Based on the structural information, a series of new derivatives have been synthesized, one of which has a higher activity on parasite cultures (IC_{50} 11 μM) and is able to decrease the reduced- $\text{T}(\text{SH})_2$ concentration in cell [25]. However, this new compound is less effective in TR inhibition (K_i 12 μM) and docking studies suggest that it prefers the second outermost binding site, indicating that it likely has other intracellular targets besides TR.

Other diaryl sulfides have been proposed previously and the binding site, predicted using docking, was different from RDS777, corresponding to the MBP and Z-site [50,51]. However, it must be considered that the bond is plausibly influenced more by the nature of the aryl substituents than by the thioether itself.

4.1.3. Metal Inhibitors

Metalloid-based drugs, such as pentavalent antimonials and arsenicals, are currently used to treat trypanosomiasis and leishmaniasis, despite having severe side effects and resistance phenomena [52]. It is known that these drugs, at least in part, act on TR by binding catalytic cysteines. In particular, Baiocco et al. [14] demonstrated that Sb(III) efficiently inhibits reduced TR (K_i 1.5 μM) by forming a stable complex with the residues involved in catalysis, namely the two cysteines (Cys52 and Cys57), His461 (the residue that together with Glu466' activates the Cys52 similar to the cysteine proteases), and Thr335. Besides antimony, silver and gold were proven to bind TR in a similar way but even more efficiently [53–55] with K_i down to 20 nM. Particularly interesting is the case of auranofin, a gold-containing drug used to treat rheumatoid arthritis [56]. Tested on *Leishmania* TR and parasites [54], auranofin was found to be 10-fold more potent than Sb on TR (K_i 0.15 μM) and, most crucially, it acts via a double mode of action. In fact, besides expected gold complexation, the thiosugar

moiety of auranofin contributes to inhibition by binding the inner part of TS₂ site. This finding suggests the opportunity to combine scaffolds that are able to bind the outer TS₂ cavity with auranofin or other metal-coordinating moieties to exploit double inhibition mechanism and to promote a selective targeting of otherwise poorly specific metal inhibitors (Figure 8).

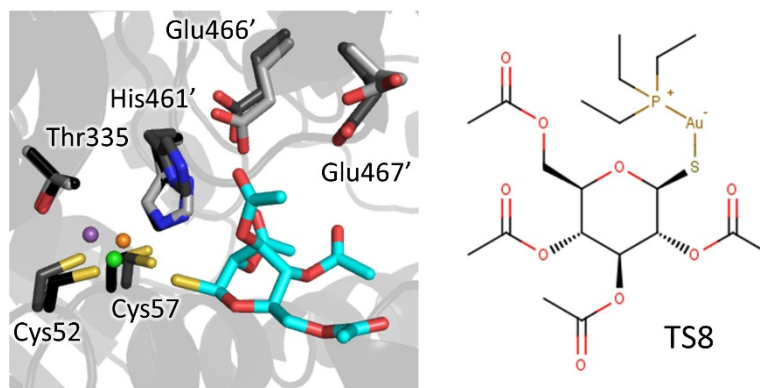


Figure 8. Metal complexation: Sb(III) (violet) forms a stable complex with catalytic residues. Similarly, Au(I) (orange) displays a planar-trigonal coordination (Ilari et al., 2012) with Cys52, Cys57, and a chloride ion (green). The thiosugar moiety (cyan) participates in the inhibition mechanism interacting with His466', Glu466', and Glu467'. Residues are shown as sticks, light grey for inhibitor-free TR (PDB: 2jk6), dark grey for Au-bound TR (PDB: 2yau), and black for Sb-bound TR (PDB: 2w0h).

4.2. Inhibitors Targeting NADPH Binding Cavity

NADPH-binding cavity is considered less appealing for the development of specific TR inhibitors clearly due to the nature of this ubiquitous cofactor involved in a number of pathways in all organisms. Nevertheless, a couple of TR inhibitors have been found to bind to this site, one of which deserves some attention.

As anticipated, diaryl sulfide RDS777 was found to bind to even the NADPH-binding site, specifically at the entrance where adenosine moiety of NADPH usually binds [32], though kinetic characterization denied competition for the cofactor so it can be speculated that binding is weak or due to crystallographic artifact.

In 2018, a new inhibitor targeting the NADPH-binding site was identified by HTS on *L. infantum* TR, based on a new luminescent assay, followed by extensive SAR evaluation [23]. The inhibitor is not particularly potent (IC₅₀ for TR 7.5 μM) but it is interesting due to some other characteristics. Indeed, it competes for NADPH but is inactive on human GR and thioredoxin reductase, and it has dose-dependent anti-proliferative effect on *L. infantum* promastigotes at micromolar concentrations (IC₅₀ 12.4 μM). Crystallographic analysis of the complex revealed that the compound binds at the entrance of NADPH site, similar to RDS777, in a pocket not conserved in human GR (Figure 9). Even if cytotoxicity data are not available and the compound could be active on other NADPH-dependent human enzymes, it represents the first proof of the existence of a druggable site in NADPH cavity.

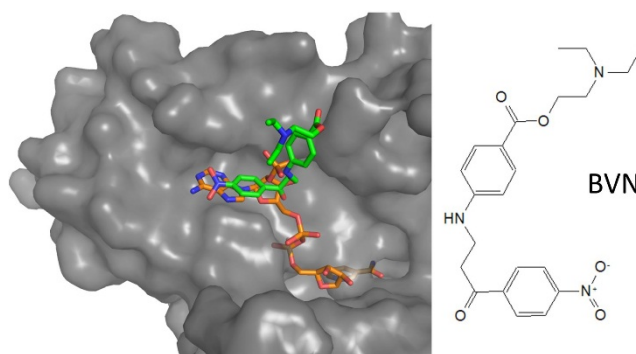


Figure 9. Mode of binding of aminoarylpropanone-derivative. Compound BVN (green) binds to NADPH (orange) binding site, where adenosine moiety locates. Protein surface is shown for BVN-bound LiTR (PDB: 6er5), superposed to NADPH-bound structure (PDB: 2w0h).

4.3. Nonpeptidic Dimerization Inhibition

The disruption of the functional dimer of TR by targeting PPI has been recently proposed as an intriguing strategy alternative to competitive inhibition. Starting from the analysis of the dimerization interface of *L. infantum* TR, Toro and colleagues identified few interaction hot-spots involving an α -helical element from which they derived linear and cyclic peptides that are able to strongly affect both dimerization (95% decrease) and activity in the low micromolar range as well as *Leishmania* viability in vitro [57]. Later, in order to improve drug-like properties such as stability and permeability, nonpeptidic small molecule analogs were synthesized and tested with modest results, in which they showed a drop in efficacy for both dimerization and activity. Attempts to gain structural information on the interaction with best performing peptidomimetics (IC₅₀: 5–9 μ M) failed due to protein precipitation, possibly induced by dimer disruption (~30% at 20 μ M concentration). Instead, a mild inhibitor (IC₅₀: 52.2 μ M), inactive on dimerization, was unexpectedly found to bind the MBS. Interaction involves stacking of pyrrolopyrimidine core on Trp21 and H-bond interactions of amide groups with Glu18 and Ser109, while the rest of the molecule protrudes out of the cavity [41].

5. Conclusions and Perspectives

Among the many pathways proposed as potential targets for antitrypanosomatid drug development, trypanothione metabolism is one of the most explored due to its critical role in redox homeostasis and its peculiarity. TR has been considered a promising target since its discovery because it satisfies most requirements for candidates, being essential, unique and druggable. Various inhibitor series have been identified and proposed as lead compounds but, to our knowledge, none of them has been advanced to clinical trials. Common reasons for that are sub-optimal potency, poor selectivity leading to toxicity, low bioavailability or biodistribution causing inactivity on animal models.

In this context, structural characterization of inhibitor binding offers precious aid to improve inhibitor performances through structure-based design. In the last few years, several studies explored TR-inhibitor interaction by X-ray crystallography, revealing important information for binding rationalization and future development. Indeed, most inhibitors characterized so far locate to the wide trypanothione cavity, mainly at the entrance of the so-called mepacrine binding site (MBS). The MBS resulted to be quite promiscuous; in fact, besides the polyamine moiety of the substrate, it is able to bind different aromatic scaffolds. Binding site promiscuity can be an advantage in drug development because it favors polypharmacology approaches, known to decrease emergence of resistance. Moreover, it allows researchers to select molecules with convenient characteristics, as is the case for two identified scaffolds, BTCP and spiro-moiety, that are able to cross the BBB, a desirable feature for the treatment of HAT.

Besides the MBS, other hot-spots have been identified in the trypanothione cavity. A hydrophobic subpocket, located deeper in the site, accommodates the hydrophobic arm of two different inhibitors,

one of which displays nanomolar activity on TR. Finally, metal ions such as Sb(III), Ag(I), and Au(I) have proven to target redox-active cysteines in the catalytic site, confirming one of the proposed mechanisms of action for antileishmanial antimonial therapy [13,14].

The broadness of the trypanothione cavity is believed to be responsible for the relatively low potency of most inhibitors identified to date, that show inhibition constants in the low micromolar range, not enough for effective action. However, the identification of multiple hot-spots for interaction provides the chance to merge different scaffolds in one molecule, as in the serendipitous case of auranofin, in order to increase efficacy and selectivity, keeping in mind the size limitations for drug-like compounds.

Despite of the most rational approach, recent results have shown that the search for lead compounds should not focus solely on the trypanothione cavity: the identification of an inhibitor addressing the NADPH cavity, selective against the main off-target GR, as well as peptides and peptidomimetics interfering with TR dimerization give a proof of concept for the idea that other sites can be exploited for TR inactivation.

It cannot be excluded that unexpected effective binding sites exist. Given the availability of well diffracting crystals for both *T. cruzi* and *T. brucei* TR, a fragment-based screen campaign could reveal new small organic molecules suitable as lead compounds, targeting already known sites or unexplored hot-spots for new mechanisms of inhibition.

Supplementary Materials: The following are available online, Table S1: IUPAC name and smiles of inhibitors.

Author Contributions: A.F. conceptualized the review. T.B. and A.F. wrote the review and gathered literature materials. A.F., T.B., A.I. and G.C. discussed the contents. All authors have read and agreed to the published version of the manuscript.

Funding: This work was founded by CNCCS s.c.a.r.l. (National Collection of Chemical Compounds and Screening Center).

Acknowledgments: Special thanks to Alexandra Elbakyan and her collaborators for their support.

Conflicts of Interest: The authors declare no conflict of interest.

References

1. World Health Organization. WHO Publishes On-line Key Information about Leishmaniasis. Available online: <https://www.who.int/news-room/fact-sheets/detail/leishmaniasis> (accessed on 30 March 2020).
2. World Health Organization. WHO Publishes On-line Key Information about Chagas Disease. Available online: [https://www.who.int/news-room/fact-sheets/detail/chagas-disease-\(american-trypanosomiasis\)](https://www.who.int/news-room/fact-sheets/detail/chagas-disease-(american-trypanosomiasis)) (accessed on 30 March 2020).
3. World Health Organization. WHO Publishes On-line Key Information about HAT. Available online: [https://www.who.int/news-room/fact-sheets/detail/trypanosomiasis-human-african-\(sleeping-sickness\)](https://www.who.int/news-room/fact-sheets/detail/trypanosomiasis-human-african-(sleeping-sickness)) (accessed on 30 March 2020).
4. Field, M.C.; Horn, D.; Fairlamb, A.H.; Ferguson, M.A.; Gray, D.W.; Read, K.D.; De Rycker, M.; Torrie, L.S.; Wyatt, P.G.; Wyllie, S.; et al. Anti-trypanosomatid drug discovery: An ongoing challenge and a continuing need. *Nat. Rev. Microbiol.* **2017**, *15*, 217–231. [[CrossRef](#)] [[PubMed](#)]
5. Sorci, G.; Faivre, B. Inflammation and oxidative stress in vertebrate host-parasite systems. *Philos. Trans. R. Soc. Lond. B. Biol. Sci.* **2009**, *364*, 71–83. [[CrossRef](#)] [[PubMed](#)]
6. Kraeva, N.; Horáková, E.; Kostygov, A.Y.; Kořený, L.; Butenko, A.; Yurchenko, V.; Lukeš, J. Catalase in Leishmaniinae: With me or against me? *Infect. Genet. Evol.* **2017**, *50*, 121–127. [[CrossRef](#)] [[PubMed](#)]
7. El-Sayed, N.M.; Myler, P.J.; Bartholomeu, D.C.; Nilsson, D.; Aggarwal, G.; Tran, A.N.; Ghedin, E.; Worthey, E.A.; Delcher, A.L.; Blandin, G.; et al. The genome sequence of *Trypanosoma cruzi*, etiologic agent of Chagas disease. *Science* **2005**, *309*, 409–415. [[CrossRef](#)]
8. Ivens, A.C.; Peacock, C.S.; Worthey, E.A.; Murphy, L.; Aggarwal, G.; Berriman, M.; Sisk, E.; Rajandream, M.A.; Adlem, E.; Aert, R.; et al. The genome of the kinetoplastid parasite, *Leishmania major*. *Science* **2005**, *309*, 436–442. [[CrossRef](#)]
9. Ilari, A.; Fiorillo, A.; Genovese, I.; Colotti, G. Polyamine-trypanothione pathway: An update. *Future Med. Chem.* **2017**, *9*, 61–77. [[CrossRef](#)]

10. Frearson, J.A.; Wyatt, P.G.; Gilbert, I.H.; Fairlamb, A.H. Target assessment for antiparasitic drug discovery. *Trends Parasitol.* **2007**, *23*, 589–595. [[CrossRef](#)]
11. Tovar, J.; Cunningham, M.L.; Smith, A.C.; Croft, S.L.; Fairlamb, A.H. Down-regulation of Leishmania donovani trypanothione reductase by heterologous expression of a trans-dominant mutant homologue: Effect on parasite intracellular survival. *Proc. Natl. Acad. Sci. USA* **1998**, *95*, 5311–5316. [[CrossRef](#)]
12. Krieger, S.; Schwarz, W.; Ariyanayagam, M.R.; Fairlamb, A.H.; Krauth-Siegel, R.L.; Clayton, C. Trypanosomes lacking trypanothione reductase are avirulent and show increased sensitivity to oxidative stress. *Mol. Microbiol.* **2000**, *35*, 542–552. [[CrossRef](#)]
13. Cunningham, M.L.; Fairlamb, A.H. Trypanothione reductase from Leishmania donovani. Purification, characterisation and inhibition by trivalent antimonials. *Eur. J. Biochem.* **1995**, *230*, 460–468. [[CrossRef](#)]
14. Baiocco, P.; Colotti, G.; Franceschini, S.; Ilari, A. Molecular basis of antimony treatment in leishmaniasis. *J. Med. Chem.* **2009**, *52*, 2603–2612. [[CrossRef](#)] [[PubMed](#)]
15. Ilari, A.; Genovese, I.; Fiorillo, F.; Battista, T.; De Ionna, I.; Fiorillo, A.; Colotti, G. Toward a Drug Against All Kinetoplastids: From LeishBox to Specific and Potent Trypanothione Reductase Inhibitors. *Mol. Pharm.* **2018**, *15*, 3069–3078. [[CrossRef](#)] [[PubMed](#)]
16. Beig, M.; Oellien, F.; Garoff, L.; Noack, S.; Krauth-Siegel, R.L.; Selzer, P.M. Trypanothione reductase: A target protein for a combined in vitro and in silico screening approach. *PLoS Negl. Trop. Dis.* **2015**, *9*, e0003773. [[CrossRef](#)] [[PubMed](#)]
17. Holloway, G.A.; Charman, W.N.; Fairlamb, A.H.; Brun, R.; Kaiser, M.; Kostewicz, E.; Novello, P.M.; Parisot, J.P.; Richardson, J.; Street, I.P.; et al. Trypanothione reductase high-throughput screening campaign identifies novel classes of inhibitors with antiparasitic activity. *Antimicrob. Agents Chemother.* **2009**, *53*, 2824–2833. [[CrossRef](#)]
18. Maccari, G.; Jaeger, T.; Moraca, F.; Biava, M.; Flohé, L.; Botta, M. A fast virtual screening approach to identify structurally diverse inhibitors of trypanothione reductase. *Bioorg. Med. Chem. Lett.* **2011**, *21*, 5255–5258. [[CrossRef](#)]
19. Martyn, D.C.; Jones, D.C.; Fairlamb, A.H.; Clardy, J. High-throughput screening affords novel and selective trypanothione reductase inhibitors with anti-trypanosomal activity. *Bioorg. Med. Chem. Lett.* **2007**, *17*, 1280–1283. [[CrossRef](#)]
20. Perez-Pineiro, R.; Burgos, A.; Jones, D.C.; Andrew, L.C.; Rodriguez, H.; Suarez, M.; Fairlamb, A.H.; Wishart, D.S. Development of a novel virtual screening cascade protocol to identify potential trypanothione reductase inhibitors. *J. Med. Chem.* **2009**, *52*, 1670–1680. [[CrossRef](#)]
21. Richardson, J.L.; Nett, I.R.; Jones, D.C.; Abdille, M.H.; Gilbert, I.H.; Fairlamb, A.H. Improved tricyclic inhibitors of trypanothione reductase by screening and chemical synthesis. *ChemMedChem* **2009**, *4*, 1333–1340. [[CrossRef](#)]
22. Salmon-Chemin, L.; Buisine, E.; Yardley, V.; Kohler, S.; Debreu, M.A.; Landry, V.; Sergheraert, C.; Croft, S.L.; Krauth-Siegel, R.L.; Davioud-Charvet, E. 2- and 3-substituted 1,4-naphthoquinone derivatives as subversive substrates of trypanothione reductase and lipoamide dehydrogenase from Trypanosoma cruzi: Synthesis and correlation between redox cycling activities and in vitro cytotoxicity. *J. Med. Chem.* **2001**, *44*, 548–565. [[CrossRef](#)]
23. Turcano, L.; Torrente, E.; Missineo, A.; Andreini, M.; Gramiccia, M.; Di Muccio, T.; Genovese, I.; Fiorillo, A.; Harper, S.; Bresciani, A.; et al. Identification and binding mode of a novel Leishmania Trypanothione reductase inhibitor from high throughput screening. *PLoS Negl. Trop. Dis.* **2018**, *12*, e0006969. [[CrossRef](#)]
24. Chacón-Vargas, K.F.; Noguera-Torres, B.; Sánchez-Torres, L.E.; Suarez-Contreras, E.; Villalobos-Rocha, J.C.; Torres-Martinez, Y.; Lara-Ramirez, E.E.; Fiorani, G.; Krauth-Siegel, R.L.; Bolognesi, M.L.; et al. Trypanocidal Activity of Quinoxaline 1,4 Di-N-oxide Derivatives as Trypanothione Reductase Inhibitors. *Molecules* **2017**, *22*, 220. [[CrossRef](#)] [[PubMed](#)]
25. Colotti, G.; Saccoliti, F.; Gramiccia, M.; Di Muccio, T.; Prakash, J.; Yadav, S.; Dubey, V.K.; Vistoli, G.; Battista, T.; Mocchi, S.; et al. Structure-guided approach to identify a novel class of anti-leishmaniasis diaryl sulfide compounds targeting the trypanothione metabolism. *Amino Acids* **2019**, *52*, 247–259. [[CrossRef](#)]
26. Da Paixão, V.G.; Pita, S.S.D.R. In silico identification and evaluation of new Trypanosoma cruzi trypanothione reductase (TcTR) inhibitors obtained from natural products database of the Bahia semi-arid region (NatProDB). *Comput. Biol. Chem.* **2019**, *79*, 36–47. [[CrossRef](#)] [[PubMed](#)]

27. De Gasparo, R.; Halgas, O.; Harangozo, D.; Kaiser, M.; Pai, E.F.; Krauth-Siegel, R.L.; Diederich, F. Targeting a Large Active Site: Structure-Based Design of Nanomolar Inhibitors of Trypanosoma brucei Trypanothione Reductase. *Chemistry* **2019**, *25*, 11416–11421. [[CrossRef](#)] [[PubMed](#)]
28. Jacomini, A.P.; Silva, M.J.V.; Silva, R.G.M.; Gonçalves, D.S.; Volpato, H.; Basso, E.A.; Paula, F.R.; Nakamura, C.V.; Sarragiotto, M.H.; Rosa, F.A. Synthesis and evaluation against Leishmania amazonensis of novel pyrazolo[3,4-d]pyridazinone-N-acylhydrazone-(bi)thiophene hybrids. *Eur. J. Med. Chem.* **2016**, *124*, 340–349. [[CrossRef](#)]
29. Jagu, E.; Pomel, S.; Diez-Martinez, A.; Rascol, E.; Pethe, S.; Loiseau, P.M.; Labruère, R. Synthesis and antikinoplastid evaluation of bis(benzyl)spermidine derivatives. *Eur. J. Med. Chem.* **2018**, *150*, 655–666. [[CrossRef](#)]
30. Ortalli, M.; Ilari, A.; Colotti, G.; De Ionna, I.; Battista, T.; Bisi, A.; Gobbi, S.; Rampa, A.; Di Martino, R.M.C.; Gentilomi, G.A.; et al. Identification of chalcone-based antileishmanial agents targeting trypanothione reductase. *Eur. J. Med. Chem.* **2018**, *152*, 527–541. [[CrossRef](#)]
31. Pandey, R.K.; Kumbhar, B.V.; Srivastava, S.; Malik, R.; Sundar, S.; Kunwar, A.; Prajapati, V.K. Febrifugine analogues as Leishmania donovani trypanothione reductase inhibitors: Binding energy analysis assisted by molecular docking, ADMET and molecular dynamics simulation. *J. Biomol. Struct. Dyn.* **2017**, *35*, 141–158. [[CrossRef](#)]
32. Saccoliti, F.; Angiulli, G.; Pupo, G.; Pescatori, L.; Madia, V.N.; Messore, A.; Colotti, G.; Fiorillo, A.; Scipione, L.; Gramiccia, M.; et al. Inhibition of Leishmania infantum trypanothione reductase by diaryl sulfide derivatives. *J. Enzyme. Inhib. Med. Chem.* **2017**, *32*, 304–310. [[CrossRef](#)]
33. Zimmermann, L.A.; de Moraes, M.H.; da Rosa, R.; de Melo, E.B.; Paula, F.R.; Schenkel, E.P.; Steindel, M.; Bernardes, L.S.C. Synthesis and SAR of new isoxazole-triazole bis-heterocyclic compounds as analogues of natural lignans with antiparasitic activity. *Bioorg. Med. Chem.* **2018**, *26*, 4850–4862. [[CrossRef](#)]
34. Bailey, S.; Smith, K.; Fairlamb, A.H.; Hunter, W.N. Substrate interactions between trypanothione reductase and N1-glutathionylspermidine disulphide at 0.28-nm resolution. *Eur. J. Biochem.* **1993**, *213*, 67–75. [[CrossRef](#)] [[PubMed](#)]
35. Baiocco, P.; Poce, G.; Alfonso, S.; Coccozza, M.; Porretta, G.C.; Colotti, G.; Biava, M.; Moraca, F.; Botta, M.; Yardley, V.; et al. Inhibition of Leishmania infantum trypanothione reductase by azole-based compounds: A comparative analysis with its physiological substrate by X-ray crystallography. *ChemMedChem* **2013**, *8*, 1175–1183. [[CrossRef](#)] [[PubMed](#)]
36. Jones, D.C.; Ariza, A.; Chow, W.H.; Oza, S.L.; Fairlamb, A.H. Comparative structural, kinetic and inhibitor studies of Trypanosoma brucei trypanothione reductase with T. cruzi. *Mol. Biochem. Parasitol.* **2010**, *169*, 12–19. [[CrossRef](#)] [[PubMed](#)]
37. Patterson, S.; Alphey, M.S.; Jones, D.C.; Shanks, E.J.; Street, I.P.; Frearson, J.A.; Wyatt, P.G.; Gilbert, I.H.; Fairlamb, A.H. Dihydroquinazolines as a novel class of Trypanosoma brucei trypanothione reductase inhibitors: Discovery, synthesis, and characterization of their binding mode by protein crystallography. *J. Med. Chem.* **2011**, *54*, 6514–6530. [[CrossRef](#)] [[PubMed](#)]
38. Fairlamb, A.H.; Cerami, A. Metabolism and functions of trypanothione in the Kinetoplastida. *Annu. Rev. Microbiol.* **1992**, *46*, 695–729. [[CrossRef](#)]
39. Stoll, V.S.; Simpson, S.J.; Krauth-Siegel, R.L.; Walsh, C.T.; Pai, E.F. Glutathione reductase turned into trypanothione reductase: Structural analysis of an engineered change in substrate specificity. *Biochemistry* **1997**, *36*, 6437–6447. [[CrossRef](#)]
40. Persch, E.; Bryson, S.; Todoroff, N.K.; Eberle, C.; Thelemann, J.; Dirdjaja, N.; Kaiser, M.; Weber, M.; Derbani, H.; Brun, R.; et al. Binding to large enzyme pockets: Small-molecule inhibitors of trypanothione reductase. *ChemMedChem* **2014**, *9*, 1880–1891. [[CrossRef](#)]
41. Revuelto, A.; Ruiz-Santaquiteria, M.; de Lucio, H.; Gamo, A.; Carriles, A.A.; Gutiérrez, K.J.; Sánchez-Murcia, P.A.; Hermoso, J.A.; Gago, F.; Camarasa, M.J.; et al. Pyrrolopyrimidine vs. Imidazole-Phenyl-Thiazole Scaffolds in Nonpeptidic Dimerization Inhibitors of Leishmania infantum Trypanothione Reductase. *ACS Infect. Dis.* **2019**, *5*, 873–891. [[CrossRef](#)]
42. Jacoby, E.M.; Schlichting, I.; Lantwin, C.B.; Kabsch, W.; Krauth-Siegel, R.L. Crystal structure of the Trypanosoma cruzi trypanothione reductase.mepacrine complex. *Proteins* **1996**, *24*, 73–80. [[CrossRef](#)]

43. Saravanamuthu, A.; Vickers, T.J.; Bond, C.S.; Peterson, M.R.; Hunter, W.N.; Fairlamb, A.H. Two interacting binding sites for quinacrine derivatives in the active site of trypanothione reductase: A template for drug design. *J. Biol. Chem.* **2004**, *279*, 29493–29500. [[CrossRef](#)]
44. Patterson, S.; Jones, D.C.; Shanks, E.J.; Frearson, J.A.; Gilbert, I.H.; Wyatt, P.G.; Fairlamb, A.H. Synthesis and evaluation of 1-(1-(Benzo[b]thiophen-2-yl)cyclohexyl) piperidine (BTCP) analogues as inhibitors of trypanothione reductase. *ChemMedChem* **2009**, *4*, 1341–1353. [[CrossRef](#)] [[PubMed](#)]
45. Eberle, C.; Lauber, B.S.; Fankhauser, D.; Kaiser, M.; Brun, R.; Krauth-Siegel, R.L.; Diederich, F. Improved inhibitors of trypanothione reductase by combination of motifs: Synthesis, inhibitory potency, binding mode, and antiprotozoal activities. *ChemMedChem* **2011**, *6*, 292–301. [[CrossRef](#)] [[PubMed](#)]
46. De Gasparo, R.; Brodbeck-Persch, E.; Bryson, S.; Hentzen, N.B.; Kaiser, M.; Pai, E.F.; Krauth-Siegel, R.L.; Diederich, F. Biological Evaluation and X-ray Co-crystal Structures of Cyclohexylpyrrolidine Ligands for Trypanothione Reductase, an Enzyme from the Redox Metabolism of Trypanosoma. *ChemMedChem* **2018**, *13*, 957–967. [[CrossRef](#)] [[PubMed](#)]
47. Turcano, L.B.T.; Torrente De Haro, E.; Missineo, A.; Alli, C.; Paonessa, G.; Colotti, G.; Harper, S.F.A.; Ilari, A.; Bresciani, A. Spiro-containing derivatives show antiparasitic activity against Trypanosoma brucei through inhibition of the trypanothione reductase enzyme. *PLoS Negl. Trop. Dis.* **2020**. accepted.
48. Chivers, J.; Jenner, P.; Marsden, C.D. Pharmacological characterization of binding sites identified in rat brain following in vivo administration of [³H]-spiperone. *Br. J. Pharmacol.* **1987**, *90*, 467–478. [[CrossRef](#)]
49. Janssen, P.A.; Niemegeers, C.J.; Schellekens, K.H.; Lenaerts, F.M.; Verbruggen, F.J.; van Nueten, J.M.; Marsboom, R.H.; Hérin, V.V.; Schaper, W.K. The pharmacology of fluspirilene (R 6218), a potent, long-acting and injectable neuroleptic drug. *Arzneimittelforschung* **1970**, *20*, 1689–1698.
50. Stump, B.; Eberle, C.; Kaiser, M.; Brun, R.; Krauth-Siegel, R.L.; Diederich, F. Diaryl sulfide-based inhibitors of trypanothione reductase: Inhibition potency, revised binding mode and antiprotozoal activities. *Org. Biomol. Chem.* **2008**, *6*, 3935–3947. [[CrossRef](#)]
51. Eberle, C.; Burkhard, J.A.; Stump, B.; Kaiser, M.; Brun, R.; Krauth-Siegel, R.L.; Diederich, F. Synthesis, inhibition potency, binding mode, and antiprotozoal activities of fluorescent inhibitors of trypanothione reductase based on mepacrine-conjugated diaryl sulfide scaffolds. *ChemMedChem* **2009**, *4*, 2034–2044. [[CrossRef](#)]
52. Colotti, G.; Fiorillo, A.; Ilari, A. Metal- and metalloid-containing drugs for the treatment of trypanosomatid diseases. *Front. Biosci.* **2018**, *23*, 954–966.
53. Baiocco, P.; Ilari, A.; Ceci, P.; Orsini, S.; Gramiccia, M.; Di Muccio, T.; Colotti, G. Inhibitory Effect of Silver Nanoparticles on Trypanothione Reductase Activity and Leishmania infantum Proliferation. *ACS Med. Chem. Lett.* **2011**, *2*, 230–233. [[CrossRef](#)]
54. Ilari, A.; Baiocco, P.; Messori, L.; Fiorillo, A.; Boffi, A.; Gramiccia, M.; Di Muccio, T.; Colotti, G. A gold-containing drug against parasitic polyamine metabolism: The X-ray structure of trypanothione reductase from Leishmania infantum in complex with auranofin reveals a dual mechanism of enzyme inhibition. *Amino Acids* **2012**, *42*, 803–811. [[CrossRef](#)] [[PubMed](#)]
55. Colotti, G.; Ilari, A.; Fiorillo, A.; Baiocco, P.; Cinellu, M.A.; Maiore, L.; Scaletti, F.; Gabbiani, C.; Messori, L. Metal-based compounds as prospective antileishmanial agents: Inhibition of trypanothione reductase by selected gold complexes. *ChemMedChem* **2013**, *8*, 1634–1637. [[CrossRef](#)] [[PubMed](#)]
56. Drugbank. Auranofin. Available online: <https://www.drugbank.ca/drugs/DB00995> (accessed on 14 April 2020).
57. Toro, M.A.; Sánchez-Murcia, P.A.; Moreno, D.; Ruiz-Santaquiteria, M.; Alzate, J.F.; Negri, A.; Camarasa, M.J.; Gago, F.; Velázquez, S.; Jiménez-Ruiz, A. Probing the dimerization interface of Leishmania infantum trypanothione reductase with site-directed mutagenesis and short peptides. *Chembiochem* **2013**, *14*, 1212–1217. [[CrossRef](#)] [[PubMed](#)]



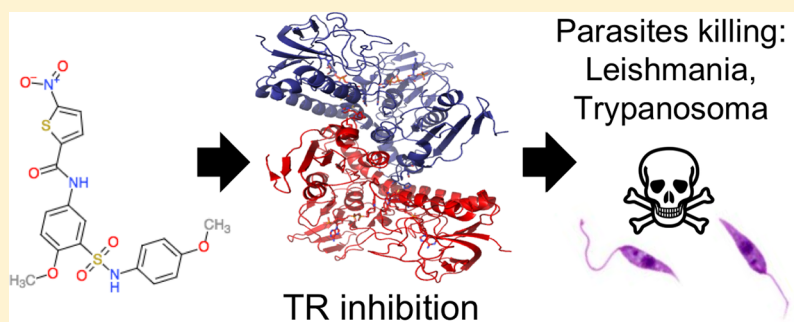
Toward a Drug Against All Kinetoplastids: From LeishBox to Specific and Potent Trypanothione Reductase Inhibitors

Andrea Ilari,^{*,†} Ilaria Genovese,[‡] Fabiana Fiorillo,[‡] Theo Battista,[‡] Ilenia De Ionna,[‡] Annarita Fiorillo,[‡] and Gianni Colotti^{*,†}

[†]Institute of Molecular Biology and Pathology, Italian National Research Council (IBPM CNR), Department of Biochemical Sciences, Sapienza University, P.le A. Moro 5, 00185 Rome, Italy

[‡]Department of Biochemical Sciences, Sapienza University, P.le A. Moro 5, 00185 Rome, Italy

S Supporting Information



ABSTRACT: Leishmaniasis, Chagas disease, and sleeping sickness affect millions of people worldwide and lead to the death of about 50 000 humans per year. These diseases are caused by the kinetoplastids *Leishmania*, *Trypanosoma cruzi*, and *Trypanosoma brucei*, respectively. These parasites share many general features, including gene conservation, high amino acid identity among proteins, the presence of subcellular structures as glycosomes and the kinetoplastid, and genome architecture, that may make drug development family specific, rather than species-specific, i.e., on the basis of the inhibition of a common, conserved parasite target. However, no optimal molecular targets or broad-spectrum drugs have been identified to date to cure these diseases. Here, the LeishBox from GlaxoSmithKline high-throughput screening, a 192-molecule set of best antileishmanial compounds, based on 1.8 million compounds, was used to identify specific inhibitors of a validated *Leishmania* target, trypanothione reductase (TR), while analyzing in parallel the homologous human enzyme glutathione reductase (GR). We identified three specific highly potent TR inhibitors and performed docking on the TR solved structure, thereby elucidating the putative molecular basis of TR inhibition. Since TRs from kinetoplastids are well conserved, and these compounds inhibit the growth of *Leishmania*, *Trypanosoma cruzi*, and *Trypanosoma brucei*, the identification of a common validated target may lead to the development of potent antikinetoplastid drugs.

KEYWORDS: *Leishmania*, *Trypanosoma*, inhibitors, LeishBOX, trypanothione reductase, neglected diseases

INTRODUCTION

Leishmania and *Trypanosoma* parasites (belonging to the Trypanosomatids family) are the causative agents of some of the most neglected and most life-threatening infective diseases, for whom only a small number of drugs exist, with poor safety, efficacy, and pharmacokinetic profiles.

Trypanosoma (T.) cruzi causes Chagas disease in humans, primarily in Central and South America. Its life cycle is complex, involving multiple distinct morphologic stages in both its mammalian hosts and the triatomine insect vectors. Although acute infections can be lethal, usually the disease evolves into a chronic stage that may result in debilitation and eventually in death. Treatment is based on nifurtimox and benznidazole, highly toxic compounds that are not effective for long-term infections and that are prone to develop resistance.¹

T. brucei is the causative agent of human African trypanosomiasis, also known as sleeping sickness, transmitted by the bite of Tsetse flies. The disease has two stages. In stage 1, the parasites remain in the bloodstream, while in stage 2, they enter the central nervous system, leading to neurological complications, with a fatal course if the disease is left untreated. Among the available drugs, suramin and pentamidine are only effective versus the stage 1 disease, because they do not penetrate the blood–brain barrier. Melarsoprol is a very toxic arsenical compound, and eflornithine (alone or in combination

Received: February 20, 2018

Revised: June 5, 2018

Accepted: June 13, 2018

Published: June 13, 2018

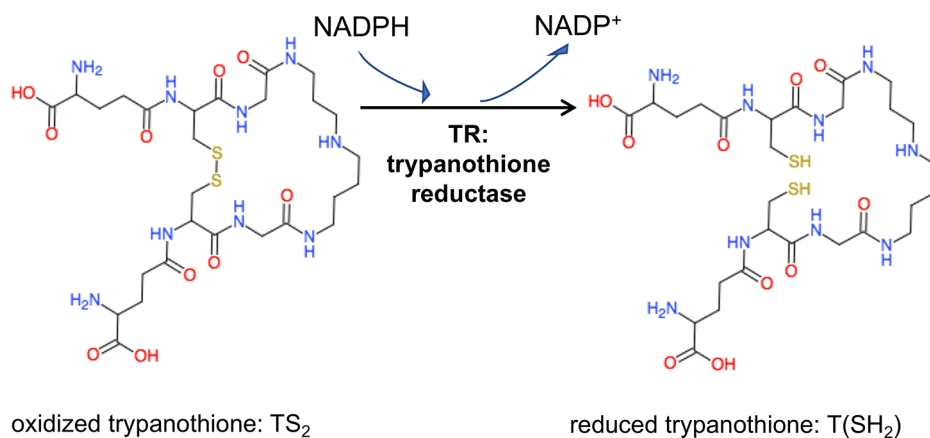


Figure 1. Enzymatic activity of trypanothione reductase. Structures designed with Chemdoodle.

				*****::*::*::*::*		
L.i.	TR	1	-MSRA	YDLVVLGAGSGGLEAGWNAAVTHKKKVAVDVQATHGPPFLFAALGGT	CVNVGCVPKMLMVTGAQYMD	71
L.d.	TR	1	-MSRA	YDLVVLGAGSGGLEAGWNAAVTHKKKVAVDVQATHGPPFLFAALGGT	CVNVGCVPKMLMVTGAQYMD	71
T.b.	TR	1	-MSKI	FDLVVIGAGSGGLEAGWNAATLYKRVAVIDVQTHGPPHYAALGGT	CVNVGCVPKMLMVTGAQYMD	71
T.c.	TR	1	MMSKI	FDLVVIGAGSGGLEAGWNAATLYKRVAVIDVQMVHGGPPFFSALGGT	CVNVGCVPKMLMVTGAQYME	72
Human	GR	1	[38] ALSRA [21]	YDYLVIAGSGGGLASARRAAEL-GARAAVVEESHK-----	LGCTCVNVGCVPKMLMVTAVHSE	121
				::::*::*::*		
L.i.	TR	72	LIRESGGFGWEMDRESLCPNWKTLIAAKNKVVNSINESYKSMFADTEGLSPHMGFGALQDAHTVVRKSEDPHSDVL---			148
L.d.	TR	72	LIRESGGFGWEMDRESLCPNWKTLIAAKNKVVNSINESYKSMFADTEGLSPHMGFGALQDAHTVVRKSEDPHSDVL---			148
T.b.	TR	72	HLRESAGFGWEPDGSVSKANWKLIAAKNEAVLDINKSYEGMFNDTEGLDFLWGSLESKNVVVRRETADPKSAVK---			148
T.c.	TR	73	HLRESAGFGWEPDRTTLRAEWKLLIAVKDEAVLNINKSYEEMFRDTEGLEFFLWGSLESKNVVVRRESADFPASAVK---			149
Human	GR	122	FMHDHADYGFPSCGKFN-NRVIVIEKRDAYSRLNAILYQNNLTKSH-TEIIRGHAAP-----			188
				::::*::*::*		
L.i.	TR	149	ETLDEYILIATG---SWPTRLGVPGEFCITSNFAFYLEDAPKRMCLCVGGYIAVEFAGIFNGYKPCGGYVDCYRGLD			225
L.d.	TR	149	ETLDEYILIATG---SWPTRLGVPGEFCITSNFAFYLEDAPKRMCLCVGGYIAVEFAGIFNGYKPCGGYVDCYRGLD			225
T.b.	TR	149	ERLQADHILLATG---SWPQMPAIPGVHEHCISSNEAFYLPPEPRRLVTGGGFIISVFAGIFNAYKFPGGKVTLCYRNL			225
T.c.	TR	150	ERLEENILLASG---SWPHMNIPIGIEHCISSNEAFYLPPEPRRLVTGGGFIISVFAGIFNAYKPKDQGVTLCYRGM			226
Human	GR	189	KKYTAPHILIAIGmpSTPHESQIPGASLIGTSGDPFLEELPGRSVIVGAGYIAVEMAGIISAL---GSRTSLMIHRDK			265
				*****::*::*::*::*		
L.i.	TR	226	ILRGFDTEVRKSLTKQLGANGIRVRTNLNPTKITKNEDGSHVHFND	GTEEDYDQVMLAIGRVPFRSQALQDKAGVR		302
L.d.	TR	226	ILRGFDTEVRKSLTKQLGANGIRVRTNLNPTKITKNEDGSHVHFND	GTEEDYDQVMLAIG-VFRSQALQDKAGVR		301
T.b.	TR	226	ILRGFDTEVIREEVTKQLTANGIEIMTNENPAKVSLLNTDGSKHVTFES	GKTLDVDVVMMAIGRIIPRTNDLQLQNVAGV-		302
T.c.	TR	227	ILRGFDTEVIREEVTKQLTANGIQLTKENPAKVELNADGSKVTFES	GKRMDFDLVMMMAIGRSFRTKDLQQLNVAGV-		302
Human	GR	266	VLRSFDSMISTNCTEELNAGVEVLKFSQVKEVKKTLGSELEVSMVA [8]	TMPIDVDLMLLWAI GRVPNTKDL SLKMLGIIQ		350
				*****::*::*::*::*		
L.i.	TR	303	TGKNGAVQVDAYSKTSVDNIYAIGDVTNRVMLTPVAINEGA-AFVETVFGGKP-RATDHTKVACAVFSIPIIGTCGMTEE			380
L.d.	TR	302	TGKNGAVQVDAYSKTSVDNIYAIGDVTNRVMLTPVAINEGACVLETVFGGKP-RATDHTKVACAVFSIPIIGTCGMTEE			380
T.b.	TR	303	LTPKGGVQVDEFSRTNPVNIYAIGDITDLRMLTPVAINEGA-ALVDTVFNGKP-RKTDHTRVASAVFSIPIIGTCGLLIEE			380
T.c.	TR	303	MIKNGGVQVDEYSRTNVSNIIYAIGDVTNRVMLTPVAINEGA-ALVDTVFNGNP-RKTDHTRVASAVFSIPIIGTCGLLIEE			380
Human	GR	351	TDDKGIHVDEPQNTNVKGIYAVDVGCKALLTPVAIAAGR-KLAHLFEYKEGSKLDYNNIPTVVFHSPIPIGTVGLTED			429
				::::*::*::*		
L.i.	TR	381	EAAKNY--ETVAVYASSFTPLMHNISGSKHKHFIRIITNESNGEVLGVHMLGDSAPETIQSVGICMRMGAKISDFHSTI			458
L.d.	TR	381	EAAKNY--ETVAVYASSFTPLMHNISGSKHKHFIRIITNESNGEVLGVHMLGDSAPETIQSVGICMRMGAKISDFHSTI			458
T.b.	TR	381	VAAKEF--ERVAVYMSFTPLMHNISGSKYKFKVAKIIVTNHSDGTVLGVHLLGDGAPEIIQAVGICLRINAISDFYNTI			458
T.c.	TR	381	VASKRY--EAVVYLSFTPLMHNISGSKYKFKVAKIIVTNHSDGTVLGVHLLGDGAPEIIQGVGICLRINAISDFYNTI			458
Human	GR	430	EAIHKYgLENVKTYS F TPMY H AVTKRKTCCVM-KMVCANKEEKVVGIHMQGLGDCEMLQGFPAVAVKMGATKADFDNTV			508
				::::*::*::*		
L.d.	TR	459	GVHPTSAE ELCSMRTPAYFYESGKRVEKL-SSNL	491		
L.d.	TR	459	GVHPTSAE ELCSMRTPAYFYESGKRVEKL-SSNL	491		
T.b.	TR	459	GVHPTSAE ELCSMRTPSYYYLKERMETLPESSL	492		
T.c.	TR	459	GVHPTSAE ELCSMRTPSYYYVKGKERMKPEASL	492		
Human	GR	509	AIHPTSEEL VTLR-----	522		

Figure 2. Alignment of sequences of trypanothione reductase from *L. infantum*, *L. donovani* (the residues changed in *L. infantum* TR are indicated in italics), *T. brucei*, and *T. cruzi*, together with human GR. * = Identities among TR residues and = similarity among TR residues. Catalytic residues of TR and GR are indicated in red; residues determining the clash of inhibitor compounds to GR in docking experiments are indicated in bold.

with nifurtimox) requires intravenous infusions and can develop drug resistance.²⁻⁴

About 20 different *Leishmania* species, spread throughout 98 countries and transmitted into mammalian hosts by the bite of sand flies (*Phlebotomus* or *Lutzomyia*), can determine parasitic infection in humans. Three main types of clinical forms of disease exist, i.e., visceral leishmaniasis, characterized by fever, low levels of red blood cells, and enlarged spleen and liver, which leads to death if left untreated; cutaneous leishmaniasis, with skin ulcers that can heal spontaneously, often leaving disfiguring scars; and mucocutaneous leishmaniasis, which presents with ulcers of the skin, mouth, and nose. Used antileishmanial treatments have poor safety, efficacy, and pharmacokinetic profiles, and they are based on pentavalent

antimonials (whose action determines depletion of trypanothione, a dithiol responsible for redox homeostasis, see below), amphotericin B (which interacts with sterol metabolism), miltefosine (which acts on the phospholipid metabolism), and paromomycin (which inhibits protein synthesis).^{3,5-9}

Although these protozoan parasites are transmitted by different insects, and the human diseases they cause are clinically diverse, much of their biology is similar. The genomes of multiple Trypanosomatidae have been sequenced and are available in TriTrypDB (<http://tritrypdb.org>), an integrated genomic and functional genomic database for pathogens of the family Trypanosomatidae, including organisms in both *Leishmania* and *Trypanosoma* genera.¹⁰ Although substantial differences in the lifestyle and pathophysiology

exist, *Leishmania* spp, *Trypanosoma cruzi*, and *Trypanosoma brucei* share many general features, including gene conservation, high synteny, high amino acid identity among proteins, the presence of subcellular structures as glycosomes and kinetoplastid, and genome architecture. In kinetoplastids, more than 6100 genes are closely related to paralogous ones, on a total of 8000–12000 genes.¹¹ Although the majority of trypanosomatid genes are conserved, which may make drug development family specific, rather than species-specific, i.e., based on the inhibition of a common, conserved parasite target, no antitrypanosomatid drugs exist.

The general rules that identify a good drug target are that it should be (i) absent in the human host; (ii) essential for the parasite survival; and (iii) druggable, i.e., a structure that allows its interaction and, possibly, its inhibition with drugs.¹² The enzymes of the trypanothione pathway are considered as one of the best possible choices in the pursuit of antitrypanosomatid drugs, since they have all three properties. In all kinetoplastids, spermidine together with glutathione is the substrate for the trypanothione synthetase-amidase (TSA), which synthesizes the trypanothione (T(SH)₂). This molecule is kept reduced by the trypanothione reductase (TR) (Figure 1), and it is used by the tryparedoxin/tryparedoxin peroxidase system (TXN/TXNPx) to reduce hydrogen peroxide and alkyl-hydroperoxide to water and alcohol, respectively, thereby detoxifying the parasites. The T(SH)₂/TR system replaces many of the antioxidant and metabolic functions of the glutathione/glutathione reductase (GR) and thioredoxin/TR systems present in other organisms and therefore is necessary for the parasite survival (for a review, see refs 13,14).

All the enzymes of trypanothione metabolism have been genetically validated as drug targets and have been shown to be essential for the parasite survival. In particular, all attempts to obtain a TR null mutant in *L. donovani* failed; mutants with a partial trisomy for the TR locus, with disruption of two TR alleles by gene targeting and a lower expression of TR mRNA, show attenuated infectivity and a markedly decreased capacity to survive within macrophages.¹⁵ Fairlamb and co-workers have shown that pentavalent antimonials, the main drugs used against leishmaniasis, in vivo interfere with the trypanothione metabolism by inducing rapid efflux of intracellular T(SH)₂ and by inhibiting TR in intact cells.¹⁶ Moreover, Ilari, Colotti, and co-workers solved the structure of TR in complex with Sb(III), disclosing the molecular basis of the interaction of antimonials with TR and of its inhibition and with other inhibiting compounds, with potential antileishmanial activity.^{17–21}

Further, TR is highly conserved in all kinetoplastids (66–100% sequence identity; 80–100% sequence homology), and selectivity over human glutathione reductase (34–37% sequence identity; 51–54% sequence homology) can be obtained on the basis of the sequence difference and the different dimensions and charges of the active site²² (Figure 2).

Since TR is essential for the parasite survival in the amastigote stage during infection,^{15,23} this enzyme has therefore been widely studied to find antitrypanosomatid compounds. Several structure-based studies showed that many different classes of compounds (ranging from tricyclic compounds to polyamine analogs, to acridines, to 1,4-naphthoquinone derivatives, to diaryl sulfides nitroheterocyclic compounds, phenothiazine derivatives, 2-aminodiphenylsulfides, *N*-(3-phenylpropyl) substituted polyamines, polyamine-peptide conjugates, and kukoamine A derivatives) are able to

inhibit TR in vitro,^{24–33} and some of them proved to be quite effective on the parasite, although *Leishmania* amastigotes are often very difficult to be selectively killed.

Here we identify potent specific TR inhibitors, based on the antiparasitic compounds identified in the GlaxoSmithKline HTS diversity set of 1.8 million compounds, and which already demonstrated to be effective by whole-cell phenotypic assays against *L. donovani*, *T. cruzi*, and *T. brucei*.³⁴

We screened the 192 compounds characterized as the best *L. donovani* inhibitors in in vitro enzymatic assays vs TR from *L. infantum* and human GR, thereby identifying 3 specific highly potent specific TR inhibitors and two partially selective TR inhibitors. The most potent compound, i.e., *N*-(4-bromo-3-methylphenyl)-5-nitrothiophene-2-carboxamide (compound C10/7), was studied to identify the type of inhibition.

The docking of the most active compounds was calculated, showing the basis of both potency and specificity of TR interaction; a SPR competition assay was also carried out to show whether the compounds compete for trypanothione binding. The most specific and potent TR inhibitors are demonstrated to efficiently inhibit the growth of *L. donovani*, *T. cruzi*, and *T. brucei*;³⁴ the inhibition of TR, a validated target conserved in all trypanosomatids, may lead to the development of antikinetoplastid drugs.

■ EXPERIMENTAL SECTION

Protein Expression and Purification: Enzymatic Assay. TR from *L. infantum* was expressed and purified as previously reported.^{17,35} Enzymatic inhibition assays were performed at 20 °C using a diode-array HP8453 spectrophotometer. In order to optimize the assay, different buffers and different enzyme and substrate concentrations were tried out. The experimental conditions that were used allowed for the determination of specific activity and K_m values for NADPH and trypanothione ($K_{m,NADPH} = 12 \mu\text{M}$; $K_{m,TS_2} = 72 \mu\text{M}$; $k_{cat} = 4800 \text{ min}^{-1}$ for trypanothione disulfide).¹⁷

LeishBox compounds were first tested at final concentration of 25 μM . The solution containing buffer (HEPES (50 mM), NaCl (40 mM) at pH 7.4), TR (5 nM), TS₂ (150 μM), and inhibitor (25 μM) were allowed to equilibrate for 2 min in a quartz Hellma 104-QS cuvette (assay volume = 800 μL). Assays were initiated by the addition of NADPH (100 μM), and the absorbance decrease was followed at 340 nm, which indicated the oxidation of NADPH. Inhibition was calculated for each experiment by measuring the velocity of oxidation of NADPH with respect to the experiments carried out in the absence of the inhibitor.

The active compounds (inhibition >80%) were tested at lower concentrations (between 10 and 0.02 μM) using the same assay, in duplicate, in order to determine compound potency (IC₅₀).

To verify selectivity, these inhibitors were also tested on GR, the most similar human enzyme. The experiment was performed as for the TR inhibition assay (GR (5 nM), GSSG (150 μM), inhibitor (25 μM), and the final addition of NADPH (100 μM), in the buffer HEPES (50 mM), NaCl (40 mM) at pH 7.4).

To calculate the K_i for the compound with the higher potency and selectivity, kinetic experiments were carried out at various concentrations of TS₂ (400 μM , 100 μM) and the inhibitor and at a fixed NADPH concentration (100 μM).

The concentration of NADPH was calculated using the molar extinction coefficient $\epsilon = 6222 \text{ M}^{-1} \text{ cm}^{-1}$ at 340 nm.

Trypanothione disulfide (Bachem), NADPH (Sigma-Aldrich), GR (Sigma-Aldrich), and GSSG (Sigma-Aldrich) were used for the experiments.

Surface Plasmon Resonance Experiments. Surface plasmon resonance (SPR) experiments were carried out using a SensiQ Pioneer system. The sensor chip (COOH5) was activated chemically by a 35 μL injection of a 1:1 mixture of *N*-ethyl-*N'*-(3-(diethylaminopropyl)carbodiimide (200 mM) and *N*-hydroxysuccinimide (50 mM) at a flow rate of 5 $\mu\text{L}/\text{min}$. TR (at a concentration of 100 nM) was immobilized on activated sensor chips via amine coupling. The immobilizations were carried out in 20 mM sodium acetate at pH 4.5; the remaining groups were blocked by injecting 1 M ethanolamine hydrochloride (35 μL). A total of 800 resonance units (RU) of TR was immobilized onto the chip for the experiment in Figure S2; a total of 3000 RU of TR was immobilized onto the chip for the competitive binding experiment. Binding of ~ 1 ng per square mm of protein at the sensorchip surface typically causes a signal change of 1000 RU.³⁶ Compounds interacting with the ligand (in 20 mM Hepes pH 7.4, 150 mM NaCl + 0.005% surfactant P20 + 2% DMSO) were injected at a concentration of 25 μM on the sensor chip at a constant flow (30 $\mu\text{L}/\text{min}$). The increase in RU relative to the baseline (0–240 s) indicates complex formation, whereas the decrease in RU represents dissociation of compounds from an immobilized ligand after the injection of buffer. As a negative control, sensor chips were treated as described above in the absence of immobilized TR. Regeneration procedures are based on two long (2000 and 500 s) injections of buffer, separated by a brief (5 s) injection of 10 mM NaOH.

For the competitive binding experiment, oxidized trypanothione (TS₂) compounds A1/7 and C10/7 were injected in 20 mM Hepes pH 7.4, 150 mM NaCl + 0.005% surfactant P20 + 2% DMSO, at a concentration of 20 μM on the sensor chip at a constant flow (30 $\mu\text{L}/\text{min}$); in addition, mixtures of compound A1/7 + TS₂ or of compound C10/7 + TS₂, each at a concentration of 20 μM , were injected in the same conditions to test whether the compounds compete with TS₂. The increase in RU relative to the baseline (0–160 s) indicates complex formation, whereas the decrease in RU after 160 s represents the dissociation of compounds and/or TS₂ from the immobilized ligand after injection of the buffer. As a negative control, sensor chips were treated as described above in the absence of immobilized TR. Regeneration procedures were based on two long (2000 and 500 s) injections of buffer, separated by a brief (5 s) injection of 10 mM NaOH.

The sensorgrams were analyzed using the SensiQ Qdat program.

Docking of Compounds in the Active Sites of TR. The AutoDock4³⁷ docking package was used for ligand flexible docking simulations. The structure of TR in oxidized form downloaded from the protein data bank (PDB code: 2JK6) was set up as the receptor for docking protocol. The.pdb coordinates of compounds A1/7, C5/7, F1/7, and C10/7 were generated using the PRODRG2 server (<http://davapc1.bioch.dundee.ac.uk/cgi-bin/prodrg>).³⁸

The TR structure was edited using the software from the ADT package to remove all water molecules and add hydrogen atoms. Nonpolar hydrogens and lone pairs were then merged into each atom within the macromolecule, and the ligands were assigned a Gasteiger partial charge. The.pdbqt files were generated with ADT for the protein and the ligands (pdb files

containing the partial charge and the autodock atom type). A grid box of 72 \times 42 \times 50 points, with a spacing of 0.436 Å, was positioned at the active-site gorge. The Lamarckian genetic algorithm (LGA) was employed to run the docking job for each ligand with the maximum number of generations and energy evaluations of 27 000 and 2 500 000, respectively.

RESULTS

Determination of Inhibiting Capacity of LeishBox Compounds vs TR from *L. infantum*. All 192 compounds of the LeishBox, identified by GlaxoSmithKline in HTS from 1.8 million compounds against *L. donovani*,³⁴ were first tested for their ability to inhibit TR enzymatic activity. A first screen was carried out at a concentration of 25 μM to measure the ability of the compounds to inhibit TR. Sixteen of the compounds (8.3% of the whole set) are able to decrease the velocity of the reduction of trypanothione disulfide by at least 50%, while 7 compounds (3.6% of tested compounds) inhibit TR by at least 80% (Table 1, Figure 3).

Table 1. TR vs GR Inhibition^a

	inhibition TR IC ₅₀ (μM)	inhibition GR IC ₅₀ (μM)	selectivity index (IC ₅₀ GR/IC ₅₀ TR)
A1/7	0.52 \pm 0.14	no inhibition at 25	$\gg 50$
F1/7	5.58 \pm 0.86	no inhibition at 25	$\gg 5$
C5/7	0.22 \pm 0.05	3.2	15
B10/7	1.96 \pm 0.30	3.7	1.9
C10/7	0.19 \pm 0.08	no inhibition at 25	$\gg 100$
G1/9	2.24 \pm 0.52	>25	>11
G2/9	5.96 \pm 0.84	>25	>4

^aIC₅₀ for each inhibitor has been calculated by fitting the experiments in Figure 3.

These 7 compounds, i.e., compounds A1/7, B10/7, C5/7, C10/7, F1/7, G1/9, and G2/9 (Figure 4), were then tested at lower concentrations (between 10 and 0.02 μM) to determine the compounds potency (IC₅₀). All of these compounds have IC₅₀ values below 6 μM (Table 1, Figure 3), and three of them (compound C10/7, *N*-(4-bromo-3-methylphenyl)-5-nitrothiophene-2-carboxamide: IC₅₀ = 190 nM; compound C5/7, 5-nitro-*N*-[4-(1-pyrrolidinylsulfonyl)phenyl]-2-thiophenecarboxamide: IC₅₀ = 220 nM, and compound A1/7, *N*-{4-methoxy-3-[(4-methoxyphenyl)sulfamoyl]phenyl}-5-nitrothiophene-2-carboxamide: IC₅₀ = 550 nM) have the highest potency, with IC₅₀ values in the nanomolar range. Compound C10/7 inhibits TR in an apparent competitive fashion, as shown by the Dixon plot (Figure S1). To rule out whether these compounds containing a nitro group were able to be reduced by NADPH or could serve as pseudosubstrates of TR, we also carried out control kinetics experiments using 25 μM compound C10/7 in the absence of trypanothione and trypanothione reductase (Figure S2).

Determination of the Inhibiting Capacity of LeishBox Compounds vs Human GR. Compounds A1/7, B10/7, C5/7, C10/7, F1/7, G1/9, and G2/9 were also tested in human GR inhibition assays (Table 1). Three compounds (1.6% of tested compounds) are also selective, i.e., do not inhibit human GR (compounds A1/7, F1/7, and C10/7), while compounds G1/9 and G2/9 are partially selective inhibitors (IC₅₀ GR > 25 μM), as is compound C5/7 (IC₅₀ GR 1 order of magnitude

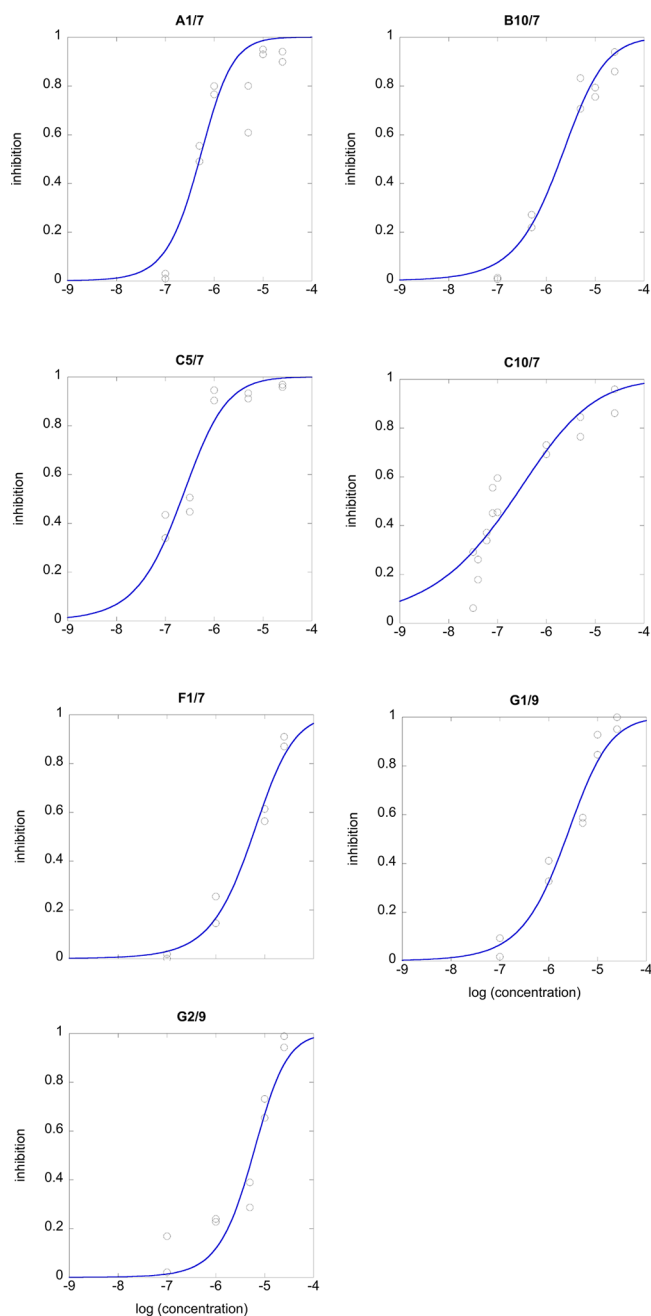


Figure 3. Inhibition experiments and calculation of IC_{50} of active compounds vs TR from *L. infantum*. For each inhibitor, inhibition (calculated for each experiment by measuring the velocity of oxidation of NADPH with respect to the experiments being carried out in the absence of inhibitor) is plotted vs \log_{10} of molar inhibitor concentration.

higher than that for IC_{50} TR), while B10/7 is a nonselective inhibitor (IC_{50} GR in the same order of magnitude as IC_{50} TR).

Selected Inhibitors Interact Directly with TR. The ability of inhibiting compounds to interact with TR was evaluated by SPR experiments. These were carried out by immobilizing TR onto COOH5 sensorchips and adding compounds as analytes. Figure S3 shows the sensorgrams of eight evaluated interactions, i.e., compounds A1/7, B10/7, C5/7, C10/7, F1/7, G1/9, and two control noninhibiting compounds (B1/7 and B2/7); the experiment indicates that

binding of the inhibitor compounds to TR occurs, while the two control compounds do not appear to bind to the target enzyme.

Structural Analysis of the Most Selective Inhibiting Compounds. The most selective inhibitors identified have quite similar structures, as shown by Figure 4. The phenyl-5-nitrothiophene-2-carboxamide moiety of *N*-(4-bromo-3-methylphenyl)-5-nitrothiophene-2-carboxamide (compound C10/7) is the core of the A1/7 and C5/7 compounds, i.e., the compounds that show the highest potency vs TR, while compound F1/7 (specific although less potent) contains a similar core with a phenyl group, a carboxamide (reversed with respect to compound C10/7), and a thiazol group instead of a thiophene. The mode of binding of these compounds to TR and the structural basis of their inhibiting capacity are therefore possibly conserved in the four compounds.

Docking of *L. infantum* TR and Human GR with Compounds A1/7, C5/7, C10/7, and F1/7 and Molecular Basis of Inhibition Specificity. We performed docking experiments with compounds A1/7, C5/7, C10/7, and F1/7 using AutoDock4 and selecting the positions of binding to TR on the basis of the lowest estimated free energy of binding, as calculated by the suite (= van der Waals energy + H bond energy + desolvation energy + electrostatic energy + final total internal energy + torsional free energy – unbound system's energy). The compounds are able to bind to the same region of TR active site, comprising catalytic C52, C57, H461', and E466', with similar orientations and very good calculated affinities (Figure 5).

Figure 5A,B reports the best docked interactions for inhibitors A1/7 to the trypanothione pocket: two different models, where the inhibitor is bound with different torsions between residues C57, K61, H461', and E466' on one side, and to P336 and the loop, including F396, P398, L399, and M400, on the other side. The two models were calculated to bind with an estimated free energy of binding of -7.88 kcal/mol (Figure 5A; estimated inhibition constant, $K_i = 1.69$ μ M at 298.15 K) and -7.55 kcal/mol (Figure 5B; estimated inhibition constant, $K_i = 2.90$ μ M at 298.15 K), respectively, values of the same order of magnitude of measured IC_{50} .

Figure 5C shows the docking of compound C5/7 with TR, identifying the very same region of interaction with respect to compound A1/7. The docking yielded a model where C5/7 binds to TR with an estimated free energy of binding of -7.75 kcal/mol (Figure 5C; estimated inhibition constant, $K_i = 2.10$ μ M at 298.15 K). Compound F1/7 binds to TR with an estimated free energy of binding of -9.58 kcal/mol (Figure 5E; estimated inhibition constant, $K_i = 94.68$ nM at 298.15 K). Compound C10/7 binds to TR with an estimated free energy of binding of -6.68 kcal/mol (Figure 5D; estimated inhibition constant, $K_i = 12.61$ μ M at 298.15 K).

In particular, all of these compounds appear to bind with the nitro group establishing bonds (with the possible exception of compound C10/7) with the nitrogens of the peptide bonds P398-L399 and L399-M400.

Superposition of the inhibitors A1/7, C5/7, C10/7, and F1/7 modeled by docking to the TR active site by the glutathione binding site of human GR was also calculated (Figure 6). In particular, in the position where the compounds are bound to GR in the modeled structures, three residues (L399, M400, and N402) are changed in M450, Y451, and A452, respectively, and the loop 396–402 (447–453 in GR) is bulkier and negatively charged. A clash between the compound

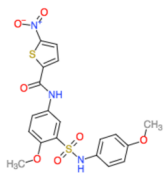
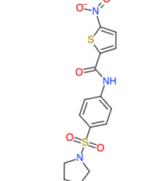
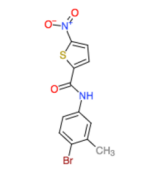
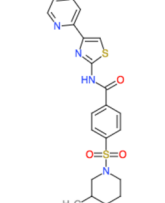
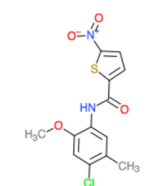
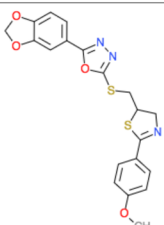
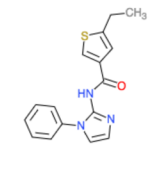
	<p>A1/7 N-(4-methoxy-3-[(4-methoxyphenyl)sulfonyl]phenyl)-5-nitrothiophene-2-carboxamide</p> <p>Formula: C₁₉H₁₇N₃O₇S₂ MW: 463.48 Aring: 3 Clogp: 2.713 Hba: 4 Hbd: 1 Heavy: 31 Tpsa: 139.55</p> <p>IC50: <i>Leishmania</i> TR: 0.52 μM human GR: no inhibition at 25 μM pIC50: L.d.: 6.1-6.3 T.c.: 7.2 T.b.: 7.3</p>
	<p>C5/7 5-Nitro-N-[4-(1-pyrrolidiny)sulfonyl]phenyl]-2-thiophenecarboxamide</p> <p>Formula: C₁₉H₁₉N₃O₅S₂ MW: 381.43 Aring: 2 Clogp: 2.541 Hba: 4 Hbd: 1 Heavy: 25 Tpsa: 112.3</p> <p>IC50: <i>Leishmania</i> TR: 0.22 μM human GR: 3.2 μM pIC50: L.d.: 5.8-6.0 T.c.: 6.7 T.b.: 6.8</p>
	<p>C10/7 N-(4-bromo-3-methylphenyl)-5-nitrothiophene-2-carboxamide</p> <p>Formula: C₁₂H₉BrN₂O₅S MW: 341.18 Aring: 2 Clogp: 3.985 Hba: 2 Hbd: 1 Heavy: 19 Tpsa: 74.92</p> <p>IC50: <i>Leishmania</i> TR: 0.19 μM human GR: no inhibition at 25 μM pIC50: L.d.: 5.5-5.8 T.c.: 6.6 T.b.: 6.5</p>
	<p>F1/7 4-[(3-methylpiperidin-1-yl)sulfonyl]-N-[4-(pyridin-2-yl)-1,3-thiazol-2-yl]-benzamide</p> <p>Formula: C₂₁H₂₂N₄O₃S₂ MW: 442.55</p> <p>Aring: 3 Clogp: 3.782 Hba: 5 Hbd: 1 Heavy: 30 Tpsa: 92.26</p> <p>IC50: <i>Leishmania</i> TR: 5.6 μM human GR: no inhibition at 25 μM pIC50: L.d.: 5.8-6.8 T.c.: 6.4 T.b.: 6.7</p>
	<p>B10/7 N-(4-chloro-2-methoxy-5-methylphenyl)-5-nitrothiophene-2-carboxamide</p> <p>Formula: C₁₃H₁₁ClN₂O₅S MW: 326.76</p> <p>Aring: 2 Clogp: 3.213 Hba: 2 Hbd: 1 Heavy: 25 Tpsa: 84.15</p> <p>IC50: <i>Leishmania</i> TR: 1.96 μM human GR: 3.7 μM pIC50: L.d.: 5.1-5.3 T.c.: 6.2 T.b.: 6.3</p>
	<p>G1/9 2-(2H-1,3-benzodioxol-5-yl)-5-([(2-(4-methoxyphenyl)-4,5-dihydro-1,3-thiazol-5-yl)methyl)sulfonyl]-1,3,4-oxadiazole</p> <p>Formula: C₂₀H₁₇N₃O₅S₂ MW: 427.48</p> <p>Aring: 3 Clogp: 3.551 Hba: 3 Hbd: 0 Heavy: 29 Tpsa: 78.97</p> <p>IC50: <i>Leishmania</i> TR: 2.2 μM human GR: >25 μM pIC50: L.d.: 6.0-6.4 T.c.: 5.6 T.b.: 5.0</p>
	<p>G2/9 5-Ethyl-N-(1-phenyl-1H-imidazol-2-yl)-3-thiophenecarboxamide</p> <p>Formula: C₁₆H₁₅N₃O₃S MW: 297.38</p> <p>Aring: 3 Clogp: 4.188 Hba: 2 Hbd: 1 Heavy: 21 Tpsa: 46.92</p> <p>IC50: <i>Leishmania</i> TR: 1.96 μM human GR: 3.7 μM pIC50: L.d.: 5.2-5.3 T.c.: 5.5 T.b.: 5.5</p>

Figure 4. Structures and chemophysical properties of the best selective TR inhibitors, i.e., A1/7, C5/7, C10/7, F1/7, B10/7, G1/9, and G2/9 compounds (Peña et al.³⁴). MW = Molecular weight; Aring = number of aromatic rings; Clogp = calculated partition-coefficient between *n*-octanol and water; Hba = hydrogen-bond acceptor; Hbd = hydrogen-bond donor; Heavy = number of heavy atoms (no hydrogen atoms); Tpsa = total polar surface area; pIC50: $-\log(\text{IC}_{50})$; all information is from the Supporting Information of Peña et al.³⁴ Structures were designed with Chemdoodle.

and the loop 447–453 of GR (396–402, TR numeration) impairs inhibitor binding to GR, and it is possibly responsible for the molecular basis of the specificity of action of these compounds toward TR.

A1/7, C5/7, C10/7, and F1/7 display different sizes and charge distributions with respect to the ligands identified in the *Li*TR trypanothione binding pocket of the TR complexes X-ray structures, namely 3,4,5-triacetyloxy-6-(acetyloxymethyl)-oxane-2thiolate (one of the Au(I) ligand in the Aurano-fin complex),²⁰ RDS-777,²¹ and compound 1 (4-((1-(4-ethylphenyl)2-methyl-5-(4-(methylthio)phenyl)-1H-pyrrol-3-yl)methyl)thiomorpholin).¹⁹ However, from the comparison between the positions occupied by the docked GSK ligands and those occupied by crystallized inhibitors, it appears that there is a partial superimposition between the volume occupied by the docking poses and the position occupied by RDS777 and the Aurano-fin component in the respective TR X-ray structures (Figure S4).

In particular, all of the A1/7, C5/7, C10/7, and F1/7 compounds, as well as RDS777 and the Aurano-fin component, occupied a volume very close to the catalytic residues, establishing electrostatic interactions with H461, E466, and E467.

SPR Competitive Binding Experiments. Oxidized trypanothione (TS₂) compounds A1/7 and C10/7 were injected in 20 mM Hepes pH 7.4, 150 mM NaCl + 0.005% surfactant P20 + 2% DMSO at a concentration of 20 μM on the sensor chip at a constant flow (30 μL/min); in addition,

mixtures of compound A1/7 + TS₂ or of compound C10/7 + TS₂, each at a concentration of 20 μM, were injected in the same conditions to test whether the compounds compete with TS₂ (Figure 7). The increase in RU relative to the baseline (0–120 s) indicates complex formation, whereas the decrease in RU after 120 s represents the dissociation of the compounds and/or TS₂ from the immobilized ligand after injection of the buffer. The experiments on one side show that TS₂ and compounds A1/7 and C10/7 appear to bind with similar curves to TR; even more importantly, sensorgrams carried out by injecting mixtures of compound A1/7 + TS₂ or of compound C10/7 + TS₂ do not show increased (additive) binding with respect to injection of TS₂ or of inhibitors alone. The experiments show that competition occurs between trypanothione and inhibitors, and the inhibitors act by binding to the trypanothione binding site.

DISCUSSION

A system of redox homeostasis based on catalase and glutathione reductase is absent in trypanosomatids that rely on a unique thiol-based redox metabolism based on trypanothione.^{39–41} Therefore, inhibition of the enzymes of the trypanothione pathway is one of the most attractive options for antikinoplastid drug discovery. Here we have characterized the ability of the 192 best antileishmanial compounds identified by GlaxoSmithKline in HTS from 1.8 million compounds against *L. donovani*.³⁴

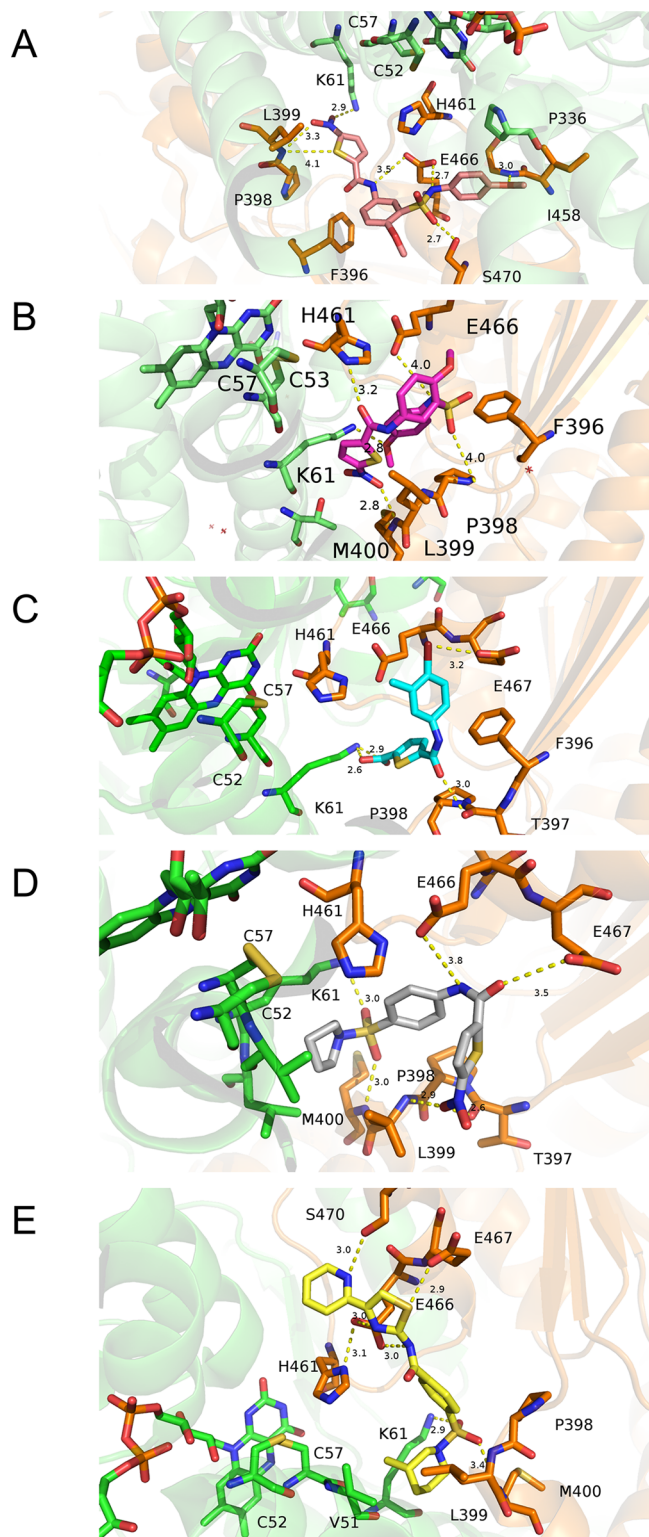


Figure 5. Model of the best docked interactions for inhibitors A1/7 (A, B), C10/7 (C), C5/7 (D), and F1/7 (E) to the trypanothione binding site of TR obtained using AutoDock4 (Trott and Olson³⁷). The distances between the structural elements of the compounds and the closest residues are indicated. The figure was designed on the basis of the docked poses using Pymol.

Among these 192 compounds, 7 (3.6% of tested compounds) are highly potent TR inhibitors, and 3

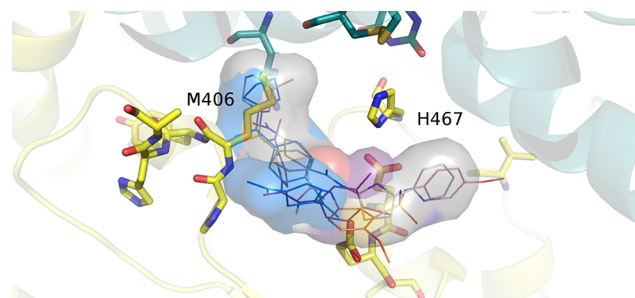


Figure 6. Superposition of inhibitors A1/7, F1/7, C5/1, and C10/7 (gray) modeled by docking to the TR active site and to the glutathione binding site of human GR (yellow). Note the clash between the compound and residues of the loop 405–409 (398–402, TR numeration), in particular M406.

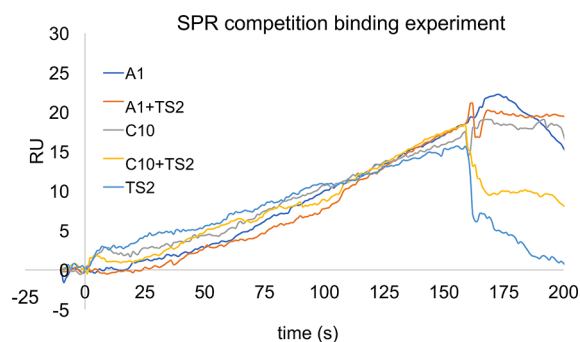


Figure 7. SPR competition experiment between oxidized trypanothione (TS₂) and compounds C10/7 and A1/7. Sensorgrams of the interaction between TR from *L. infantum* immobilized on a COOHs sensorchip and oxidized trypanothione, compounds C10/7 and A1/7 of the LeishBox at concentrations of 20 μ M, in parallel with sensorgrams of mixtures TS₂ + C10/7 and TS₂ + A1/7, each at a concentration of 20 μ M. The experiment shows that competition occurs between compounds and TS₂.

compounds (1.6% of tested compounds) are also selective, which do not inhibit human GR.

Although many quite efficient TR in vitro inhibitors have been identified, most of these compounds are less effective against the parasite. TR inhibitors can be considered potentially good lead compounds only if they possess submicromolar IC₅₀ and K_i values, as demonstrated in conditioned TR knockout models, where the redox metabolism of the parasite is affected only when the level of TR is depleted to less than 5% of normal content.^{39,42}

Compound C10/7 efficiently inhibits TR, with nanomolar IC₅₀ and K_i values about 8 times better than the K_i value of Sb(III). The actual TR inhibitor derived from in vivo reduction of pentavalent antimonial prodrugs is currently used against Leishmaniasis. Antimony, however, may also bind (and possibly inhibit) other thiol-containing enzymes;⁴³ this can represent a potential advantage in terms of multitarget action but poses a problem of toxicity (binding and inhibition of human enzymes) and resistance (development of mechanisms to overcome the presence of the drug).^{44,45}

The potent TR selective inhibitors identified in this study act by binding to the trypanothione pocket of TR, while the same region of the glutathione pocket of human GR is blocked by the substitution of L399 and M400 into a methionine and a tyrosine, respectively. In GR, these residues form a bulky loop that impairs inhibitor binding: this may provide an explanation

for the ability of these compounds to efficiently kill *Leishmania* parasites in both axenic promastigote and microphage-infecting amastigote forms, while having little effect with respect to human cells.³⁴ In addition, the pocket, altered in GR, is not only conserved in TR from *L. donovani* (and *L. infantum*) but also in TR from *T. cruzi* and *T. brucei*. Compounds A1/7, C5/7, C10/7, and F1/7 not only evade toxicity problems but can be good lead compounds also against *T. cruzi* and *T. brucei*, setting the basis for a potential antiketoplastid therapy. Structural analysis of these four best compounds shows that the phenyl-5-nitrothiophene-2-carboxamide moiety of *N*-(4-bromo-3-methylphenyl)-5-nitrothiophene-2-carboxamide (compound C10/7) is the core of the A1/7 compound and of the C5/7 compound, which may bind in the same position at the trypanothione binding site. Also, compound F1/7 contains a similar core with a phenyl group, a carboxamide (reversed with respect to C10/7), and a thiazol group instead of a thiophene, and it can bind to the same site of C10/7, A1/7, and C5/7 compounds. Docking of A1/7, C5/7, F1/7, and C10/7 shows that they bind to the same sites and inhibit TR with the same mechanism. These compounds bear some structural similarity to other compounds, previously demonstrated to be good inhibitors of TR, such as azole compounds identified in structure-based TR-inhibitor identification studies, able to bind at the entrance of the trypanothione binding site as compound C10/7.¹⁹

SPR competitive binding experiments show that competition occurs between trypanothione and inhibitors, and the inhibitors act by binding to the trypanothione binding site. The experiment was carried out using TR in the oxidized state to avoid further complication of the analysis, since a nucleophilic attack by the NADPH-reduced cysteines of the active site to the nitrothiophene moiety of some inhibitors is, in principle, possible.⁴⁶ This is not irrelevant for the presence of a nitrothiophene in the most effective inhibitors: docking shows that the nitro group can interact with the nitrogen of the peptide bond at L399 and/or with the amino-group of the side chain of K61 (Figure 5).

In this context, it is worth noting that the most selective inhibitors identified in this study were already demonstrated to be effective by whole-cell phenotypic assays against *L. donovani*, *T. cruzi*, and *T. brucei*³⁴ (Figure 3), and that one of these three compounds (compound A1/7: *N*-{4-methoxy-3-[(4-methoxyphenyl)sulfamoyl]phenyl}-5-nitrothiophene-2-carboxamide) is the only compound present in all three LeishBox, ChagasBox, and HATBox.

In conclusion, we have identified *Leishmania* (and *Trypanosoma*) targets for compounds identified by GlaxoSmithKline in HTS from 1.8 million compounds against *L. donovani*, *T. cruzi*, and *T. brucei*.³⁴ We will now proceed to the structure-based optimization of compounds derived by C10/7.

■ ASSOCIATED CONTENT

Supporting Information

The Supporting Information is available free of charge on the ACS Publications website at DOI: 10.1021/acs.molpharmaceut.8b00185.

A Dixon plot of TR inhibition by compound C10/7, control experiments performed in the absence of trypanothione, a SPR experiment showing interaction between TR from *L. infantum* immobilized on a COOH5 sensorchip and compounds of the LeishBox

at a concentration of 20 μ M, and a comparison between the positions occupied by the docked GSK ligands and those occupied by crystallized inhibitors, i.e., RDS777 and Auranofin (PDF)

■ AUTHOR INFORMATION

Corresponding Authors

*E-mail: andrea.ilari@uniroma1.it; Phone: +39-06-49910910; Fax: +39-06-4440062.

*E-mail: gianni.colotti@uniroma1.it; Phone: +39-06-49910910; Fax: +39-06-4440062.

ORCID

Andrea Ilari: 0000-0002-7754-399X

Gianni Colotti: 0000-0002-9913-0635

Notes

The authors declare no competing financial interest.

■ ACKNOWLEDGMENTS

We thank GlaxoSmithKline, and in particular, Dr. Julio Martin and Dr. Albane Kessler (GSK DDW, Tres Cantos, Spain), for the availability of the LeishBox compounds and for useful discussions. This work was funded by CNCCS s.c.a.r.l. (National Collection of Chemical Compounds and Screening Center 2015) and by MIUR PRIN 20154JRJPP.

■ REFERENCES

- (1) Rodrigues Coura, J.; de Castro, S. L. A critical review on Chagas disease chemotherapy. *Memorias do Instituto Oswaldo Cruz* **2002**, *97* (1), 3–24.
- (2) Barrett, M. P.; Boykin, D. W.; Brun, R.; Tidwell, R. R. Human African trypanosomiasis: pharmacological re-engagement with a neglected disease. *Br. J. Pharmacol.* **2007**, *152* (8), 1155–71.
- (3) Barrett, M. P.; Croft, S. L. Management of trypanosomiasis and leishmaniasis. *Br. Med. Bull.* **2012**, *104*, 175–96.
- (4) Vincent, I. M.; Creek, D.; Watson, D. G.; Kamleh, M. A.; Woods, D. J.; Wong, P. E.; Burchmore, R. J.; Barrett, M. P. A molecular mechanism for efloornithine resistance in African trypanosomes. *PLoS Pathog.* **2010**, *6* (11), e1001204.
- (5) Chawla, B.; Jhingran, A.; Panigrahi, A.; Stuart, K. D.; Madhubala, R. Paromomycin affects translation and vesicle-mediated trafficking as revealed by proteomics of paromomycin -susceptible -resistant *Leishmania donovani*. *PLoS One* **2011**, *6* (10), e26660.
- (6) Colotti, G.; Baiocco, P.; Fiorillo, A.; Boffi, A.; Poser, E.; Chiaro, F. D.; Ilari, A. Structural insights into the enzymes of the trypanothione pathway: targets for antileishmaniasis drugs. *Future Med. Chem.* **2013**, *5* (15), 1861–75.
- (7) Lux, H.; Heise, N.; Klenner, T.; Hart, D.; Opperdoes, F. R. Ether–lipid (alkyl-phospholipid) metabolism and the mechanism of action of ether–lipid analogues in *Leishmania*. *Mol. Biochem. Parasitol.* **2000**, *111* (1), 1–14.
- (8) Ouellette, M.; Drummelsmith, J.; Papadopoulou, B. Leishmaniasis: drugs in the clinic, resistance and new developments. *Drug Resist. Updates* **2004**, *7* (4–5), 257–66.
- (9) Singh, N.; Kumar, M.; Singh, R. K. Leishmaniasis: current status of available drugs and new potential drug targets. *Asian Pac. J. Trop. Med.* **2012**, *5* (6), 485–97.
- (10) Aslett, M.; Aurrecochea, C.; Berriman, M.; Brestelli, J.; Brunk, B. P.; Carrington, M.; Depledge, D. P.; Fischer, S.; Gajria, B.; Gao, X.; Gardner, M. J.; Gingle, A.; Grant, G.; Harb, O. S.; Heiges, M.; Hertz-Fowler, C.; Houston, R.; Innamorato, F.; Iodice, J.; Kissinger, J. C.; Kraemer, E.; Li, W.; Logan, F. J.; Miller, J. A.; Mitra, S.; Myler, P. J.; Nayak, V.; Pennington, C.; Phan, I.; Pinney, D. F.; Ramasamy, G.; Rogers, M. B.; Roos, D. S.; Ross, C.; Sivam, D.; Smith, D. F.; Srinivasamoorthy, G.; Stoeckert, C. J., Jr.; Subramanian, S.; Thibodeau, R.; Tivey, A.; Treatman, C.; Velarde, G.; Wang, H.

TriTrypDB: a functional genomic resource for the Trypanosomatidae. *Nucleic Acids Res.* **2010**, *38*, D457–D462.

(11) El-Sayed, N. M.; Myler, P. J.; Blandin, G.; Berriman, M.; Crabtree, J.; Aggarwal, G.; Caler, E.; Renauld, H.; Worthey, E. A.; Hertz-Fowler, C.; Ghedin, E.; Peacock, C.; Bartholomeu, D. C.; Haas, B. J.; Tran, A. N.; Wortman, J. R.; Alsmark, U. C.; Angiuoli, S.; Anupama, A.; Badger, J.; Bringaud, F.; Cadag, E.; Carlton, J. M.; Cerqueira, G. C.; Creasy, T.; Delcher, A. L.; Djikeng, A.; Embley, T. M.; Hauser, C.; Ivens, A. C.; Kummerfeld, S. K.; Pereira-Leal, J. B.; Nilsson, D.; Peterson, J.; Salzberg, S. L.; Shallom, J.; Silva, J. C.; Sundaram, J.; Westenberger, S.; White, O.; Melville, S. E.; Donelson, J. E.; Andersson, B.; Stuart, K. D.; Hall, N. Comparative genomics of trypanosomatid parasitic protozoa. *Science* **2005**, *309* (5733), 404–409.

(12) Frearson, J. A.; Wyatt, P. G.; Gilbert, I. H.; Fairlamb, A. H. Target assessment for antiparasitic drug discovery. *Trends Parasitol.* **2007**, *23* (12), 589–95.

(13) Colotti, G.; Ilari, A. Polyamine metabolism in Leishmania: from arginine to trypanothione. *Amino Acids* **2011**, *40* (2), 269–85.

(14) Ilari, A.; Fiorillo, A.; Genovese, I.; Colotti, G. Polyamine-trypanothione pathway: an update. *Future Med. Chem.* **2017**, *9* (1), 61–77.

(15) Dumas, C.; Ouellette, M.; Tovar, J.; Cunningham, M. L.; Fairlamb, A. H.; Tamar, S.; Olivier, M.; Papadopoulou, B. Disruption of the trypanothione reductase gene of Leishmania decreases its ability to survive oxidative stress in macrophages. *EMBO journal* **1997**, *16* (10), 2590–2598.

(16) Cunningham, M. L.; Fairlamb, A. H. Trypanothione reductase from Leishmania donovani. Purification, characterisation and inhibition by trivalent antimonials. *Eur. J. Biochem.* **1995**, *230* (2), 460–8.

(17) Baiocco, P.; Colotti, G.; Franceschini, S.; Ilari, A. Molecular basis of antimony treatment in leishmaniasis. *J. Med. Chem.* **2009**, *52* (8), 2603–12.

(18) Baiocco, P.; Ilari, A.; Ceci, P.; Orsini, S.; Gramiccia, M.; Di Muccio, T.; Colotti, G. Inhibitory Effect of Silver Nanoparticles on Trypanothione Reductase Activity and Leishmania infantum Proliferation. *ACS Med. Chem. Lett.* **2011**, *2* (3), 230–3.

(19) Baiocco, P.; Poce, G.; Alfonso, S.; Coccozza, M.; Porretta, G. C.; Colotti, G.; Biava, M.; Moraca, F.; Botta, M.; Yardley, V.; Fiorillo, A.; Lantella, A.; Malatesta, F.; Ilari, A. Inhibition of Leishmania infantum trypanothione reductase by azole-based compounds: a comparative analysis with its physiological substrate by X-ray crystallography. *ChemMedChem* **2013**, *8* (7), 1175–83.

(20) Ilari, A.; Baiocco, P.; Messori, L.; Fiorillo, A.; Boffi, A.; Gramiccia, M.; Di Muccio, T.; Colotti, G. A gold-containing drug against parasitic polyamine metabolism: the X-ray structure of trypanothione reductase from Leishmania infantum in complex with aurano-fin reveals a dual mechanism of enzyme inhibition. *Amino Acids* **2012**, *42* (2–3), 803–11.

(21) Saccoliti, F.; Angiulli, G.; Pupo, G.; Pescatori, L.; Madia, V. N.; Messori, A.; Colotti, G.; Fiorillo, A.; Scipione, L.; Gramiccia, M.; Di Muccio, T.; Di Santo, R.; Costi, R.; Ilari, A. Inhibition of Leishmania infantum trypanothione reductase by diaryl sulfide derivatives. *J. Enzyme Inhib. Med. Chem.* **2017**, *32* (1), 304–310.

(22) Spinks, D.; Shanks, E. J.; Clegghorn, L. A.; McElroy, S.; Jones, D.; James, D.; Fairlamb, A. H.; Frearson, J. A.; Wyatt, P. G.; Gilbert, I. H. Investigation of trypanothione reductase as a drug target in Trypanosoma brucei. *ChemMedChem* **2009**, *4* (12), 2060–9.

(23) Tovar, J.; Cunningham, M. L.; Smith, A. C.; Croft, S. L.; Fairlamb, A. H. Down-regulation of Leishmania donovani trypanothione reductase by heterologous expression of a trans-dominant mutant homologue: effect on parasite intracellular survival. *Proc. Natl. Acad. Sci. U. S. A.* **1998**, *95* (9), 5311–6.

(24) Smith, H. K.; Bradley, M. Comparison of resin and solution screening methodologies in combinatorial chemistry and the identification of a 100 nM inhibitor of trypanothione reductase. *J. Comb. Chem.* **1999**, *1* (4), 326–32.

(25) Chitkul, B.; Bradley, M. Optimising inhibitors of trypanothione reductase using solid-phase chemistry. *Bioorg. Med. Chem. Lett.* **2000**, *10* (20), 2367–9.

(26) Khan, M. O.; Austin, S. E.; Chan, C.; Yin, H.; Marks, D.; Vaghjani, S. N.; Kendrick, H.; Yardley, V.; Croft, S. L.; Douglas, K. T. Use of an additional hydrophobic binding site, the Z site, in the rational drug design of a new class of stronger trypanothione reductase inhibitor, quaternary alkylammonium phenothiazines. *J. Med. Chem.* **2000**, *43* (16), 3148–56.

(27) Girault, S.; Davioud-Charvet, T. E.; Maes, L.; Dubremetz, J. F.; Debreu, M. A.; Landry, V.; Sergheraert, C. Potent and specific inhibitors of trypanothione reductase from Trypanosoma cruzi: bis(2-aminodiphenylsulfides) for fluorescent labeling studies. *Bioorg. Med. Chem.* **2001**, *9* (4), 837–46.

(28) Persch, E.; Bryson, S.; Todoroff, N. K.; Eberle, C.; Thelemann, J.; Dirdjaja, N.; Kaiser, M.; Weber, M.; Derbani, H.; Brun, R.; Schneider, G.; Pai, E. F.; Krauth-Siegel, R. L.; Diederich, F. Binding to large enzyme pockets: small-molecule inhibitors of trypanothione reductase. *ChemMedChem* **2014**, *9* (8), 1880–1891.

(29) Beig, M.; Oellien, F.; Garoff, L.; Noack, S.; Krauth-Siegel, R. L.; Selzer, P. M. Trypanothione reductase: a target protein for a combined in vitro and in silico screening approach. *PLoS Neglected Trop. Dis.* **2015**, *9* (6), e0003773.

(30) Patterson, S.; Alphey, M. S.; Jones, D. C.; Shanks, E. J.; Street, I. P.; Frearson, J. A.; Wyatt, P. G.; Gilbert, I. H.; Fairlamb, A. H. Dihydroquinazolines as a novel class of Trypanosoma brucei trypanothione reductase inhibitors: discovery, synthesis, and characterization of their binding mode by protein crystallography. *J. Med. Chem.* **2011**, *54* (19), 6514–30.

(31) Hamilton, C. J.; Saravanamuthu, A.; Fairlamb, A. H.; Eggleston, I. M. Benzofuranyl 3,5-bis-polyamine derivatives as time-dependent inhibitors of trypanothione reductase. *Bioorg. Med. Chem.* **2003**, *11* (17), 3683–93.

(32) Stump, B.; Eberle, C.; Kaiser, M.; Brun, R.; Krauth-Siegel, R. L.; Diederich, F. Diaryl sulfide-based inhibitors of trypanothione reductase: inhibition potency, revised binding mode and antiprotozoal activities. *Org. Biomol. Chem.* **2008**, *6* (21), 3935–47.

(33) Venkatesan, S. K.; Shukla, A. K.; Dubey, V. K. Molecular docking studies of selected tricyclic and quinone derivatives on trypanothione reductase of Leishmania infantum. *J. Comput. Chem.* **2010**, *31* (13), 2463–2475.

(34) Pena, I.; Pilar Manzano, M.; Cantizani, J.; Kessler, A.; Alonso-Padilla, J.; Bardera, A. L.; Alvarez, E.; Colmenarejo, G.; Cutillo, I.; Roquero, I.; de Dios-Anton, F.; Barroso, V.; Rodriguez, A.; Gray, D. W.; Navarro, M.; Kumar, V.; Sherstnev, A.; Drewry, D. H.; Brown, J. R.; Fiandor, J. M.; Julio Martin, J. New compound sets identified from high throughput phenotypic screening against three kinetoplastid parasites: an open resource. *Sci. Rep.* **2015**, *5*, 8771.

(35) Baiocco, P.; Franceschini, S.; Ilari, A.; Colotti, G. Trypanothione reductase from Leishmania infantum: cloning, expression, purification, crystallization and preliminary X-ray data analysis. *Protein Pept. Lett.* **2009**, *16* (2), 196–200.

(36) Chaiken, I.; Rose, S.; Karlsson, R. Analysis of macromolecular interactions using immobilized ligands. *Anal. Biochem.* **1992**, *201* (2), 197–210.

(37) Trott, O.; Olson, A. J. AutoDock Vina: improving the speed and accuracy of docking with a new scoring function, efficient optimization, and multithreading. *J. Comput. Chem.* **2009**, *31* (2), 455–461.

(38) Schuttelkopf, A. W.; van Aalten, D. M. PRODRG: a tool for high-throughput crystallography of protein-ligand complexes. *Acta Crystallogr., Sect. D: Biol. Crystallogr.* **2004**, *60* (8), 1355–1363.

(39) Comini, M. A.; Flohé, L., Trypanothione-Based Redox Metabolism in Trypanosomatids. In *Trypanosomatid Diseases*; Wiley-VCH Verlag GmbH & Co. KGaA, 2013; pp 167–199.

(40) Krauth-Siegel, R. L.; Comini, M. A. Redox control in trypanosomatids, parasitic protozoa with trypanothione-based thiol metabolism. *Biochim. Biophys. Acta, Gen. Subj.* **2008**, *1780* (11), 1236–48.

(41) Oza, S. L.; Shaw, M. P.; Wyllie, S.; Fairlamb, A. H. Trypanothione biosynthesis in *Leishmania major*. *Mol. Biochem. Parasitol.* **2005**, *139* (1), 107–16.

(42) Krieger, S.; Schwarz, W.; Ariyanayagam, M. R.; Fairlamb, A. H.; Krauth-Siegel, R. L.; Clayton, C. Trypanosomes lacking trypanothione reductase are avirulent and show increased sensitivity to oxidative stress. *Mol. Microbiol.* **2000**, *35* (3), 542–52.

(43) Navarro, M.; Gabbiani, C.; Messori, L.; Gambino, D. Metal-based drugs for malaria, trypanosomiasis and leishmaniasis: recent achievements and perspectives. *Drug Discovery Today* **2010**, *15* (23–24), 1070–8.

(44) Ashutosh; Sundar, S.; Goyal, N. Molecular mechanisms of antimony resistance in *Leishmania*. *J. Med. Microbiol.* **2007**, *56* (2), 143–153.

(45) Halder, A. K.; Sen, P.; Roy, S. Use of antimony in the treatment of leishmaniasis: current status and future directions. *Mol. Biol. Int.* **2011**, *2011*, 571242.

(46) Morley, J. O.; Matthews, T. P. Structure-activity relationships in nitrothiophenes. *Bioorg. Med. Chem.* **2006**, *14* (23), 8099–108.